Electronic Thesis and Dissertation Repository

4-19-2017 12:00 AM

Cerebral lactate metabolism and memory: Implications for Alzheimer's disease

Richard Andrew Harris, *The University of Western Ontario*

Abstract

Alzheimer's disease (AD) is a neurodegenerative disease characterized by amyloid plaques that are comprised of aggregated amyloid-β peptides. These toxic proteins promote mitochondrial dysfunction and neuronal cell death. A shift in metabolism away from oxidative phosphorylation and toward aerobic glycolysis, with the concomitant production of lactate, affords neurons a survival advantage against amyloid-β toxicity. Recent evidence now suggests that aerobic glycolysis in the brain plays a critical role in supporting synaptic plasticity, learning, and memory. However, the role of aerobic glycolysis and lactate metabolism in AD-mediated cognitive decline is unknown. My objective was to test the hypotheses that aerobic glycolysis is upregulated in neurons to mediate amyloid-β resistance and promote memory processes *in vivo* using the APP/PS1 mouse model of AD. Cerebral lactate levels within the frontal cortex of control mice were found to decline with age, whereas lactate levels remained unaltered in APP/PS1 mice. An age-dependent decline in levels of key aerobic glycolysis enzymes and an increase in lactate transporter expression were detected in control mice. Increased expression of lactate-producing enzymes correlated with improved memory performance in control mice, yet the opposite effect was detected in APP/PS1 mice. To determine if aerobic glycolysis plays a role in mediating spatial memory processes, mice were injected with dichloroacetate, an inhibitor of pyruvate dehydrogenase kinase. Dichloroacetate caused a reduction in conversion of pyruvate to lactate in the brain and a decline in phosphorylation of pyruvate dehydrogenase, the target of dichloroacetate, yet there was no significant effect on memory. In agreement with previous observations, a correlation analysis of cortical extracts revealed that increased phosphorylation of pyruvate dehydrogenase correlated with better spatial memory in control mice. These observations indicate that production of lactate, via aerobic glycolysis, is beneficial for memory function during normal aging, yet is not explicitly required for spatial memory tasks. In addition, elevated lactate levels in APP/PS1 mice indicate perturbed lactate processing, a factor that may contribute to memory impairment in AD. Collectively, this research demonstrates several novel observations that will lead to a better understanding of cerebral lactate metabolism in the AD brain and aid in the development of metabolic strategies to treat this devastating disease.

Keywords

Co-authorship statement

Parts of Chapter 1 were published as a review article in *Biogerontology* (reprint permission in Appendix B). I was the first author of this publication. The co-authors were Lauren Tindale (LT), who created the figures and Robert C. Cumming (RCC), who contributed in the conception of the ideas and helped in writing the manuscript.

Sections 2.1 to 2.7 and 3.1 to 3.6 were published in *The Journal of Neuroscience* (reprint permission in Appendix B). I was the first author, and the co-authors were LT, Asad Lone (AL), Olivia Singh (OS), Shannon L. Macauley (SLM), Molly Stanley (MS), David M. Holtzman (DMH), Robert Bartha (RB), and RCC. LT, AL, and OS helped in the implementation of the experiments, and RB and RCC contributed in the experimental design. SLM, MS, and DMH performed the microdialysis measurements of interstitial lactate in the hippocampus. RCC contributed to the preparation of the manuscript and involved in the synthesis of many of the ideas.

Sections 2.8 to 2.12 and 3.11 to 3.14 are currently being prepared for publication. I will be the first author, and co-authors will be AL, OS, Ariel Frame (AF), Andrew Powell (AP), Alex Kozlov (AK), Patrick Lim (PL), Trung Nguyen Thanh Le (TNTL), Timothy Scholl (TS), and RCC. AL, OS, AF, AP, and AK helped in the implementation of the experiments. PL, TNTL, and TS performed the hyperpolarized ^{13}C-pyruvate magnetic resonance spectroscopy experiment. RCC contributed to the preparation of the manuscript.

Ariel Frame performed the LDHA/LDHB enzyme activity assay from the hippocampus of mice injected with vehicle and Isosafrol (Figure 24C) and contributed to the writing of the materials and methods for that section.

Acknowledgments

There are so many people to thank for their help and support. First and foremost, I'd like to thank my advisor, Dr. Robert Cumming. Rob, I've learned more from you over the past five years than I think you realize. You truly lead by example. You've taught me how to properly manage a laboratory and inspire passion in students. You always put your students first, often at the expense of your own needs, and it is this dedication and selflessness that I will try to emulate over my career. Thank you for all of your time and energy over the years. It is truly appreciated and will not be forgotten.

I would also like to thank members of my advisory committee, Dr. Marco Prado and Dr. Kathleen Hill, for your guidance throughout this process and for challenging my assumptions. Thank you also Dr. Hill and Dr. Shiva Singh for sharing your animal colony space and equipment. I am grateful to Dr. Robert Bartha, Miranda Bellyou, and Alex Li for their technical expertise in running the ^{1}H-MRI for lactate scanning and Dr. Timothy Scholl, Jennifer Hadway, Patrick Lim, Trung (Adam) Le, and Yonathan Araya for their expert administration of the hyperpolarized ^{13}C-pyruvate MRI experiment. The ACVS staff deserves recognition for their management of the mouse colony and the Biology Department administrative staff has been wonderfully helpful every step of the way.

Special thanks to Dr. Jordan Newington for jumpstarting this direction of research and showing me the ropes. To Asad Lone, Olivia Singh, Chunhui Li, Ariel Frame, James Vinnai, Mohamed Gatie, Andrew Powell, Alex Kozlov, David Hawke, Michael Lee, Lauren Tindale, Tyler Tam, and all other official and unofficial members of the Cumming lab, each and every one of you has contributed to the success of this work.

Finally, I am very lucky to be surrounded by friends and family that provide unconditional love and support. This work would not have been possible without the love from Sarah Mackrell, Timothy Harris, Audrey Mackrell, Hannah Mackrell, and Harlow Mackrell. Thank you Ashley Kirley, Michael Smith, and Peter Zeman for making this a fun ride. I also wish to thank my parents, Robert and Cille Harris and my brothers, Michael, Jeffrey, and Andrew for their unwavering encouragement and support.

Table of Contents

List of Tables

List of Figures

List of Appendices

List of Abbreviations

2DG	2-deoxyglucose
4-CIN	α-cyano-4-hydroxycinnamate
Acetyl-CoA	Acetyl coenzyme A
AD	Alzheimer's disease
ADNI	Alzheimer's Disease Neuroimaging Initiative
ADP	Adenosine diphosphate
AICD	Amino-terminal APP intracellular domain
Akt	Protein kinase B
AMPA	α-amino-3-hydroxy-5-methyl-4-isoxazolepropionate
ANLSH	Astrocyte-neuron lactate shuttle hypothesis
ANOVA	Analysis of variance
API	Alzheimer's Prevention Initiative
APLP	Amyloid precursor-like protein
APOE	Apolipoprotein E
APP	Amyloid precursor protein
ATP	Adenosine triphosphate
Aβ	Amyloid-β
BACE1	β-site APP-cleaving enzyme 1
CAA	Cerebral amyloid angiopathy
CMC	Carboxymethylcellulose
CMRa	Cerebral metabolic rate of acetoacetate
CMRglc	Cerebral metabolic rate of glucose
$CMRO_2$	Cerebral metabolic rate of oxygen
CNS	Central nervous system
COX	Cytochrome oxidase
CREB	cAMP response element-binding protein
CSF	Cerebrospinal fluid
DAB	1,4-dideoxy-1,4-imino-D-arabinitol
DCA	Dichloroacetate
DIAN	Dominantly Inherited Alzheimer's Network
DMN	Default mode network
DNP	Dynamic nuclear polarization
DSM-IV	Diagnostic and Statistical Manual of Mental Disorders, Fourth Edition
EGFR	Epidermal growth factor receptor
ELISA	Enzyme-linked immunosorbent assay
ERK	Extracellular signal-regulated kinase

ETC	Electron transport chain
ETL	Echo train length
FADH$_2$	Flavin adenine dinucleotide (reduced)
FDG	Fluorodeoxyglucose
FID-CSI	Free induction decay chemical shift imaging
FIESTA	Fast imaging employing steady-state acquisition
fMRS	Functional magnetic resonance spectroscopy
FOV	Field of view
FOXO	Forkhead box protein O
FSE	Fast spin echo
FTDP-17	Frontotemporal dementia and Parkinsonism linked to chromosome 17
G6PDH	Glucose-6-phosphate dehydrogenase
GAPDH	Glyceraldehyde 3-phosphate dehydrogenase
GFAP	Glial fibrillary acidic protein
GLT	Glutamate transporter
Glucose-6P	Glucose-6-phosphate
GLUT	Glucose transporters
GPR81	G-protein coupled receptor 81
GSH	Glutathione
HCA1	Hydroxycarboxylic receptor 1
HIF	Hypoxia-inducible factor
HK	Hexokinase
IL	Interleukin
ISF	Interstitial fluid
ITI	Inter-trial interval
LDH	Lactate dehydrogenase
LTD	Long-term depression
LTP	Long-term potentiation
MAPT	Microtubule-associating protein tau
MCI	Mild cognitive impairment
MCT	Monocarboxylate transporter
MELAS	Mitochondrial myopathy, encephalopathy, lactic acidosis, and stroke-like episodes
MRS	Magnetic resonance spectroscopy
mTOR	Mammalian target of Rapamycin
MWM	Morris water maze
NAA	*N*-acetylaspartate
NADH	Nicotinamide adenine dinucleotide (reduced)

NADPH	Nicotinamide adenine dinucleotide phosphate (reduced)
NDAN	Non-demented individuals with AD neuropathology
NFT	Neurofibrillary tangle
NMDA	N-methyl-D-aspartate
NMR	Nuclear magnetic resonance
NOS	Nitric oxide synthase
NOX	NADPH oxidase
OGI	Oxygen-to-glucose index
PBS	Phosphate-buffered saline
pCREB	Phosphorylated-cAMP response element-binding protein
PDH	Pyruvate dehydrogenase
PDK	Pyruvate dehydrogenase kinase
PDP	Pyruvate dehydrogenase phosphatase
PEP	Phosphoenolpyruvate
PET	Positron emission tomography
PFK	Phosphofructokinase-1
PFKFB3	6-phosphofructose-2-kinase/fructose-2,6-bisphosphatase-3
PGE_2	Prostaglandin E_2
PI3K	Phosphoinositide 3-kinase
PiB	Pittsburgh compound B
PK	Pyruvate kinase
PPP	Pentose phosphate pathway
PSEN	Presenilin
R5P	Ribose-5-phosphate
rCBF	Regional cerebral blood flow
ROS	Reactive oxygen species
rtTA	Reverse tetracycline transactivator
sAPP	Secreted amyloid precursor protein
SEM	Standard error of the mean
SMEI	Severe myoclonic epilepsy in infancy
Tau	Tubulin-associated unit
TCA	Tricarboxylic acid
TE	Echo time
TOM	Translocase of the outer membrane
TR	Repetition time
TUJ1	Class III β-Tubulin
α-KGDHC	α-Ketoglutarate dehydrogenase complex

Chapter 1

1   Literature review

The motivation for this work comes primarily from two research questions that I aim to answer: does lactate metabolism in the brain mediate resistance to amyloid-β plaques, and does lactate metabolism in the brain contribute to memory? This literature review will provide background information on three main areas of research that all converge in this thesis: (1) Alzheimer's disease, (2) the link between cerebral metabolism and Alzheimer's disease, and (3) the link between cerebral metabolism and memory. First, I provide a background of the underlying causes of Alzheimer's disease and the current state of Alzheimer's disease research, which is shifting toward early diagnosis and prevention. Second, I introduce the link between Alzheimer's disease and glucose metabolism, as well as the metabolic phenotype of aerobic glycolysis and associated lactate metabolism that is central to this work. I also introduce relevant components of the metabolic pathways involved in aerobic glycolysis because they are integral to several experiments performed. Third, I review neuron and astrocyte metabolic coupling and the role of lactate in memory. Finally, I provide the rationale for the questions driving this research, as well as the specific aims of this work, and the central hypotheses.

1.1   Alzheimer's disease

Alzheimer's disease (AD) is a progressive and irreversible neurodegenerative disease that affects the elderly and is the most common form of dementia worldwide. AD represents a considerable challenge to the Canadian health care system due to its high prevalence in the population (564,000 Canadians in 2016, or 1.5% of the population), rising incidence (projected 937,000 Canadians in 2032, or 2.8% of the population), and high cost of care for individuals with dementia ($10.4 billion in annual cost to Canadians in 2016)[1]. There are two different types of AD: early-onset (familial) and late-onset (sporadic). Familial AD affects less than 1% of all cases of AD and is directly caused by a genetic mutation resulting in the development of AD before the age of 65, sometimes as early as 30[2,3]. The vast majority of AD patients have the sporadic version, in which the exact cause is unknown although several risk factors have been identified including age, genetics, diet,

and lifestyle[4]. Diagnosis of dementia is based on a physician's evaluation of cognitive tests and criteria given in the Diagnostic and Statistical Manual of Mental Disorders, Fourth Edition (DSM-IV), yet an individual with AD will progress through different stages of the disease as cognitive and functional abilities decline. Symptoms of AD commonly begin with mild cognitive impairment (MCI) characterized by confusion or loss of memory that disrupts daily life and eventually leads to loss of executive functions including speaking, swallowing, and walking. As the disease progresses, more pronounced dementia arises leading to physical complications, such as immobility and malnutrition, which can increase the risk of other serious complications, including pneumonia, ultimately leading to death of the individual[5]. The median survival time of individuals with AD depends on age and is approximately 8 years from diagnosis to death for individuals over 65 years of age, and less than 4 years for individuals aged over 90 years[6].

1.1.1 Causes of Alzheimer's disease

AD was first characterized in 1906 by Alois Alzheimer after post-mortem analysis of a 55 year old woman with pre-senile dementia revealed the presence of dense protein deposits in both the intracellular and extracellular regions of the brain[7]. The intracellular deposits, commonly known as neurofibrillary tangles (NFTs), are composed of aggregates of the microtubule-associating protein tau (tubulin-associated unit), that arise from abnormal hyperphosphorylation[8–10]. The extracellular deposits are known as amyloid plaques and are primarily comprised of an aggregated peptide called the amyloid-β peptide (Aβ) derived from the proteolytic cleavage of the amyloid precursor protein (APP)[11,12]. These two distinct pathologies, amyloid plaques and neurofibrillary tangles, have formed the neuropathological criteria for post-mortem diagnosis of AD[13]. The etiology of AD has evolved over the past 100 years and has now been attributed to the accumulation of several different pathological features in the brain that collectively lead to neurodegeneration and dementia. Researchers have attempted to understand the causes of AD by focusing on the specific mechanisms that lead to AD pathology in order to design effective interventions for the prevention, attenuation, or reversal of disease progression.

Tau Protein

In 1986, a link between tau and neurodegenerative diseases was established with the extraction and subsequent identification of hyperphosphorylated tau as the primary component of NFTs in the AD brain[8–10,14]. The tau protein, also known as the microtubule-associating protein tau (MAPT), is one member of a family of microtubule-associating proteins, including MAP1(A/B) and MAP2, that are functionally redundant and widely expressed, especially in the central nervous system[15]. The tau protein functions to promote assembly and organization of microtubules, which are important for growth of axons and dendrites in neurons[16]. Tau is regulated by phosphorylation; the degree of which can lead to a conformational change that impairs its ability to promote microtubule assembly[17,18]. Mutations in the tau gene *MAPT* cause Frontotemporal dementia and Parkinsonism linked to chromosome 17 (FTDP-17), a neurogenerative disease known as a "taupathy"[19–21]. While hyperphosphorylation of tau and accumulation of NFTs are common in taupathies, they lack the characteristic amyloid plaques of AD, suggesting that NFTs alone cannot cause AD. In addition, no mutations in *MAPT* have been found associated with familial AD, suggesting that Aβ is the initiator of AD pathogenesis[22]. Human genetic and biomarker studies have suggested Aβ deposition precedes tau hyperphosphorylation and that neurofibrillary tangles are a late-stage pathology correlating more closely with symptom severity in AD patients than amyloid plaques[23–26]. A recent study using transgenic mice expressing a human tau repeat domain demonstrated that amyloid plaques are necessary but not sufficient for the conversion of wild-type to pathological tau, suggesting that a second risk determinant (risk alleles/factors) is required to drive the pathological conversion of tau[27].

Amyloid precursor protein processing to generate amyloid-β peptides

The most prevalent theory for the root cause of AD is the amyloid cascade hypothesis, which posits that AD arises from the abnormal deposition, or improper clearance, of Aβ in the brain[28]. This was largely supported by the discovery that all of the familial versions of AD are caused by mutations within the *APP* gene itself or within genes that directly affect APP processing in favor of Aβ production[29]. In contrast, a mutation in *APP* that

results in a reduction of Aβ was found to be protective against AD and age-related cognitive decline[30]. The discovery of the *APP* gene was made possible by the identification of the amino acid sequence of the Aβ peptide isolated from the AD brain[11,31] and was subsequently used to clone the *APP* gene and map the location to chromosome 21[32]. Consistent with this discovery, individuals with trisomy 21 (Down syndrome) develop dementia at an early age and display plaques and tangles consistent with AD pathology[33].

APP is one member of a family of single-pass transmembrane proteins that includes the amyloid precursor-like proteins (APLP1 and APLP2) in mammals, all of which are highly homologous and functionally redundant[34]. APP and APLP2 are ubiquitously expressed but APLP1 expression is restricted to the nervous system[35]. The biological function of the APP is still unclear although several studies have suggested that APP participates in cell adhesion, neurite outgrowth, synaptogenesis, and neuron survival[36–39]. Knockout mice individually lacking APP, APLP1, or APLP2 are viable and fertile with a small growth deficit, minor behavioural phenotypes, and a reduced number of synaptic vesicles at presynaptic terminals[40–42]. Mice lacking both APP and APLP2, or APLP1 and APLP2, display perinatal lethality[41]. Yet mice lacking APP and APLP1 are viable and fertile, indicating a key physiological role for APLP2[41]. Despite the functional redundancy of the APP family, APP itself is the only member that generates the amyloidogenic peptide, due to sequence differences at the internal Aβ cleavage site[43]. APP is highly expressed in neurons and is processed in the Golgi apparatus and transported in vesicles down the axon where it collects at the cell surface of the synapse[44]. APP undergoes proteolytic processing in two distinct pathways: amyloidogenic and non-amyloidogenic[45] (Figure 1).

Figure 1. Schematic of amyloid precursor protein processing

APP is a transmembrane protein that is cleaved in two distinct pathways: non-amyloidogenic (left) or amyloidogenic (right). Cleavage by the α-secretase followed by the γ-secretase generates the non-amyloidogenic P3 fragment. In contrast, cleavage by the β-secretase followed by the γ-secretase results in the generation of the amyloidogenic Aβ peptide, which can subsequently form oligomers and fibrils that are neurotoxic.

In the non-amyloidogenic pathway, APP is first cleaved by the α-secretase to release the extracellular secreted α-APP (sAPPα) ectodomain. APP is then cleaved by the γ-secretase, which generates the non-amyloidogenic extracellular P3 fragment and the APP intracellular domain (AICD) C-terminal fragment . In the amyloidogenic pathway, APP is first cleaved by the β-site APP-cleaving enzyme 1 (BACE1), which produces the extracellular secreted β-APP cleavage product (sAPPβ). Subsequent cleavage of APP by the γ-secretase then generates the intracellular AICD fragment and releases the extracellular Aβ (pathogenic) fragment. The γ-secretase cuts at one of several different sites to produce Aβ peptides of varying sizes with $A\beta_{(1-40)}$ and $A\beta_{(1-42)}$ being most common. Presenilin 1 (PSEN1) and presenilin 2 (PSEN2) are homologous proteins that form the active site of the γ-secretase complex. Autosomal dominant mutations have been identified in both *PSEN1* and *PSEN2* that favor the cleavage of $A\beta_{(1-42)}$ in familial AD[46–48]. The $A\beta_{(1-42)}$ peptide in particular is hydrophobic and highly prone to undergo self-aggregation forming insoluble fibers leading to the development of amyloid plaques[49,50]. Until recently there was no known biological function of the Aβ peptides, but a recent study reported that injection of *Salmonella typhimurium* in a mouse model of severe amyloid pathology accelerated amyloid plaque deposition which co-localized to invading bacteria and prevented their attachment to host cells, suggesting that Aβ might play a role in antimicrobial defense[51]. Aβ is actively metabolized and cleared in the normal brain, however individuals with AD have increased production or reduced clearance which leads to an age-dependent accumulation of Aβ and deposition of plaque in the brain[52,53].

Apolipoprotein E

Aside from the characteristic plaques and tangles of AD pathology, several genetic and environmental risk-factors have been shown to be directly associated with AD onset. The most prominent genetic risk factor for sporadic AD is the ε4 polymorphism in the apolipoprotein E (*APOE*) gene, which increases the risk of AD 5- to 15-fold depending

on the allelic dosage[54–56]. The prevalence of the ε4 allele in AD patients is greater than 50%, while individuals homozygous for ε4 have a 95% chance of developing AD by the age of 80 years old[57]. Although the epidemiological link between APOE-ε4 and AD is well established, the mechanism by which ε4 is a risk factor for AD remains largely unclear. APOE is a 34 kDa lipid binding protein that transports cholesterol and triglycerides throughout the body by binding to cell surface lipoprotein receptors[58]. In humans, there are three different APOE isoforms (ε2, ε3, and ε4), which differ from each other by a single amino acid affecting lipid association and receptor binding[59,60]. The ε4 allele is the only variant that increases risk of AD, while the ε2 allele is associated with protection against AD and the ε3 allele has no correlation with AD[55,61]. The link between APOE and AD is likely through clearance mechanisms of Aβ. APOE is a chaperone molecule that binds directly with amyloid plaques[54]. The ε3 isoform binds to Aβ with higher affinity and clears more efficiently than ε4[62]. Accordingly, APOE-ε3 mice displayed fewer amyloid plaques than ε4 mice[63,64]. AD patients with APOE-ε4 display increased plaque load in both sporadic and familial variants, as well as in subjects with amyloid load but are cognitively normal [65–67]. Interestingly, the ε4 iosoform has also been implicated as a transcription factor that promotes the activation of genes associated with programmed cell death, microtubule disassembly, synaptic function, and insulin resistance[68]. It is also a known risk factor for other neurodegenerative diseases including cerebral amyloid angiopathy (CAA), taupathies, Parkinson's disease, and multiple sclerosis, suggesting it plays a general role in susceptibility to neurodegeneration[69–72].

Age

The single greatest risk factor for AD is age. Epidemiological evidence suggests that beyond the age of 60 the incidence of sporadic AD rises exponentially with the risk doubling every 5 years after 65[73–75]. Even in individuals afflicted with familial AD, the disease rarely develops before the age of 45, suggesting significant Aβ accumulation or age-associated brain changes are necessary before the onset of cognitive decline[2,3]. The aging process itself carries an inherent risk of cognitive dysfunction. Normal aging is associated with reductions in gross brain volume[76–79], accelerated atrophy in the

hippocampus and cortex[76,80–82], and disruption of episodic memory[83,84]. In fact, significant Aβ accumulation also occurs in cognitively normal elderly individuals and may simply be a part of normal aging[85–87]. These features of the aging brain make it difficult to tease apart the relative contributions of aging and AD-pathology to cognitive decline[88], which has led to a new proposed diagnostic criteria for AD that incorporates the use of biomarkers showing underlying pathogenesis[89–92]. The link between aging and AD likely involves the progressive accumulation of Aβ either through over production in familial AD or through reduced ability to clear Aβ in sporadic AD[52,93,94]. Evidence in support of this model comes from preclinical investigation using multi-modal imaging strategies to demonstrate that abnormal Aβ biomarkers are the earliest indicators of AD[95]. Yet at some point a pathological threshold of Aβ accumulation is reached which triggers a cascade of downstream processes that mediates neurodegeneration[96,97].

1.1.2   Toward Alzheimer's disease prevention

Since 2002, there have been over 400 clinical trials for AD therapeutics with an overall failure rate of 99.6%[98]. Current FDA-approved treatment options for AD patients are limited to acetylcholinesterase inhibitors for mild-to-moderate dementia and the *N*-methyl-D-aspartate (NMDA)-receptor antagonist Memantine for moderate to severe dementia[99–103]. These therapies reduce the severity of symptoms for AD patients but do not alter the course of the disease progression. In fact, there are currently no FDA-approved therapies that prevent or reverse cognitive decline in AD[104]. A growing consensus has emerged that the problem with failed clinical trials may not be related to the strategy of targeting AD pathology, or even the animal models for testing pre-clinical candidate drugs, but that the therapies are applied to human patients too late to alter the course of sustained brain damage[105,106]. In recent years a large initiative toward prevention of AD has been undertaken, in which the goal is to discover the earliest reliable biomarker for probable AD in order to implement therapeutic or lifestyle interventions for at-risk individuals before the onset of neurodegeneration and dementia[107]. In 2005, the Alzheimer's Disease Neuroimaging Initiative (ADNI) was launched with the goal of tracking the progression of AD and establishing criteria for early diagnosis[108,109]. In 2008 an international partnership called the Dominantly

Inherited Alzheimer's Network (DIAN) was initiated to develop a database of AD individuals carrying familial mutations while their non-carrier siblings act as genetically similar controls[110]. The goal is to determine a temporal sequencing of preclinical AD biomarkers in order to identify the most ideal therapeutic window for treatment of at-risk AD patients. More recently an initiative called the Alzheimer's Prevention Initiative (API) was started with the goal of evaluating the extent to which AD-modifying treatments predict clinical benefit in at-risk individuals[111,112]. Despite the fact that all individuals registered with the DIAN carry autosomal dominant mutations for AD, the pathological phenotype of familial AD is largely similar to sporadic AD, which has prompted some to suggest that they are the same disease just with an age delay in sporadic individuals[113,114]. Another reason why subjects with autosomal dominant AD mutations are recruited for these clinical trials is because defining preclinical AD in sporadic individuals is difficult even when significant Aβ is detected in the brain by positron emission tomography (PET) and in the cerebrospinal fluid (CSF) by ELISA analysis[115–117].

These neuroimaging initiatives use a variety of techniques to measure pathological changes in the brain, of which the two most reliable biomarkers of AD pathophysiology are measurements of the CSF and PET imaging. The CSF can be used to detect alterations in Aβ and tau as a reflection of physiological changes to amyloid plaques and neurofibrillary tangles occurring in the brain. Reductions in $A\beta_{(1-42)}$ and increased phosphorylated-tau or total tau in the CSF correlate well with late-stage neurodegeneration and cognitive decline[115,118–121]. PET scans are a useful imaging technique to measure a wide variety of parameters depending on the radio-labelled tracer used in the analysis. The two most commonly used tracers are the ^{11}C-labeled Pittsburgh compound B (PiB) that binds with high specificity and high affinity to fibrillar-Aβ found predominantly in amyloid plaques[122], and the ^{18}F-fluorodeoxyglucose (FDG) compound that is an analog of glucose used to measure glucose metabolism in the brain[123,124]. Biomarker research from the ADNI and DIAN programs provided a clear picture of preclinical AD progression that begins with Aβ accumulation in the brain and follows in a sequence of cerebral inflammation, oxidative stress, synaptic loss, regional

hypometabolism, tau pathology accumulation, and finally atrophy, neurodegeneration, and dementia[125–132]. These studies also identified an interesting phenomenon in AD pathogenesis: Aβ accumulation begins decades before clinical diagnosis of AD-dementia. PiB-PET scans suggest that deposition of amyloid plaque can begin 20 to 30 years before the onset of cognitive decline, while reductions of $A\beta_{(1\text{-}42)}$ in CSF are present up to 25 years before symptom onset[25,131,133,134]. Pathological changes in CSF tau were detected up to 15 years before the onset of clinical symptoms, while individuals with both abnormal Aβ and tau CSF biomarkers were associated with a more rapid progression to a clinical state[25,133,135–137]. Cerebral hypometabolism and impaired episodic memory also occurred 10 years before expected symptom onset, suggesting that neurodegeneration precedes clinical diagnosis by up to a decade[25].

Non-demented individuals with Alzheimer's disease neuropathology

Although Aβ accumulation and tau hyperphosphorylation have been consistent pathological features of AD, the presence of these biomarkers is also observed in cognitively normal elderly people[138]. This group of individuals, which have been called non-demented individuals with AD neuropathology (NDANs), were first discovered in 1968 after autopsy of cognitively normal individuals found 8 of 28 brains to have amyloid plaque deposition and neurofibrillary tangles similar to AD patients[139]. Since then it has been established that approximately 30-50% of the elderly (aged 57 to 102) are cognitively normal yet have Aβ and tau pathology indistinguishable from AD patients of the same age[140–143,85,144–148]. In fact, the distribution of amyloid plaques and NFTs matches the pattern in AD patients and the sequence of pathological events is the same as AD irrespective of cognitive status[149–151]. However, it is currently unclear if all cognitively normal individuals with AD biomarkers will eventually develop AD-related dementia. Some have argued that NDAN individuals are in the preclinical stages of AD and will eventually progress to AD with increased age[152–156], while others suggest that AD pathology may be a normal part of the aging process[157]. Several studies have shown that CSF $A\beta_{(1\text{-}42)}$ and tau can predict cognitive decline in healthy individuals with a mean follow up of at least 3 years[158–160]. One study demonstrated that NDAN individuals

meeting criteria for intermediate likelihood or high likelihood of AD displayed subtle deficits in episodic memory after adjusting for age, sex, and education[161]. Yet, another study found that measures of cognition did not correlate with any of the measured AD biomarkers within cognitively normal individuals[162]. In addition, some longitudinal studies showed only about 20% of individuals positive for AD biomarkers will progress from cognitively normal to MCI or AD-related dementia with a mean follow-up of 2.8 years[25,131]. Due to an estimated lag time of 15 to 20 years between the appearance of AD biomarkers and onset of cognitive impairment, it is still unknown if all individuals positive for AD biomarkers will progress to AD. However, it is clear that certain environmental and lifestyle factors can either increase or reduce the risk of developing AD-related dementia in cognitively normal individuals.

Epidemiological evidence suggests that several different environmental factors can reduce or increase the risk of developing dementia[163]. The dementia risk reducing factors include: higher education, aerobic exercise, cognitive training, social engagement, and healthy diet; while the dementia risk increasing factors include: smoking, diabetes, obesity, hypertension, traumatic brain injury, depression, and sleep disturbances[163]. Collectively these findings suggest that certain adjustable lifestyle choices can impact the healthy aging of the brain despite the presence of neuropathology and has led to the argument that a greater emphasis should be placed on preventative measures to treat AD in at-risk individuals[164]. While it is clear that environmental factors can alter the risk of developing dementia, the biological mechanisms underlying this effect are still unknown. The association between lifestyle effects and progression of AD pathology has been inconsistent. It has been shown that physical activity and cognitive engagement can reduce Aβ and tau pathology in middle-aged at-risk individuals[165–167], yet this finding was not replicated in a follow up study[168]. In addition, these observations do not explain how some individuals can tolerate AD neuropathology and remain cognitively normal. One prevalent theory that explains the discrepancy between neuropathological changes and their clinical expression is called "cognitive reserve", which refers to the capacity of the brain to tolerate pathological insult[169]. The proposed mechanism involves both passive and active models[170]. The passive model simply refers to an anatomical

difference in brain size with increased neuron count and a higher threshold for AD pathology or neurodegeneration. The active model refers to the adaptive use of underlying neurological networks to compensate for neuropathology and localized insult. Taken together, individuals with higher cognitive reserve will tolerate an overall higher burden of AD pathology before succumbing to cognitive impairment[171,172]. In fact, cognitive decline is delayed in individuals with higher reserve[173–175], yet progresses more rapidly than lower reserve individuals once a pathological threshold is reached[173,176–179]. Several studies have shown associations between higher cognitive reserve and structural changes in the brain, including neurogenesis, synaptic density, synaptic protein expression, neuronal density, dendritic complexity, and neuronal hypertrophy[180–186]. Yet, a causal mechanism underlying cognitive reserve and maintenance of brain function in the presence of AD pathology has yet to be demonstrated.

1.2 Glucose metabolism and Alzheimer's disease

A progressive decline in brain glucose metabolism, called cerebral hypometabolism, is a common feature of AD that correlates temporally with symptom severity and has high predictive value for onset of dementia[153,187–191]. Current estimates suggest that cerebral glucose metabolism is 20-25% lower in the AD brain[192]. Cerebral hypometabolism has been traditionally perceived as a result of decreased energy demand due to synaptic dysfunction and neuronal loss at later stages of the disease[193]. However, there is a growing consensus that impaired glucose metabolism precedes clinical symptoms in AD and may serve as a preclinical biomarker[153,188,190,191,194–196]. Impaired glucose metabolism is likely due to mitochondrial dysfunction, which is directly caused by Aβ interference with mitochondrial enzymes. The Aβ peptide has been shown to progressively accumulate in the mitochondria of CNS neurons in both AD patients and AD transgenic mice prior to amyloid plaque deposition and cognitive deficits[197–200]. In addition, embryonic neurons derived from the hippocampus of triple-transgenic AD female mice displayed reduced mitochondrial respiration and increased glycolysis, suggesting that mitochondrial dysfunction occurs early in AD pathogenesis[199]. Defects in mitochondrial metabolism are also well documented in the human AD brain[201].

Amyloid-β and the mitochondrion

The mitochondrion is a vital organelle responsible for producing the majority of cellular ATP and regulating cell survival. Several *in vitro* and *in vivo* studies have directly linked Aβ exposure to mitochondrial dysfunction including the inhibition of respiratory chain complexes, reduced membrane potential and ATP levels, and increased reactive oxygen species (ROS) production, as well as mitochondrial swelling and depolarization leading to the induction of apoptosis[202–211]. Consistent with the targeted production of Aβ in synaptic terminals, Aβ preferentially accumulates in synaptic mitochondria and likely contributes to early synaptic dysfunction in AD[212]. Certain soluble species of oligomeric Aβ are amphipathic in nature and have the ability to permeabilize lipid bilayers thereby passively entering the mitochondria[213–216]. APP also contains a mitochondrial targeting signal and can be actively imported into the mitochondria by the translocase of the outer membrane (TOM) machinery[217,218]. Once inside the mitochondria, Aβ directly binds to and impairs the activity of the pyruvate dehydrogenase (PDH) complex, which is responsible for converting pyruvate to acetyl-coenzyme A (acetyl-CoA) and is the first committed step for pyruvate to oxidative phosphorylation in the mitochondria[204]. Aβ also impairs activity of proteins in the tricarboxylic acid (TCA) cycle and the electron transport chain (ETC), including the α-ketoglutarate dehydrogenase complex (α-KGDHC) and cytochrome oxidase (COX)[204,219]. Reduced activity and expression of these enzymes in the AD brain has been well documented[220–222]. This diminished enzyme activity leads to a reduction in oxygen consumption rate and ATP production, suggesting a direct link between defective mitochondrial and preclinical hypometabolism in AD[209].

Defective mitochondria can produce high levels of ROS, which can lead to a state of oxidative stress and is a common feature of AD. Under normal circumstances, physiological levels of ROS function as important redox-dependent signaling molecules that regulate cellular growth and homeostasis[223]. The ETC of the mitochondria is the main source of cellular ROS via the reduction of oxygen to the superoxide free radical anion and subsequent conversion to hydrogen peroxide by superoxide dismutase[224]. An overproduction of ROS or a decline in antioxidant response can lead to oxidative damage

and ultimately cell death. The AD brain displays several markers of oxidative damage to biomacromolecules including proteins, nucleic acids and lipids[225,226]. *In vitro* work has demonstrated a dose-dependent effect between Aβ and mitochondrial-derived oxidative stress and neuronal toxicity[227,228]. Synergistic effects between Aβ and tau have been observed in the mitochondria of triple-transgenic AD mice leading to reduced ATP production and an increase in oxidative stress[229]. Moreover, mitochondrial-derived oxidative stress has been shown to potentiate Aβ formation and suggests a feed-forward mechanism in AD pathogenesis[230]. This has led to the oxidative stress hypothesis of AD, which posits that the generation of oxygen free radicals from the mitochondria participate in the cascade of events that lead to neuronal death in AD[231].

Cerebral hypermetabolism in Alzheimer's disease

In contrast to cerebral hypometabolism in AD, the exact opposite effect (cerebral hypermetabolism) has also been observed in the AD brain at very early stages of the disease. This may represent an early compensatory mechanism in response to Aβ accumulation and mitochondrial dysfunction. A recent PET study of autosomal dominant AD mutation carriers revealed regionally higher glucose uptake ~25 years before the estimated age of onset[232]. PET imaging of cognitively normal people at risk for AD revealed area-specific increases in both Aβ deposition and glucose metabolism in individuals before MCI[233]. Although reduced glucose metabolism was observed 5 to 10 years before the estimated age of onset in many cortical areas with Aβ deposition, a divergent pattern was observed subcortically; the caudate and pallidum did not show either metabolic decline or atrophy, despite markedly elevated PiB uptake[232]. APP/PS1 transgenic-AD mice display an age-dependent increase in glucose uptake in the hippocampus and cortex that precedes cognitive impairment and correlates spatially with amyloid plaque deposition[234]. In addition to these observations, the same enzymes that were shown to be inhibited by Aβ at later stages of the disease, COX and α-KGDHC, can also be up-regulated before the appearance of amyloid plaques in the APP(Tg2576) mouse model of AD[235].

Cerebral hypermetabolism in the preclinical AD brain may be accounted for by the compensatory up-regulation of glycolytic machinery in response to mitochondrial damage. Glycolysis is the metabolic pathway in the cytosol that breaks down glucose to pyruvate with the concomitant production of ATP and NADH. The specific activity of the glycolytic rate-limiting enzymes phosphofructokinase-1 (PFK), hexokinase (HK), and pyruvate kinase (PK) were found to be increased in the frontal and temporal cortex of AD patients[236–238]. Increased activity was also found for lactate dehydrogenase (LDH), the enzyme responsible for the production of lactate as the end-product of glycolysis[238]. Embryonic neurons derived from the triple-transgenic AD mouse hippocampus displayed reduced mitochondrial respiration but increased rates of glycolysis[199]. In addition, recent evidence has revealed that nerve cells can be made to be resistant to Aβ toxicity by undergoing a metabolic shift toward enhanced glycolysis and reduced oxidative phosphorylation in the mitochondria[239,240]. Thus, glycolytic metabolism may be elevated in certain regions of the brain as a compensatory mechanism in response to Aβ accumulation and mitochondrial dysfunction. Loss of this protective mechanism may render certain areas of the brain susceptible to Aβ-induced neurotoxicity.

1.2.1   Aerobic glycolysis and amyloid-β resistance

Under normal conditions, the majority of glucose consumed by the cell is oxidized to carbon dioxide and water in the mitochondria to yield large amounts of ATP to support cellular functions. Glycolysis can be up-regulated in a state of low oxygen (hypoxia) or mitochondrial dysfunction in order to compensate for energy demand with the production of lactic acid (lactate) as an end-product[241,242]. However, a characteristic feature of rapidly proliferating cells is the extensive reliance on glycolysis for energy needs, even under normoxic conditions. In cancer cells, this type of metabolism is known as the Warburg effect in recognition of its discovery by Otto Warburg[243]. The reliance on glycolysis in the presence of oxygen is commonly referred to as "aerobic glycolysis" and is a characteristic feature of cancer cells and stem cells[244]. It is now understood that aerobic glycolysis occurs in many different cell types including: endothelial cells, skeletal muscle, vascular smooth muscle, monocytes and leukocytes of the immune system, as well as astrocytes and neurons of the brain[245–252]. The relative contribution of glycolysis

to ATP production highly depends on the cell type, growth environment, and phase of cell cycle. Through precise measurements of oxygen consumption and lactate production rates, it has been estimated that glycolysis can account for between 0.94% to 65% of total ATP produced in the cell with an average of approximately 17% in most tissues[253]. Interestingly, aerobic glycolysis has been estimated to account for up to 85% of ATP produced in endothelial cells despite their direct contact with oxygenated blood[251].

A high glycolytic rate has several advantages for energy-demanding cells. First, despite its low efficiency at producing energy (2 ATP per glucose) compared to oxidative phosphorylation in the mitochondria (34 ATP per glucose), glycolysis can generate ATP at a faster rate when the supply of glucose is abundant[254]. This feature has obvious benefits for cellular processes that have a rapid energy demand, such as in maintaining resting membrane potential via the ATP-dependent Na^+/K^+-ATPase pump. For neurons, the Na^+/K^+-ATPase pump can account for up to 50% of total expended energy[255]. Second, proliferating cells require metabolites to support the biosynthetic requirements of mitosis and glycolytic intermediates can provide the carbon building blocks for the *de novo* synthesis of nucleotides, lipids, and non-essential amino acids[256,257]. In addition to glycolysis in the cytosol, the supply of acetyl-CoA and glutamine to the TCA cycle within mitochondria drives the production of metabolites that can be siphoned off to the cytosol and participate in the anabolic metabolism of amino acids and lipids[257]. Finally, the conversion of pyruvate to lactate produces NAD^+, which is an important cofactor for continued glycolytic flux and biosynthesis of nucleotides and amino acids, in addition to maintaining the NAD^+/NADH redox balance of the cytosol[258,259]. These metabolic pathways will be described in greater detail in later sections. Thus, when glucose is not rate-limiting, aerobic glycolysis provides several advantages to the cell and may persist as the predominant metabolic phenotype despite the presence of oxygen.

Our lab has previously demonstrated that nerve cells selected for resistance to Aβ toxicity undergo metabolic reprogramming and shift toward aerobic glycolysis through the stabilization of the transcription factor hypoxia-inducible factor 1α (HIF-1α) and up-regulation of pyruvate dehydrogenase kinase-1 (PDK1) and lactate dehydrogenase-A (LDHA)[260]. Over-expression of either PDK1 or LDHA enzymes in nerve cell lines

represses mitochondrial respiration and confers resistance to Aβ and other neurotoxins, whereas chemical or genetic inhibition of these enzymes results in re-sensitization of resistant lines to Aβ toxicity[239,240]. Moreover, mitochondrial-derived ROS, which are closely associated with Aβ toxicity, are markedly diminished in resistant relative to sensitive cells. By repressing mitochondrial respiration, Aβ-resistant cells are less likely to produce ROS and are more resistant to mitochondrial depolarization; two events tightly linked to induction of apoptosis[261]. In support of this discovery, a recent multimodal PET imaging study has revealed a strong correlation between the spatial distribution of elevated aerobic glycolysis in healthy resting individuals and Aβ deposition in the brains of both healthy individuals and AD patients[262]. In contrast, brain regions that rely primarily on oxidative phosphorylation for energy needs displayed little amyloid burden. The observation that Aβ deposition in the AD brain closely matches the spatial pattern of elevated aerobic glycolysis in both the healthy and AD brain suggests that aerobic glycolysis may arise as a mechanism to counter the toxic effects of Aβ in the AD brain.

1.2.2   Cerebral glucose metabolism

Glucose is nearly the sole fuel source of the human brain[263]. The metabolism of glucose in the brain is a complex process integrating several different cell types and competing biochemical pathways in order to sustain the energy needs of neuronal activation. Here I describe each step of glucose metabolism as it relates to aerobic glycolysis, the shuttling of metabolites between astrocytes and neurons, as well as any connections to AD pathophysiology. Considering the tight connection between aerobic glycolysis and proliferation, many of the properties of glycolytic enzymes and regulators were characterized in cancer cells. The first rate-limiting step in cerebral glucose metabolism is the facilitated transport of glucose across the blood brain barrier. This is mediated by the glucose transporter (GLUT)-family of integral membrane proteins of which there are 14 members in humans, each with different affinities for glucose and related sugars[264]. GLUT-1 is primarily expressed in astrocytes and the capillary endothelium that form the blood-brain barrier[265]. Astrocytes are generally believed to act as an intermediary cell between glucose uptake from the blood and delivery to neurons, yet current models

suggest that glucose can also diffuse from endothelial cells through the basal lamina and interstitial fluid (ISF) to neurons where it is directly imported via GLUT-3[266–268]. GLUT-1 and GLUT-3 expression is decreased in the AD brain which correlates spatially with cerebral hypometabolism[269–272]. GLUT-1 expression can also be up-regulated by HIF-1α in response to hypoxia[273–275]. Once glucose is taken into the cell it is irreversibly phosphorylated by HK1 to form glucose-6-phosphate (glucose-6P), which traps it in the cell by adding a negative charge to prevent it from diffusing back through the membrane[276]. Glucose-6P is the precursor to three main metabolic pathways: glycolysis, the pentose phosphate pathway (PPP), and glycogenesis (Figure 2).
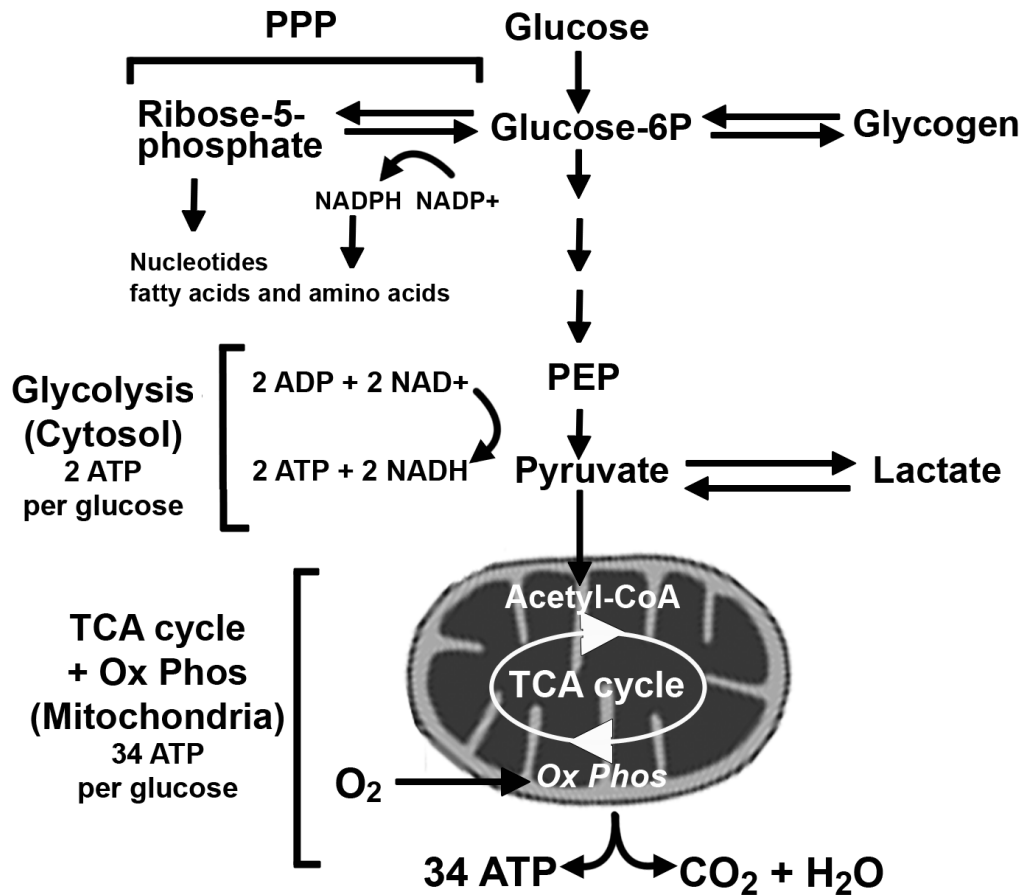
Figure 2. Schematic representation of cerebral glucose metabolism

Glucose enters cells via glucose transporters and is phosphorylated by hexokinase to produce glucose-6-phosphate (Glucose-6P). In astrocytes, glucose-6P can be reversibly converted to glycogen by glycogen phosphorylase. Glucose-6P can also enter the pentose phosphate pathway (PPP) to generate two molecules of NADPH and Ribose-5-phosphate for the biosynthesis of nucleotides, fatty acids, and amino acids. Glucose-6P is further metabolized in the cytosol through glycolysis giving rise to two molecules of pyruvate, ATP, and NADH. Pyruvate is further processed in the mitochondria through the tricarboxylic acid (TCA) cycle to produce NADH which fuels oxidative phosphorylation thereby generating ATP and CO_2 while consuming oxygen. The complete oxidation of glucose produces far larger amounts of energy in the form of ATP in the mitochondria (34 ATP) compared to glycolysis (2 ATP). During aerobic glycolysis pyruvate is reduced to lactate by lactate dehydrogenase which is subsequently released in the extracellular space.

The pentose phosphate pathway

The main fate of glucose-6P is to continue through the glycolytic pathway to generate pyruvate, NADH, and ATP, but it can also be funnelled into the PPP depending on the redox and energy status of the cell. The PPP is a metabolic branch that runs parallel to glycolysis and is primarily responsible for generating reducing equivalents in NADPH and biosynthetic precursors for growing or dividing cells. The first committed step to the PPP is catalyzed by the enzyme glucose 6-phosphate dehydrogenase (G6PDH), which oxidizes glucose-6P to 6-phosphogluconolactone while reducing $NADP^+$ to $NADPH$[277]. G6PDH is strongly inhibited by NADPH, while $NADP^+$ is a cofactor for its proper conformation, thus the cytosolic ratio of $NADP^+/NADPH$ is the main modulator of G6PDH and entry to the PPP[278,279]. The $NADP^+/NADPH$ ratio is also a redox sensor. NADPH is a necessary cofactor for the reduction of glutathione (GSH) molecules, which are the primary reducing agents for the cell. Consequently, the PPP is upregulated in response to oxidative stress in order to replenish depleted glutathione levels[280,281]. The PPP is also important for the synthesis of nucleotides and fatty acids. Ribose-5-phosphate (R5P), an intermediate metabolite of the PPP, is the requisite building block for nucleotides, while NADPH is a necessary reducing agent for the synthesis of nucleotides, fatty acids, and amino acids[257]. Therefore, the PPP is also up-regulated in highly proliferating cells, including cancer cells, in order to meet the increased demands for synthesis of biological building blocks[282].

Glycogenesis

In astrocytes, glucose-6P can also be converted to glycogen, a polymer composed of glucose residues that serves as a fuel reserve of the brain[283]. The prominent role of glycogen storage in astrocytes is to act as an energy buffer in times of glucose deprivation or high glucose consumption[284–287]. Yet, in recent years it has been hypothesized that the storage and mobilization of astrocytic glycogen serves to enhance the availability of glucose for neuronal metabolism[286,288–291]. Neuronal activation can trigger glycogen breakdown in astrocytes by as much as 20%[292], while decreased neuronal activity during anesthesia is accompanied by an increase in glycogen storage by

up to 85%[293]. Recent evidence also points to a direct association between glycogen mobilization and functional memory through synthesis of glutamate in astrocytes[294,295]. In addition, glycogen-derived lactate has also been shown to contribute to memory processing via shuttling between astrocytes and neurons[296]. However, the role of lactate in brain energy metabolism is still unresolved. Another study has suggested that glycogen mobilization in astrocytes functions primarily to preserve glucose supply for neurons, rather than provide neurons with glycogen-derived lactate[297]. Thus, glycogen storage and metabolic coupling between astrocytes and neurons are important for proper metabolic homeostasis during neuronal activity or in cases of severe energy crisis.

Glycolysis

The final rate-limiting step in glycolysis is the conversion of phosphoenolpyruvate (PEP) and ADP into pyruvate and ATP. This is catalyzed by the enzyme pyruvate kinase (PK), of which there are four isoforms (M1, M2, L, and R). The L and R isoforms of PK are exclusively expressed in liver and red blood cells, respectively, while PKM1 and PKM2 are expressed in most adult tissues and arise from alternative splicing of the same M-gene under regulation of the oncogene *C-MYC*[298,299]. The PKM1 isoform assembles as a constitutively active tetramer for rapid substrate turnover[300]. In contrast, PKM2 is among the most tightly regulated enzymes of the glycolytic pathway and is important for controlling levels of ATP and glycolytic intermediates in the cell. PKM2 can exist as a tetramer (high activity), or as a dimer (low activity). The dimeric form of PKM2 is characterized by low affinity for PEP which results in accumulation of glycolytic intermediates and increased flux through the PPP[301]. The ratio of PKM2/PKM1 is an indication of the metabolic phenotype of the cell, whereby high levels of PKM2 promote aerobic glycolysis and high levels of PKM1 promote oxidative phosphorylation[299]. Consistent with this observation, cancer cells preferentially splice the M2 isoform over M1 through the action of C-MYC in order to promote aerobic glycolysis and proliferation[302]. Replacing PKM2 expression with PKM1 effectively inhibited the growth of xenograft tumors by impairing nucleotide production and promoting cell cycle arrest[303,304]. PKM2 is also sensitive to oxidative stress as it can be inhibited by cysteine

oxidation to divert more glucose-6P toward the PPP to generate NADPH as an antioxidant response[305].

As the end product of glycolysis, pyruvate has two major fates: conversion to acetyl-CoA in order to fuel oxidative phosphorylation in the mitochondria, or conversion to lactate to regenerate NAD^+ in the cytosol. The breakdown of pyruvate in the mitochondria occurs over a series of successive reactions in the citric acid cycle that ultimately produces NADH and $FADH_2$ as reducing equivalents to drive the proton gradient necessary for oxidative phosphorylation and ATP production. The first committed step in this process is the irreversible decarboxylation and acetylation of pyruvate to acetyl-CoA with the concomitant reduction of NAD^+ to NADH. This is catalyzed by PDH, which is a ubiquitously expressed protein complex composed of four sub-complex proteins (E1, E2, E3, and the E3 binding protein)[306]. The PDH complex serves as a critical link between glycolysis and the citric acid cycle, and thus its activity is highly regulated at the transcriptional and post-translational levels. For example, during starvation, the genes of the PDH complex are repressed in the liver in order to reduce pyruvate metabolism and maintain glucose levels in the blood stream[307]. In addition, the products of the PDH reaction, acetyl-CoA, NADH, and ATP, can exhibit direct feedback inhibition when their concentrations are sufficiently elevated in the mitochondria[308,309]. Yet, the principal mode of PDH regulation is reversible phosphorylation. The E1 subunit of the PDH complex forms the active site for the oxidative decarboxylation of pyruvate and contains three target serine residues (at positions Serine-232, -293, and -300) that are susceptible for post-translational modification by phosphorylation[310]. Phosphorylation of any serine is sufficient to completely inhibit the activity of the PDH complex, which allows for the rapid and reversible regulation of pyruvate metabolism or to maintain energy homeostasis[311].

Pyruvate dehydrogenase kinase

Pyruvate dehydrogenase kinase (PDK) phosphorylates the regulatory serine residues of PDH, while the pyruvate dehydrogenase phosphatase (PDP) removes the phosphate groups. There are four isoforms of PDK (PDK1-4), each with unique and overlapping

tissue expression. PDK1 and PDK2 are expressed ubiquitously while predominantly in the heart and nervous system, respectively. PDK3 is found only in heart and skeletal muscle, and PDK4 is expressed in the kidneys, brain, liver, heart and skeletal muscle[312]. The PDK isoforms also have different specificity to the PDH-E1 serine residues. All PDK isoforms are able to phosphorylate Serine-232 and Serine-293, while only PDK1 can phosphorylate all three sites[313]. The PDK enzymes are themselves tightly regulated at the transcriptional and post-translational levels. All PDK isoforms are allosterically activated by high levels of acetyl-CoA, NADH, and ATP (the opposite effect occurs with the PDH complex), and are inhibited by the mitochondrial accumulation of pyruvate, NAD^+, and ADP[314]. The expression of PDK2 and PDK4 are upregulated in the heart, liver, and kidneys during starvation, yet this trend is not observed in the brain[315,316]. More recently a growing body of evidence links the expression of PDK1 to cancer cells through transcriptional activation by HIF-1α as a means of reducing mitochondrial metabolism and preventing ROS production[317–319]. Less is known about the role of pyruvate metabolism in aging or AD. One study has shown that aged rats display a reduction in the expression of PDK1 and PDK2 in the brain[320]. Alzheimer's patients also typically show a reduction in PDH activity, and increased pyruvate levels in the cerebrospinal fluid may be a potential biomarker of AD[321,322].

Lactate dehydrogenase

Pyruvate that is not imported into the mitochondria can be converted to lactate in the cytosol. Lactate dehydrogenase (LDH) is the enzyme complex that catalyzes the reversible conversion of pyruvate to lactate with the concomitant oxidation of NADH to NAD^+. LDH is a ubiquitously expressed tetramer composed of two different subunits, LDHA and LDHB, which can assemble into five different combinations (LDH-1 through LDH-5) depending on the relative expression levels of each subunit in the cytosol[323,324]. LDH-1 is comprised entirely of LDHB subunits while LDH-5 is comprised entirely of LDHA subunits. LDHA favors the forward reaction of pyruvate and NADH to lactate and NAD^+, while LDHB favors the reverse reaction of lactate and NAD^+ back to pyruvate and NADH. The LDHA gene promoter contains two hypoxia response elements, the essential binding sites of HIF-1, which implicates a role of LDHA in cellular response to

hypoxia and oxidative stress[325]. LDHA is also commonly over-expressed in many tumours and is a promising target for cancer therapy[326,327]. Previous evidence has suggested that neurons exclusively express LDHB, while astrocytes can express both LDHA and LDHB[328]. However, a more recent report has demonstrated that primary cultures of rat neurons and astrocytes both preferentially express LDHA, yet are capable of expressing all isofoms of LDH[329]. In addition, LDHB expression was higher in freshly isolated synaptic terminals, which implicates that lactate conversion to pyruvate in neurons is specific to synapses[329]. A recent study using a mouse model of advanced aging demonstrated a progressive shift toward higher LDHA/LDHB ratio resulting in higher cortical lactate levels with age[330]. Yet, it has been suggested that the observed elevation in lactate is unlikely to be caused by a shift in the isoform ratio of LDH due to the near steady-state conditions of the reaction[331]. The age-dependent change in LDH expression and its effect on cerebral lactate metabolism and AD remains to be elucidated.

Hypoxia-inducible factor

Cellular metabolism is a complex process regulated by many intrinsic and extrinsic factors. Shifts in metabolic states occur naturally in order to meet the energy demands of active cellular processes while responding to a dynamic environment and changing nutrient availability. Hypoxia inducible factor-1 (HIF-1) is the master transcriptional regulator of anaerobic respiration and also plays a key role in promoting aerobic glycolysis. HIF-1 is a heterodimeric transcription factor comprised of two subunits that are constitutively expressed: a stable β subunit, and an α subunit that is highly regulated by changing oxygen levels[332]. Under normal oxygen conditions, HIF-1α is hydroxylated by prolyl hydroxylases and targeted for ubiquitin-mediated degradation[333]. Under hypoxic conditions, HIF-1α is stabilized and translocates to the nucleus where it dimerizes with HIF-1β and induces expression of genes regulated by hypoxic response elements[334]. These genes include glucose transporters GLUT-1 and GLUT-3, as well as glycolytic enzymes and regulators LDHA, and PDK1[335]. HIF-1α activation represents a well-characterized mechanism by which the cell can quickly respond to hypoxic environments by up-regulating glycolysis and inhibiting mitochondrial respiration in

order to meet cellular energy demands. However, even when oxygen is abundant, HIF-1 can be stabilized and transcriptionally active during periods of rapid proliferation and increased metabolic demand. HIF-1α expression can be elevated under normoxic conditions through the PI3K/Akt/mTOR pathway, which results in transcriptional up-regulation of PKM2 and promotes cell proliferation[336]. Expression of HIF-1α is induced by the glycolytic intermediates pyruvate, lactate and NAD^+, in addition to other TCA cycle metabolites[319,335]. This feed-forward mechanism perpetuates HIF-1 activity and contributes to prolonged aerobic glycolysis commonly associated with proliferating cells. HIF-1α is over-expressed in many human cancers and loss of HIF-1α dramatically slows tumor growth in nude mice[337–340]. HIF-1α activation promotes several cellular responses that are beneficial for a growing tumor, including vascular remodelling, increased glucose uptake, oxidative stress response, and cell survival. As such, it also directly opposes known deleterious effects of AD pathophysiology, including reduced cerebral blood flow, impaired glucose uptake and metabolism, increased oxidative stress, and uncontrolled cell death[341]. Aβ has also been shown to decrease HIF-1α expression in activated astrocytes resulting in a reduced rate of glycolysis[342]. In addition, nerve cell lines and primary cortical neurons can be made resistant to Aβ toxicity by activating HIF-1α resulting in enhanced glycolysis[260].

1.3   Cerebral metabolism and memory

The brain is a very energetically demanding organ. Despite being 2% of the total body weight, the human brain accounts for approximately 20% of basal metabolism in healthy adults[343,344]. An updated account of ATP consumed in the cerebral cortex predicts that most of the energy is directed at the maintenance of post-synaptic receptors, which includes the energy used to reverse glutamate-evoked Na^+ and Ca^{2+} fluxes[255]. The remaining energy is directed at pumping Na^+ ions out of neurons for the maintenance of resting membrane potentials and the generation of action potentials, while only a small fraction of total energy consumed is used for neurotransmitter recycling[255,345]. Current estimates suggest that approximately 10-12% of the total glucose consumed by the resting brain is in excess of oxygen consumption, suggesting a role for non-oxidative (glycolytic) metabolism[346–351]. Different regions of the resting brain also display different

levels of glycolytic metabolism. Aerobic glycolysis accounts for nearly 25% of glucose consumed in two distinct cortical systems: the default mode network (DMN) and areas of the frontal and parietal cortex[351]. The DMN is defined as the region of the brain that shows high levels of activity when no explicit task is performed, while the frontal and parietal cortex are associated with task control processes[352–355]. In contrast to these brain regions displaying higher levels of aerobic glycolysis, the cerebellum relies almost entirely on oxidative phosphorylation for energy needs. These observations could be explained by the ratio of neurons to astrocytes in each brain region. The cerebral cortex contains only about 19% of the brains' total neurons and 72% of non-neuronal cells, while the cerebellum contains approximately 80% of the brains' neurons and only 19% of non-neuronal cells, which supports the hypothesis that neurons preferentially exhibit a phenotype of oxidative metabolism[356].

Cerebral activation and aerobic glycolysis

The brain must also rapidly respond to changing energy demand and supply, as reflected by task-dependent cerebral activation, changes in localized blood flow, and glucose utilization[357]. It was traditionally perceived that most of the energy needed for brain function is derived by the complete oxidation of glucose to carbon dioxide and water. Therefore, it was postulated that blood-flow increases accompanied by cerebral activation must be related to an increased demand for oxygen[358]. However, several early observations during cerebral activation suggested regional cerebral blood flow (rCBF) and cerebral metabolic rate of glucose (CMRglc) increase in excess oxygen consumption[346,359,360]. In fact, there is a very close correlation between rCBF and CMRglc, but not between rCBF and oxygen consumption[346,361,362]. It is now known that during cerebral activation, aerobic glycolysis is quickly up-regulated and can account for up to 40% of the glucose consumed by activated regions[361,363]. A recent multimodal PET analysis identified high rates of aerobic glycolysis in cortical regions of the adult brain known to participate in cognitive control networks[351]. Local aerobic glycolysis can also persist for up to 40 minutes following activation despite the return of physiological conditions back to baseline[349]. Correspondingly, it is well documented that there is an increase in local brain lactate efflux during cerebral activation[363–368]. Yet, this lactate

efflux accounts for only about 50% of the excess glucose consumed by glycolysis and suggests that some of the lactate is also recycled as a fuel source.

Recent work has provided a potential mechanism between rCBF and glycolytic metabolism through changes to the lactate/pyruvate ratio and the cytosolic $NADH/NAD^+$ ratio. Experiments in support of this hypothesis are based on lactate and pyruvate injections, whereby the intravenous injection of lactate augmented rCBF in response to visual stimulus, while the injection of pyruvate attenuated this response[369–371]. The $NADH/NAD^+$ ratio is a sensor of the redox state of the cell that increases when NADH is produced by glycolysis and the citric acid cycle at a faster rate than can be used by the mitochondria to synthesize ATP. The excess electrons from NADH can be transferred to oxygen by NADPH oxidase (NOX) to generate superoxide, which elevates cytosolic Ca^{2+} levels and activates nitric oxide production by nitric oxide synthase (NOS)[372,373]. Nitric oxide is a signaling molecule in endothelial cells that causes cerebral vasodilation and increases local blood flow[374]. Lactate has also been shown to directly promote the ability of astrocytes to induce vasodilation through accumulation of prostaglandin E_2 (PGE_2), a well characterized vasodilating agent[375]. The induction of rCBF serves to remove excess lactate and promotes the delivery of glucose and oxygen to activated tissues. Taken altogether, under resting conditions, glucose is almost entirely oxidized to carbon dioxide to generate large amounts of ATP. Cerebral activation triggers the up-regulation of aerobic glycolysis to rapidly synthesize ATP with the concomitant production of lactate as an end product. The rapid increase in glycolysis raises the $NADH/NAD^+$ ratio and promotes an increase in rCBF. The increased blood flow serves to remove the excess lactate and promotes the delivery of glucose and oxygen to activated tissues in order to sustain metabolic flux.

1.3.1 Neuron-astrocyte metabolic coupling

The question of how glucose is utilized by the different cell types of the brain, namely neurons and astrocytes, has been extensively investigated yet remains to be fully characterized. Astrocytes are the most common non-neuronal cell in the brain and play a key role in cerebral homeostasis, including neurotransmitter recycling, ion and water regulation, defense against oxidative stress, and synapse formation and remodeling[376].

Despite the general assumption that the human brain contains about 100 billion neurons and ten-times as many astrocytes, it was recently calculated that the human brain contains approximately equal numbers of neurons and astrocytes with a total of 86.1 ± 8.1 billion neurons and 84.6 ± 9.8 billion astrocytes[356]. While neurons traditionally account for the majority of energy consumed in the brain, astrocytes are thought to regulate the energy supply from the blood stream to neurons in a process called "metabolic coupling".

The astrocyte-neuron lactate shuttle hypothesis

In 1994, a seminal discovery by Pellerin and Magistretti identified glutamate as the molecular trigger for glucose uptake and up-regulation of aerobic glycolysis in response to brain activation[377]. Glutamate is the principal excitatory neurotransmitter of the central nervous system, accounting for well over 80% of all synaptic activity in the human brain[378]. In response to axon depolarization, glutamate is released into the synapse from the pre-synaptic terminal and propagates the action potential in the post-synaptic neuron by binding to specific ionotropic and metabotropic receptors[379]. Glutamate is then quickly removed by glutamate transport 1 (GLT-1), located on astrocytes and neurons, in order to terminate signal propagation and prevent excitotoxicity. Glutamate transport is coupled with the import of three Na^+ ions into the cell, which leads to the activation of the Na^+/K^+-ATPase to restore the osmotic balance[380]. This is an energetically demanding process that increases ATP consumption and triggers an increase in glucose uptake to compensate for energy demand. Pellerin and Magistretti observed an increase in glucose uptake and lactate released by primary mouse cortical astrocytes in response to glutamate stimulation[377]. It is proposed that the increased lactate production implicates aerobic glycolysis in astrocytes as the key mechanism coupling neuronal activity to glucose utilization. The discovery led to the long-standing hypothesis called the astrocyte-neuron lactate shuttle hypothesis (ANLSH). The ANLSH posits that astrocytes can rapidly mobilize glucose from either glycogen stores, or directly from cerebral blood vessels, and process it through glycolysis to generate lactate which is exported and subsequently used as a fuel source for oxidative phosphorylation in the mitochondria of neurons (Figure 3)[377,381–383].
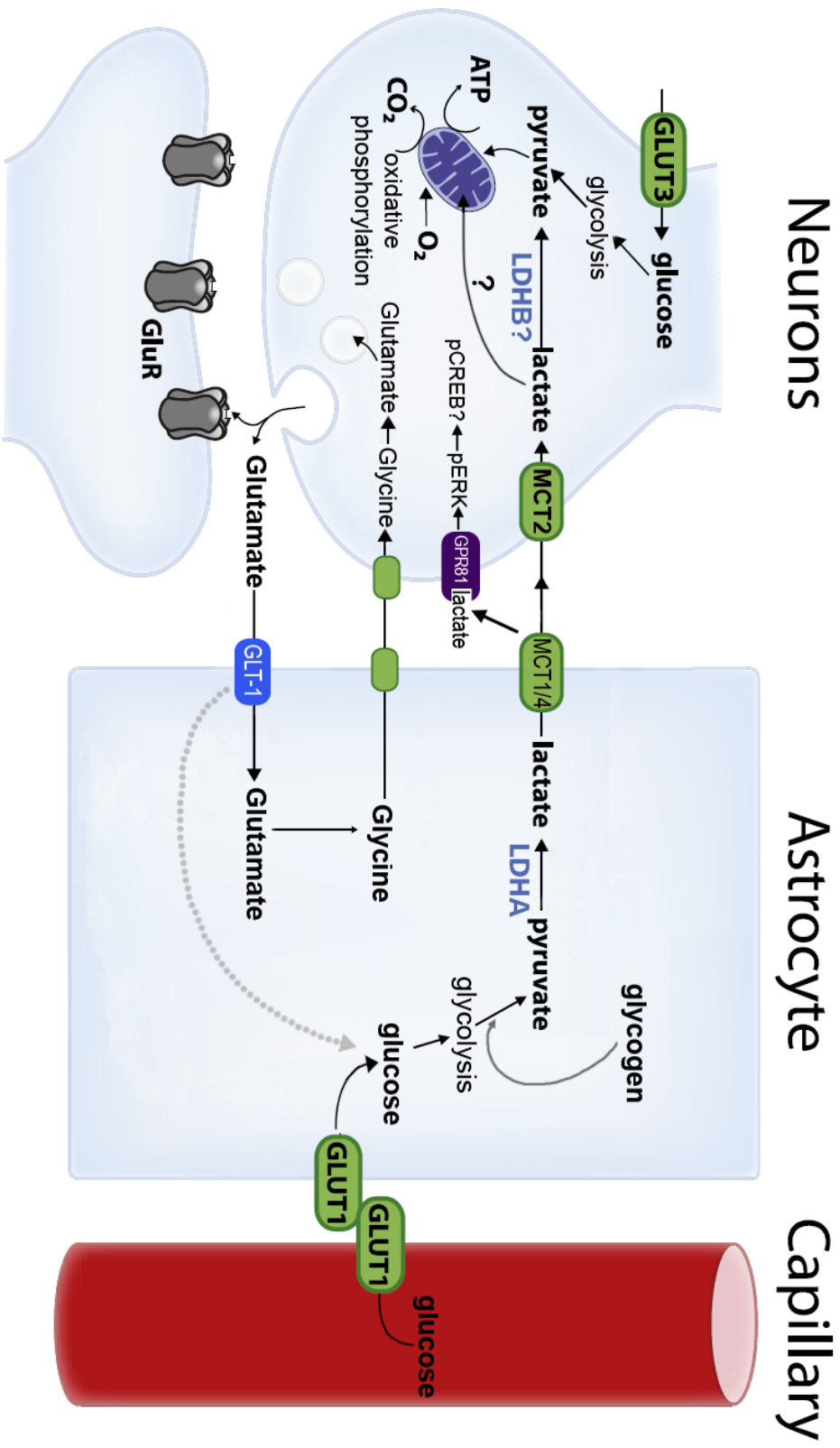
Figure 3. The astrocyte-neuron lactate shuttle model

The astrocyte-neuron lactate shuttle model proposes that astrocytes readily take up glucose from cerebral blood vessels, via glucose transporters (GLUT-1) and process it at a high capacity, by aerobic glycolysis, to produce lactate by lactate dehydrogenase A (LDHA) which is released into the extracellular space via monocarboxylate transporters 1 or 4 (MCT1/4). Extracellular lactate is then taken up by neurons (via MCT2) and converted to pyruvate by LDHB, which enters the TCA cycle followed by oxidative phosphorylation in the mitochondria. Lactate may also be transported and oxidized in the mitochondria through an unknown process. Recent studies suggest that extracellular lactate may also bind GPR81 (a G-protein coupled receptor) on neurons and trigger a phosphorylation of ERK and possibly activate downstream signaling events, including phosphorylation of the cAMP-binding protein (CREB), that may affect memory. In addition, astrocytes remove the excitatory neurotransmitter glutamate from synapses via glutamate transporters (GLT-1) and convert it to glutamine as part of a recycling of the neurotransmitter. In doing so, glutamate triggers a cascade of molecular events leading to an enhancement of glucose utilization by astrocytes. Astrocytes can also breakdown glycogen for entry into glycolysis. Neurons also have the capacity to fully oxidize glucose following uptake by the neuron-specific glucose transporter (GLUT-3).

Monocarboxylate transporters

The shuttling of lactate and other monocarboxylates, including pyruvate and ketone bodies, is dependent on the proton-linked monocarboxylate transporter (MCT) family of transmembrane proteins[384]. There are a total of 14 members of MCT, yet only four isoforms are well-characterized (MCT1 to MCT4), each with different tissue-specific expression patterns and substrate specificity. Among the three MCTs that are known to be expressed in the brain, MCT2 is almost exclusively expressed in neurons, while MCT4 is almost exclusively expressed in astrocytes, and MCT1 is expressed in astrocytes, oligodendrocytes, and endothelial cells of cerebral blood vessels[385–390]. In addition to neurons, MCT2 has also been observed specifically in the foot processes of astrocytes and has a ten-fold higher affinity for substrates than MCT1 and MCT4, suggesting it is particularly suited to lactate import[391,392]. The transport of lactate via MCTs is dependent on H^+ co-transport and thus movement of lactate is pH-sensitive, whereby lactate transport is enhanced at low pH on the H^+ binding side or high pH on the opposite side[393]. In this manner, the export of lactate out of the cell is regulated by the redox potential and is enhanced by a high glycolytic rate[394]. The transport of lactate is also freely reversible with a trans-acceleration effect, which means that shuttling is accelerated if the lactate concentration is increased on the opposite side[395]. Given the tissue-specific expression and the kinetic characteristics of each, the distribution of MCTs in the brain supports the ANLSH whereby astrocytes are a lactate 'source' and neurons are a lactate 'sink'[396,397]. The low lactate-affinity of MCT1 and MCT4 in astrocytes would ensure that lactate is exported to continue a high glycolytic rate and prevent lactate accumulation inside the cell. In contrast, the high lactate-affinity of MCT2 in neurons would ensure a high degree of lactate import and consumption.

Support for the astrocyte-neuron lactate shuttle hypothesis

Several lines of evidence support the ANLSH. First, from an anatomical standpoint, astrocytes are positioned in such a manner to support the coupling between glucose supply from blood vessels and energetic demand in neurons. Astrocytes project specialized processes called perivascular end-feet to surround cerebral blood vessels in

order to form the blood-brain-barrier and express GLUT-1 at the surface to promote glucose import into the brain[398,399]. In parallel, astrocytes have perisynaptic end-feet that enclose synaptic clefts in order to recycle glutamate released from neurons[400–402]. Therefore, astrocytes are positioned to respond to synaptic activity and supply glucose to neurons from the blood stream. Astrocytes and neurons also display markedly different metabolic phenotypes. Astrocytes typically present a high glycolytic rate and release lactate in the extracellular space[403–408]. The glycolytic phenotype of astrocytes may be maintained through either the low expression of PDH, or a high degree of the phosphorylation-mediated inactivation of PDH, in order to promote the conversion of pyruvate to lactate[409,410]. In contrast to astrocytes, neurons sustain a high rate of oxidative metabolism and even prefer lactate as a fuel source over glucose when both are present[403,405,411–416]. Further, neurons have a reduced capacity to perform glycolysis due to the constant proteasomal degradation of the enzyme 6-phosphofructose-2-kinase/fructose-2,6-bisphosphatase-3 (PFKFB3), which is an activator of the rate-limiting glycolytic enzyme PFK[407]. In contrast, astrocytes express high levels of PFKFB3[407]. In addition, the LDH isoforms display differential cell-type specific expression in the hippocampus and occipital cortex of post-mortem tissues: neurons exclusively express with LDHB, while astrocytes express both LDHA and LDHB isoforms[328]. Thus the enrichment of LDHB in neurons favors lactate metabolism as a fuel source, while astrocytes are capable of both lactate metabolism and production. Perhaps the most convincing evidence in support of the ANLSH comes from *in vivo* studies using ^{13}C-labeling of lactate and nuclear magnetic resonance (NMR) spectroscopy. These experiments demonstrated that lactate is almost exclusively metabolized by neurons and that lactate produced by glycolysis in astrocytes serves as a substrate for neurons[413,417–419]. In addition to these observations, it has been demonstrated that a decline in neuronal synaptic transmission arising from glucose deprivation could be rescued by exogenous delivery of glucose or lactate specifically to astrocytes[267]. This effect was abolished in the presence of an MCT inhibitor, which indicates a role in metabolic trafficking of pyruvate or lactate in astrocytic networks to sustain neuronal activity[267].

Controversy regarding astrocytic versus neuronal aerobic glycolysis

The role of lactate as an intermediate metabolite shuttled between astrocytes and neurons to meet active energy requirements of the brain is still highly debated[266,420–425]. The ANLSH posits that neurons preferentially consume lactate over glucose as a fuel source, which is provided by astrocytes following activation-induced glycolytic metabolism. Yet, both cell types are capable of consuming glucose as a fuel source and producing lactate *in vitro* under various conditions[425–427]. Astrocytes also have a considerable capacity to perform oxidative metabolism and rely on their mitochondria for approximately 75% of total ATP produced[428]. In fact, it was estimated that astrocytes exhibit no preferential utilization of either glycolysis or oxidative phosphorylation to support the Na^+/K^+ ATPase pump[428,429]. Neurons also have a high capacity for glycolysis and it has been suggested from several studies using isolated synaptosomes from the adult brain that neuronal glycolysis increases in response to cerebral activation[430–433]. Several lines of evidence also suggest that lactate is not a major fuel source during normal brain activation, yet can be used as peripheral supply from the blood when glucose availability is inadequate such as during physical exercise[434–438]. Some researchers have argued that glycogen mobilization in astrocytes may simply help to offset the energy requirements of neurons, thereby reducing astrocytic utilization of blood-borne glucose and increasing glucose availability for activated neurons[297,439]. Interestingly, alternative theories have been proposed counter to the ANLSH called the neuron-to-astrocyte lactate shuttle. The authors used concentration and kinetic parameters of GLUT-1 and MCTs in endothelial cells, astrocytes, and neurons, to simulate neuronal uptake of glucose during activation and release of lactate to be taken up by astrocytes[266,440]. This model was further supported by *in vivo* functional magnetic resonance spectroscopy (fMRS) to demonstrate that neurons, not astrocytes, are the primary source of glucose uptake and lactate production[424]. Yet, regardless of the direction of lactate flow during cerebral activation, these authors suggested that the overall contribution of lactate to glucose metabolism is so small that it should be considered negligible[441]. Taken altogether, cerebral activation triggers an up-regulation of aerobic glycolysis in affected brain regions with the

associated production of lactate, yet the role of lactate as an intermediate metabolite shuttled between astrocytes and neurons remains a contentious issue.

1.3.2   The role of lactate in memory

Memory is a complex cognitive process regulated by several different cellular and molecular signaling cascades in the brain working together to encode and retrieve information. Memory is often described as a process that can divided into three distinct stages: acquisition, consolidation, and retrieval. Memory acquisition (encoding) is the process by which an animal learns the association between a cause and effect in a given context, while memory consolidation (storage) involves the stabilization of the association into a long-term memory trace, and retrieval (recall) is the process by which a memory trace is accessed to modulate future behaviour[442]. A large body of literature implicates the role of different brain regions in these sequential processes: in general, memory acquisition involves synaptic changes in the hippocampus, while memory consolidation involves the transfer of information from the hippocampus to the frontal and temporal cortex where it is stored for long-term retention, and memory retrieval links neural connections between the hippocampus and cortex to elicit a recall of information[443–447]. The specific transfer of information between two neurons was originally proposed to involve cellular changes such that the repeated and persistent activity of one neuron induces a lasting increase in efficiency of firing the other neuron[448]. This mechanism is now commonly referred to as synaptic plasticity, which describes the ability of synapses to change their strength over time in response to changes in their activity[449]. The molecular changes occurring at the synapse that strengthen or weaken the connection are referred to as long-term potentiation (LTP) and long-term depression (LTD), respectively. While short-term changes at the synapse involve post-translational modifications, changes associated with consolidation or stabilization of long-term memory requires changes in gene expression and new protein synthesis[450]. The role of LTP in the hippocampus associated with memory formation has been examined extensively and reviewed in great detail[451–455]. On a molecular level, long-term LTP begins with the depolarization of the post-synaptic site through the α-amino-3-hydroxy-5-methyl-4-isoxazolepropionate (AMPA) receptor and the coincident binding of

glutamate to the NMDA receptor, which stimulates an influx of Ca^{2+} into the cell and triggers a signaling cascade that activates Ca^{2+}-dependent protein kinases. This ultimately leads to activation of the transcription factor cAMP-response element binding protein (CREB), which promotes gene expression of proteins that remodel the actin cytoskeleton and are required for long-term LTP and memory consolidation[456–458]. Several studies have demonstrated that genetic loss of *CREB* impaired long-term memory formation[459–461].

A growing body of evidence suggests that lactate participates in LTP and memory formation. Inhibitory avoidance training in rats caused an increase in activated CREB and its downstream targets, ARC and COFILIN. This effect was completely blocked with administration of 1,4-dideoxy-1,4-imino-D-arabinitol (DAB), which blocks glycogen breakdown, and led to impaired memory formation[462]. Exogenous lactate can rescue CREB activation back to a level comparable to vehicle-injected rats, although glucose was not tested. A recent meta-analysis of whole-genome microarray data revealed a strong correlation between aerobic glycolysis and changes in gene expression associated with synapse formation and neurite growth in the adult brain[463]. This observation may be explained by results from a recent study showing that lactate can potentiate NMDA signaling and promote the expression of synaptic plasticity-related genes downstream of CREB by raising the cytosolic $NADH/NAD^+$ ratio in cultured neurons and *in vivo* in the mouse sensory-motor cortex[464]. This is in agreement with previous studies showing redox-dependent regulation of the NMDA receptor[465,466]. Lactate has also been implicated as a receptor-mediated signaling molecule independent of metabolic coupling[467]. Lactate was identified as a natural ligand of a G protein-coupled receptor 81 (GPR81), also known as hydroxycarboxylic receptor 1 (HCA1)[468]. This receptor is expressed on post-synaptic terminals of excitatory synapses as well as the perivascular astrocytic processes and endothelial cells that comprise the blood-brain barrier, although it is expressed at 100-fold levels in adipose tissues where it plays a prominent role inhibiting lipolysis[468–471]. Activation of GPR81 causes an inhibition in adenylyl cyclase activity resulting in a decline in cAMP levels, which in turn reduces calcium-spiking activity in cortical neurons[471,472]. The ability of lactate to suppress neuronal activity has

been observed previously in hippocampal slices, yet a direct role for GPR81 in synaptic plasticity and memory has yet to be discovered[473].

Perhaps the most convincing evidence that implicates a role of lactate in memory processes is directly through metabolic coupling and fuel delivery. Given that aerobic glycolysis is quickly up-regulated in active regions of the brain and cognitive tasks are energetically demanding processes, lactate production and transport may simply comprise a system of energy delivery to brain regions participating in memory processes. The first evidence of this emerged from experiments demonstrating that glycogen is mobilized from astrocytes in neonatal chicks following training in a taste-aversion task[474,475]. Administration of DAB or 2-deoxyglucose (2DG), which impaired glycogen breakdown and glycolysis respectively, impaired memory performance[476,477]. Supplementation with lactate was sufficient to rescue memory in the presence of DAB or 2DG, while glucose was able to rescue memory from DAB but not 2DG. These observations suggested that mobilization of glycogen and glycolysis both play a key role in memory formation. A similar study demonstrated that IA training in rats caused an increase in extracellular lactate in the hippocampus that was completely blocked with DAB[462]. Administration of DAB had no effect on short-term memory (tested after an hour) but blocked long-term memory (tested after 24 hours) that was rescued with exogenous lactate[462]. The authors also demonstrated that knock down of MCT1, MCT2, or MCT4 expression impaired memory that was rescued with administration of lactate following disruption of MCT1 or MCT4 (astrocytic) but not MCT2 (neuronal) expression. Pharmacological blockage of MCT2 with α-cyano-4-hydroxycinnamate (4-CIN) also caused an inhibition of spatial working memory formation in rats that could not be rescued with lactate or glucose administration[296].These results have been confirmed by independent groups using a cocaine-induced model of conditioned responses[478]. Ultimately, these studies demonstrating lactate production through glycogen breakdown in astrocytes and subsequent transport to neurons plays a key role in memory formation[479]. However, it remains to be discovered how neuronal activation, aerobic glycolysis, and lactate shuttling varies during aging and in AD and contributes to cognitive decline under physiological conditions.

1.4   Research questions

Aerobic glycolysis and glycogen breakdown both play a central role in long-term memory formation through the production of lactate in astrocytes and subsequent transport to neurons. Lactate may act as a redox-mediated signaling molecule to directly promote the expression of synaptic plasticity genes or bind directly to a receptor to elicit downstream signaling cascades that regulate neuronal activity. Aerobic glycolysis is up-regulated in activated regions of the brain to quickly support the energy demands of firing neurons and promote the *de novo* synthesis of biosynthetic building blocks for synaptic remodeling. Aerobic glycolysis also shares a close spatial distribution to amyloid deposition in AD patients and confers a survival advantage to neurons in culture when exposed to Aβ. However, the changes in aerobic glycolysis that occur with age and the role of lactate production and transport in memory decline associated with Alzheimer's disease have yet to be investigated. Furthermore, the transgenic-AD mouse line used in this study, $APP_{swe}/PS1_{\Delta E9}$, develops memory loss with age, yet does not exhibit extensive neuron loss consistent with atrophy in the human AD brain[480]. This has remained a contentious issue for decades and has given rise to several research questions that I aim to answer including:

1. Does aerobic glycolysis mediate resistance to Aβ *in vivo*?

2. Does aerobic glycolysis play a role in memory performance during both normal aging and under the conditions of high Aβ deposition?

1.5   Hypothesis

I hypothesize that neurons upregulate aerobic glycolysis in response to Aβ deposition to promote Aβ resistance *in vivo*. Furthermore, I hypothesize that aerobic glycolysis contributes to memory processes in both normal aging and under conditions of high Aβ deposition.

1.6   Specific aims

In order to test the hypothesis that neurons upregulate aerobic glycolysis in response to Aβ deposition, a mouse model of cerebral amyloid pathology, APP/PS1, and control littermates will be treated with DCA (an inhibitor of PDK1) in the drinking water over the course of age. I predict that APP/PS1 mice treated with DCA will undergo neurodegeneration and succumb to memory decline at an earlier age than untreated APP/PS1 mice. In order to test the hypothesis that aerobic glycolysis contributes to memory, a standard memory test will be used to compare the spatial memory performance of control mice and APP/PS1 mice to the expression of aerobic glycolysis enzymes measured by Western blot analysis. This will determine if a correlation between aerobic glycolysis enzyme expression and memory exists during normal and pathological conditions. In addition, the effect of chemical inhibition of aerobic glycolysis on memory in control and APP/PS1 mice will be assessed. I predict that the expression of aerobic glycolysis enzymes in the brain will correlate with memory performance in both control and APP/PS1 mice. Moreover, inhibition of aerobic glycolysis will have a more adverse effect on memory in APP/PS1 mice due to the reliance of this metabolism to preserve neuronal function under pathological conditions.

Chapter 2

2 Materials and Methods

2.1 Animals

Male APP$_{swe}$/PS1$_{\Delta E9}$ mice[481] were maintained on a C57BL/6J background (Charles River Laboratories International, Inc.) and will henceforth be referred to as APP/PS1 mice. Age-matched male C57BL/6J littermates were used as controls and will henceforth be referred to as control mice. All animals were housed in groups of up to 3 animals per cage under a 12 hour light/dark cycle with *ad libitum* access to water and the Mouse Diet 5015 breeder chow base diet (LabDiet). A single red, transparent plastic house was placed in each cage with cotton nesting material and corn cob bedding and that was changed weekly. Animals were weaned at 3 weeks of age and ear punches were used for identification and PCR-based genotyping. All animal procedures were conducted in compliance with the Canadian Council of Animal Care (CCAC) guidelines with approved animal protocol from the Institutional Animal Care and Use Committees at the University of Western Ontario (protocol number 2011-079).

2.2 ^{1}H-Magnetic resonance spectroscopy

Animals were anesthetized starting with 3.5% isoflurane and then reduced to 2% combined with 30% oxygen. Mice were scanned using a 9.4 T small animal MRI scanner equipped with a 30 mm millipede volume radiofrequency coil (Agilent, Palo Alto, CA, USA). T$_2$-weighted images were acquired using a 2-dimensional fast spin echo (FSE) pulse sequence with parameters: repetition time (TR)/echo time (TE) = 4000/10 ms, echo train length (ETL) = 4, effective TE = 40 ms, field of view (FOV) = 19.2 x 19.2 mm^2, matrix size = 128 x 128, slice thickness= 0.5 mm, 25 slices, 4 averages. Based on the T$_2$-image, a voxel (2 x 4 x 3 mm^3) was localized to the frontal cortex for magnetic resonance spectroscopy using a LASER pulse sequence with the following parameters: TR/TE = 4000/270 ms, 384 averages for the metabolite spectrum with water suppressed. An unsuppressed water spectrum (8 averages) was also acquired and a QUECC correction was applied. Metabolite levels were measured by fitting spectra using fitMAN

software incorporated into a graphical user interface written in the IDL (Version 5.4, Research Systems Inc.) programming language[482].

2.3 *In vivo* microdialysis and interstitial fluid lactate measurements

In vivo microdialysis was performed as previously described[483]. Briefly, guide cannulae (BR-style, Bioanalytical Systems, West Lafayette, IN, USA) were stereotaxically implanted into the hippocampus and secured into place with dental cement. Twenty-four hours post-cannulation, mice were transferred to Raturn sampling cages (Bioanalytical Systems) and microdialysis probes (2 mm; 38 kDa molecular weight cut-off; BR-style, Bioanalytical Systems) were inserted into the guide cannula, connected to a syringe pump and infused with artificial cerebrospinal fluid (aCSF; 1.3 mM $CaCl_2$, 1.2 mM $MgSO_4$, 3 mM KCl, 0.4 mM KH_2PO_4, 25 mM $NaHCO_3$ and 122 mM NaCl; pH 7.35) at a flow rate of 1 μl/minute. Following an 8-hour habituation period, hippocampal ISF was collected in hourly fractions and lactate measurements using a lactate oxidase method were quantified for each hour using the YSI 2900 analyzer (YSI Incorporated, Yellow Springs, OH, USA) per the manufacturer's instructions.

2.4 SDS-PAGE and Western blot analysis of brain extracts

Mice were euthanized by cervical dislocation and then immediately perfused with PBS, pH 7.4 ± 0.1. The frontal cortex and hippocampus of the right hemisphere were removed and snap frozen in dry ice. Tissues were homogenized by hand using a pestle in an extraction buffer containing 50 mM Tris pH 7.5, 2% SDS, 100 mM EDTA, protease inhibitors: 2 mM leupeptin, 0.1 mM pepstatin A, and 1 mM PMSF, and the phosphatase inhibitor 0.5 mM sodium orthovanadate. Protein extracts were separated by 10% SDS-PAGE, and electroblotted onto PVDF membrane (Bio-Rad, Hercules, CA, USA). Membranes were probed with the following antibodies: PDK1 (Enzo, Farmingdale, NY, USA), PDH-E1α (pSer^{232}) (Millipore, Darmstadt, Germany), PDH-E1α (pSer^{293}) (Millipore), PDH-E1α (AbCam, Cambridge, UK), LDHA (Cell Signaling, Danvers, MA, USA), LDHB (AbCam), PKM2 (Cell Signaling), PKM1 (Cell Signaling), MCT2 (Millipore), MCT4 (Millipore) and β-actin (Cell Signaling), followed by incubation with

an appropriate horseradish peroxidase-conjugated secondary antibody (Bio-Rad). The blots were developed using Pierce ECL western blotting substrate (Thermo Fisher Scientific, Waltham, MA, USA) and visualized with a Bio-Rad Molecular Imager (ChemiDoc XRS, Bio-Rad). Densitometric analysis was performed using Quantity One software (Bio-Rad).

2.5   The Morris water maze

Spatial learning and memory was assessed as previously described[484] using the Morris water maze (MWM) with the following specifications: A white circular tank with diameter 48" and height 30" (San Diego Instruments, San Diego, CA, USA) was filled with water and maintained at a temperature of 26 ± 1 ℃ using a 300 W submersible aquarium heater (Aqueon, Franklin, WI, USA) that was removed immediately before mice were brought into the testing room. Spatial visual cues in the form of different shaped cardboard pictures were placed on the walls surrounding the water tank, including a white diamond at the North position, a blue cross at the North-East, a yellow triangle at the South-East, a green circle at the South, a pink heart at the South-West, and a red square at the North-West (Figure 4). Visual data were collected using a HD Pro Webcam C920 (Logitech, Romanel-sur-Morges, Switzerland) and analyzed by the video tracking software ANY-maze v4.98 (Stoelting Company, Wood Dale, IL, USA). A circular, clear plastic platform (diameter 10.16 cm) was submerged 1 cm below the surface of the water. The platform was positioned in the correct quadrant according to virtual tracer lines generated by the ANY-maze software with a radial grid from the center spaced at 45 degrees as well as a square grid spaced to the edge of the water line and a concentric grid spaced to the edge of the square. The platform was positioned in the tank in the correct quadrant with its center at the intersection of the radial and concentric lines.
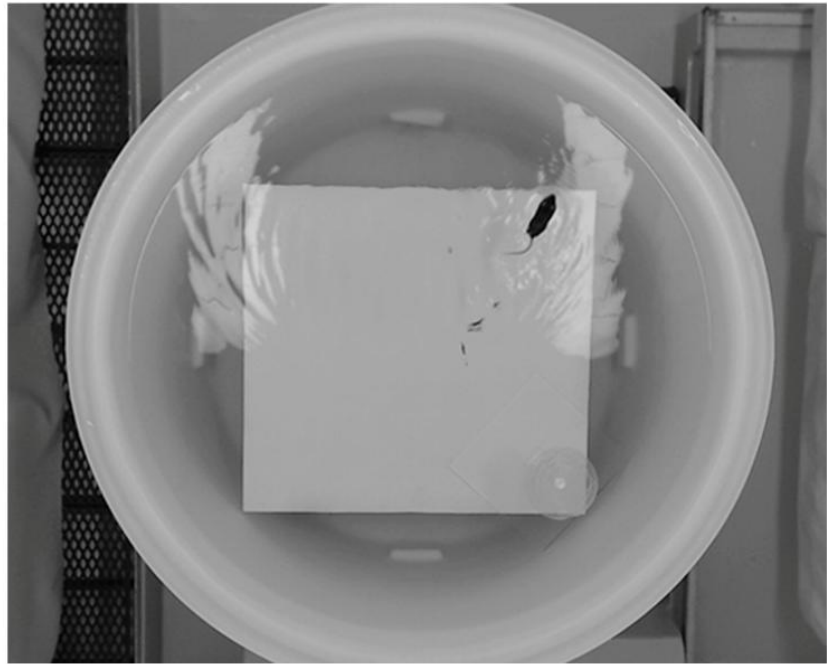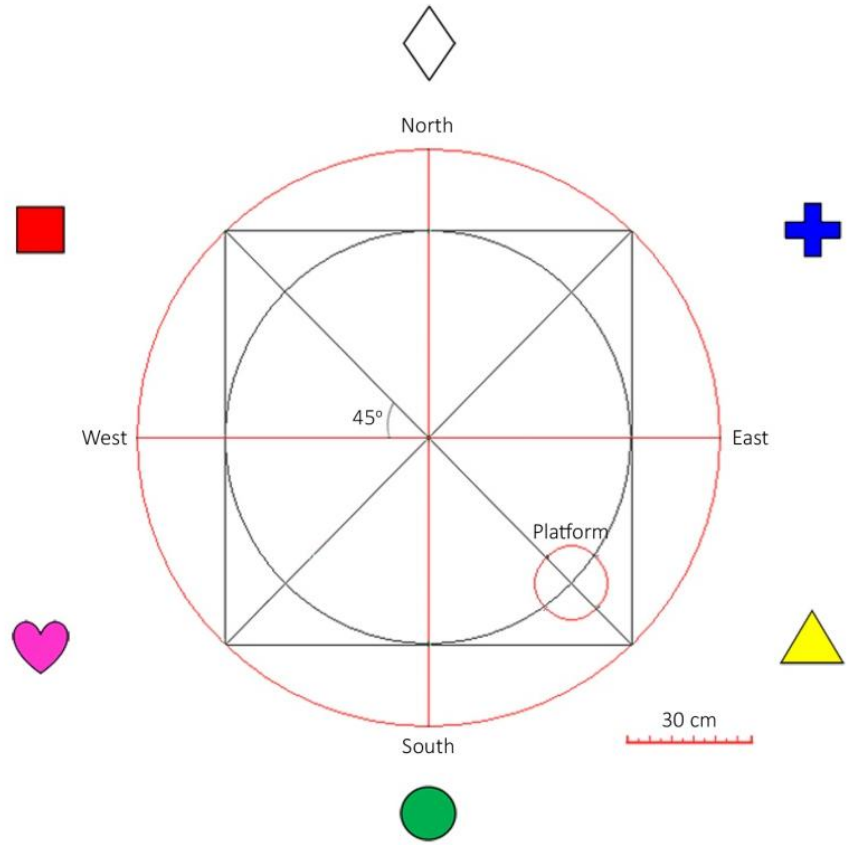
Figure 4: Configuration of the Morris water maze.

(Top) Virtual tracer lines in red outline the edge of the water level and the division of the tank into four quadrants, as well as the platform in the South-East quadrant. Virtual tracer lines in black outlining the positioning of the platform using a radial grid from the center spaced at 45 degrees as well as a square grid spaced to the edge of the water line and a concentric grid spaced to the edge of the square. Representative images are shown of cardboard pictures placed on the walls surrounding the water tank, including a white diamond at the North position, a blue cross at the North-East, a tallow triangle at the South-East, a green circle at the South, a pink heart at the South-West, and a red square at the North-West. Scale bar in the bottom right is 30 cm. (Bottom) Photograph taken of the MWM with a mouse swimming and platform located in the South-East quadrant.

Before the first training day, mice were acclimatized to the experimental room and water tank. For mice naïve to the MWM, the acclimatization period lasted three consecutive days: on the first day, mice spent 30 minutes in the experimental room in their native cages; on the second day, mice spent 30 minutes in the experimental room in their native cages followed by 15 seconds on the platform located in the center of the tank and allowed 90 seconds to swim to the platform if they jumped off, or guided to the platform if they did not find it within 90 seconds; on the third day, mice spent 30 minutes in the experimental room in their native cages followed by 15 seconds on the platform located in the center of the tank, then followed by a release into the water at the North release point of the tank and allowed 90 seconds to find the platform, or guided to the platform if they did not find it in 90 seconds. For mice that were not naïve to the MWM, an acclimatization period of one day was performed consisting of 30 minutes spent in the experimental room in their native cages followed by 15 seconds spent on the platform located in the center of the tank, then followed by a release into the water at the North release point of the tank and allowed 90 seconds to find the platform, or guided to the platform if they did not find it in 90 seconds. For all subsequent training days mice were first acclimatized to the experimental room for 30 minutes before the beginning of the first trial.

Mice were then trained for 4 consecutive days with 4 trials per day to find the location of the platform submerged in the correct quadrant. The release point of the first trial corresponded to the cardinal directions (North, East, South, and West) rotating with each training day (Table 1). For each of the 4 trials in one day, mice were released into the water with a clockwise rotation of release placements for each trial that day. A trial lasted until the mouse found the platform or until 90 seconds had elapsed, at which point the mouse was gently guided to the platform. The mouse was then placed for 15 seconds on the platform before it was removed and briefly dried in paper towel before placing it back in its cage. An inter-trial interval (ITI) of 10 minutes was used to ensure consistency of timing between trials for each mouse.

Table 1: Release point schedule for mice training in the Morris water maze

Training Day	Release Point (4 per day)			
	Trial 1	Trial 2	Trial 3	Trial 4
1	N	E	S	W
2	E	S	W	N
3	S	W	N	E
4	W	N	E	S
Probe	Center			

On the fifth day, mice were exposed to a probe trial in which the platform was removed and the mouse was released in the center of the tank and given 60 seconds to attempt to find the missing platform. After swimming in the probe trial, the mouse was then removed from the tank and briefly dried in paper towel before placing it back into its cage. A flag trial was then performed in which the platform was placed back into the water in the opposite quadrant that originally held the platform and a small red plastic pole was inserted into the platform so it was sticking out of the water. The mouse was released in the center of the tank and given 90 seconds to find the location of the platform. A trial lasted until the mouse found the platform or until 90 seconds had elapsed, at which point it was gently guided to the platform. The mouse was then given 15 seconds on the platform before it was removed and briefly dried in paper towel before placing it back into its cage.

Mice were disqualified from the data analysis of the MWM according to criteria that they did not appear to be using visual spatial strategies to actively search for the platform, or they appeared unable or unmotivated to escape[485]. This behavior could occur in the following ways: (1) the mouse frequently swims around the edge of the pool in an attempt to climb up the wall of the tank and does not make a clear attempt to find the

platform; (2) the mouse frequently stops swimming and floats on the surface of the water for long periods of time. If the mouse attempted to climb up the wall of the tank and continued to swim on the edge of the pool, the timer continued until the end of the trial. If at any point the mouse stopped swimming and floated in the water, the timer was paused until it started swimming again and continued until the end of the trial. A mouse was disqualified from analysis if it failed to demonstrate active searching behavior on consecutive training days or on the probe trial. If a mouse was disqualified from analysis it was removed from all training days as well as the probe and flag trials for that particular training phase.

For acute exposure to chemical inhibitors of aerobic glycolysis, the location of the platform was moved to different quadrants between each set of chemical treatments (Table 2). The platform was located in the south-east quadrant for the 1st training phase (Vehicle), the north-west quadrant for the 2nd training phase (Isosafrol), the north-east quadrant for the 3rd training phase (DCA), and the south-west quadrant for the 4th training phase (Saline). During the probe trial, mice were injected intraperitoneally with the specified treatment (vehicle, Isosafrol, DCA, or saline) 30 minutes prior to the start of the probe trial.

Table 2: Treatment schedule for mice in memory testing with Isosafrol and dichloroacetate

Training Phase	Age (months)	Treatment	Platform Location
1	12-13	Vehicle	SE
2	13-14	Isosafrol	NW
3	14-16	DCA	NE
4	16-17	Saline	SW
Euthanization	17-18	Saline or DCA	

2.6 Preparation of mouse brain soluble and insoluble amyloid-β-extracts and ELISA

Mouse brain tissue from the frontal cortex was extracted in a 50 mM Tris pH 7.5, 2% SDS buffer with a protease inhibitor cocktail containing AEBSF (Millipore), then sonicated briefly and centrifuged at $100,000 \times g$ for 1 hour at 4ºC. The supernatant was collected as the soluble Aβ fraction and initially diluted in cold Reaction buffer BSAT-DPBS (Dulbecco's phosphate buffered saline at pH7.4 containing 5% BSA and 0.03% Tween-20), then diluted as necessary for ELISA analysis. To analyze the insoluble Aβ fraction, the pellet was dissolved in 70% formic acid and sonicated briefly before centrifugation at $100,000 \times g$ for 1 hour at 4 ºC. The supernatant was neutralized by 1 M Tris phosphate buffer, pH 11, and then initially diluted in cold BSAT-DPBS, followed by dilution as necessary for the ELISA. ELISAs for $A\beta_{40}$ and $A\beta_{42}$ (Thermo Fisher Scientific) were performed according to standard protocol and measured at 450 nm using an Infinite M1000 microplate reader (TECAN, Männedolf, Switzerland).

2.7 Cryo-immunohistochemistry and confocal microscopy

Left hemi-brains were fixed in 4% paraformaldehyde at 4 ºC overnight, then incubated in 30% sucrose at 4 ºC for 48 hours, and snap frozen in freezing microtome cassettes containing Tissue-Tek® O.C.T. compound (Sakura Finetek USA Inc., Torrance, CA, USA). Brain tissues were sectioned on a serial sagittal plane using a CM350 Cryostat (Leica, Wetzlar, Germany) at a thickness of 30 μm and free-floating brain slices were stored in 25 % glycerol in PBS at 4 ºC for up to three weeks. Sections were washed in PBS, then permeabilized using PBST (PBS and 0.1 % Triton X-100), and blocked overnight at 4 ºC in 10% goat serum in PBST. Sections were incubated in primary antibody solutions at a 1:100 dilution in PBST + 1% BSA overnight at 4 ºC: PDK1 (Enzo), LDHA (Cell Signaling), GFAP (AbCam), and TUJ1 (AbCam). Sections were washed in PBS and incubated in secondary antibodies: AlexaFluor® 488 and AlexaFluor® 647 (Thermo Fisher Scientific) at a 1:1000 dilution in PBST + 1% BSA for 1 hour at room temperature then washed with PBS and mounted with ProLong® Gold reagent with DAPI (Thermo Fisher Scientific) on Superfrost slides (Fisher Scientific, Waltham, MA,

USA). For staining of Aβ plaques, sections were dehydrated with 80% ethanol then incubated in 0.01%Thioflavin S (Sigma, St. Louis, MO, USA) for 15 min at room temperature, followed by rehydration in PBS and mounting with ProLong® Gold antifade reagent without DAPI (Thermo Fisher Scientific) on Superfrost slides (Fisher Scientific).

2.8   Dichloroacetate

Dichloroacetate (DCA) is an analog of acetic acid in which two of the hydrogens of the methyl group are replaced by chlorine atoms. Humans have a long history of exposure to DCA through chlorinated drinking water with an average daily consumption at approximately 4 mg/kg[486]. DCA has been used as a metabolic treatment in laboratory animals since 1973[487] and in humans since 1980[488]. DCA is a selective inhibitor of PDK, thereby preventing the phosphorylation of PDH and promoting the active form[489].

2.9   Isosafrol

Isosafrol is an analog of stiripentol, an inhibitor of cytochrome P450, which has been used for the treatment of severe myoclonic epilepsy in infancy (SMEI), a rare congenital form of epilepsy called Dravet syndrome[490]. Isosafrol lacks the hydroxyl group and tertiary-butyl group of stiripentol. It was recently discovered that isosafrol is a potent inhibitor of LDHA and strongly prevented pyruvate-to-lactate conversion *in vitro*[491].

2.10 Chronic exposure to dichloroacetate through oral administration in drinking water

DCA (Sigma) was orally administered to mice at a daily dose of 200 mg/kg (pH 7.4 ± 0.1) by changing the drinking immediately water after weaning (3 weeks of age), based on an average daily water consumption of 5mL per mouse. Mice were weighed twice weekly and the average weight of mice in each cage was used to calculate the amount of DCA to add to drinking water of each bottle per cage. Drinking water was replaced twice per week with freshly prepared DCA.

2.11 Acute exposure to Isosafrol and dichloroacetate through intraperitoneal injection

The chemical inhibitor of LDH, Isosafrol (Sigma) was prepared fresh the day of injection at a concentration of 15mg/mL in a sterile solution of 1% Carboxymethylcellulose (CMC) (Sigma) in 0.9% NaCl (saline). Mice were weighed and then injected intraperitoneally with the correct volume of Isosafrol solution for a dosage of 300 mg/kg (1 mL for a 50 mg animal). The vehicle injection was a sterile solution of 1% CMC (Sigma) in saline. Mice were weighed and then injected intraperitoneally with the correct volume of vehicle assuming a dosage of 300 mg/kg of Isosafrol from a 15 mg/mL concentration. DCA (Sigma), was prepared fresh the day of injection at a concentration of 10 mg/mL in a sterile solution of saline and neutralized to pH 7.4 ± 0.1 with NaOH. Mice were weighed and then injected intraperitoneally with the correct volume of DCA solution for a dosage of 200 mg/kg (1 mL for a 50 mg animal). For saline injections, mice were weighed and injected intraperitoneally with the correct volume of sterile saline assuming a dosage of 200 mg/kg of DCA from a 10 mg/mL solution.

2.12 Preparation of mouse brain extracts and LDHA/LDHB enzyme activity assay

Mice were injected intraperitoneally with vehicle (1% CMC) or Isosafrol (300 mg/kg) and euthanized 30 minutes later by cervical dislocation. The hippocampus was dissected and snap frozen in dry ice. Tissues were homogenized in PPB buffer (100 mM Potassium Phosphate Buffer, pH 7.0 ± 0.1, with 0.1% Triton X-100 (Sigma), 2 mM EDTA, 2 mM leupeptin, 0.1 mM pepstatin A, 1 mM PMSF, and 0.5 mM sodium orthovanadate). Protein extracts were added to a standard reaction formula for either LDHA (pyruvate to lactate) or LDHB (lactate to pyruvate). The LDHA reaction formula included 30 mM sodium pyruvate (Sigma), 0.192 mM NADH (Sigma), and approximately 3 μg of protein extract in 500 mM PPB, pH 7.4 ± 0.1 for a total volume of 50 μL in a single well of a Nunc™ Black Polystyrene 96-well plate (Thermo Fisher Scientific). The LDHB reaction formula included 90 mM sodium lactate (Sigma), 1.287 mM NAD^+ (Sigma), 218.4 μM Hydrazine (Sigma), and approximately 3 μg of protein extract in a buffer containing 0.5 M Glycine and 2.5 mM EDTA, pH 9.5 ± 0.1 for a total volume of 50 μL in a single well

of a Nunc™ Black Polystyrene 96-well plate (Thermo Fisher Scientific). The rate of NADH consumption or production (LDHA and LDHB reactions, respectively) was determined by measuring NADH fluorescence at excitation/emission of 340/460 nm using a Infinite M1000 microplate reader (TECAN) at 20 second intervals for 5 minutes. Concentration of NADH was determined at each time point by comparing each fluorescence value to a NADH fluorescence standard curve. One Unit of enzyme is defined as the amount of enzyme that catalyzes conversion of 1μmol of substrate per minute. A line-of-best-fit was modeled from a linear regression analysis and enzyme activity was expressed in Units per mg of protein, calculated using the slope (ΔNADH(μM)/min) of the reaction and the volume of the reaction (50 μL) according to the following equation:

$$\text{Units/mg} = [\Delta\text{NADH}(\mu M)/\text{min}]/(\text{mg of protein}/0.05 \text{ mL})$$

2.13 Hyperpolarized ^{13}C-pyruvate magnetic resonance spectroscopy

Images were acquired using a GE MR750 3.0T MRI (GE, Fairfield, CT, USA). A custom-built dual-tuned ^{13}C-^{1}H solenoid radiofrequency coil was used as and ^{1}H and ^{13}C images were inherently registered. A hyperpolarized [1-^{13}C]-pyruvate buffered solution was prepared using a dynamic nuclear polarizer, Hypersense (Oxford Instruments, Abingdon, UK). The solution had a final concentration of 150 mM pyruvate with pH 7.4 at 37 °C and with ~10% polarization at 3 T with T_1 of ~60 seconds. The imaging session consisted of fast imaging employing steady-state acquisition (FIESTA) imaging and hyperpolarized ^{13}C-MRS imaging. FIESTA images were acquired with the following imaging parameters: 30 x 30 mm field of view (FOV), 0.2 mm isotropic in-plane resolution, 0.4 mm slice thickness, repetition time (TR) = 10.3 ms, echo time (TE) = 5.2 ms, bandwidth = 12.58 Hz, and phase cycling = 8. For hyperpolarized ^{13}C-MRS imaging, a ~0.3 ml bolus of the hyperpolarized [1-^{13}C]-pyruvate buffered solution was injected via a tail vein catheter. 15 seconds after the injection, 2D ^{13}C-spectra were acquired using free induction decay chemical shift imaging (FID-CSI) with the following parameters: 30 x 30 mm FOV, 2.5 mm isotropic in-plane resolution, slice thickness = 10~15 mm, TR = 80 ms, spectral width = 5000 Hz and number of points = 256. DCA was freshly prepared

at a concentration of 40 mg/mL in sterile saline and neutralized to pH 7.4 ± 0.1 using NaOH. Mice were given 30 minutes to recover following hyperpolarized ^{13}C-pyruvate injection before injection of DCA at 200 mg/kg via tail vein catheter. Mice were then given another 30 minutes to recover and another bolus of hyperpolarized ^{13}C-pyruvate was injected and mice were scanned again as previously described.

2.14 Statistical analysis

Two-way ANOVA and Tukey's *post hoc* comparisons were used for the following analyses: the difference between the genotypes over the course of aging for lactate levels deduced by ^{1}H-MRS analysis, the difference between genotypes over the course of aging for band density derived from western blot analysis, as well as the levels of soluble and insoluble $A\beta_{(1-40)}$ and $A\beta_{(1-42)}$ from cortical extracts of APP/PS1 mice. A Bonferroni correction for multiple comparisons was used to adjust the significance value for western blot analysis. A two-way ANOVA with repeated measures was used to analyze the difference between genotypes for the latency to find the platform over the course of training days in the MWM. A Welch's T-test was used to evaluate the difference between genotypes for individual measures of the MWM: total distance traveled, percent time spent in the correct quadrant, and latency to find the flag platform. A multiple linear regression model and ANCOVA was used to analyze the difference between genotypes for correlation of memory performance in the MWM and the relative band density by western blot analysis, in addition to the correlation of soluble and insoluble $A\beta$ levels with the relative band density by western blot analysis. A one-way ANOVA with repeated measures was used to analyze the difference between genotypes for each training phase of injected chemicals Isosafrol and DCA. Two-way ANOVA and Tukey's *post hoc* comparisons were used to analyze the difference between the genotypes and chemical treatments on memory performance with the MWM. A Welch's t-test with a Bonferroni correction for multiple comparisons was used to analyze the difference between saline- and DCA-injected control mice on band densitometry from western blot analysis. A Welch's paired t-test was used to evaluate the difference between lactate-to-pyruvate ratios for ^{13}C-pyruvate MRS measurements of before and after DCA injection. A Welch's t-test with a Bonferroni correction for multiple comparisons was used to

evaluate the difference between control mice injected saline and DCA for measures of memory performance in the MWM. A multiple linear regression model was used to analyze the difference between saline- and DCA-injected mice for the correlation of memory performance in the MWM and relative band density by western blot. Statistical evaluation was performed with Microsoft Excel 2007, RStudio v0.99.891, and GraphPad Prism v6.01.

Chapter 3

3 Results

3.1 Examination of lactate levels in the frontal cortex and hippocampus of APP/PS1 mice over the course of age

To examine changes to brain lactate levels over the course of normal aging, *in vivo* [1]H-magnetic resonance spectroscopy (^{1}H-MRS) was performed on the frontal cortex and hippocampus of control and APP/PS1 mice (Figure 5A). Lactate was identified as a peak at 1.33 ppm (Figure 5B) and quantified as a ratio to the metabolite, *N*-acetylaspartate (NAA). Lactate was measured at 3, 6, 9, and 12 months of age in the frontal cortex (Figure 6A). A two-way ANOVA (age × genotype) was performed, which revealed a significant effect of age ($F(3,47) = 4.200$, $p = 0.010$), and genotype ($F(3,47) = 4.575$, $p = 0.037$). A Tukey's *post hoc* comparison test determined that cortical lactate levels progressively declined starting at 9 months of age ($p = 0.008$) to 12 months of age ($p = 0.002$). In contrast, lactate levels did not significantly change for APP/PS1 mice throughout the course of aging. In order to ensure that the standard reference metabolite did not change over the course of age, NAA was measured as a ratio to creatine at 3, 6, 9, and 12 months of age in the frontal cortex (Figure 6B). A two-way ANOVA (age × genotype) was performed, which revealed no significant effect for age ($F(3,48) = 2.561$, $p = 0.066$) or genotype ($F(3,48) = 0.082$, $p = 0.776$), which indicated that NAA levels did not change and was suitable as a reference metabolite for measuring lactate over the course of aging. In addition to the frontal cortex, lactate levels in the hippocampus of control and APP/PS1 mice was assessed by ^{1}H-MRS and expressed as a ratio to NAA at 6 and 12 months of age (Figure 7A). A two-way ANOVA (age × genotype) was performed and revealed no significant effect of genotype on lactate levels in the hippocampus for age ($F(1,54) = 3.863$, $p = 0.055$) or genotype ($F(1,54) = 0.349$, $p = 0.557$). The same analysis for levels of NAA/creatine (Figure 7B) revealed no significant effect of treatment for age ($F(1,54) = 3.323$, $p = 0.074$) or genotype ($F(1,54) = 0.005$, $p = 0.941$), which indicated that NAA was a good reference metabolite for measuring lactate over the course of aging.
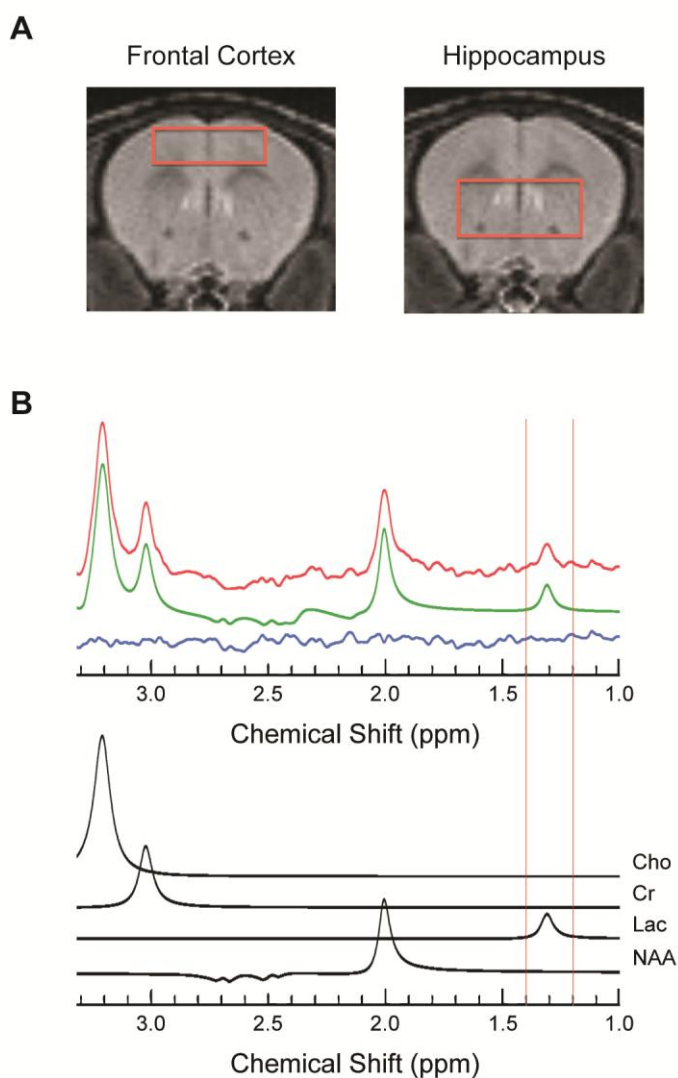
Figure 5: Representation of lactate levels in the frontal cortex and hippocampus of APP/PS1 mice measured by ^{1}H-magnetic resonance spectroscopy.

(A) Volume of interest in frontal cerebral cortex (left) and hippocampus (right) in the coronal plane. (B) Representative spectrum showing the raw data (red line) obtained from the frontal cortex of a 6-month-old APP/PS1 mouse, the fitted result (green line), and the residual line (blue line), which is the difference between the fit and the spectrum. Cho, choline; Cr, creatine; Lac, lactate (highlighted by vertical red lines between 1.2 and 1.4 ppm); NAA, N-acetylaspartate.
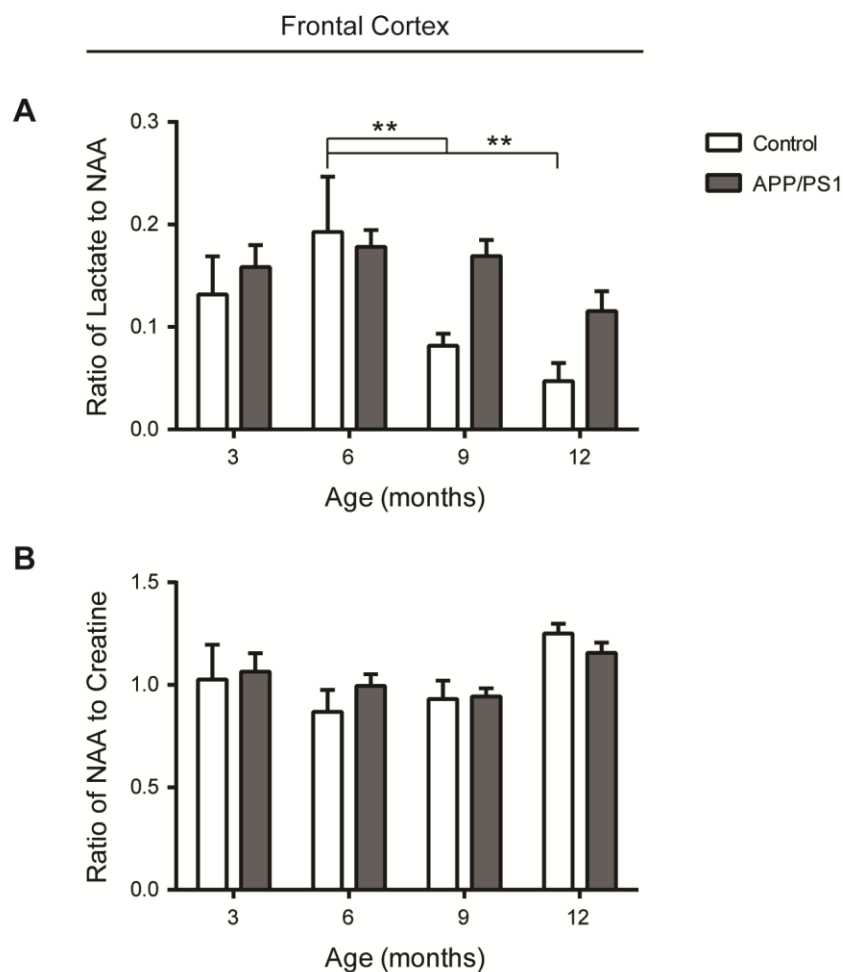
Figure 6. Lactate levels remain unaltered in APP/PS1 mice from 3 to 12 months of age, but decline in aged control mice.

(A) ^{1}H-MRS spectra were quantified and average lactate levels in the frontal cortex from 3 to 12 months of age were expressed as a ratio to total NAA for control mice and APP/PS1 mice. (B) Quantification of average NAA levels in the frontal cortex expressed as a ratio to total creatine for control mice and APP/PS1 mice. Data are shown as mean + SEM, **$p < 0.01$, $n = 5$ and 12, respectively, for control and APP/PS1 mice at ages 3 - 9 months; $n = 4$ and 3, respectively, for control and APP/PS1 mice at age 12 months.
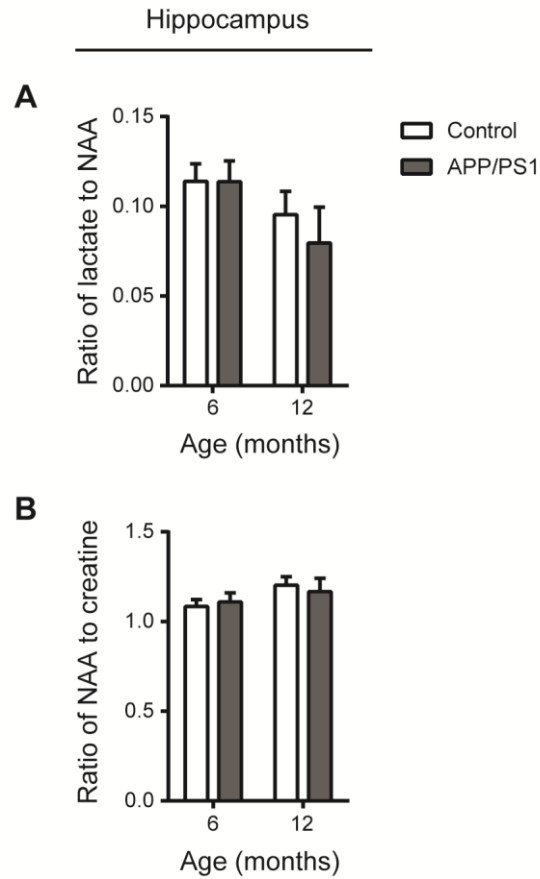
Figure 7. Lactate levels remain constant in the hippocampus over the course of age in both control and APP/PS1 mice.

(A) ^{1}H-MRS spectra were quantified and average lactate levels in the hippocampus at 6 and 12 months of age were expressed as a ratio to total NAA for control mice and APP/PS1 mice. (B) Quantification of average NAA levels in the frontal cortex expressed as a ratio to total creatine for control mice and APP/PS1 mice. Data are shown as mean + SEM, $n = 16$ and 11, respectively, for control and APP/PS1 mice.

To rule out the possibility that the anesthetic isoflurane might influence brain metabolism during MRS analysis, *in vivo* microdialysis was performed in awake, freely moving mice to assess lactate levels in the hippocampal ISF (Figure 8). A one-way ANOVA followed by a Tukey's *post-hoc* test revealed a significant age-dependent rise in lactate levels in APP/PS1 mice from 3 to 18 months of age ($F(2,84) = 20.53$, $p < 0.001$). Furthermore, hippocampal ISF lactate levels were significantly elevated in APP/PS1 mice at 12 months of age compared with control mice as determined by a two-way ANOVA (age × genotype) followed by a Bonferroni's *post-hoc* test ($F(1,75) = 5.870$, $p < 0.05$). These observations reveal an age-dependent elevation in lactate levels within the cortex and hippocampal ISF of APP/PS1 mice compared with control mice.
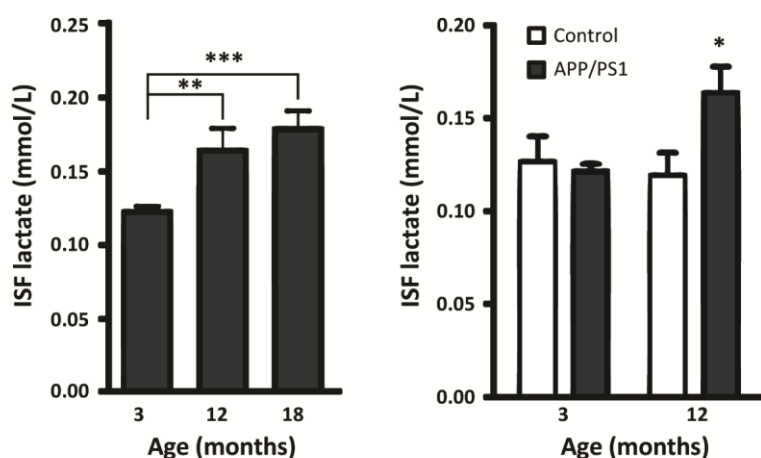
Figure 8. Interstitial lactate levels in the hippocampus are elevated in older APP/PS1 mice.

Hippocampal ISF lactate levels in APP/PS1 mice are significantly elevated at 12 and 18 months of age compared with 3-month-old mice (left). A significant difference in hippocampal ISF lactate levels between control and APP/PS1 mice was detected at 12 months of age (right). *$p < 0.05$, **$p < 0.01$, ***$p < 0.001$. Data are shown as mean + SEM.

3.2 Age-dependent changes in expression of lactate metabolism and transporting proteins in the frontal cortex and hippocampus of APP/PS1 mice

To explore the mechanism by which lactate levels can change in the brain with age, I next examined the expression of proteins responsible for lactate metabolism and transport (Figure 9). Protein extracts from the frontal cortex of control and APP/PS1 mice euthanized at 6 and 12 months of age were resolved by SDS-PAGE and then immunoblotted using the antibodies indicated (Figure 10). The band density was quantified using β-actin as a loading control and measurements were expressed as a ratio of density relative to control mice at 6 months of age (Figure 11). A two-way ANOVA (age × genotype) with a Bonferroni correction for multiple comparisons ($\alpha = 0.00625$) revealed a significant age-dependent decline for proteins involved in lactate metabolism, including the following: PDK1 ($F(1,12) = 39.677$, $p < 0.001$), LDHA ($F(1,12) = 24.008$, $p < 0.001$), and PKM1 ($F(1,12) = 22.118$, $p < 0.001$). An age-dependent decline was observed in several markers of aerobic glycolysis markers, including PDH-p/PDH ($F(1,12) = 9.006$, $p = 0.011$), LDHB ($F(1,12) = 4.720$, $p = 0.050$), and PKM2 ($F(1,12) = 7.168$, $p = 0.020$), yet these did not reach the threshold set by the Bonferroni correction ($\alpha = 0.00625$). In contrast, expression of the lactate transporters was elevated with age: MCT2 ($F(1,12) = 5.590$, $p = 0.036$) and MCT4 ($F(1,12) = 38.685$, $p < 0.001$). A significant effect of genotype was found for PDK1 ($F(1,12) = 9.718$, $p = 0.009$), LDHB ($F(1,12) = 7.960$, $p = 0.015$), PKM1 ($F(1,12) = 5.083$, $p = 0.044$), and MCT4 ($F(1,12) = 6.237$, $p = 0.028$). In addition, a significant interaction between age and genotype was found for PDK1 ($F(1,12) = 13.417$, $p = 0.003$) and PKM1 ($F(1,12) = 5.181$, $p = 0.042$).
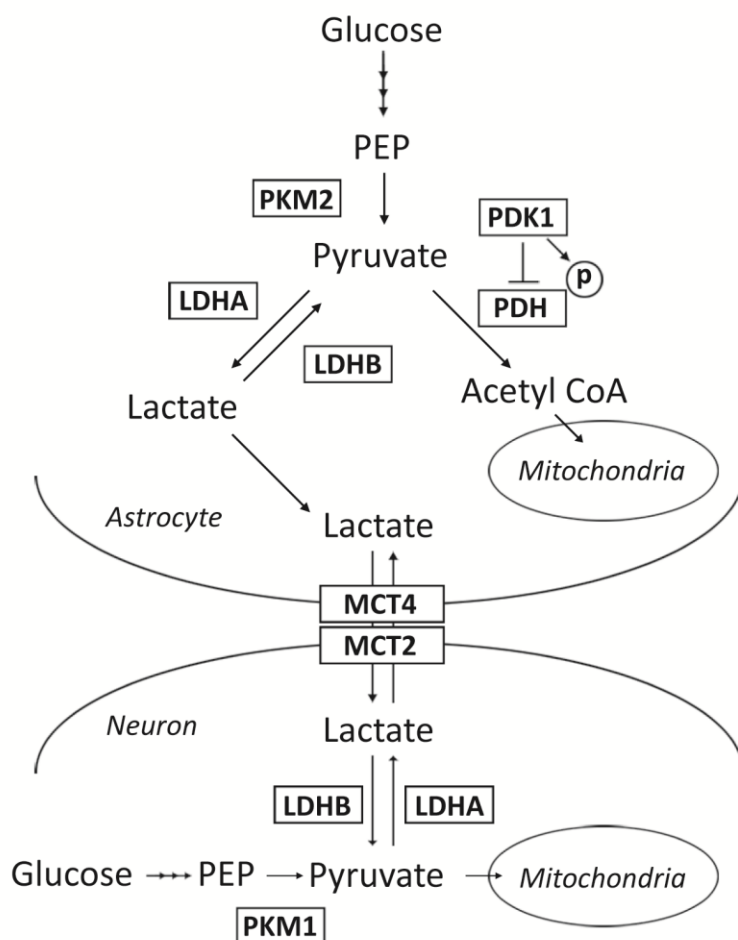
Figure 9. Proposed metabolic pathway of lactate metabolism and transport in the brain.

Glucose is broken down via glycolysis into phosphoenol pyruvate (PEP). PEP is then converted to pyruvate via pyruvate kinase M2 (PKM2) or pyruvate kinase M1 (PKM1). Pyruvate can be metabolized to acetyl-CoA and used as a substrate for oxidative phosphorylation in the mitochondria, or converted to lactate as a by-product of aerobic glycolysis. Pyruvate dehydrogenase kinase 1 (PDK1) phosphorylates and inhibits the pyruvate dehydrogenase complex (PDH), which is responsible for converting pyruvate to acetyl-CoA. Lactate dehydrogenase A (LDHA) converts pyruvate to lactate primarily in astrocytes, while lactate dehydrogenase B (LDHB) catalyzes the reverse reaction of lactate to pyruvate mainly within neurons. Monocarboxylate transporter 4 (MCT4) and monocarboxylate transporter 2 (MCT2) are involved in shuttling lactate between astrocytes and neurons, respectively.
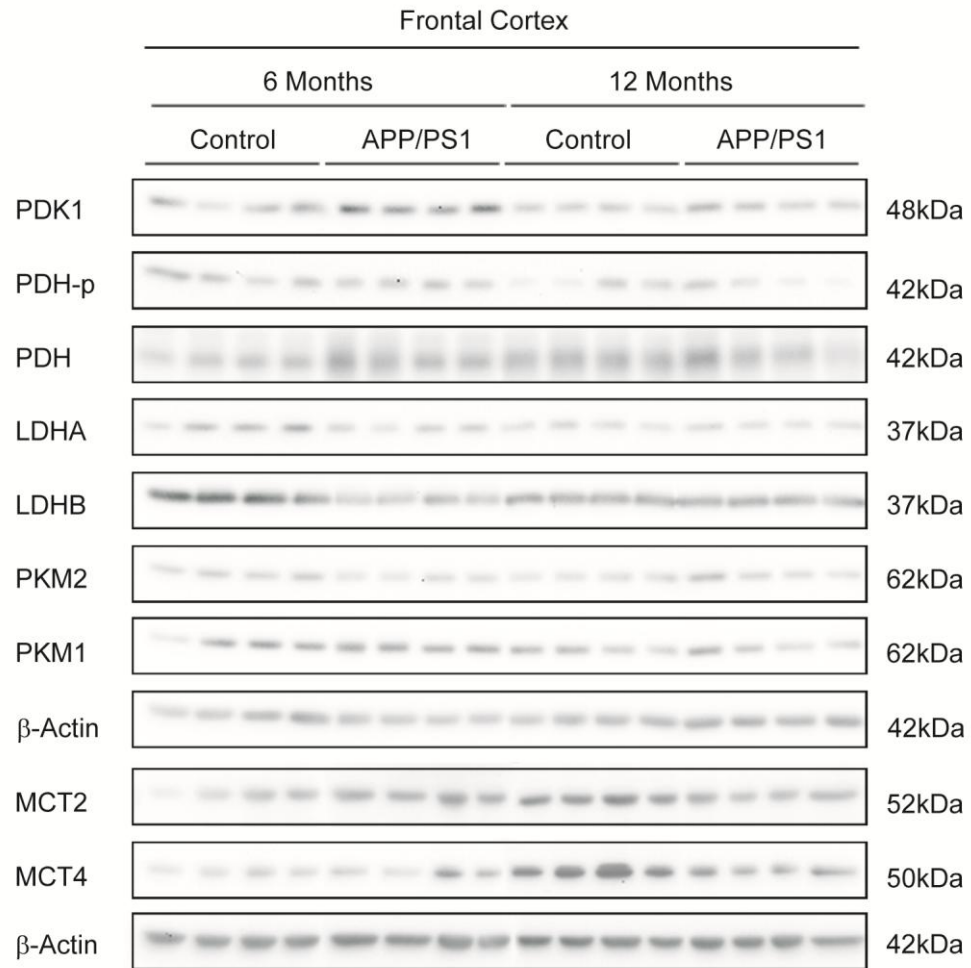
Figure 10. Age-dependent decline in expression of aerobic glycolysis proteins in the frontal cortex.

Western blot analysis of mouse frontal cortex extracts from 6-month-old and 12-month-old control mice and APP/PS1 mice using indicated antibodies as markers of aerobic glycolysis and lactate metabolism. The upper β-Actin panel was used as a loading control for all indicated proteins above this panel whereas the lower β-Actin panel was used as loading control for MCT2 and MCT4 protein levels. $n = 4$ for each set of control mice and APP/PS1 mice at 6 and 12 months of age.
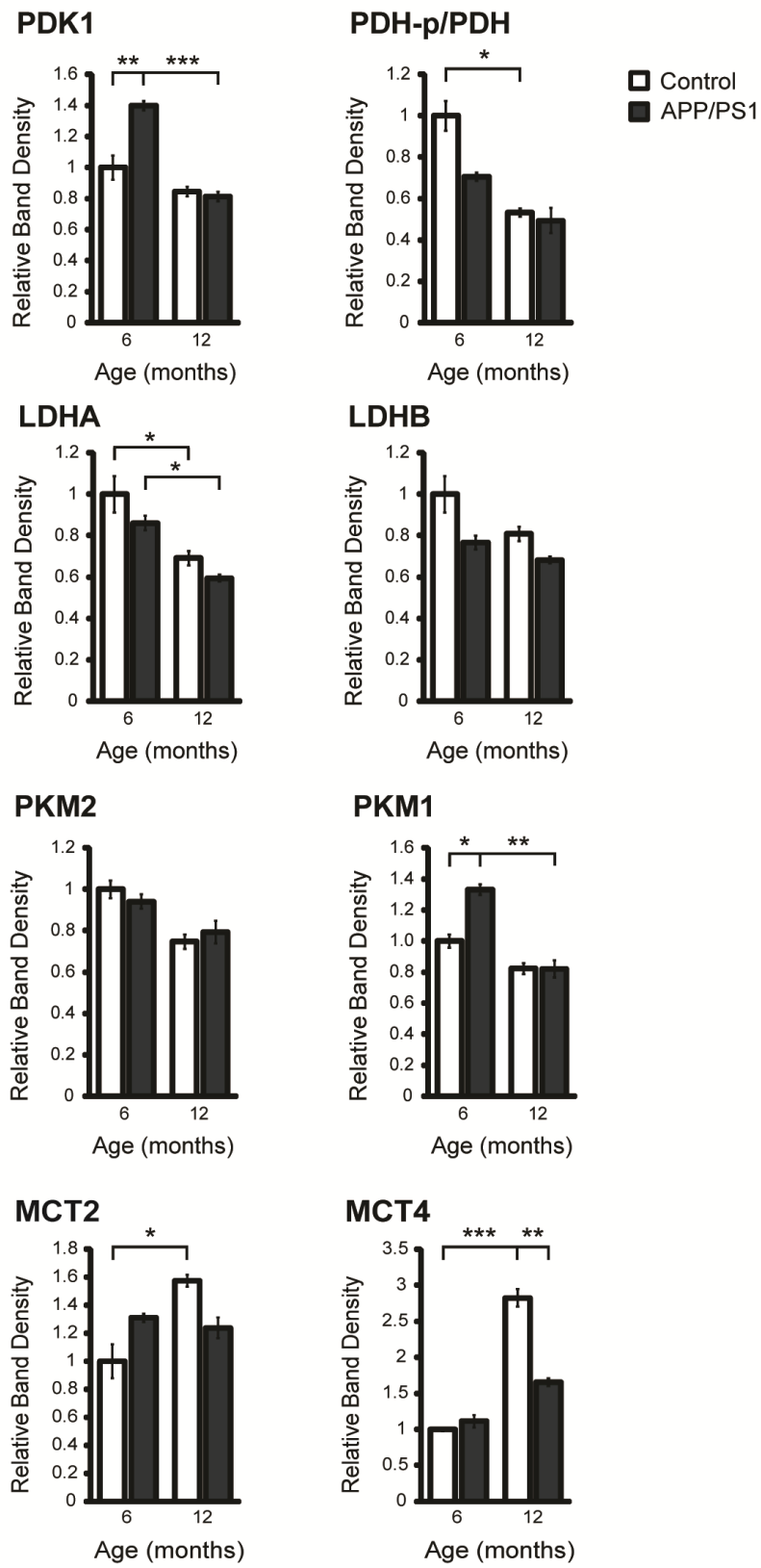
Figure 11. Age-dependent decline in expression of aerobic glycolysis proteins in the frontal cortex: Band densitometry analysis.

Quantification of band densitometry for western blots of extracts from the frontal cortex of 6-month-old and 12-month-old control mice and APP/PS1 mice probed with the indicated antibodies. Relative band density was calculated relative to β-actin. Data are shown as mean ± SEM, $*p < 0.05$, $**p < 0.01$, $***p < 0.001$, $n = 4$ for each set of control mice and APP/PS1 mice at 6 and 12 months old.

Western blot analysis was also performed using extracts from the hippocampus of control and APP/PS1 mice euthanized at 6 and 12 months of age (Figure 12). Band densitometry measurements of proteins involved in lactate metabolism and transport were measured relative to β-actin and a two-way ANOVA (age × genotype) with a Bonferroni correction for multiple comparisons ($\alpha = 0.00625$) (Figure 13). This analysis revealed a significant age-dependent decline in markers of lactate metabolism, including the following: PDH-p/PDH ($F(1,19) = 23.106$, $p < 0.001$), LDHA ($F(1,19) = 28.244$, $p < 0.001$), and PKM1 ($F(1,19) = 20.912$, $p < 0.001$). Interestingly, in contrast to the measurements in the frontal cortex, there was an age-dependent increase in expression of certain lactate metabolism enzymes in the hippocampus including LDHB ($F(1,19) = 19.496$, $p < 0.001$) and PKM2 ($F(1,19) = 13.746$, $p = 0.002$). In contrast to expression patterns in the cortex, a decrease in the lactate transport protein MCT4 ($F(1,19) = 17.068$, $p < 0.001$) was found in the hippocampus of both control and APP/PS1 mice with age. These data indicated that there is an age-dependent change in proteins involved in lactate metabolism and transport in the hippocampus that is distinct from that of the frontal cortex.
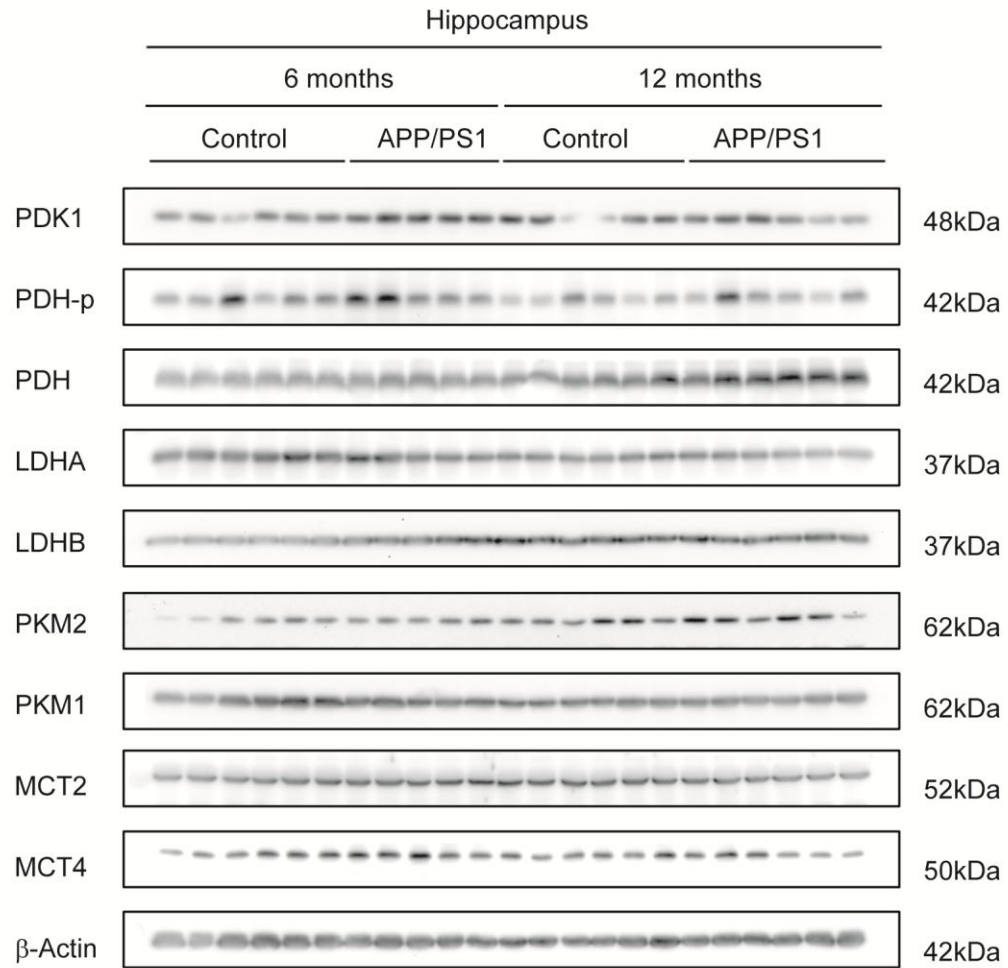
Figure 12. Differential expression of aerobic glycolysis proteins in the hippocampus with age.

Western blot analysis of mouse hippocampal extracts from 6-month-old and 12-month-old control mice and APP/PS1 mice probed with the indicated antibodies. $n = 6$ for each set of control mice and APP/PS1 mice at 6 and 12 months old.
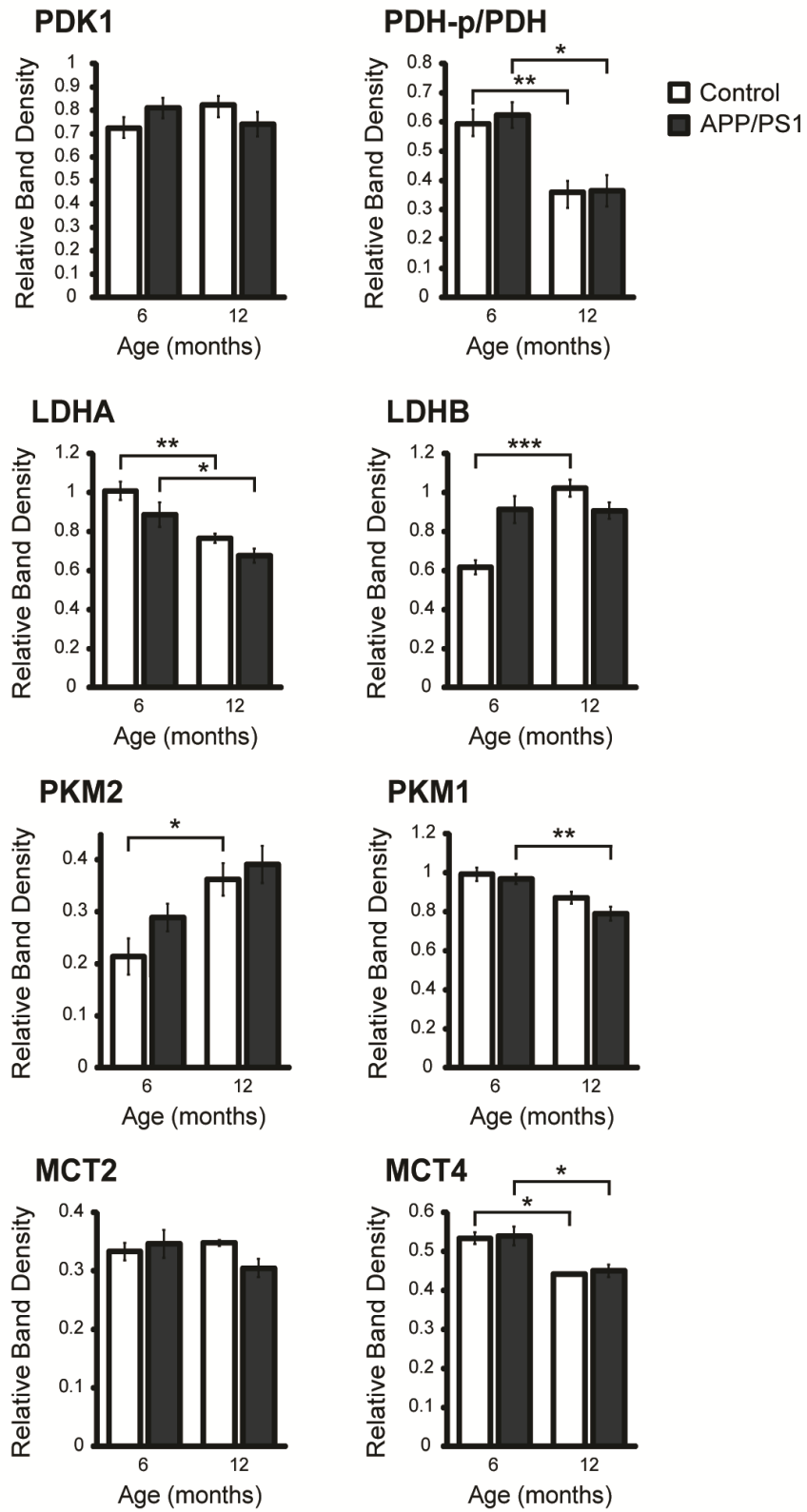
Figure 13. Differential expression of aerobic glycolysis proteins in the hippocampus with age: Band densitometry analysis.

Quantification of band densitometry for western blots of extracts from the hippocampus of 6-month-old and 12-month-old control mice and APP/PS1 mice probed with the indicated antibodies. Relative band density was calculated relative to β-actin. Data are shown as mean ± SEM, *$p < 0.05$, **$p < 0.01$, ***$p < 0.001$, $n = 6$ for each set of control mice and APP/PS1 mice at 6 and 12 months old.

3.3 Correlation analysis of aerobic glycolysis enzyme expression in the frontal cortex and amyloid-β dynamics

Considering that a tight spatial correlation exists between Aβ deposition and areas of high aerobic glycolysis in both the resting normal brain, it has been suggested that aerobic glycolysis may contribute to Aβ processing[262]. In order to determine if aerobic glycolysis influences the production of Aβ, or if the deposition of Aβ influences the expression of aerobic glycolysis enzymes, soluble and insoluble fractions of Aβ were extracted from the frontal cortex of APP/PS1 mice at 12 months of age. The levels of unique Aβ species, $Aβ_{(1-40)}$ and $Aβ_{(1-42)}$, were quantified by ELISA selective for Aβ peptides with C-termini ending at residue 40 or 42, respectively. The average amount of Aβ in each brain extract was calculated as a ratio to total protein and a two-way ANOVA was performed (fraction × Aβ species). This analysis revealed a significant interaction between the type of fraction and Aβ species suggesting that the burden of amyloid in the frontal cortex exists predominantly as insoluble $Aβ_{(1-42)}$ ($F(1,20) = 22.00$, $p < 0.001$) (Figure 14). A multiple linear regression was then performed for relative band density of aerobic glycolysis enzymes and amount of $Aβ_{(1-40)}$ or $Aβ_{(1-42)}$ in either soluble or insoluble fractions (Figure 15). This analysis revealed no correlation between levels of soluble $Aβ_{(1-40)}$ and $Aβ_{(1-42)}$ with expression of aerobic glycolysis proteins: LDHA/LDHB ($R^2 = 0.418$, $p = 0.125$), PDK1 ($R^2 = 0.269$, $p = 0.513$), PDH-p/PDH ($R^2 = 0.352$, $p = 0.220$), and PKM2/PKM1 ($R^2 = 0.512$, $p = 0.055$). The same analysis was performed for relative band density with insoluble Aβ species and revealed no significant correlation with expression of aerobic glycolysis enzymes: LDHA/LDHB ($R^2 = 0.779$, $p = 0.075$), PDK1 ($R^2 = 0.765$, $p = 0.564$), PDH-p/PDH ($R^2 = 0.755$, $p = 0.896$), or PKM/PKM1 ($R^2 = 0.808$, $p = 0.419$). These data suggested that expression of aerobic glycolysis enzymes likely has no influence on the tendency of Aβ peptides to form insoluble species.
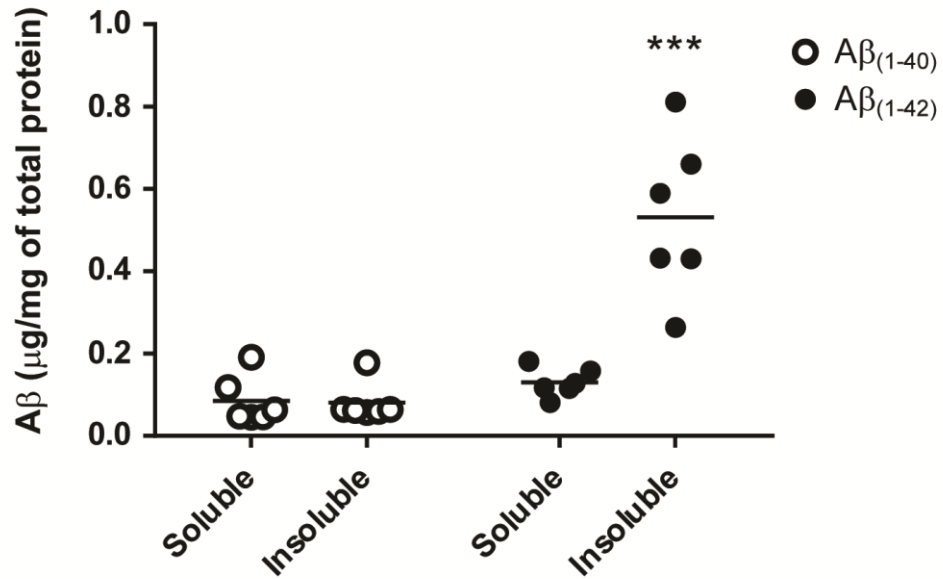
Figure 14. Soluble and insoluble Aβ(1-40) and Aβ(1-42) in the frontal cortex of APP/PS1 mice at 12 months old.

Levels of Aβ(1-40) and Aβ(1-42) were quantified with ELISA using extracts from the frontal cortex of APP/PS1 mice at 12 months old in both soluble and insoluble fractions. Amount of Aβ was expressed as a ratio to the total amount of protein as measured by Lowry assay. Data are shown as individual animals with mean as horizontal line, ***$p < 0.001$, $n = 6$ mice.
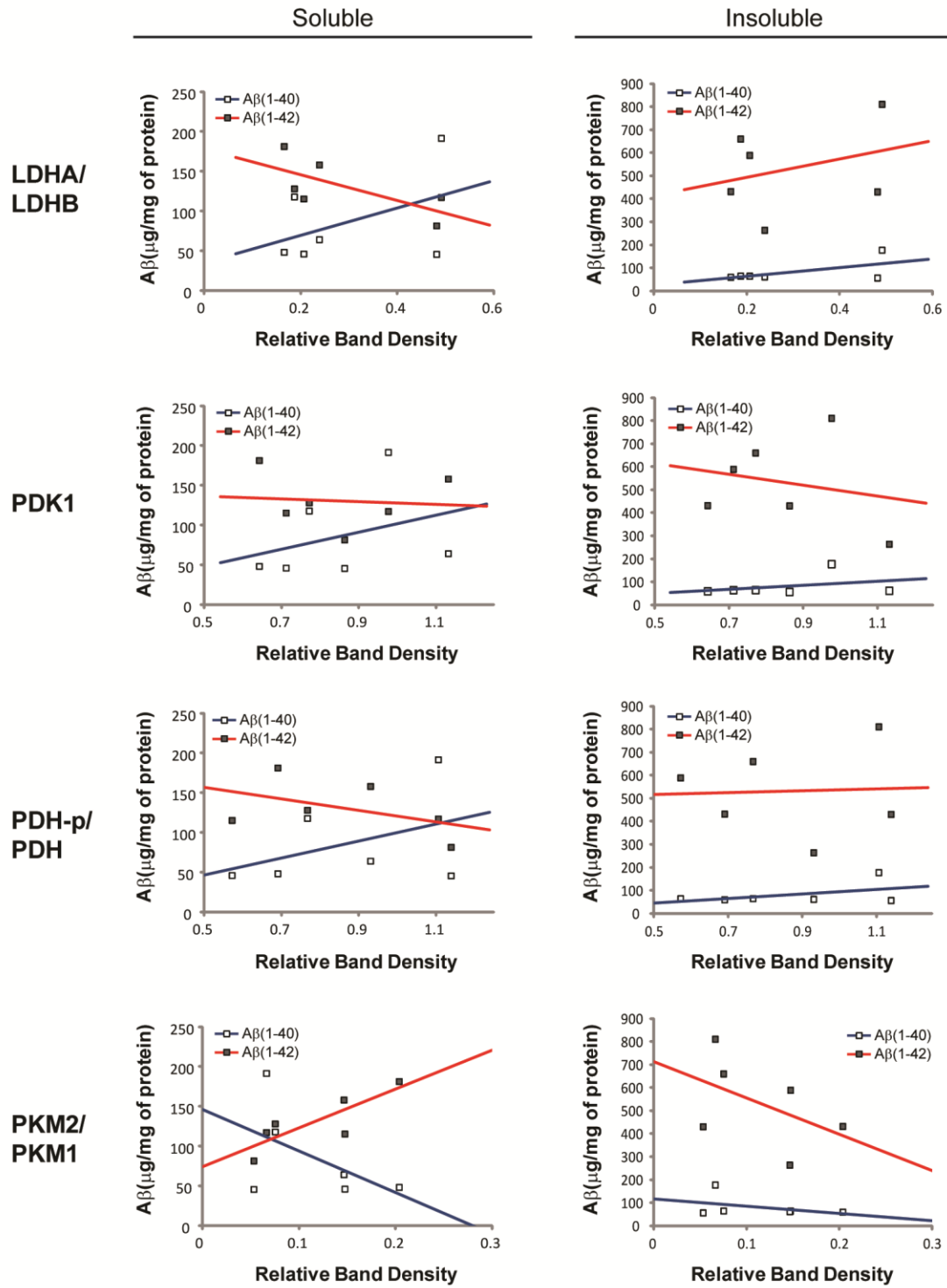
Figure 15. Deposition of Aβ in APP/PS1 mice does not correlate with expression of aerobic glycolysis enzymes.

Levels of $A\beta_{(1-40)}$ and $A\beta_{(1-42)}$ in both soluble (left) and insoluble (right) cortical extracts from APP/PS1 mice at 12 months old were correlated with expression of aerobic glycolysis enzymes: the ratio of LDHA/LDHAB, PDK1, the ratio of phosphorylated-PDH/PDH, and the ratio of PKM2/PKM1. n = 6 mice. No significant associations were detected.

3.4 Determining the cell-specific localization of aerobic glycolysis enzyme expression in control and APP/PS1 mice

To identify which cell types are expressing the enzymes responsible for aerobic glycolysis, frozen brain sections from control and APP/PS1 mice at 12 months of age were immunostained using antibodies specific for PDK1 and LDHA and co-stained with glial fibrillary acidic protein (GFAP) antibodies for reactive astrocytes and Class III β-Tubulin (TUJ1) for neurons. The sections were also stained with Thioflavin S (ThioS), which stains amyloid plaques. Within the frontal cortex of control mice, PDK1 and LDHA were exclusively expressed in the soma of TUJ1+ neurons (Figure 16). Within the frontal cortex of APP/PS1 mice, the expression of PDK1 and LDHA were observed primarily in the soma of TUJ1+ neurons and also in GFAP+ reactive astrocytes surrounding amyloid plaques. The same staining pattern was observed within the dentate gyrus of the hippocampus: PDK1 and LDHA expression was limited to the soma of TUJ1+ neurons in control mice and expression also observed in GFAP+ reactive astrocytes surrounding amyloid plaques in APP/PS1 mice (Figure 17). These observations indicate that PDK1 and LDHA are expressed primarily in the cell bodies of neurons, suggesting that this cell type is also capable of producing lactate through aerobic glycolysis.

Frontal Cortex

Control
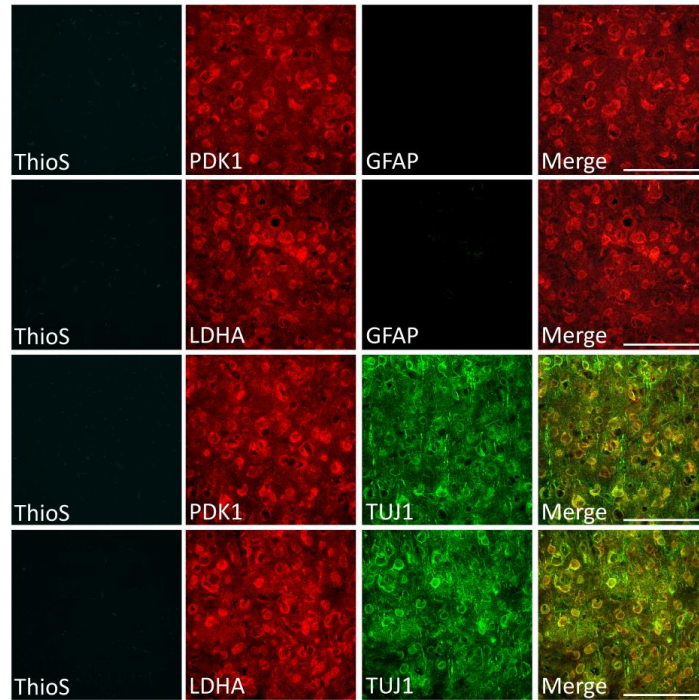
APP/PS1
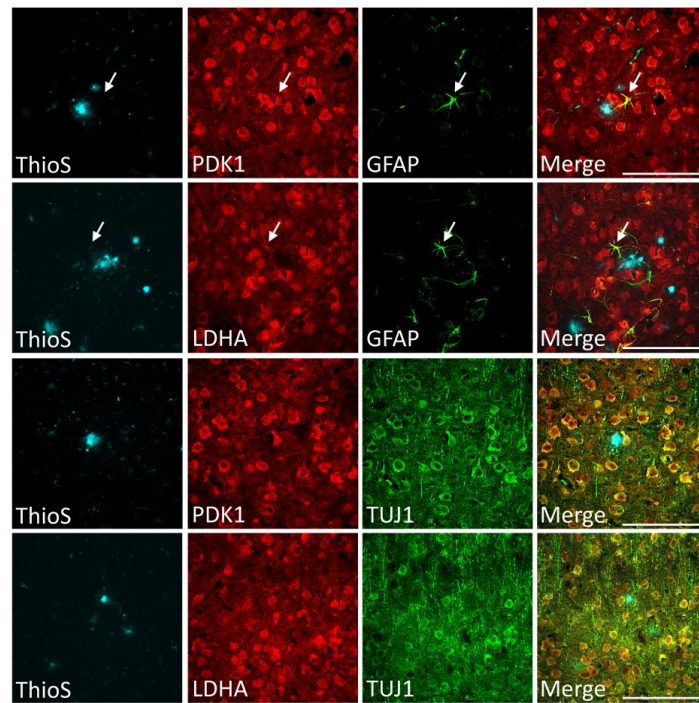
Figure 16. PDK1 and LDHA are expressed in neurons of the frontal cortex of control and APP/PS1 mice and astrocytes co-localized to Aβ plaques of APP/PS1 mice.

Fluorescence micrographs of the frontal cortex in control mice (top) and APP/PS1 mice (bottom) at 12 months old. Thioflavin S was used to visualize Aβ plaque deposits (blue), while immunofluorescence was used to colocalize expression of PDK1 (red) and LDHA (red) with markers for astrocytes (GFAP +, green) and neurons (TUJ1 +, green). Merged images indicate that PDK1 and LDHA are primarily expressed in the soma of neurons in control mice and also in reactive astrocytes surrounding Aβ plaques of APP/PS1 mice (bottom). White arrows indicate co-localized expression of PDK1 and LDHA in cortical GFAP + cells in APP/PS1 mice. Scale bar, 100 μm.

Dentate Gyrus

Control
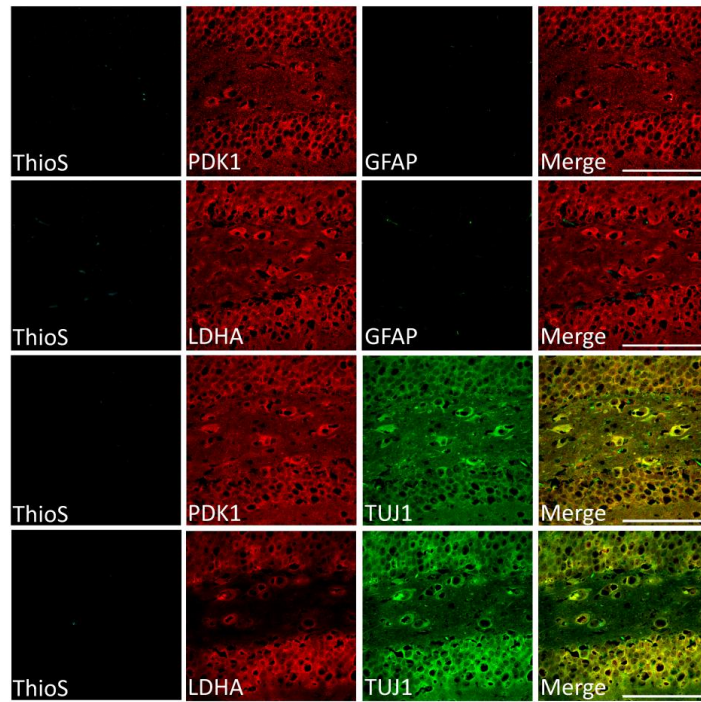
APP/PS1
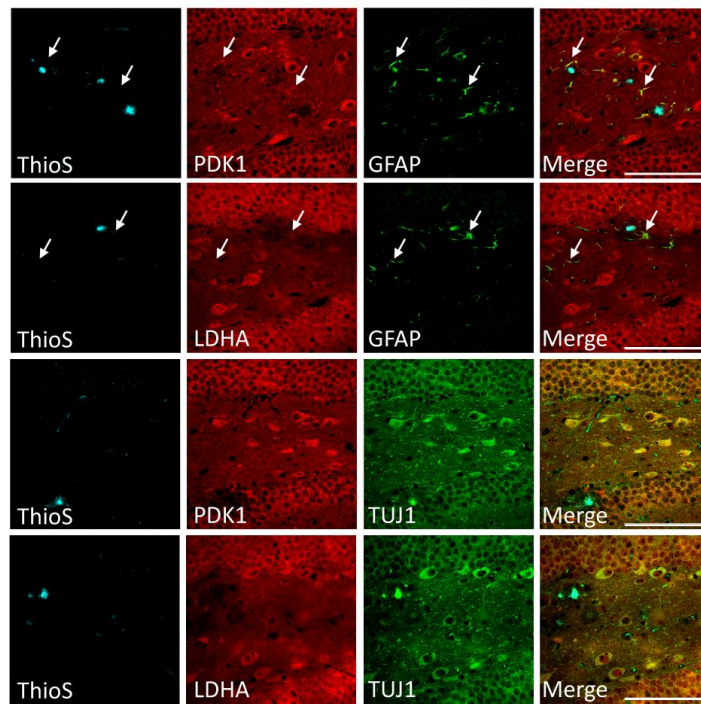
Figure 17. PDK1 and LDHA are expressed in both neurons and astrocytes co-localized to Aβ plaques in the dentate gyrus of the hippocampus.

Fluorescence micrographs of the dentate gyrus of the hippocampus in control mice (top) and APP/PS1 mice (bottom) at 12 months old. Thioflavin S was used to visualize Aβ plaque deposits (blue), while immunofluorescence was used to colocalize expression of PDK1 (red) and LDHA (red) with markers for astrocytes (GFAP +, green) and neurons (TUJ1 +, green). Merged images indicate that PDK1 and LDHA are primarily expressed in the soma of neurons in control mice and also in reactive astrocytes surrounding Aβ plaques of APP/PS1 mice (bottom). White arrows indicate co-localized expression of PDK1 and LDHA in cortical GFAP + cells in APP/PS1 mice. Scale bar, 100 μm.

3.5 Determining the age of onset for visual-spatial memory deficit in APP/PS1 mice

The MWM was used as a test of visual-spatial learning and memory at 12 months of age. Control mice and APP/PS1 mice were evaluated on their ability to learn the location of a hidden platform in the North-West quadrant of the water tank over the course of 4 training days with 4 trials per day (Figure 18A). The latency time to find the platform was measured as an average of the 4 trials for each mouse and a two-way ANOVA with repeated measures (training day × genotype) was performed. This analysis revealed a significant effect of training day on the ability of mice to find the platform ($F(3,72) = 20.08$, $p < 0.001$), but there was no significant effect with genotype ($F(3,72) = 2.709$, $p = 0.1128$), or the interaction between training day and genotype ($F(3,72) = 0.114$, $p = 0.952$). This analysis revealed that there is no difference between control mice and APP/PS1 mice in their ability to learn the location of the hidden platform during training. On the fifth day of testing, the hidden platform was removed and a probe trial was performed in which mice were allowed to swim for 60 seconds. The swim path of each mouse was used to compile a heat map representation of swimming behavior of each group of control and APP/PS1 mice during the probe trial (Figure 18B). The total distance covered during the probe trial was measured in order to determine if genotype had an effect on the physical ability of mice to swim in the tank of water (Figure 18C). A Welch's t-test revealed no significant effect on total distance covered ($t(21) = 1.516$, $p = 1.445$). The ability of mice to remember the location of the platform was assessed as the percent time spent in the correct quadrant (Figure 18D). A Welch's t-test revealed a significant effect between genotypes ($t(21) = 2.688$, $p = 0.007$), which indicated that APP/PS1 mice have worse memory performance than control mice at 12 months of age. After the probe trial, a flag trial was performed to assess the ability of mice to use a visual cue to find the platform. Mice were allowed to swim in the tank for 90 seconds and the latency to find the flag-marked platform was recorded (Figure 18E). A Welch's t-test revealed no significant effect between genotypes ($t(22) = 1.301$, $p = 0.207$), which indicated that both control mice and APP/PS1 mice were able to use the flag as a visual cue to determine the location of the hidden platform.
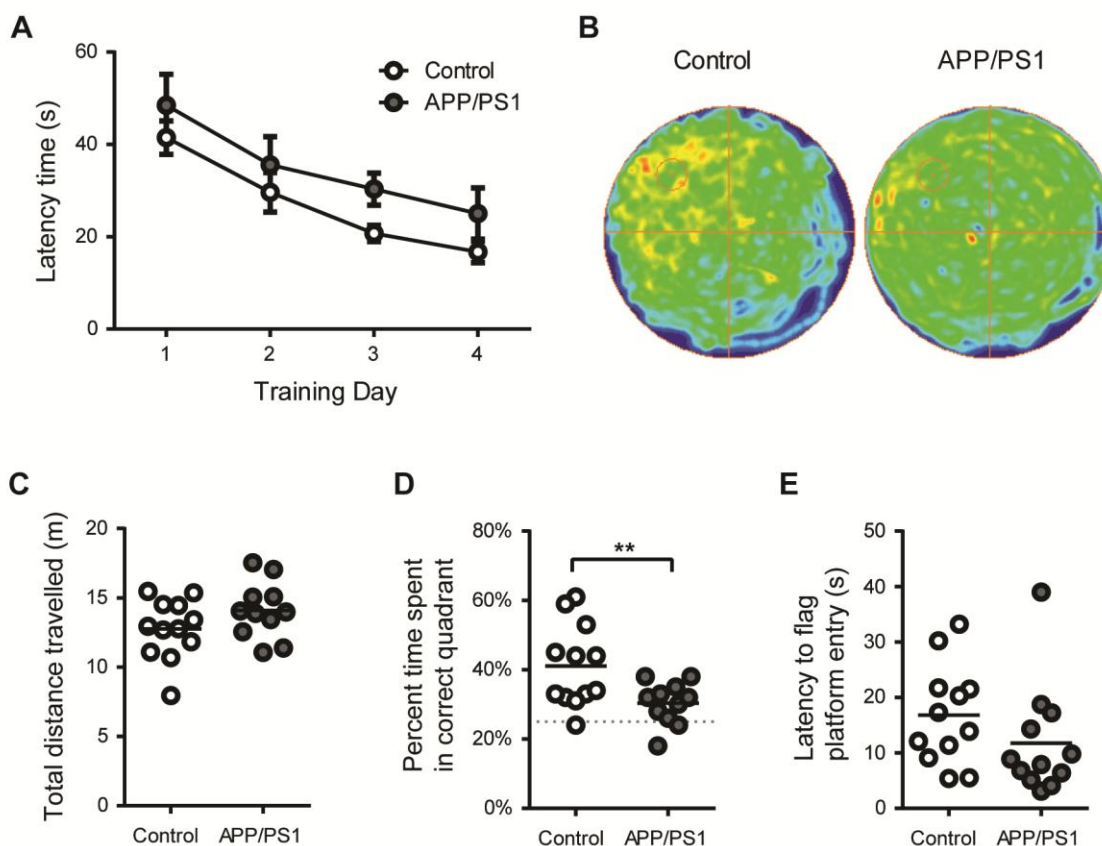
Figure 18. APP/PS1 mice have impaired visual-spatial memory at 12 months of age.

Memory performance in control mice and APP/PS1 mice at 12 months of age was assessed using the Morris water maze. (A) Mice were trained for 4 consecutive days to find the location of a hidden platform in the NW quadrant and the latency to escape was recorded. On day 5 a probe trial was performed in which the platform was removed and mice were allowed to swim for 60 seconds (B-E). (B) The swim path for each group of mice was recorded and compiled into heat map representations. Measurements were taken for the total distance traveled (C) and the percentage of time spent in the correct quadrant (D). Immediately after the probe trial, a flag trial was performed to assess the ability of mice to use visual cues to find the platform. The platform was placed back in to the tank in the opposite quadrant and the latency to find the flag was recorded (E). Data shown are mean ± SEM, **$p < 0.01$, $n = 12$ and 11 for control and APP/PS1 mice, respectively.

3.6 Correlation analysis of aerobic glycolysis enzyme expression and memory performance in APP/PS1 mice at 12 months of age

To determine whether aerobic glycolysis in the frontal cortex affects memory, the expression of aerobic glycolysis enzymes in the frontal cortex was compared with individual performances in the MWM at 12 months of age (Figure 19). A one-way ANCOVA was conducted on the linear regression of relative band density and percent time spent in the correct quadrant, controlling for genotype. This analysis revealed that genotype was a significant covariate for the enzymes involved in lactate production: LDHA ($F(1,9) = 12.467$, $p = 0.008$), PDH-p/PDH ($F(1,9) = 5.588$, $p = 0.046$), and PKM2/PKM1 ($F(1,9) = 7.119$, $p = 0.028$). This suggests that higher expression of these proteins correlates with better memory performance in control mice and worse performance in APP/PS1 mice. Genotype was not a significant covariate for the linear regression of LDHB expression on memory performance ($F(1,9) = 2.161$, $p = 0.180$). These data suggest that metabolism toward lactate production in the frontal cortex may be beneficial for memory processes in control mice and may in fact be detrimental to APP/PS1 mice.
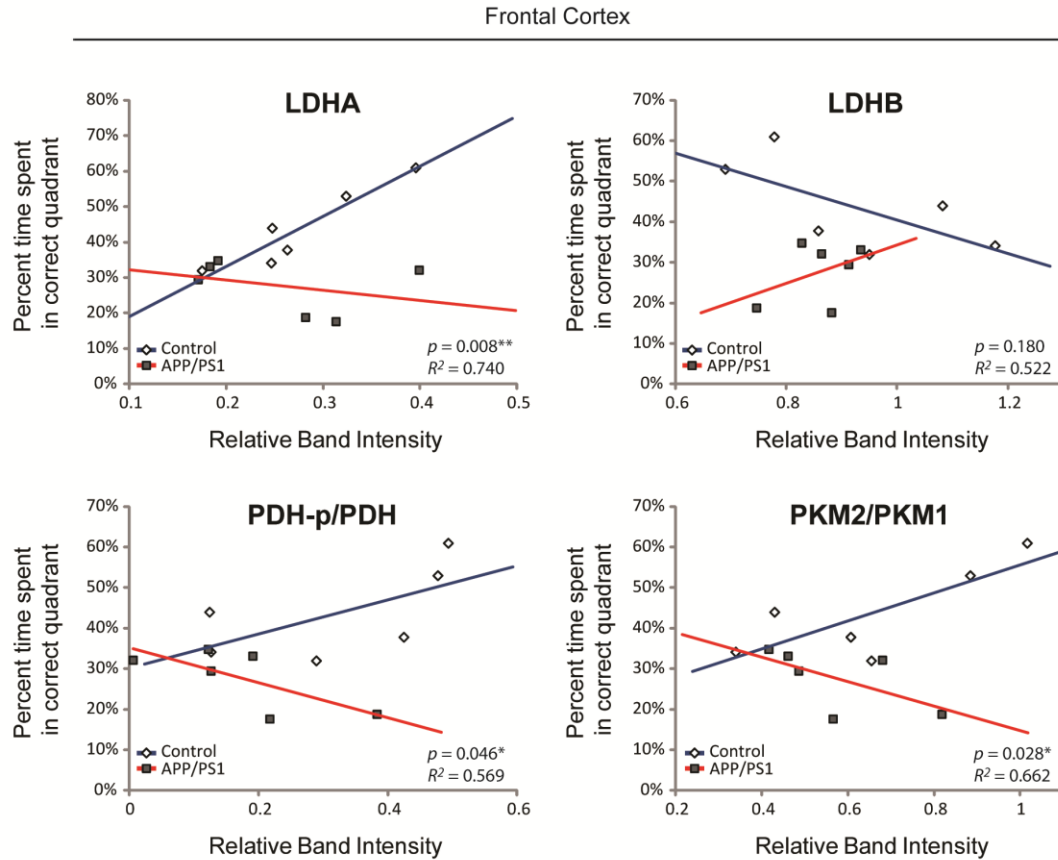
Frontal Cortex

Figure 19. Inverse relationship between expression of aerobic glycolysis enzymes in the frontal cortex and memory performance in APP/PS1 mice.

Memory performance in the Morris water maze, as measured by percent time spent in the correct quadrant during the probe trial, was correlated with the expression of aerobic glycolysis enzymes in the frontal cortex of both control mice and APP/PS1 mice at 12 months of age. Higher expression of enzymes involved in lactate production, including LDHA, the ratio of PKM2/PKM1, and the ratio of phosphorylated-PDH/PDH, correlated with better memory performance in control mice, but not for APP/PS1 mice. Higher expression of LDHB, the enzyme that catalyzes the reverse reaction of LDHA, correlated with decreased memory performance for control mice, but an increase in memory performance for APP/PS1 mice. $*p < 0.05$, $**p < 0.01$, $n = 6$ for each group of control and APP/PS1 mice.

A similar analysis examining the relationship between expression of aerobic glycolysis enzymes and memory was performed on extracts from the hippocampus (Figure 20). A one-way ANCOVA was conducted on the linear regression of relative band density and percent time spent in the correct quadrant, controlling for genotype. This analysis revealed that genotype was not a significant covariate for any of the markers of lactate metabolism: LDHA (R^2 = 0.374, p = 0.073), LDHB (R^2 = 0.148, p = 0.738), PDH-p/PDH (R^2 = 0.141, p = 0.416), and PKM2/PKM1 (R^2 = 0.168, p = 0.737). Altogether, these data indicate that aerobic glycolysis in the frontal cortex, and the concomitant production of lactate, may play a key role in memory processes. In contrast, the role of lactate metabolism in the hippocampus is less clearly defined.

Hippocampus
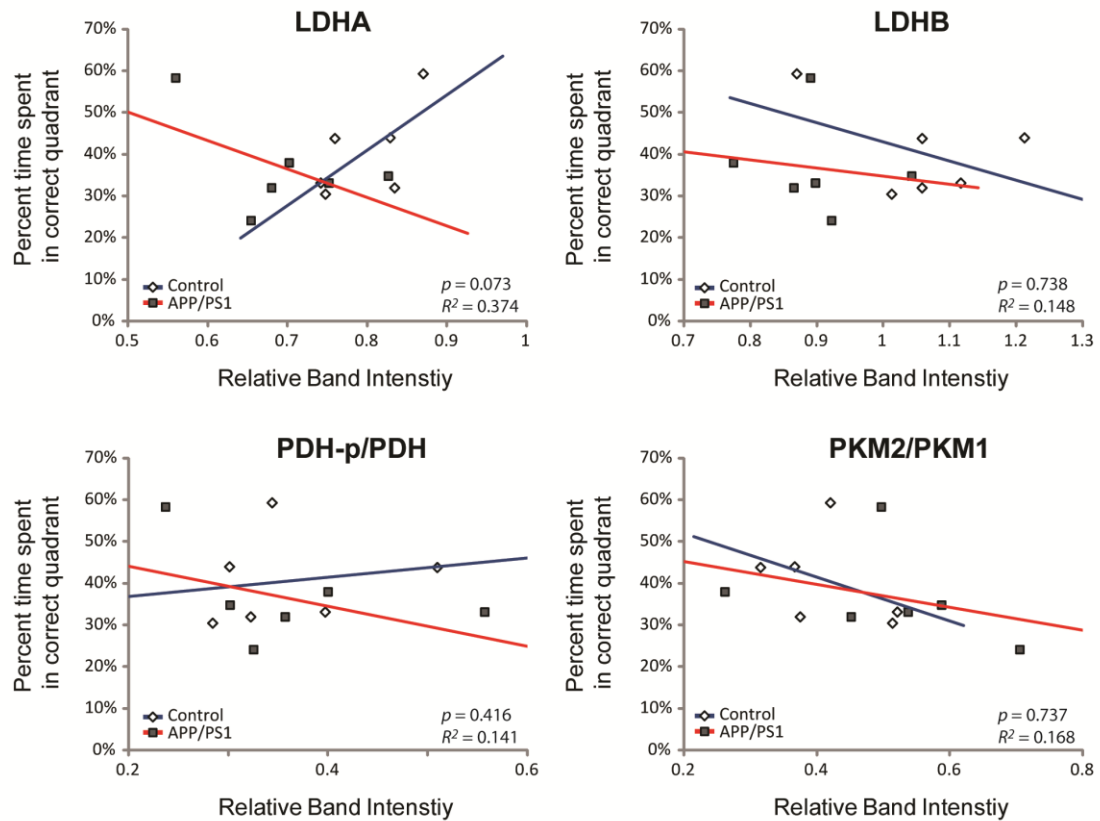
Figure 20. Correlation analysis between expression of aerobic glycolysis enzymes in the hippocampus and memory performance in APP/PS1 mice.

Memory performance in the Morris water maze, as measured by percent time spent in the correct quadrant during the probe trial, was correlated with the expression of aerobic glycolysis enzymes in the hippocampus of both control mice and APP/PS1 mice at 12 months old. $n = 6$ for each group of control mice and APP/PS1 mice. No significant interactions were detected.

3.7 Examining the effect of chronic oral administration of dichloroacetate on memory at 12 months of age

Dichloroacetate (DCA) is a chemical inhibitor of PDK and is used in the treatment of congenital lactic acidosis[492]. DCA-mediated inhibition of PDK results in increased PDH activity and more glycolytic flux through the mitochondria with a concomitant decrease in lactate production[239]. Animal and clinical experiments indicate that a single oral dose of DCA has excellent bioavailability and can induce a lactate-lowering effect within 30 minutes of administration[492]. In order to determine if DCA caused an effect on the memory performance, mice were exposed to 200 mg/kg of DCA in the drinking water from the time of weaning to 12 months of age when they were memory tested with the MWM. During the training phase of the MWM, mice were tasked with finding the location of a hidden platform in one of the quadrants of the tank. Mice were given 4 trials a day over 4 consecutive training days and the average time required to find the platform for each day was recorded (Figure 21A). A two-factor repeated measures ANOVA (genotype x treatment) was performed and revealed no significant interaction between genotype, treatment, and training day ($F(3,123) = 0.106$, $p = 0.370$). This indicated that the DCA in the drinking water did not have a preferential effect on one genotype over another in their ability to learn the location of the platform over the course of four training days. There was no effect from the interaction between treatment and training day ($F(3,123) = 0.038$, $p = 0.999$), indicating that DCA had no effect on mice of either genotype to learn the location of the platform. There was also no effect between genotype and training day ($F(3,123) = 1.046$, $p = 0.375$), indicating that control mice did not learn the location of the platform any faster than APP/PS1 mice. This analysis did reveal a significant effect from training day ($F(3,123) = 35.743$, $p < 0.001$), demonstrating that all mice from both genotypes and treatments found the platform faster over the course of four training days. In addition, there was a significant effect from genotype ($F(1,41) = 8.258$, $p = 0.006$), suggesting that APP/PS1 mice took longer to find the platform on average for each training day regardless of DCA treatment. This indicated that the APP/PS1 mice have an impaired ability to learn the location of the platform at 12 months of age.

During the probe trial, the platform was removed from the tank and the mice were given 60 seconds to swim and attempt to find the platform. The swimming path of the animals was recorded along with the time spent in the correct quadrant and the total distance covered during the swim. In order to visualize the memory performance of each group of mice, a heat map analysis was constructed that compiles the swimming path of each mouse into a collective representation of areas covered by the swimming group (Figure 21B). The percentage of time spent in the correct quadrant was recorded during the probe trial as a measure of memory performance (Figure 21C). A two-way ANOVA (genotype $\times$ treatment) revealed a significant effect of genotype on memory performance ($F(1,37) =$ 10.63, $p = 0.002$), while there was no effect from DCA treatment ($F(1,37) = 0.103$, $p =$ 0.751) or interaction between genotype and treatment ($F(1,37) = 0.028$, $p = 0.867$). This indicated that chronic DCA treatment had no effect on memory performance for either genotype. The total distance covered during the probe trial was measured to evaluate the physical ability of mice to swim in the MWM (Figure 21D) and a two-way ANOVA (genotype $\times$ treatment) was performed. This analysis revealed no significant difference between genotypes ($F(1,37) = 1.330$, $p = 0.256$) or DCA treatment ($F(1,37) = 0.085$, $p =$ 0.772). These results suggest that the chronic treatment of DCA in the drinking water at 200 mg/kg had no effect on the memory performance of either control or APP/PS1 mice at 12 months of age. Further, the only variable contributing to a difference in memory at this age was genotype of the animals.
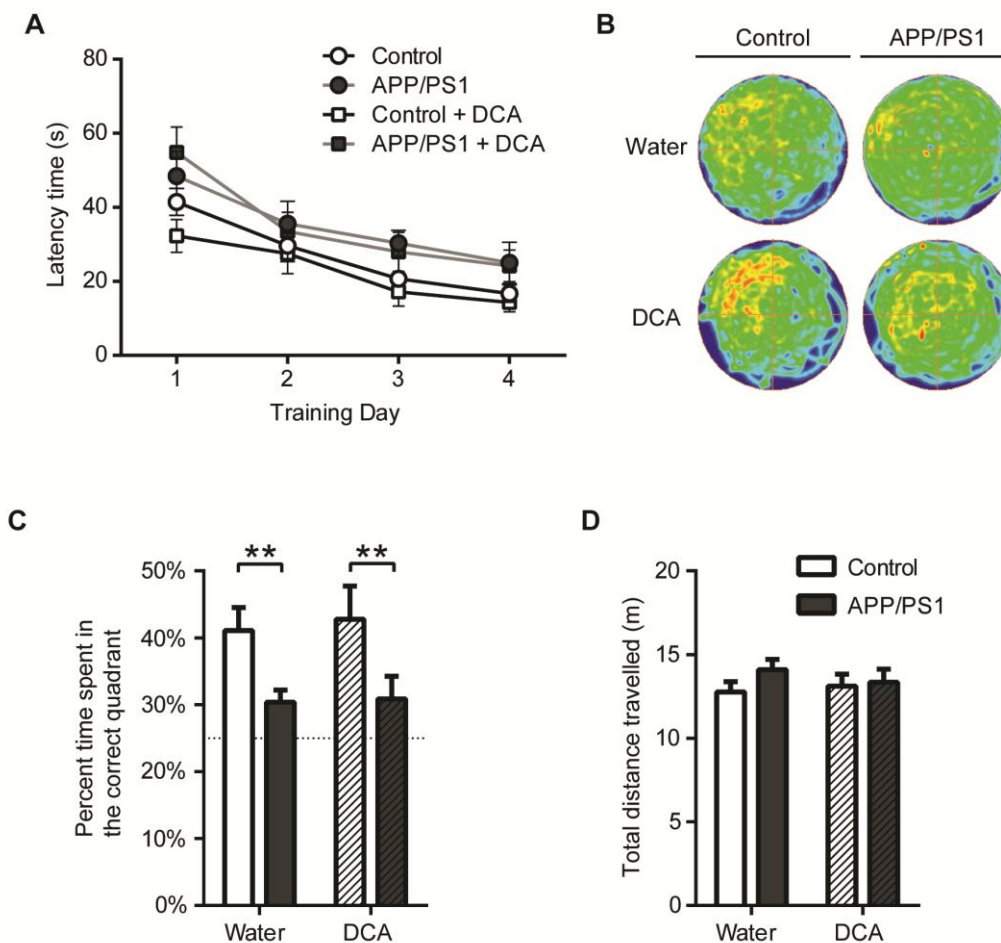
Figure 21. Chronic exposure to dichloroacetate does not affect memory performance at 12 months of age.

Memory performance of 12-month-old control mice and APP/PS1 mice provided either normal water or DCA-water (200 mg/kg) was assessed by the Morris water maze. (A) Mice were trained for 4 consecutive days (4 trials per day) to find the location of a hidden platform in the NW quadrant and the latency to escape was recorded. On day 5 a probe trial was performed in which the platform was removed and mice were allowed to swim for 60 seconds (B-D). (B) The swim path for each group of mice was recorded and compiled into heat map representations. Measurements were taken for the percentage of time spent in the correct quadrant (C) and the total distance traveled (D). The dashed horizontal line at 25% represents the amount of time spent in the correct quadrant by random chance. Data shown are mean $\pm$ SEM, **$p < 0.01$, $n = 12$ and 11 for control and APP/PS1 mice provided normal water, respectively, and $n = 10$ and 9 for control and APP/PS1 mice provided DCA water, respectively.

3.8 Determining the effect of chronic oral dichloroacetate administration on PDH phosphorylation in the brain

Although short-term oral administration of DCA has been shown to diminish cortical lactate levels[493], the effect of chronic oral DCA administration on PDH phosphorylation and metabolism in the brain has never been examined. The expression of aerobic glycolysis enzymes was examined at 12 months of age by western blot analysis in the frontal cortex of control mice provided either normal water or DCA-water (Figure 22). Band densitometry analysis was then performed (Figure 23) and a Welch's t-test (treatment) revealed no significant effect on the ratio of phosphorylated-PDH to total PDH ($t(12) = 0.204$, $p = 0.842$), or the protein expression of PDK1 ($t(12) = 1.042$), $p = 0.327$), LDHA ($t(12) = 1.480$, $p = 0.167$), LDHB ($t(12) = 1.020$, $p = 0.3348$, PKM2 ($t(12) = 2.081$, $p = 0.060$), or PKM1 ($t(12) = 0.211$, $p = 0.837$). These observations collectively suggest that chronic exposure to 200 mg/kg of DCA in the drinking water had no effect on the phosphorylation level of PDH or the expression of lactate metabolism enzymes at 12 months of age.
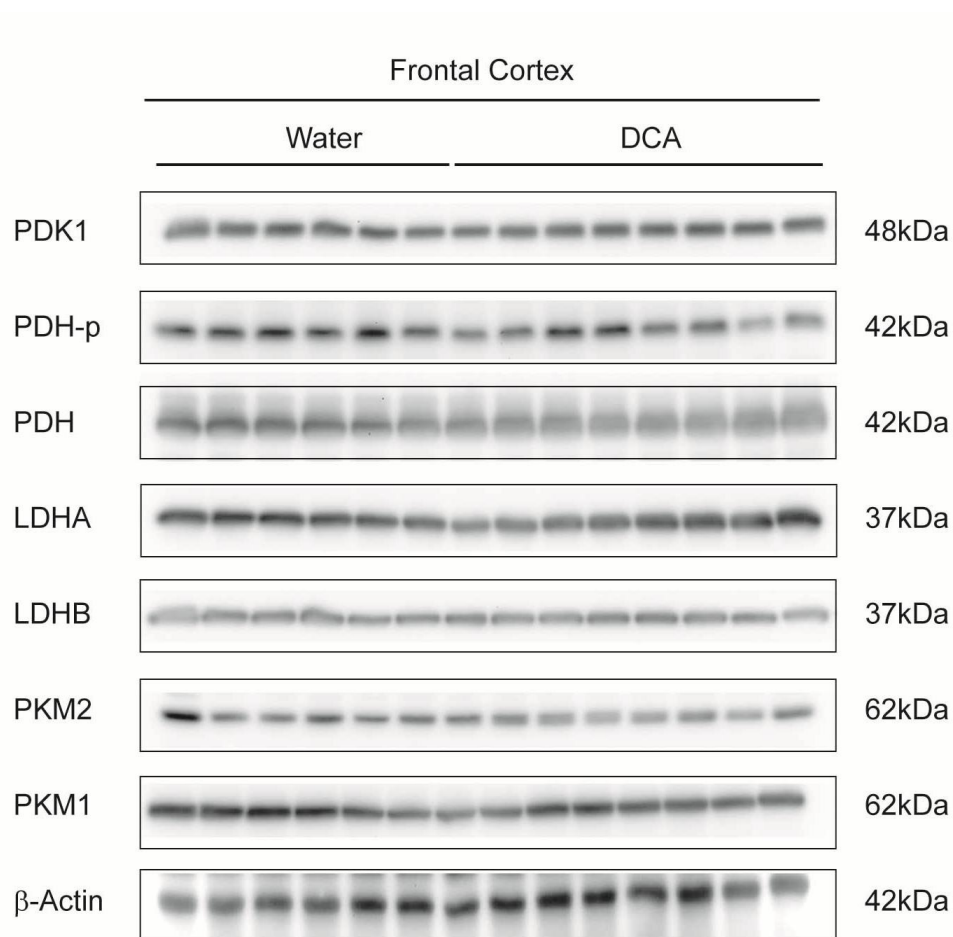
Figure 22. Chronic exposure to dichloroacetate in the drinking water does not affect phosphorylation levels of PDH or expression of aerobic glycolysis enzymes in the frontal cortex of control mice.

Western blot analysis of extracts from the frontal cortex of 12 month old control mice drinking either normal water or DCA water (200 mg/kg) using indicated antibodies as markers of aerobic glycolysis and lactate metabolism. $n = 6$ and 8, respectively, for control mice with normal water and DCA water.
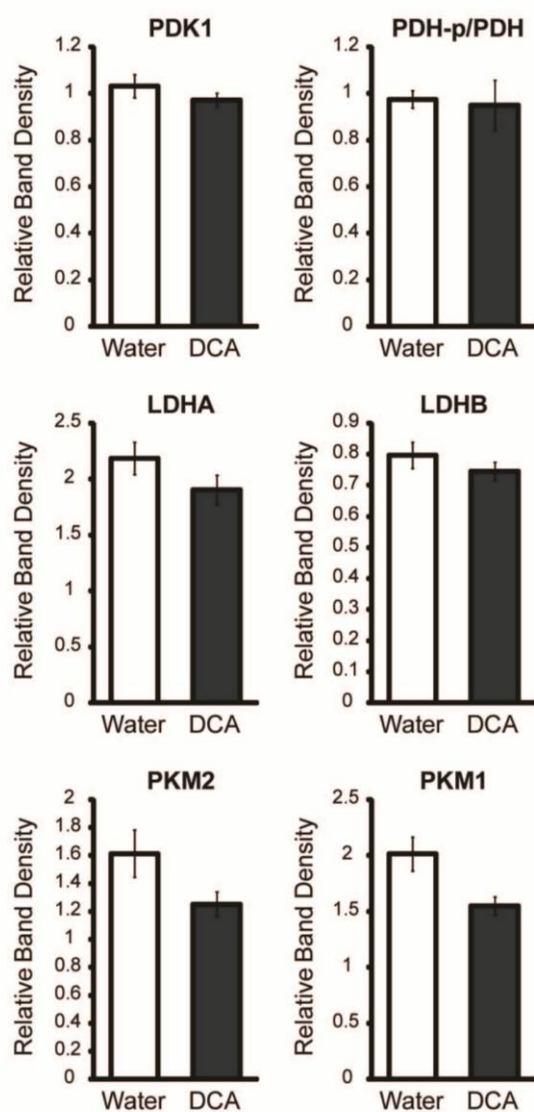
Figure 23. Chronic exposure to dichloroacetate in the drinking water does not affect phosphorylation levels of PDH or expression of aerobic glycolysis enzymes in the frontal cortex of control mice: Band densitometry analysis.

Quantification of band densitometry for western blots of extracts from the frontal cortex of 12 month old control mice drinking either normal water or DCA water (200 mg/kg) using indicated antibodies as markers of aerobic glycolysis and lactate metabolism. Relative band density was calculated relative to β-actin. Data are shown as mean ± SEM, *n* = 6 and 8, respectively, for control mice with normal water and DCA water.

3.9 Determining the effect of acute dichloroacetate injection on PDH phosphorylation in the brain

Due to the inability of chronic oral administration of DCA to inhibit PDH phosphorylation, alternative strategies were considered to deliver chemical inhibitors. I decided to perform an acute injection of both Isosafrol and DCA. Isosafrol is a specific inhibitor of LDHA that has been shown to cross the blood-brain barrier and prevent chemically induced seizures in mice[491]. To determine if acute exposure to DCA had an effect on brain metabolism, the expression of aerobic glycolysis enzymes was examined at 17 - 18 months of age by western blot analysis in the frontal cortex of control mice injected with either saline or DCA (200 mg/kg) 30 minutes before euthanization (Figure 24A). Band densitometry analysis was then performed and expressed as standardized ratio to saline-injected mice relative to β-actin (Figure 24B). A Welch's t-test revealed a significant effect on the ratio of phosphorylated-PDH to total PDH at Serine-232 ($t(10) = 9.083$, $p < 0.001$) and Serine-293 ($t(10) = 16.261$, $p < 0.001$) in DCA-injected mice compared to saline-injected mice. This analysis also revealed a significant effect of treatment on PDK1 levels ($t(10) = 2.837$), $p = 0.018$). These data indicated that intraperitoneal injection of DCA at 200mg/kg inhibited phosphorylation of PDH in the frontal cortex. In addition, extracts from the hippocampus of mice injected intraperitoneally with either vehicle or Isosafrol were tested for LDHA or LDHB activity with a fluorescence-based enzyme activity assay (Figure 24C). A decrease in LDHA activity was observed in the hippocampus of mice injected with Isosafrol (14.31 ± 1.340 Units/mg) as compared to mice injected with vehicle (21.23 ± 4.712 Units/mg). A Welch's t-test revealed that this difference was not significant ($p = 0.09$). Injection of Isosafrol caused no difference in LDHB activity ($p = 0.405$). These findings demonstrate that both DCA and Isosafrol affect their protein targets in the brains of mice within 30 minutes of injection.
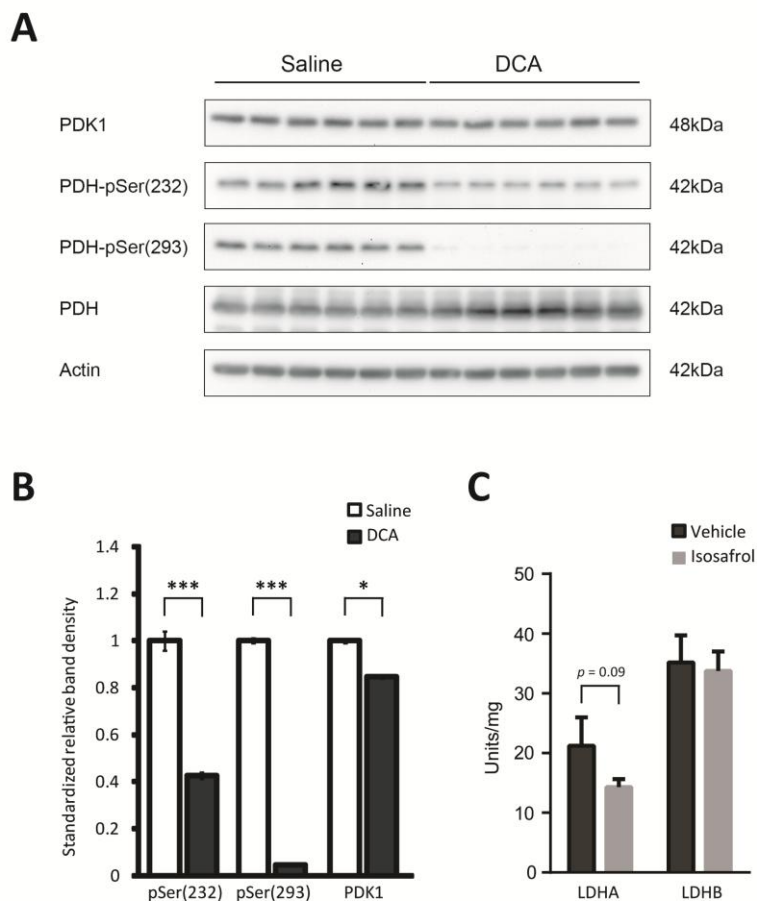
Figure 24. Acute exposure to dichloroacetate decreases phosphorylation of PDH and Isosafrol may alter enzyme activity in the frontal cortex.

(A) Western blot analysis of frontal cortex extracts from 18-month-old control mice euthanized 30 minutes after intraperitoneal injection with either saline or DCA (200 mg/kg). Levels of phosphorylated-PDH at Serine-232 or Serine-293, total PDH, and PDK1 were measured using indicated antibodies. (B) Quantification of band densitometry for western blots of extracts. Relative band density was calculated relative to β-actin. $n = 6$ for each set of saline- and DCA-injected mice. (C) Isosafrol decreases LDHA, but not LDHB activity in the frontal cortex. Mice injected intraperitoneally with either vehicle or Isosafrol (300 mg/kg). After 30 minutes mice were sacrificed, perfused with PBS and brains were snap frozen. Hippocampal extracts were analyzed for LDHA and LDHB activity. $n = 1$ mouse with 6 technical repeats. Data are shown as mean ± SEM, *$p < 0.05$, ***$p < 0.001$.

3.10 Examining the effect of acute Isosafrol and dichloroacetate injection on memory performance

A single cohort of control mice and APP/PS1 mice were assessed using the MWM over the course of 12 to 18 months of age in four consecutive training and probe trial experiments. The location of the platform was moved after each exposure so the mice had to re-learn the location at each training session. All mice were injected with the treatment on the day of the probe trial, 30 minutes before entering the pool. The treatments for each probe trial were as follows: (1) the vehicle of Isosafrol (1% carboxymethylcellulose) with platform location South-East, (2) Isosafrol (300 mg/kg) with platform location North-West, (3) DCA (200 mg/kg) with platform location North-East, and (4) the vehicle of DCA (saline) with platform location South-West. During the training phase, the mice were given 4 trials a day over 4 consecutive days to find the location of the hidden platform and the average latency time for each day was recorded (Figure 25). A one-way ANOVA with repeated measures (genotype x training day) revealed a significant delay in the latency time for APP/PS1 mice to find the platform for the first three training sessions compared to control mice: Vehicle ($F(1,23) = 12.920$, $p = 0.002$), Isosafrol ($F(1,22) = 21.100$, $p < 0.001$), and DCA ($F(1,21) = 5.631$, $p = 0.0273$). However, there was no significant difference in latency times between control and APP/PS1 mice in the fourth training session: Saline ($F(1,16) = 2.185$, $p = 0.159$). This analysis indicated that the APP/PS1 mice were slower at learning to find the platform than the control mice during the first three training periods, yet by the fourth training session they performed equally to control mice. These data suggest that APP/PS1 mice at an age of up to 18 months are capable of learning the location of the platform just as well as control mice following repeated training.
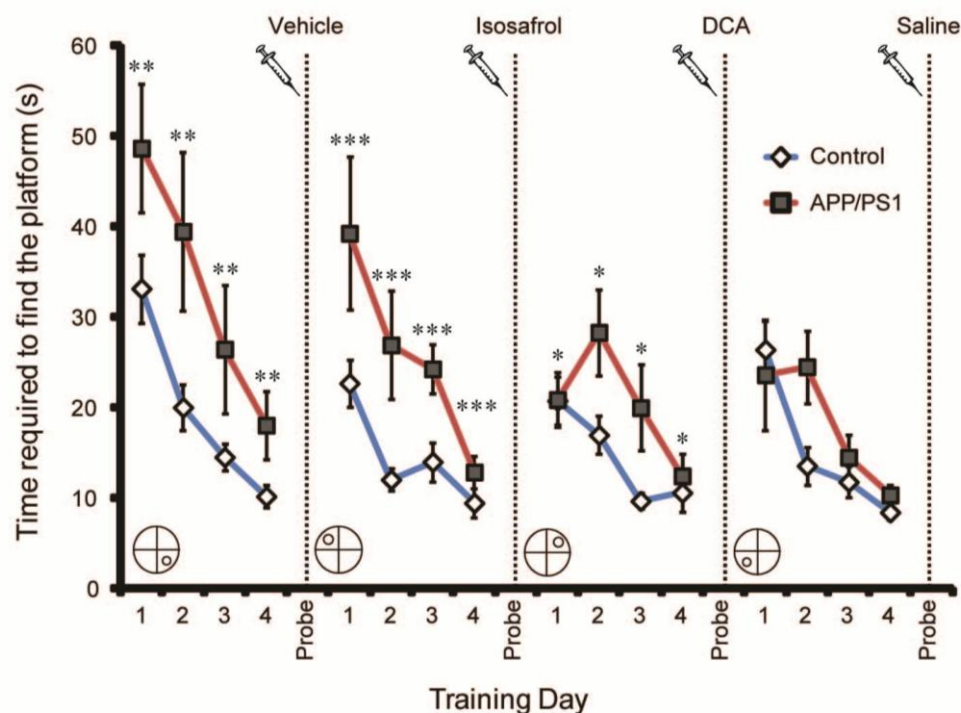
Figure 25. Overview of training program in the Morris water maze for mice treated with Isosafrol and dichloroacetate.

The effect of metabolic inhibitors on memory performance in control mice and APP/PS1 mice starting at 12 months of age was repeatedly tested using the Morris water maze. Mice were given four training trials a day to find the location of a hidden platform in one quadrant of the water tank (position indicated on bottom left of each training phase). On the fifth day, the platform was removed from the tank and a probe trial was performed 30 minutes after intraperitoneal injection of the indicated treatment (indicated by syringe). Mice were given a two week recovery period between training phases and the location of the platform changed for each treatment. Data shown are mean ± SEM, asterisks indicate a significant difference between genotype for a particular training phase as determined by a two-way ANOVA with repeated measures, $*p < 0.05$, $**p < 0.01$, $***p < 0.001$, $n = 17$ and 8, respectively, for control mice and APP/PS1 mice for vehicle phase, $n = 16$ and 8, respectively, for control mice and APP/PS1 mice for Isosafrol phase, $n = 15$ and 8, respectively, for control mice and APP/PS1 mice for DCA phase, and $n = 13$ and 5, respectively, for control mice and APP/PS1 mice for saline phase.

The memory performance of each mouse on the probe trial was then compared over the course of treatments to determine if there was an observable effect from acute exposure to Isosafrol or DCA. The ability of mice to remember the location of the platform was measured as the percent time spent in the correct quadrant (Figure 26A). A two-way ANOVA analysis (genotype × treatment) of the time spent in the correct quadrant revealed a significant effect associated with genotype ($F(1,81) = 4.280$, $p = 0.042$), and treatment ($F(3,81) = 5.651$, $p = 0.001$), as well as the interaction between genotype and treatment ($F(3,81) = 3.453$, $p = 0.021$). In order to compare the memory of control mice over the course of different treatments, a Tukey's *post-hoc* test was performed and revealed no significant difference between vehicle and Isosafrol treatment ($p = 0.236$), but there was a significant difference between vehicle and DCA treatment ($p < 0.001$), as well as the difference between DCA and saline treatment ($p = 0.004$). This analysis revealed no significant difference in memory for control mice between vehicle and saline treatments ($p = 0.999$), which indicated that these mice are just as capable of remembering the location of the platform at an older age than when they started the first training session. Interestingly, the APP/PS1 mice exhibited better memory (43.9% ± 5.4%) than the control mice (37.8% ± 2.0%) with the DCA treatment, although this difference was not significant ($p = 0.698$). This analysis also revealed that memory performance in APP/PS1 mice were unaffected by acute exposure to metabolic inhibitors of aerobic glycolysis. The total distance covered during the probe trial was measured in order to determine if genotype or treatment had an effect on the physical ability of mice to swim in the tank of water (Figure 26B). A two-way ANOVA (genotype × treatment) revealed no significant effect of genotype ($F(1,81) = 0.004$, $p = 0.952$) or treatment ($F(3,81) = 1.606$, $p = 0.195$), or the interaction between genotype and treatment ($F(3,81) = 2.213$, $p = 0.093$) on swimming distance. Thus, neither the genotype nor chemical treatment had any effect on locomotor activity in mice. Altogether, these data collected from the MWM suggested that acute exposure to chemical inhibitors of aerobic glycolysis had a significant effect on the memory performance of control mice, yet had no effect on APP/PS1 mice. Further, acute exposure to DCA appeared to exert a more pronounced effect on memory processes than Isosafrol in control mice.
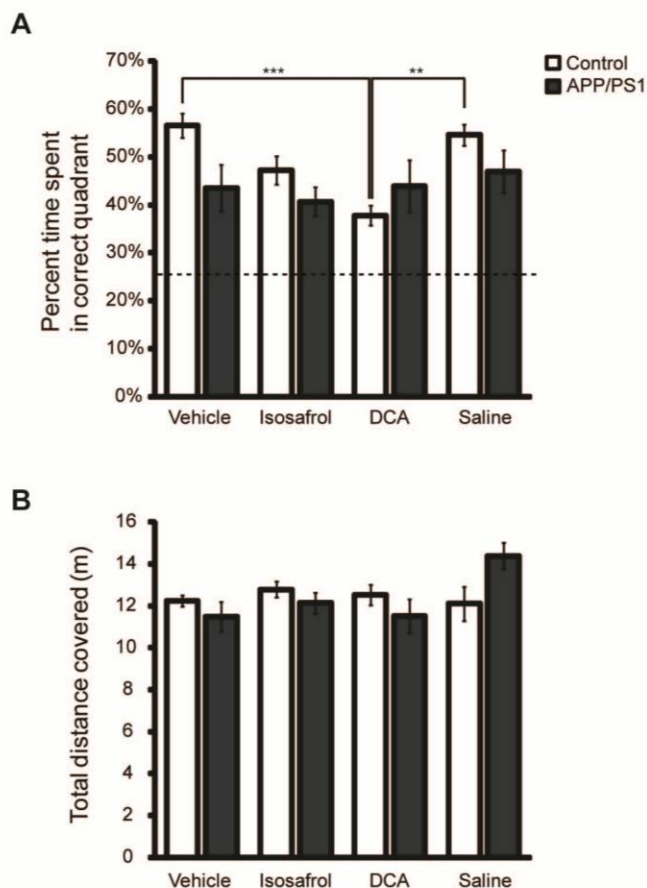
Figure 26. Acute exposure to dichloroacetate impairs memory performance in control mice.

The Morris water maze was used to evaluate memory performance, as measured during a 60 second probe trial by the percent time spent in the quadrant that contained the hidden platform during training (A). Mice were exposed to the probe trial 30 minutes after intraperitoneal injection of the indicated treatment. Horizontal dotted line at 25% represents the percent of time spent in the correct quadrant by random chance. Control mice injected with DCA (200 mg/kg) performed significantly worse than when injected with vehicle or saline. (B) Total distance covered during the probe trial was used as a measure of locomotor ability. Data shown are mean ± SEM, asterisks indicate a significant difference between treatments as determined by a two-way ANOVA followed by Tukey's post-hoc test, $**p < 0.01$, $***p < 0.001$, $n = 17$ and 8, respectively, for control mice and APP/PS1 mice for vehicle phase, $n = 16$ and 8, respectively, for control mice and APP/PS1 mice for Isosafrol phase, $n = 15$ and 8, respectively, for control mice and APP/PS1 mice for DCA phase, and $n = 13$ and 5, respectively, for control mice and APP/PS1 mice for saline phase.

3.11 Replicating the effect of acute dichloroacetate injection on memory performance in control mice

In the initial study, we attempted to determine the effect of the aerobic glycolysis inhibitors Isosafrol and DCA on memory performance using a single group of mice with repeated memory testing under different treatment conditions. This experimental design introduces the confounding factor of repeated testing, which could influence the outcome of successive memory tests. Previous studies have shown that repeated memory testing influence the successive behavior outcome on the MWM[494]. Thus, it was important to test the effect of aerobic glycolysis inhibitors on mice that had no previous exposure to any agent. Considering that DCA had a more pronounced effect on memory performance in the MWM than Isosafrol (Figure 26), DCA was selected as a single experimental treatment with saline as a negative control.

A new group of 20 control mice aged 9-months was randomly divided into saline and DCA treatment groups. The mice were given 2 weeks to acclimatize to their environment before beginning memory testing as described above with the platform located in the south-west quadrant. The latency to find the location of the platform during the training phase was recorded and a two-way ANOVA with repeated measures (training day $\times$ treatment) was performed (Figure 27A). This analysis revealed no significant effect on memory by DCA treatment ($F(1,17) = 0.525$, $p = 0.478$), or the interaction between treatment and training day ($F(3,51) = 0.880$, $p = 0.458$), which suggested that there was no difference in the ability of the two treatment groups to learn the location of the platform during training. On the fifth day of training, the platform was removed and the mice were injected intraperitoneally with either saline or DCA (200 mg/kg) 30 minutes before entering the pool for a probe trial. The swimming path of each mouse was recorded and a heat map representation of swimming behaviour was constructed for the two treatment groups (Figure 27B). The total distance covered during the probe trial was recorded (Figure 27C), and a Welch's t-test revealed no significant effect of DCA treatment on total distance covered ($t(18) = 0.805$, $p = 0.4331$). Several different measures of memory performance were collected during the probe trial and a Welch's t-test with a Bonferroni correction for multiple comparisons ($\alpha < 0.01$) was performed to

determine if there was a difference between the two treatment groups. There was no significant effect on the following measures of memory performance: (Figure 27D) the percent of time spent in the correct quadrant ($t(18) = 0.516$, $p = 0.307$), (Figure 27E) the number of entries to the platform location ($t(18) = 0.766$, $p = 0.227$), and (Figure 27F) the latency to the first entry to the platform location ($t(18) = 1.322$, $p = 0.102$). The latency to the first entry to the platform location during the probe trial was then compared to the average latency of each mouse to find the platform during the last day of training (Figure 27G). This analysis was performed to determine if there was an effect of DCA exposure on the ability of mice to continue learning the location of the platform. On average, mice injected with saline before the probe trial crossed the boundary of the platform 4.88 ± 1.09 seconds faster than the average of their previous attempts on the last day of training. In contrast, mice injected with DCA before the probe trial crossed the boundary of the platform on average 0.16 ± 1.96 seconds slower than the average of their previous attempts on the last day of training. A Welch's t-test was performed on the difference in latency to the platform between the probe trial and the final day of training. This analysis revealed a potential effect ($t(18) = 2.241$, $p = 0.021$), yet it did not reach the threshold determined by the Bonferroni correction for multiple comparisons ($a = 0.01$). Although this result should be interpreted with caution, it suggested that DCA may have had an effect on the ability of mice to continue learning the location of the hidden platform. After the probe trial, the platform was placed back into the tank in the opposite quadrant and a red flag was attached to the platform as a visual cue of its location. Mice were allowed to swim in the tank for 90 seconds and the latency to find the flag-marked platform was recorded (Figure 27H). A Welch's t-test revealed no significant effect ($t(18) = 0.158$, $p = 0.438$), which indicated that the ability of mice to use the flag as a visual cue to determine the location of the hidden platform was not compromised by DCA treatment. Altogether, these data suggested that acute exposure to DCA did not have an observable effect on the memory performance of mice, yet may impair the ability of mice to continue learning the location of the platform.
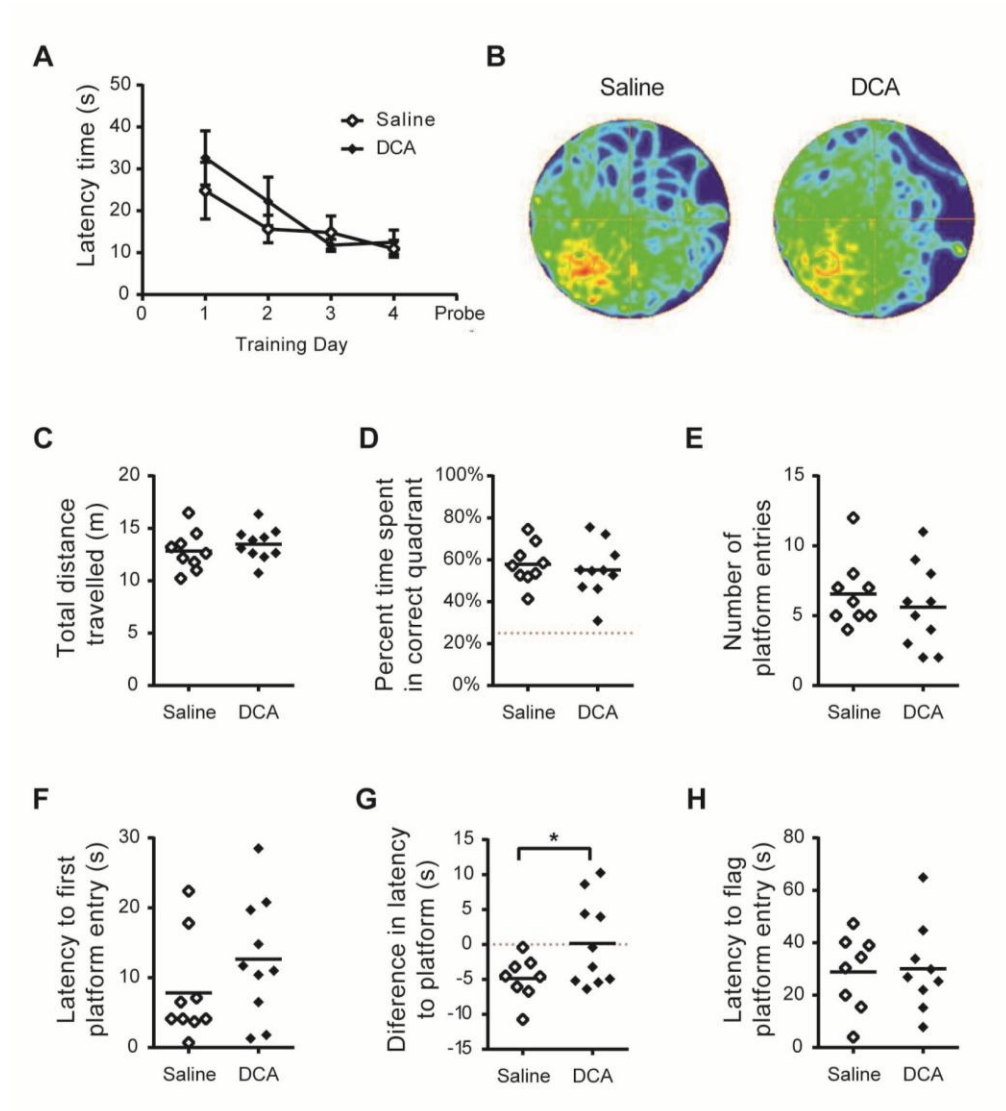
Figure 27. Acute exposure to dichloroacetate does not alter spatial memory performance in naïve mice.

Naïve control mice were intraperitoneal injected with saline or DCA (200 mg/kg) at 9 months of age followed by memory assessment using the Morris water maze. (A) Mice were trained for 4 consecutive days (4 trials per day) to find the location of a hidden platform in the SW quadrant and the latency to escape was recorded. On day 5 a probe trial was performed in which the platform was removed and mice were allowed to swim for 60 seconds (B-H). (B) The swim path for each group of mice was recorded and compiled into heat map representations. Measurements were taken for the total distance traveled (C), the percentage of time spent in the correct quadrant (D), the number of times crossing the boundary of the platform (E), the latency to the first platform entry (F), and the difference in latency between the average of training day 4 and the first platform entry during the probe trial (G). Immediately after the probe trial, a flag trial was performed to assess the ability of mice to use visual cues to find the platform. The platform was placed back in to the tank in the opposite quadrant and the latency to find the flag was recorded (H). Data shown are mean ± SEM, *$p < 0.05$, $n = 9$ and 10 for saline and DCA treatments, respectively.

3.12 Assessing the efficacy of acute dichloroacetate injection to reduce the conversion of pyruvate to lactate in the brain

In order to determine if DCA injection had a metabolic effect on the brain, mice were scanned with a 3T-MRI after injection with hyperpolarized ^{13}C-pyruvate (Figure 28A). Hyperpolarized ^{13}C-pyruvate MRS measures the kinetic conversion of pyruvate to lactate *in vivo.* ^{13}C-substrates can be highly magnetized (hyperpolarized) by dynamic nuclear polarization (DNP) *in vitro* and then used as injectable agents to probe *in vivo* metabolism[495]. This hyperpolarization technique provides signal-to-noise enhancements on the order of 10,000-fold over non-hyperpolarized ^{13}C-imaging methods[495]. In addition, the metabolic rate of conversion of pyruvate to lactate in the brain can be measured over the course of ~1 minute following injection of hyperpolarized ^{13}C-pyruvate. Mice were injected with ^{13}C-pyruvate and its conversion to lactate was measured 30 minutes before and 30 minutes after injection of DCA (200 mg/kg) using an intravenous tail-vein catheter and the ratio of lactate-to-pyruvate peaks was quantified as an indication of pyruvate breakdown to lactate in the mouse brain (Figure 28B). This analysis revealed that the ratio of lactate-to-pyruvate peaks was reduced from 0.104 ± 0.013 before DCA exposure to 0.056 ± 0.196 after DCA exposure (Figure 28C). However, due to variability in the conversion rate, a paired Welch's t-test revealed that there was no significant difference between before and after DCA injections ($t(4) = 2.010$, $p = 0.069$). These data indicate that DCA may reduce the conversion of pyruvate-to-lactate in the brain, although there was variability in the degree to which DCA interfered with this conversion and additional mice need to be tested.

A
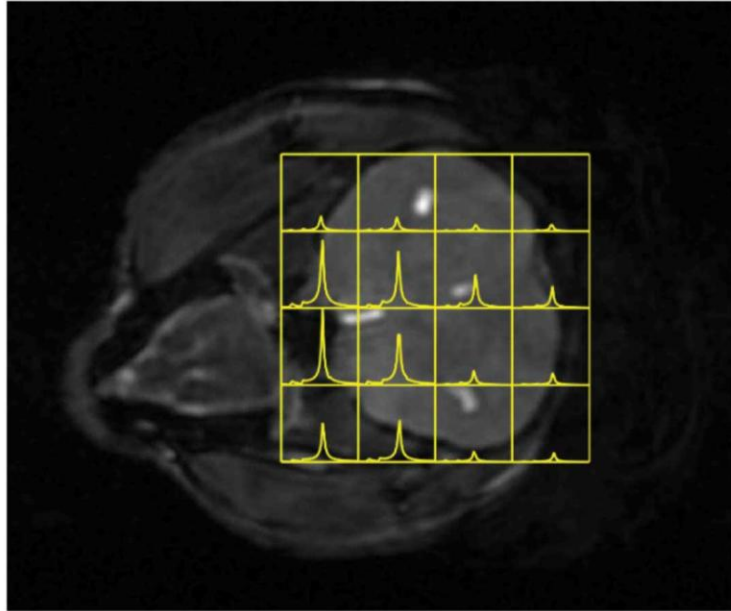
B
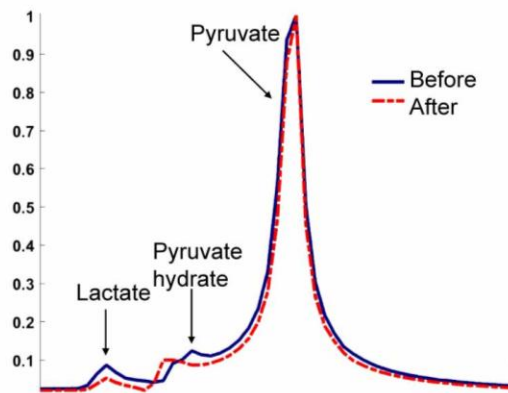
C
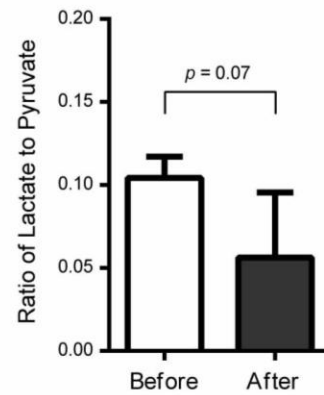
Figure 28. Hyperpolarized ^{13}C-pyruvate magnetic resonance spectroscopy revealed a potential decrease in conversion of pyruvate to lactate in DCA-injected mice.

Control mice at 9 months old were injected with a 0.3 mL bolus of hyperpolarized [1-^{13}C]-pyruvate via tail vein catheter and the conversion of pyruvate-to-lactate was measured using free induction chemical shift imaging (FID-CSI). (A) ^{1}H-MRI image of the brain in the coronal field overlaid with voxels of 13C-pyruvate spectra (yellow). (B) Conversion of pyruvate-to-lactate was measured as a ratio of the observed lactate peak to pyruvate peak. A pyruvate hydrate peak was also recorded. 30 minutes after the first ^{13}C-pyruvate injection was measured (before), DCA (200 mg/kg) was injected using the tail vein catheter followed by a 30 minute recovery time, after which another injection of ^{13}C-pyruvate was performed (after). The difference in the ratio of lactate-to-pyruvate peaks from before DCA injection (blue line) and after (red dashed line) was used to evaluate the effect of DCA on pyruvate conversion to lactate in the brain. (C) The ratio of lactate-to-pyruvate peaks was measured following hyperpolarized ^{13}C-pyruvate injection before and after DCA (200 mg/kg) exposure in control mice at 9 months old. Data shown are mean ± SEM, $p = 0.068$, as calculated by paired Welch's t-test, $n = 5$ mice.

3.13 Replicating the effect of acute dichloroacetate injection on PDH phosphorylation in the brain

In order to evaluate the physiological effect of DCA injection on the brain of affected mice, mice were euthanized 30 minutes after injection of saline or DCA. Brain extracts from the frontal cortex were analyzed by western blotting using antibodies targeting key proteins involved in lactate metabolism and transport (Figure 29). The band density was quantified using β-Actin as a loading control and a Welch's t-test was performed with a Bonferroni correction for multiple comparisons ($\alpha = 0.00625$) to determine the difference between saline- and DCA-injected mice (Figure 30). This analysis revealed a significant effect for the phosphorylation level of PDH ($t(14) = 8.198$, $p < 0.001$), which indicated that phosphorylation levels were reduced in DCA-injected mice. A significant effect was also revealed for the expression of PDK1 ($t(14) = 3.362$, $p = 0.005$), indicating an increase in expression in DCA-injected mice. There was no effect on the expression of the following enzymes: LDHA ($t(14) = 1.647$, $p = 0.122$), LDHB ($t(14) = 0.966$, $p = 0.350$), PKM2 ($t(14) = 1.680$, $p = 0.115$), and PKM1 ($t(14) = 0.321$, $p = 0.753$). This analysis also revealed a significant effect for the expression of the astrocyte-specific lactate transporting protein: MCT4 ($t(14) = 3.468$, $p = 0.004$). Mice injected with DCA had lower expression of MCT4 than saline-injected mice. There was no effect for expression of the neuron-specific MCT2 ($t(14) = 0.636$, $p = 0.535$). These observations indicated that the injection of DCA caused a significant decline in phosphorylation levels of PDH in the frontal cortex, and may also influence expression of PDK1 and the lactate transporter protein, MCT4.
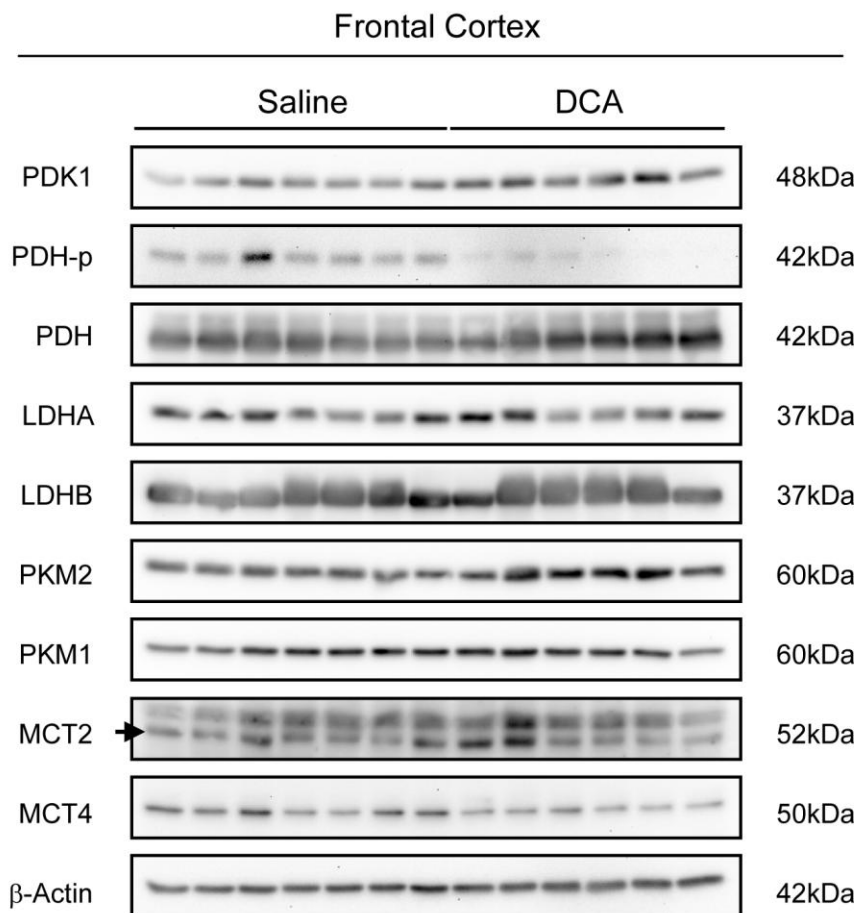
Figure 29. Acute exposure to dichloroacetate reduces phosphorylation levels of PDH in the frontal cortex.

Western blot analysis was performed on extracts from the frontal cortex of control mice intraperitoneal injected with either saline or DCA (200 mg/kg) 30 minutes prior to euthanization. Indicated antibodies were used to detect proteins involved in aerobic glycolysis and lactate metabolism. $n = 10$ and 9, respectively, for saline- and DCA-injected mice.
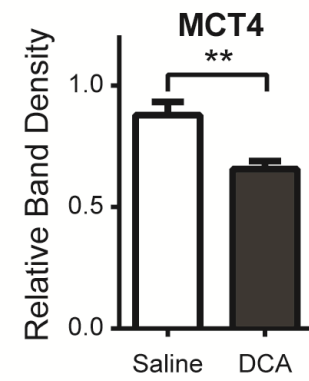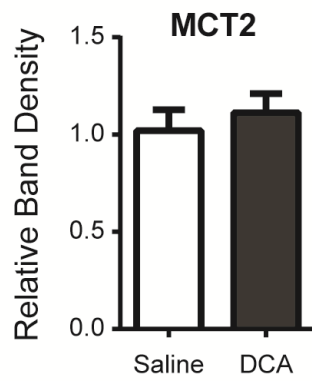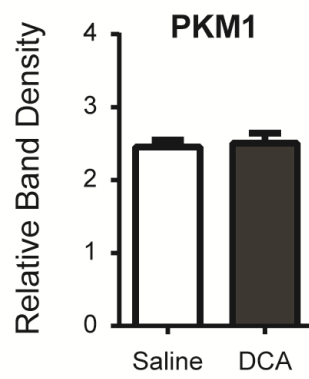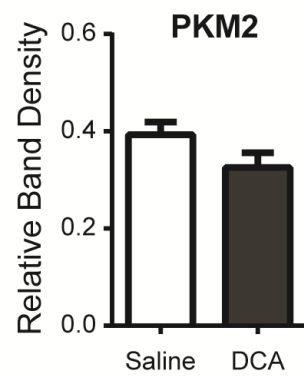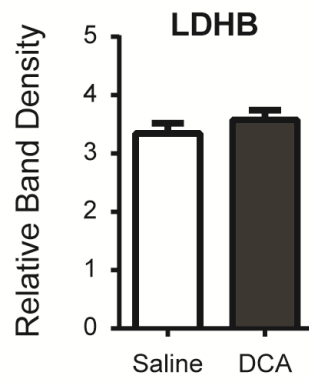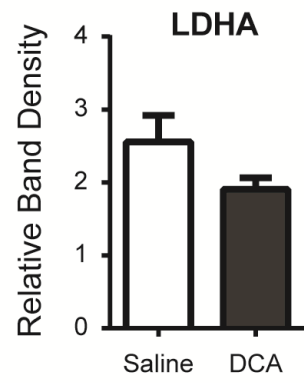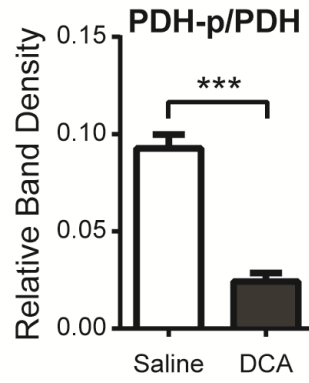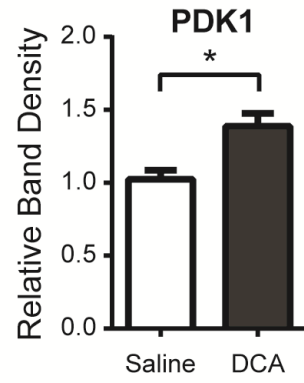
Figure 30. Acute exposure to dichloroacetate reduces phosphorylation levels of PDH in the frontal cortex: Band densitometry analysis.

Quantification of band densitometry for western blots of extracts from the frontal cortex of control mice injected with saline or DCA (200 mg/kg) 30 minutes prior to euthanization. Indicated antibodies were used as markers of aerobic glycolysis and lactate metabolism. Relative band density was calculated relative to β-actin. A significant decline in phosphorylation levels of PDH was measured following DCA injection. Data are shown as mean + SEM, *$p < 0.05$, **$p < 0.01$, ***$p < 0.001$, $n = 10$ and 9, respectively, for saline- and DCA-injected mice.

Extracts from the hippocampus were also analyzed by western blotting with antibodies for lactate metabolism and transport (Figure 31). Band densitometry analysis was performed using β-actin as a loading control and a Welch's t-test with a Bonferroni correction for multiple comparisons ($\alpha = 0.00625$) was used to evaluate the effect of DCA injection (Figure 32). This analysis revealed a significant effect for the phosphorylation levels of PDH ($t(14) = 4.493$, $p < 0.001$), which indicated that phosphorylation of PDH was reduced in DCA-injected mice. This analysis also revealed a potential effect for the expression of LDHA ($t(14) = 2.249$, $p = 0.041$) and the neuron-specific lactate transporter MCT2 ($t(14) = 2.276$, $p = 0.039$), yet these did not reach the threshold determined by the Bonferroni correction for multiple comparisons. There were no other significant effects for any of the following lactate metabolism or transporting proteins: PDK1 ($t(14) = 0.910$, $p = 0.379$), LDHB ($t(14) = 1.790$, $p = 0.095$), PKM2 ($t(14) = 2.002$, $p = 0.065$), PKM1 ($t(14) = 0.524$, $p = 0.609$), or the astrocyte-specific lactate transporter MCT4 ($t(14) = 1.373$, $p = 0.191$). Altogether, these analyses indicated that injection of DCA caused a reduction in phosphorylation of PDH in the frontal cortex and hippocampus of affected mice.
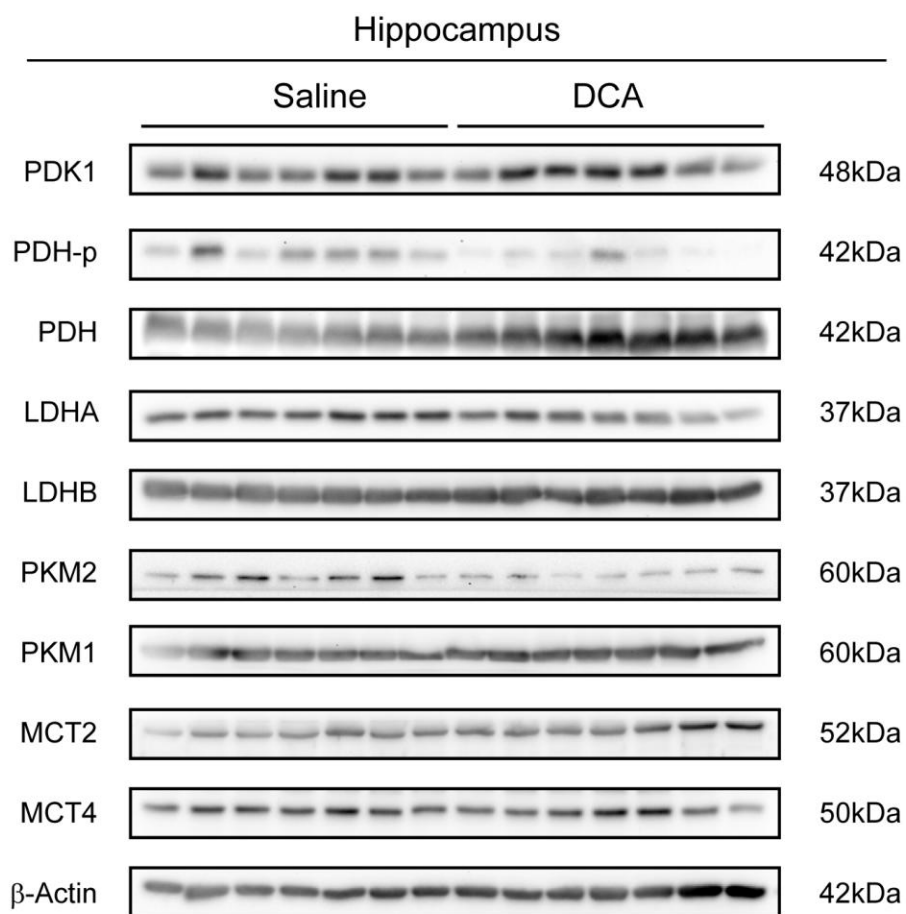
Figure 31. Acute exposure to dichloroacetate reduces phosphorylation levels of PDH in the hippocampus.

Western blot analysis was performed on extracts from the hippocampus of control mice intraperitoneal injected with either saline or DCA (200 mg/kg) 30 minutes prior to euthanization. Indicated antibodies were used to detect proteins involved in aerobic glycolysis and lactate metabolism. $n = 10$ and 9, respectively, for saline- and DCA-injected mice.
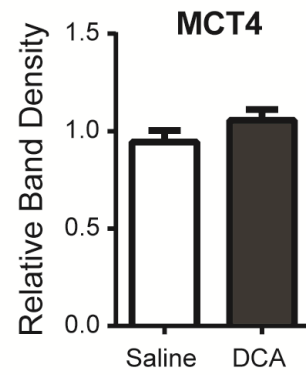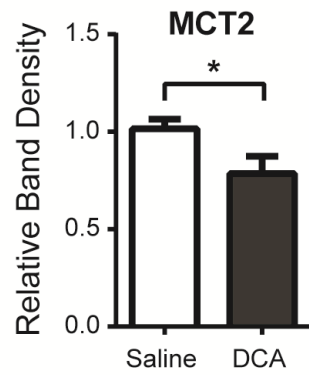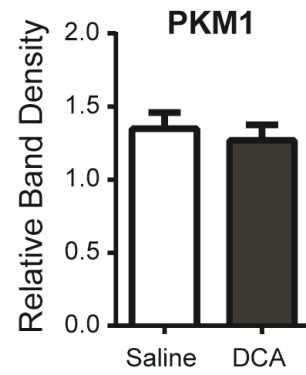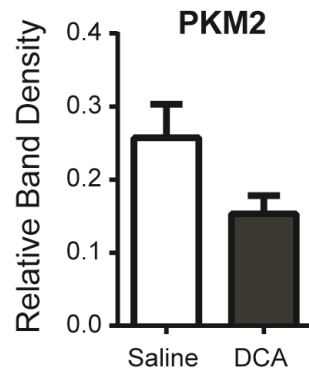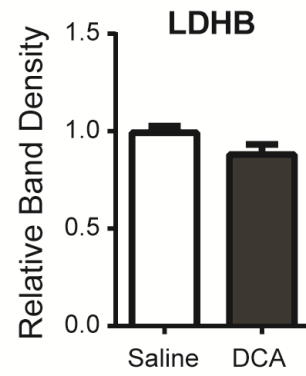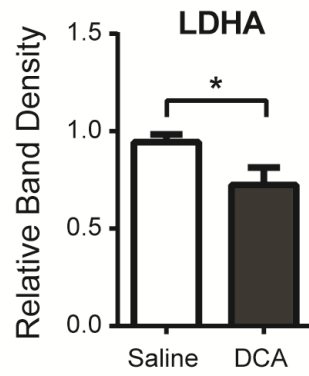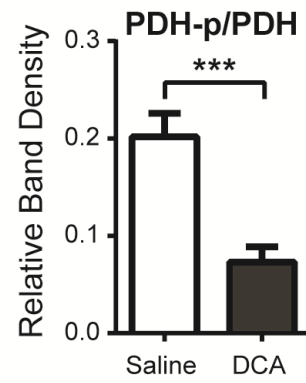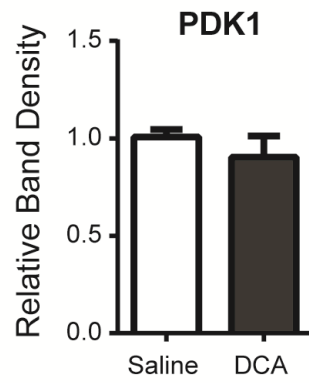
Figure 32. Acute exposure to dichloroacetate reduces phosphorylation levels of PDH in the hippocampus: Band densitometry analysis.

Quantification of band densitometry for western blots of extracts from the hippocampus of control mice injected with saline or DCA (200 mg/kg) 30 minutes prior to euthanization. Indicated antibodies were used as markers of aerobic glycolysis and lactate metabolism. Relative band density was calculated relative to β-actin. A significant decline in phosphorylation levels of PDH was measured following DCA injection. Data are shown as mean + SEM, $*p < 0.05$, $***p < 0.001$, $n = 10$ and 9, respectively, for saline- and DCA-injected mice.

3.14 Replicating the correlation analysis of PDH phosphorylation and memory performance in control mice

Considering that there was an inverse correlation between expression of aerobic glycolysis enzymes in the frontal cortex and memory performance of control mice and APP/PS1 mice (Figure 19), the expression of these same proteins was compared to memory performance of saline-injected and DCA-injected mice. Band densitometry measurements in the frontal cortex were correlated to the individual measures of percent time spent in the correct quadrant during the MWM probe trial and a multiple linear regression model (relative band density x treatment) was performed (Figure 33). This analysis revealed a significant positive correlation for the level of phosphorylation of PDH in saline-injected mice ($R^2 = 0.7443$, $p = 0.006$), which indicated that mice with higher phosphorylation levels performed better in the memory task. There was no correlation for phosphorylated-PDH in DCA-injected mice ($R^2 = 0.049$, $p = 0.600$). A correlation was also detected in saline-injected mice for the expression of PKM1 ($R^2 = 0.528$, $p = 0.041$), indicating that mice with higher PKM1 performed better in memory testing. This analysis also revealed a significant correlation in DCA-injected mice for expression of the astrocyte-specific lactate transporter MCT4 ($R^2 = 0.746$, $p = 0.012$), yet there was no correlation for MCT4 expression in saline-injected mice ($R^2 = 0.004$, $p = 0.883$). A one-way ANCOVA was conducted on the linear regression of relative band density and percent time spent in the correct quadrant, controlling for treatment. This analysis revealed that DCA treatment was not a significant covariate for any of the measured proteins. The memory performance of mice injected with saline or DCA was also correlated with the expression of lactate metabolism and transport enzymes in the hippocampus. The same analysis was performed on relative band densitometry and percent time spent in the correct quadrant for saline- and DCA-injected mice (Figure 34). A multiple linear regression model (relative band density x treatment) was then performed and revealed only one significant correlation for expression of PKM1 ($R^2 = 0.625$, $p = 0.020$) in saline-injected mice. This analysis suggested that mice with higher expression of PKM1 in the hippocampus performed worse on the memory task. Interestingly, this is opposite to the trend observed in the frontal cortex.
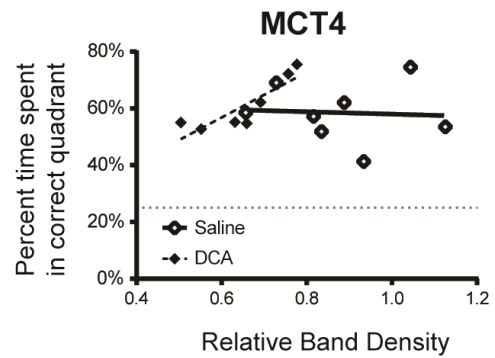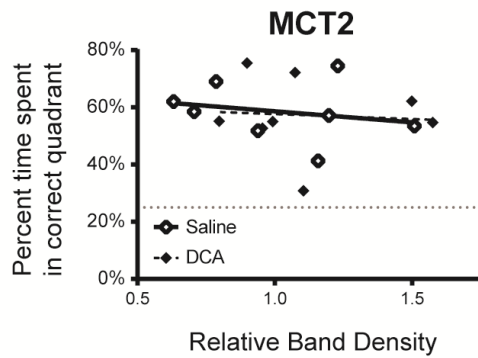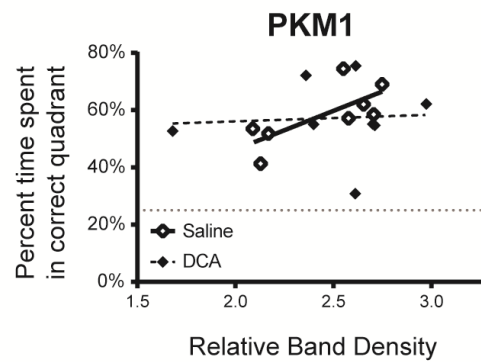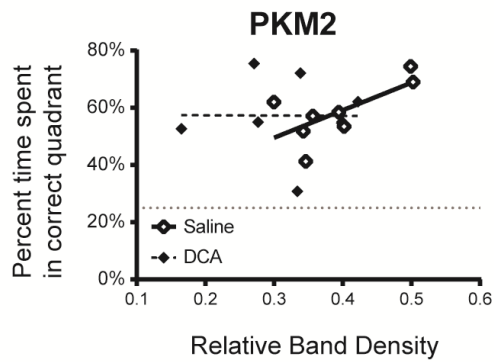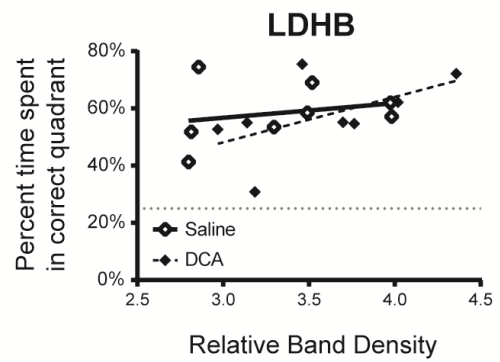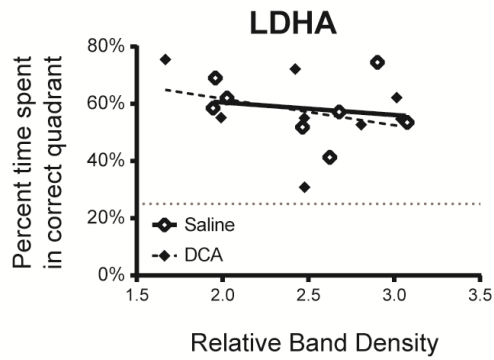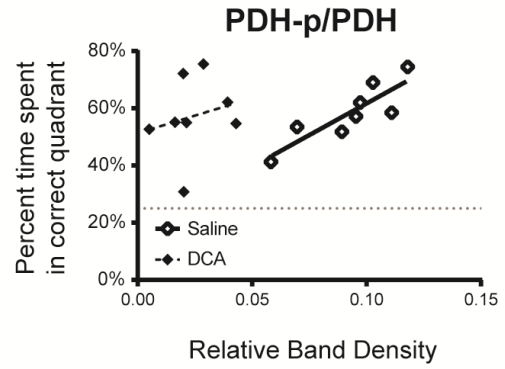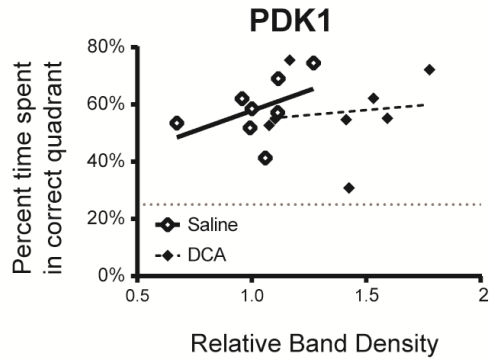
Figure 33. Memory performance correlates with phosphorylation of PDH in saline-injected mice and MCT4 expression in dichloroacetate-injected mice within the frontal cortex.

Band densitometry measurements using indicated antibodies in the frontal cortex were compared with memory performance of control mice injected with saline (open diamond) and DCA (closed diamond) in the Morris water maze probe trial as a measure of percent time spent in the correct quadrant. Lines-of-best-fit are overlaid for saline-injected mice (solid) and DCA-injected mice (dashed). A significant positive correlation was observed for phosphorylated-PDH in saline-injected mice and also for MCT4 in DCA-injected mice. Horizontal dotted line at 25% represents the probability of spending the same amount of time in the correct quadrant by chance. $n = 8$ for each group of saline- and DCA-injected mice.
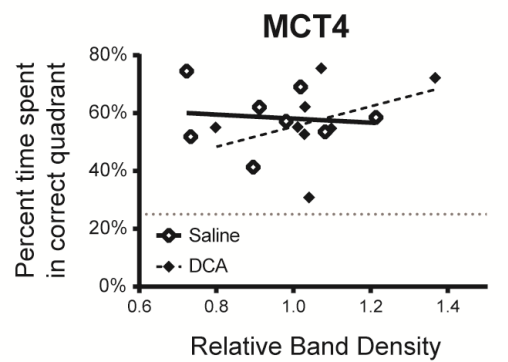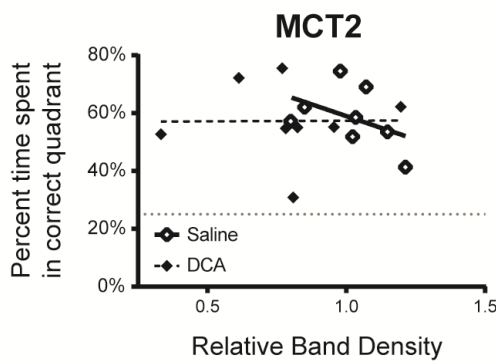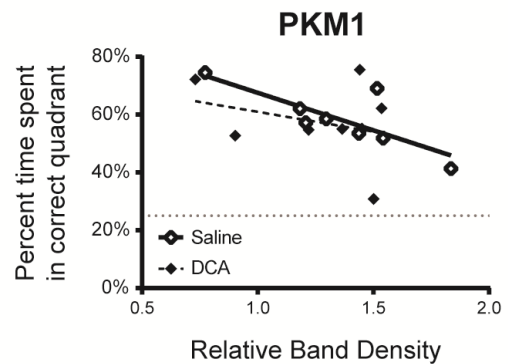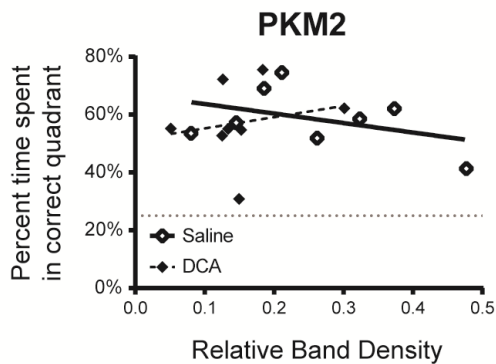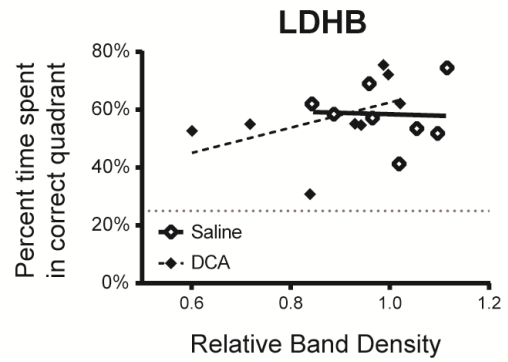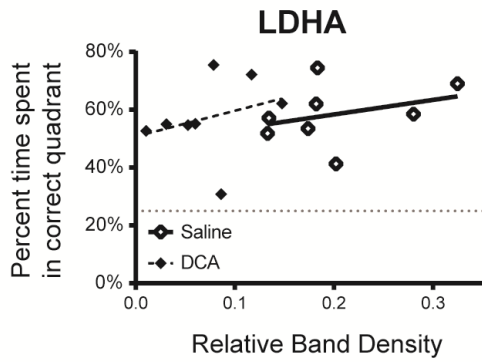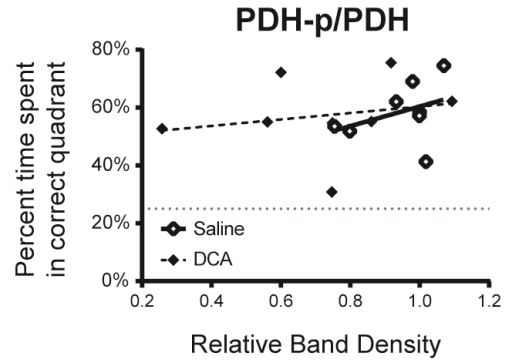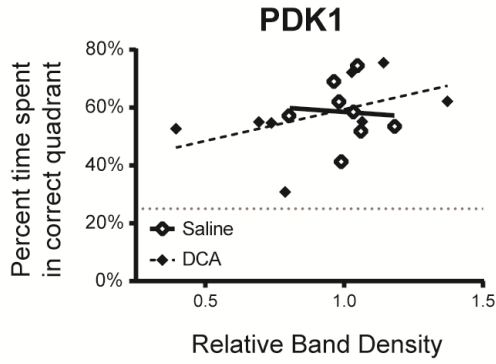
Figure 34. Correlations of memory performance with band densitometry in the hippocampus.

Band densitometry measurements using indicated antibodies in the hippocampus were compared with memory performance of control mice injected with saline (open diamond) and DCA (closed diamond) in the Morris water maze probe trial as a measure of percent time spent in the correct quadrant. Lines-of-best-fit are overlaid for saline-injected mice (solid) and DCA-injected mice (dashed). Horizontal dotted line at 25% represents the probability of spending the same amount of time in the correct quadrant by chance. $n = 8$ for each group of saline- and DCA-injected mice.

In order to further validate the correlation between phosphorylation of PDH in the frontal cortex and memory performance in saline-injected mice, the relative band density was correlated to several other measures of memory performance in the MWM (Figure 35). A multiple linear regression (relative band density x treatment) was performed on the number of platform entries with phosphorylation of PDH and revealed a significant positive correlation for saline-injected mice ($R^2 = 0.546$, $p = 0.036$). This correlation was not observed for DCA-injected mice ($R^2 = 0.003$, $p = 0.900$). This indicated that saline-injected mice with higher phosphorylation of PDH crossed the platform boundary more often. A one-way ANCOVA was conducted on the linear regression of relative band density and number of platform entries, controlling for treatment. This analysis revealed that DCA treatment was not a significant covariate. The latency to the first entry of the platform boundary was then compared to phosphorylation of PDH using an exponential decay equation. This analysis revealed a strong correlation ($R^2 = 0.967$), which suggested that saline-injected mice with higher phosphorylation of PDH were able to find the platform boundary faster. This correlation was not observed in DCA-injected mice ($R^2 = 0.227$). Finally, the difference in latency to the first platform entry between the probe trial and the final training day was correlated to phosphorylation of PDH using a multiple linear regression (relative band density x treatment). This analysis revealed no correlation for saline-injected mice ($R^2 = 0.324$, $p = 0.182$) and no correlation for DCA-injected mice ($R^2 = 0.057$, $p = 0.570$). Altogether, these data indicate that phosphorylation level of PDH in the frontal cortex was positively correlated to several measures of memory performance in the MWM.
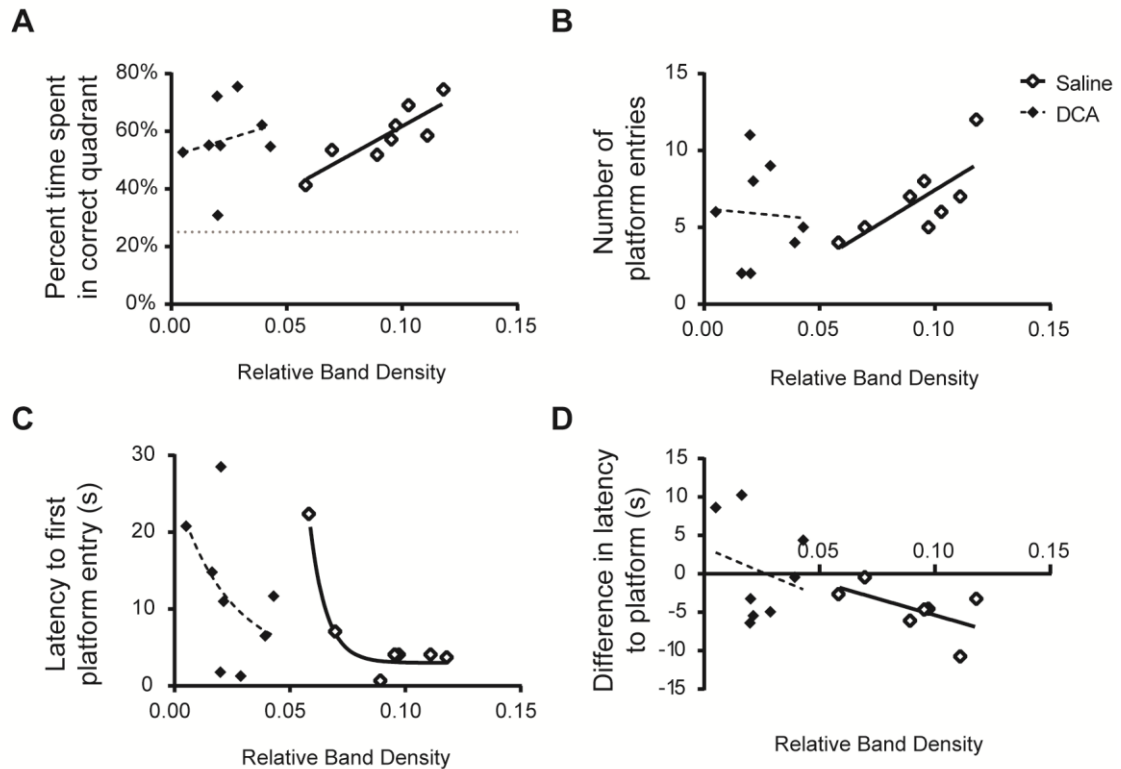
Figure 35. Phosphorylation of PDH correlates with memory performance in control mice.

Band densitometry measurements of phosphorylated PDH in the frontal cortex of control mice injected with either saline (open diamond) or DCA (closed diamond) were compared with memory performance in the Morris water maze probe trial for measures of (A) percent time spent in the correct quadrant, (B) number of platform entries, (C) latency to the first platform entry, and (D) the difference in time between average latency to find the platform on training day 4 and the latency to the first entry of the platform on the probe trial. Lines-of-best-fit are overlaid for saline-injected mice (solid) and DCA-injected mice (dashed). Levels of phosphorylated PDH in control mice correlate with all measures of memory performance. $n = 9$ and 10 for saline and DCA treatments, respectively.

Chapter 4

4 Discussion

This work produced several novel observations, which gave rise to some conclusions that need to be addressed. This chapter is split into two main categories of discussion: examining the temporal and spatial expression of aerobic glycolysis enzymes and lactate levels, and examining the relationship between cerebral aerobic glycolysis and memory performance. Each conclusion is addressed independently by interpreting the results and determining how they fit into the context of the greater research field.

4.1 Examining the temporal and spatial expression of aerobic glycolysis enzymes and lactate levels

4.1.1 Cerebral lactate levels decline with age

Lactate production, consumption, and transport between astrocytes and neurons has been examined extensively[425], yet little emphasis has been placed on examining changes in this metabolism with age. *In vivo* ^{1}H-MRS is a powerful tool to detect metabolic signatures of different brain regions non-invasively over the course of normal aging. In this study, ^{1}H-MRS was used to measure lactate in the frontal cortex and hippocampus of control mice and APP/PS1 mice from 3 to 12 months of age. This analysis revealed a decline in lactate levels from 6 to 12 months of age in the frontal cortex of control mice (Figure 6), whereas the hippocampus revealed no significant decline in lactate levels between 6 and 12 months of age (Figure 7). Consistent with this finding, a ^{1}H-MRS longitudinal study of metabolites in healthy C57BL/6 mice between 3 and 24 months of age also revealed a progressive decline in lactate levels in the cortex but not hippocampus[496]. However, in contrast to our findings, a study using ^{1}H-MRS reported that cortical lactate levels increased with age in a mitochondrial DNA mutator mouse model of advanced aging[330]. However, it is not clear if brain metabolism in mutant advanced-aging mice is an accurate reflection of brain metabolism that occurs during normal aging. Collectively, these observations suggest that a decline in glycolytic metabolism occurs with advanced age in the frontal cortex, whereas the hippocampus appears to be less affected.

Examination of lactate levels by ^{1}H-MRS revealed a decline in the frontal cortex of aged control mice and no change in APP/PS1 mice. In addition, there was found to be no significant change with age or genotype in the hippocampus. Maintained lactate in the frontal cortex of aged APP/PS1 mice could be attributed to an increase in regional glucose uptake and glycolytic metabolism. An increase in glucose uptake in the cortex and hippocampus, as measured by ^{18}F-FDG-PET, was reported in 12-month-old APP/PS1 mice when compared to control animals[234]. The authors ruled out the contribution of cerebral blood flow by demonstrating that cerebral perfusion is reduced in APP/PS1 mice at this age. A similar study measured an increase in glucose utilization in the frontal cortex and hippocampus of APP/PS1 mice at 3.5 and 5 months of age, which correlated with improved performance in the MWM[497]. Increased glucose uptake has also been measured using ^{18}F-FDG-PET in the cortex, hippocampus, and striatum of 7- and 9-month old $APP_{(Tg2576)}$ mice[498], in 12-month old $PDAPP_{V717F}$ mice[499,500], in 16-month-old $APP_{(Tg2576)}/PS1_{M146L}$ mice[501]and in 12-month-old 5xFAD mice[502]. However, a decline in glucose uptake has also been measured by ^{18}F-FDG-PET in several animal models of AD, including 18-month-old 3xTG mice[503]. Hypometabolism is a common pathological feature of AD indicating a reduction in neuronal energy demand from loss of synaptic activity at later stages of the disease, yet inconsistencies in glucose uptake measurements using ^{18}F-FDG-PET have been noted in AD animal models[504]. Different states of glucose uptake have been reported, even among the same transgenic strains, including $APP_{(Tg2576)}$ mice[498,505] and 5xFAD mice[502,506]. However, in APP/PS1 mice, only increases in glucose uptake have been measured at 3.5, 5, and 12 months of age[234,497].

The majority of ^{1}H-MRS studies of AD in rodent models do not report lactate measurements[507–509]. This is because the lactate peak is largely obscured by lipid signals with similar resonance frequencies and is difficult to measure[510,511]. In many cases, brain extracts from post-mortem tissue are analyzed instead of *in vivo* longitudinal measurements over the course of age. A ^{1}H-MRS metabolomics study of extracted brain samples revealed an elevation in lactate levels in the hippocampus and frontal cortex of the TgCRND8 mice compared to controls at both 2-3 months of age and 12-13 months of age[512]. However, a recent high-throughput metabolomics study on 6-month-old APP/PS1 mice using ultra performance liquid chromatography followed by gas chromatograph

mass spectrometry measured a decline in lactate, creatine, and NAA in the hippocampus and cortex compared to controls[513]. These observations highlight the need for consistency in measuring metabolites, including lactate, across animal models of AD to reliably evaluate the age-associated changes in brain metabolism. The concentration of metabolites detected by ^{1}H-MRS can be quantified using an unsuppressed water signal from the same volume of interest as an internal reference[496], yet in this study lactate was measured using NAA as a reference metabolite and has been previously reported[514]. Second only to the neurotransmitter glutamate, NAA is the most abundant metabolite in the brain and is mainly produced in neurons where it is shuttled to oligodendrotyes and is used for myelin production[515]. In order to determine if NAA levels change with age, NAA in the frontal cortex and hippocampus was quantified as a ratio to total creatine, which is frequently used as a reference metabolite in ^{1}H-MRS studies[508,514]. We found that the ratio of NAA to creatine in both the frontal cortex and hippocampus did not change over the course of age in control mice or APP/PS1 mice (Figure 5 and Figure 6), which is consistent with the findings of other groups[496,507–509]. Therefore, NAA was a suitable metabolite to standardize lactate measurements over the course of aging.

Although we did not detect a difference in hippocampal lactate levels using ^{1}H-MRS analysis, we did observe an increase in hippocampal ISF lactate levels using microdialysis analysis in awake mice (Figure 8). The discrepancies in measured lactate levels using the two methods may be due to the low level of sensitivity for the detection of lactate by ^{1}H-MRS and the small size of the hippocampus. In contrast, microdialysis has higher detection capabilities for lactate and was performed in awake mice. The use of isoflurane anesthetic during ^{1}H-MRS analysis may have influenced lactate levels in the hippocampus and obscured genotype-specific differences[516]. These findings underscore the need to develop more sensitive and non-invasive techniques for measuring lactate levels *in vivo*.

4.1.2 The expression of lactate metabolism and transport proteins declines with age in both control mice and APP/PS1 mice

Maintained lactate levels in the APP/PS1 brain is indicative of higher levels of aerobic glycolysis and resembles the metabolic profile of the Warburg effect in cancer cells[243]. It

has been previously demonstrated that nerve cells selected for resistance to Aβ toxicity up-regulate aerobic glycolysis as a protective mechanism[239]. Chemical or genetic disruption to key aerobic glycolysis enzymes PDK1 or LDHA resulted in re-sensitization of resistant lines, while over-expression of PDK1 or LDHA conferred resistance to Aβ and other neurotoxins in naïve lines[240]. Elevated lactate in the frontal cortex and hippocampus of APP/PS1 mice at this age may indicate the up-regulation of glucose uptake or a metabolic shift from oxidative phosphorylation to aerobic glycolysis as a protective resistance to Aβ toxicity. Nerve cell lines and primary cortical neurons that are resistant to Aβ toxicity had enhanced glucose consumption, increased activity of glycolytic enzymes including HK, glyceraldehyde 3-phosphate dehydrogenase (GAPDH), and PK, and increased flux through the PPP[260]. The Aβ-induced changes to metabolism were found to be due to activation of the transcription factor HIF-1, which regulates cellular responses to low oxygen by up-regulating glycolytic metabolism, including enzymes PDK and LDHA. It was anticipated that western blot analysis of brain extracts would reveal an increase in aerobic glycolysis enzyme expression in APP/PS1 mice compared to control mice at the same age. A two-way ANOVA identified an increase in expression of PDK1 at 6 months of age in the frontal cortex of APP/PS1 mice when compared to controls, indicating a possible up-regulation of aerobic glycolysis. However, these mice also had an increase in PKM1 (non-glycolytic isozyme) and no significant difference in expression of LDHA, PKM2, or the phosphorylation levels of PDH (Figure 11). These observations indicate a lack of collective up-regulation of enzymes involved in aerobic glycolysis in APP/PS1 mice. Interestingly, this analysis revealed a significant age-dependent decline in all proteins involved in glucose metabolism for both control and APP/PS1 mice from 6 to 12 months of age indicating a general decline in glucose metabolism with age. The cerebral CMRglc can be estimated using ^{18}F-FDG PET imaging as a marker of glucose uptake and metabolism. Several studies have demonstrated that CMRglc declines significantly in older individuals in several brain regions including the parietal, temporal, and frontal cortex, with the greatest reduction observed in the frontal cortex[517–520]. Furthermore, the metabolism of ketones, the brains' major alternative fuel source, can be measured using ^{11}C-AcAc PET as a marker of cerebral metabolic rate of acetoacetate (CMRa). In contrast to CMRglc,

the CMRa does not decline with age in the same brain regions[521]. It has been suggested that the decline in CMRglc may be due to brain atrophy and lower cortical thickness in cognitively normal individuals[519,522], yet even after correction for partial volume effects, the same trends in CMRglc and CMRa were observed[523]. These studies suggest that a general decline in cerebral glucose uptake and metabolism occurs with age that may not be adequately compensated by the metabolism of ketones as an alternative fuel source, and is consistent with the age-dependent decline in expression of glycolytic enzymes observed in the frontal cortex of both control and APP/PS1 mice in this study.

If we assume that glucose influx and metabolism is elevated in aged APP/PS1 mice, then an increase in lactate levels measured by ^{1}H-MRS in the frontal cortex of 9-12-month-old APP/PS1 mice supports the hypothesis that aerobic glycolysis is up-regulated in neurons in order to promote Aβ resistance. Yet, given a general decline in expression of glycolytic enzymes with age in both control and APP/PS1 mice, an alternate explanation may be that lactate efflux from the brain is diminished in APP/PS1 mice. Western blot analysis of brain extracts revealed an age-dependent increase in expression of the lactate transporters: MCT2 (neuronal-specific) and MCT4 (astrocyte-specific), in the frontal cortex of control mice, but not in APP/PS1 mice. At 12 months of age, the expression of MCT4 was found to be significantly elevated in the frontal cortex of control mice compared to APP/PS1 mice (Figure 11). This indicates that lactate transport may be compromised in APP/PS1 mice. During neuronal activation, a high energy demand is placed on astrocytes, which need to rapidly clear glutamate from the synapse and necessitating aerobic glycolysis for rapid energy production. As a result, the majority of lactate released from astrocytes is beyond the metabolic need of activated neurons, and thus is expelled from the brain[524]. There is substantial evidence that suggests astrocytes in the AD brain become "reactive" or "activated" in response to inflammatory cytokines produced by microglia, including Interleukin-1 (IL-1) and IL-6[525,526]. Reactive astrocytes change their phenotype by interweaving themselves within amyloid plaques and up-regulating expression of several marker proteins including GFAP and the S100 calcium-binding protein B (S100β)[527,528]. Yet it was recently discovered in APP/PS1 mice that reactive astrocytes do not migrate to plaques; instead they respond to plaque-induced

injury by changing phenotype and function[529]. Consequently, reactive astrocytes may provide less support to neurons because they are functionally different and can no longer fulfill their normal roles[530,531]. The data presented here suggest that a decline in glycolytic metabolism occurs in the cortex during normal aging while a concurrent increase in MCT expression arises as a possible compensatory response to maintain neuronal activity. In contrast, while a decline in glycolytic metabolism occurs in the APP/PS1 brain, no increase in MCT expression was detected. Thus, in the absence of enhanced lactate transport, lactate may accumulate either within reactive astrocytes or in the extracellular space.

4.1.3 The interaction between the frontal cortex and the hippocampus

In this study, both the frontal cortex and the hippocampus were examined in parallel as both these brain regions play key roles in memory. It is understood that the hippocampus and the frontal cortex both participate in memory consolidation and retrieval. Many of the pioneering studies investigating the involvement of specific brain regions in memory come from lesion studies in humans. The most famous of these cases being the patient H.M., who had most of his medial temporal lobe (which includes the hippocampus) bilaterally removed in an attempt to cure his epilepsy. Following surgery, H.M. developed severe anterograde amnesia, meaning he could not develop any new memories or consolidate newly acquired memories[532]. This evidence strongly implicated the hippocampus as the central mediator of episodic memory formation and has encouraged decades of research detailing the interaction of the hippocampus with other brain regions to support memory consolidation and retrieval[533]. In a similar study of brain lesions using paired-associate learning tasks, in which two lists of cue words are paired with different response words, patients with damage to the frontal cortex have difficulty with the second-list learning[534]. This suggests that the frontal cortex is responsible for control of memory associations as part of a memory-filtering mechanism. Several studies using animal models have shown that damage to the frontal cortex impairs the ability of the brain to alter behaviour in response to stimuli with different emotional significance[535], learn the association of different perceptual stimuli with a food reward[536], or to switch

between memory associations of odor or place stimuli[537]. These studies demonstrate that the frontal cortex is involved in memory consolidation and retrieval by associating incoming stimuli with a context of familiar experiences within related memories. The association between hippocampus and frontal cortex is best understood using the railroad metaphor in which the hippocampus is responsible for placing new railroad tracks (memory formation), while the frontal cortex is responsible for flexibly switching between tracks that have already been laid (memory association)[538,539].

The frontal cortex and hippocampus also have dramatically different metabolic profiles. The regional distribution of aerobic glycolysis can be measured using multimodal PET by comparing the cerebral metabolic rate for oxygen ($CMRO_2$) using [^{15}O-H_2O] and CMRglc using [^{18}F-FDG]. Aerobic glycolysis is estimated as the oxygen-glucose index (OGI), which compares the molar ratio of oxygen-to-glucose. An OGI of 6 indicates that all glucose is converted to carbon dioxide and water, and an OGI of less than 6 indicates that non-oxidative glucose metabolism (aerobic glycolysis) is occurring. In a recent study measuring the OGI from different brain regions of normal young adults at rest, aerobic glycolysis was found to be elevated in the DMN and in areas of the frontal and parietal cortex, while the cerebellum and the hippocampus had reduced aerobic glycolysis relative to the brain average[351]. In a follow up study, the authors demonstrated that the brain regions with high aerobic glycolysis in young healthy adults strongly correlated with the regions of high Aβ deposition, as measured by PET using [^{11}C-PiB] retention[540]. Yet, the age-associated metabolic changes in the frontal cortex and hippocampus of the AD brain have yet to be investigated. In this study, ^{1}H-MRS analysis of the hippocampus revealed that lactate levels decline with age for both control mice and APP/PS1 mice, although not significantly, and there was no difference between control mice and APP/PS1 mice. In contrast, microdialysis sampling revealed elevated extracellular lactate in the hippocampus of aged APP/PS1 mice compared to controls. These data suggest that either aerobic glycolysis declines with age in the hippocampus, or lactate export increases, and is counter to the hypothesis that aerobic glycolysis is promoted in neurons in response to Aβ deposition.

Western blot analysis of brain extracts from the hippocampus revealed a significant change in expression of aerobic glycolysis enzymes from 6 to 12 months in both control and APP/PS1 mice. A two-way ANOVA revealed a significant age-dependent decline in phosphorylated PDH levels, LHDA and PKM1 expression, along with an increase in expression of LDHB and PKM2 (Figure 13). The decline in phosphorylated PDH levels suggests an increase in PDH activity, while a decline in LDHA and an increase in LDHB suggest an increase in lactate oxidation with age. This analysis also revealed a significant interaction between age and genotype for PDK1 and LDHB, indicating that PDK1 increases in control mice and decreases in APP/PS1 mice with age, while LDHB expression increases in control mice and does not change in APP/PS1 mice with age. These changes indicate a shift in metabolism toward oxidative phosphorylation in both control and APP/PS1 mice. The age-dependent decline in PKM2 and increase in PKM1 is unexpected since expression of PKM2 is closely associated with aerobic glycolysis in cancer cells[301,336,541,542]. Expression of PKM2 is induced by insulin signaling and mTOR activation[336], as well as epidermal growth factor receptor (EGFR) activation[543]. Elevated PKM2 expression is also found in adult stem cells while PKM1 is expressed in differentiated cells of the brain[544,545]. Western blot expression analysis of the lactate transporters MCT2 (neuron-specific) and MCT4 (astrocyte-specific) in the hippocampus revealed an age-dependent decline in MCT4 for both control and APP/PS1 mice, but no difference in age or genotype for MCT2. These findings suggest that lactate efflux may decline within hippocampal astrocytes with a concomitant metabolic shift toward oxidative phosphorylation with age. Further investigation is warranted to discern how expression of aerobic glycolysis enzymes is regulated over the course of age and in different regions of the AD brain.

The ^{1}H-MRS analysis of cerebral lactate levels was complemented by microdialysis measurements of hippocampal ISF of control and APP/PS1 mice performed by Macauley and colleagues. This analysis revealed an age-dependent increase in ISF lactate for APP/PS1 mice from 3 to 18 months of age, as well as a significant increase at 12 months of age compared to control mice (Figure 8). These results appear counter to the unaltered hippocampal lactate levels in APP/PS1 mice as measured by ^{1}H-MRS (Figure 7), as well as the age-dependent decline in expression of aerobic glycolysis enzymes and lactate

transporters in the hippocampus as measured by western blot analysis (Figure 13). One important distinction between these experiments is the physiological condition of the animal. During *in vivo* microdialysis sampling of ISF lactate, mice are awake and freely moving, while ^{1}H-MRS measurements of lactate was performed under isoflurane anesthesia. Isoflurane has been shown to influence brain metabolism[516]. In addition, *in vivo* ^{1}H-MRS has a low level of sensitivity for the detection of lactate, a limitation that is further compounded by the small size of the hippocampus.

It is well established that aerobic glycolysis is upregulated during neuronal activation with a concomitant increase in ISF lactate concentration[346,349,361,363,377,546]. The age-dependent increase in hippocampal ISF lactate concentrations in APP/PS1 mice may be indicative of an increased capacity to perform aerobic glycolysis during neuronal activation, which is supportive of my hypothesis that neurons upregulate aerobic glycolysis in response to Aβ deposition. Moreover, MCT2 expression levels did not decline with age, suggesting that neuronal-generated lactate may be exported at a higher level in APP/PS1 mice relative to control aged mice. These findings underscore the need to develop more sensitive and non-invasive techniques for measuring lactate levels *in vivo*.

4.1.4   Aerobic glycolysis does not influence amyloid-β processing

The interplay between Aβ production and glycolytic metabolism may occur through neuronal activity. Regional ISF measurements using *in vivo* microdialysis in APP$_{(Tg2576)}$ transgenic mice at 3 months of age demonstrated that neuronal activity increases ISF Aβ and lactate concentrations[547]. The acute injection of glucose increases hippocampal ISF lactate concentration, Aβ levels, and neuronal activity in both 3-month-old and 18-month old APP/PS1[93,483,548]. Interestingly, ^{1}H-MRS measurements of lactate levels in the frontal cortex of 24-month-old PS2APP mice correlated significantly with higher plaque levels[514]. Neuronal activation may also promote Aβ production through altered APP processing. In a study that used primary neuronal cultures harvested from APP$_{(Tg2576)}$ embryos, neuronal activation was found to promote Aβ production while neuronal inhibition decreased Aβ production by mediating the interaction between APP and

PS1[549]. In a similar study, activation of the NMDA receptor increased the production and secretion of Aβ by shifting APP processing from the α-secretase to the β-secretase[550]. Perhaps the most compelling evidence linking neuronal activation to aerobic glycolysis and Aβ production comes from PET imaging. The regional distribution of aerobic glycolysis in the resting human brain is predominantly in the DMN, a region that correlates spatially with deposition of Aβ in the AD brain[540]. The authors suggest this may be due to a persistent level of neuronal activity in the DMN when individuals are not engaged in specific goal-directed behaviours[352,551,552]. The DMN is also active during light sleep[553,554] and persists in deep sleep yet connectivity between frontal and posterior regions is lost during this time[555]. ISF lactate and Aβ levels exhibit diurnal fluctuation that are co-regulated and consistent with neuronal activity during sleep/wake cycles in both normal mice and APP/PS1 mice; Aβ production increases during wakefulness and decreases with sleep[547,556–558]. Furthermore, Aβ plaque formation can interrupt the normal sleep-wake cycle of 9-month-old APP/PS1 mice resulting in increased wakefulness and decreased sleep in a feed-forward loop that promotes Aβ production[557]. This is consistent with diurnal fluctuations in CSF Aβ levels and disrupted sleep-wake cycles observed in humans[556,559–561]. These observations indicate a possible feed-forward mechanism between regional neuronal activity and increases in glucose uptake, aerobic glycolysis, and Aβ production, but it is currently unknown if aerobic glycolysis promotes Aβ production or whether it is merely a consequence of neuronal activity.

In order to measure Aβ dynamics in the APP/PS1 mouse brain, an ELISA was performed on extracts from the frontal cortex of 12 month-old mice. The relative concentrations of $A\beta_{(1\text{-}40)}$ and $A\beta_{(1\text{-}42)}$ were measured as a ratio to total protein in either soluble or insoluble fractions from the frontal cortex of APP/PS1 mice. This analysis revealed that the majority of Aβ in the brains of these mice was insoluble $A\beta_{(1\text{-}42)}$ (Figure 14). This finding is in agreement with the genetic elements of APP/PS1 mice: the Swedish mutation (K670N:M671L) in *APP* increases production and secretion of both $A\beta_{(1\text{-}40)}$ and $A\beta_{(1\text{-}42)}$[562–566], while expression of PSEN1 lacking exon 9 (ΔE9) shifts the cleavage of APP to favor $A\beta_{(1\text{-}42)}$ over $A\beta_{(1\text{-}40)}$[96]. The levels of Aβ in APP/PS1 mice have been examined extensively and the majority of Aβ burden in the brain is consistently the $A\beta_{(1\text{-}42)}$ species

in insoluble (plaque) fractions[96,481,567–570]. Interestingly, the levels of soluble $A\beta_{(1-40)}$ and $A\beta_{(1-42)}$ in the cortex and hippocampus both correlate negatively with measures of spatial learning and memory in the MWM, but not insoluble $A\beta_{(1-40)}$ and $A\beta_{(1-42)}$[570]. In order to test the hypothesis that aerobic glycolysis influences $A\beta$ production, the levels of soluble and insoluble $A\beta_{(1-40)}$ and $A\beta_{(1-42)}$ were correlated with the expression of aerobic glycolysis enzymes in the frontal cortex (Figure 15). There were significant relationships detected for levels of soluble $A\beta_{(1-40)}$ and $A\beta_{(1-42)}$ with PDK1, LDHA/LDHB, PDH-p/PDH, or PKM2/PKM1. In addition, there were no significant interactions between levels of insoluble $A\beta_{(1-40)}$ and $A\beta_{(1-42)}$ with expression of any of the aerobic glycolysis enzymes investigated. This analysis indicates that aerobic glycolysis in the frontal cortex does not influence the production of $A\beta$ or the cleavage of APP to favor $A\beta_{(1-40)}$ or $A\beta_{(1-42)}$. Further studies using neuronal cell culture models evaluating the effect of altered aerobic glycolysis enzyme expression on $A\beta$ dynamics would help elucidate the interplay between these two processes.

4.1.5 Aerobic glycolysis enzymes are expressed primarily in neurons and reactive astrocytes surrounding plaques

The cell-specific spatial expression of enzymes responsible for aerobic glycolysis and lactate production in the mouse brain has not previously been investigated. Several lines of evidence support distinct metabolic phenotypes between neurons (mainly oxidative) and astrocytes (mainly glycolytic)[378]. Measurements of cerebral lactate by ^{1}H-MRS or western blot analysis of protein extracts do not distinguish between these two predominant cell types. To identify which cell types are expressing the enzymes responsible for aerobic glycolysis, frozen brain sections from control and APP/PS1 mice at 12 months of age were immunostained using antibodies specific for PDK1 and LDHA and co-stained with antibodies for astrocytes (GFAP) and neurons (TUJ1). Within the frontal cortex and hippocampus of control mice, PDK1 and LDHA expression was localized primarily to the soma of TUJ1+ neurons (Figure 16 and Figure 17). This observation demonstrates that neurons are capable of using aerobic glycolysis in both control mice and APP/PS1 mice. In support of this observation, LDHA has been found to be expressed in the cytosol of rat primary cortical neurons and astrocytes, while LDHB

expression was prevalent in synaptosomes[329]. In contrast, previous studies have found neurons exclusively immunoreactive with LDHB antibodies, while astrocytes were immunoreactive with both LDHA and LDHB antibodies in the human hippocampus and occipital cortex[328,409]. In a similar study of primary astrocyte and neuron cultures from chick embryos, astrocytes were found to predominantly express LDHA and neurons were found to predominantly express LDHB[571]. Interestingly, in this study PDK1 and LDHA were also expressed in GFAP+ reactive astrocytes surrounding amyloid plaques in the frontal cortex and hippocampus of APP/PS1 mice. It was surprising to find an absence of PDK1 or LDHA expression in astrocytes of control mice. The GFAP antibody used for this experiment may not have been sensitive enough to visualize astrocytes in control mice and future experiments should make use of an antibody that reliably stains native astrocytes. However, if PDK1 and LDHA were expressed in astrocytes of the control mouse brain then fluorescence signal would have labeled these cells red in the merged confocal image, and this was not detected. The expression of PDK1 and LDHA in reactive astrocytes, but not in native astrocytes, may indicate that these cells up-regulate aerobic glycolysis as a consequence of disease pathogenesis. A similar staining pattern has been characterized in TgCRND8 mice at 12 months of age showing co-immunostaining of reactive astrocytes with PFKFB3 expression, a main regulator of glycolysis[572]. Up-regulation of aerobic glycolysis in reactive astrocytes may be responsible for the increase in lactate observed in the frontal cortex of APP/PS1 at 9 and 12 months of age. Further investigation is warranted to test if reactive astrocytes display metabolic reprogramming toward aerobic glycolysis. Collectively these observations indicate that PDK1 and LDHA are expressed primarily in the cell bodies of neurons, yet both cell types may be capable of producing lactate through aerobic glycolysis.

4.2 Examining the relationship between cerebral aerobic glycolysis and memory performance

4.2.1 Expression of aerobic glycolysis enzymes in the frontal cortex correlates with memory performance

Previous work has demonstrated that both the hippocampus and the frontal cortex are involved in spatial memory retrieval using the MWM[573–576]. More recently, it was

demonstrated that lesions to the frontal cortex impaired memory in a partial-cue environment, showing that an interaction between the frontal cortex and hippocampus was required for pattern completion during memory retrieval[577]. However, it has yet to be determined if aerobic glycolysis in the frontal cortex or hippocampus plays a role in spatial memory recall. In order to test the hypothesis that aerobic glycolysis contributes to memory processes, a correlation analysis was performed comparing expression of aerobic glycolysis proteins in extracts from the frontal cortex and hippocampus at 12 months of age (Figure 19 and Figure 20). A multiple linear regression model was then fit on the percentage of time spent in the correct quadrant during the probe trial. This analysis revealed a significant interaction with memory for enzymes involved in lactate production including LDHA, the ratio of phosphorylated PDH to total PDH, and the ratio of PKM2 to PKM1, suggesting that higher expression, or phosphorylation, of these proteins correlates with better memory performance in control mice and worse performance in APP/PS1 mice. These observations support the hypothesis that aerobic glycolysis contributes to memory processes in control mice, but not in APP/PS1 mice. It stands to reason that if neuronal activity is linked to a focal elevation of aerobic glycolysis and lactate efflux[578], then a higher expression of aerobic glycolysis would enhance neuronal activation.

It is currently unknown why higher aerobic glycolysis may be detrimental to memory in the AD brain. In the context of AD in humans, elevated lactate levels correlate negatively with memory performance. Increased lactate within the precuneus/posterior cingulate of individuals with MCI is associated with poorer memory performance[579]. AD patients also show a significant increase in CSF lactate levels compared with age-matched non-demented individuals or patients with vascular dementia[580,581]. In addition, intravenous lactate infusion does not improve semantic memory in AD patients[582]. These findings suggest that perturbed lactate metabolism may be involved in the pathophysiological processes in AD. One possible explanation may be that enhanced aerobic glycolysis and neuronal activation promote Aβ deposition leading to interference with synaptic transmission and memory processes[570]. However, the ELISA analysis of soluble and insoluble levels of $A\beta_{(1-40)}$ and $A\beta_{(1-42)}$ demonstrated no such relationship in the frontal

cortex (Figure 15). The same multiple linear regression analysis in the hippocampus revealed no significant interaction between relative band intensity and genotype on percent time spent in the correct quadrant for any of the markers of aerobic glycolysis (Figure 20). This finding suggests that aerobic glycolysis may play a role in memory processes in the frontal cortex but not the hippocampus.

4.2.2 Chronic oral administration of dichloroacetate does not affect memory at 12 months of age

The behaviour of APP/PS1 mice is well characterized but the age of cognitive decline varies between laboratories and husbandry conditions. In the MWM, impairment in spatial memory has been reported as early as 3.5 months of age[583] and 6 months of age[584], yet 8-14 months of age is the most commonly reported age for onset of spatial memory impairment in APP/PS1 mice when using the MWM[97,569,570,585,586]. In order to test the two central hypotheses, that neurons upregulate aerobic glycolysis to promote Aβ resistance, and aerobic glycolysis contributes to memory processes, a chemical inhibitor of aerobic glycolysis, DCA, was orally administered to control and APP/PS1 mice at a dose of 200 mg/kg per day via drinking water, beginning at the age of weaning. It was anticipated that APP/PS1 mice exposed to DCA would lose a protective resistance mechanism and succumb to neurodegeneration at an earlier age than APP/PS1 mice exposed to normal drinking water. Spatial learning and memory was assessed using the MWM at 12 months of age (Figure 18). The ability of mice to learn the location of the platform was measured as the change in latency time required to find the platform over the course of 4 training days. APP/PS1 mice showed a delay in finding the platform on each training day compared to control mice. This is in agreement with similar studies demonstrating a spatial learning impairment at this age[97,584], yet disagrees with one report showing no difference between genotypes[585]. Interestingly, a study using the visual platform water maze demonstrated that APP/PS1 mice have a significant increase in thigmotaxis, or tendency to cling to or follow the wall instead of actively search for the platform, and also demonstrated more excessive floating in the pool than control mice[587]. This indicates that stress may be a confounding factor for spatial memory performance for these mice. In order to account for this possibility, mice that displayed excessive thigmotaxis or

floating in either genotype were eliminated from analysis in both the training phase and probe trials.

On day 5 a probe trial was performed in which the platform was removed and mice were tested on their ability to remember the location of the platform, as measured by the percent time spent in the correct quadrant. A two-way ANOVA revealed that APP/PS1 mice have a significant decrease in the percent time spent in the correct quadrant, regardless of DCA exposure. There was no effect from treatment or the interaction between genotype and treatment, suggesting that DCA had no effect on the ability of mice of either genotype to remember the location of the platform. This indicated that either chronic exposure to DCA had no physiological effect on the brain, or that aerobic glycolysis did not participate in Aβ resistance and memory performance. As a measure of physical ability to perform the task, the total distance covered during the probe trial was measured and a two-factor ANOVA was performed. This analysis revealed no significant effect from genotype or treatment, or the interaction between genotype and treatment, indicating that all mice swam a comparable distance. This suggests that impairment in memory performance of APP/PS1 mice is reflective of impaired spatial memory and not altered physical ability. It also demonstrates that chronic oral exposure to DCA does not have a negative consequence to physical ability.

4.2.3 Chronic oral administration of dichloroacetate does not have a physiological effect on the brain at 12 months of age

The effect of DCA exposure has been well documented in humans due to its ability to reduce lactate levels in patients with congenital forms of MELAS (mitochondrial myopathy, encephalopathy, lactic acidosis, and stroke-like episodes)[588] and preclinical evidence that it might be beneficial in cancer [589]. Acute administration of DCA at 35-50 mg/kg increases PDH activity by 3-6 fold and reduces lactate levels by more than 60% in muscle tissue[590,591]. It has been estimated that the maximal reduction in circulating lactate levels is achieved at an acute dose of DCA at 100 mg/kg, yet a dose-dependent reduction in lactate continues beyond 200 mg/kg[493]. In order to confirm the physiological effect of DCA, brain extracts were harvested at 12 months of age from the frontal cortex of control mice exposed to chronic DCA and compared to mice that were provided normal drinking

water. DCA is a specific inhibitor of PDK, the kinase that phosphorylates and inhibits the PDH complex[489,592]. It was expected that mice exposed to DCA would have a decline in PDH phosphorylation levels when compared to mice that were provided normal drinking water. However, this analysis revealed that there was no difference in PDH phosphorylation between these two groups (Figure 23). In addition, there was no difference in expression levels of any other marker of aerobic glycolysis between the two treatment groups. This indicates that chronic exposure to DCA at an oral dose of 200mg/kg daily since the age of weaning does not have a physiological effect on the mouse at 12 months of age.

Despite several studies demonstrating the effectiveness of acute DCA exposure activating PDH and lowering lactate levels, the physiological effect of chronic DCA exposure is less clear. In one study of four MELAS patients, chronic oral exposure to DCA at a daily dose of 25 mg/kg appeared to maintain lower serum lactate levels, yet there was no change in CSF lactate levels over a course of 5 years[593]. In a larger study of 30 MELAS patients given a chronic daily DCA dose of 25 mg/kg, there was no significant difference between DCA and placebo groups in ^{1}H-MRS estimation of cerebral lactate, CSF lactate, or venous lactate, over the course of 24 months[594]. In addition, all 15 of the patients randomly assigned to DCA had to prematurely discontinue the study due to side effects from peripheral nerve toxicity. DCA is cleared more efficiently from plasma after an initial acute dose than after 6 months of 25 mg/kg daily exposure[595]. Moreover, older subjects aged 14 – 33.9 years were less efficient at clearing DCA from plasma than younger subjects aged 2.2 – 7.1 years after 6 months of 25 mg/kg daily exposure[595]. This finding has also been recapitulated in rats, demonstrating an age-associated effect on DCA plasma clearance after chronic exposure for 6 months at 25 mg/kg daily[596]. These studies demonstrate a lack of knowledge on the physiological effect between acute and chronic DCA exposure. In this study, one control mouse and 3 APP/PS1 mice were euthanized after approximately 5 months of 200 mg/kg daily oral DCA exposure due to tissue damage to the ends of their tails and hind feet. All other mice appeared to tolerate DCA well up to 12 months of age. During the probe trial of the MWM, there was no significant effect of DCA treatment on the total distance covered, suggesting that there was no physical impairment due to DCA exposure on the ability of these mice to swim.

In summary, these observations indicate that chronic oral administration of DCA at 200 mg/kg daily for 12 months has no discernible effect on lactate levels or phosphorylation levels of PDH in the frontal cortex. This suggests that chronic oral DCA administration may be unsuitable for the long-term modulation of aerobic glycolysis in the brain.

4.2.4   Acute inhibition of aerobic glycolysis impairs memory

In order to further test the hypothesis that aerobic glycolysis contributes to memory processes, the chemicals DCA and Isosafrol were used to inhibit the activity of PDK and LDHA, respectively. Instead of a chronic exposure to these chemicals, an acute intraperitoneal injection was used to deliver the treatment 30 minutes before entering the MWM on the probe trial. The ability of these agents to target their intended protein in the CNS after a single intraperitoneal injection was confirmed by western blot and enzyme activity analysis (Figure 24). A single cohort of control mice and APP/PS1 mice starting at 12 months of age was selected for this experiment and all mice were injected with the same treatment at each of the probe trials (Figure 25). Mice were trained to learn the location of the platform over the course of 4 training days and the latency to find the platform was recorded for each training phase. This analysis revealed a significant difference in latency time to find the platform between genotypes for the vehicle phase, Isosafrol phase, and the DCA phase, but not the final saline phase of training. This suggests that APP/PS1 mice may show an improvement in memory over the course of repeated memory testing. However, the pre-exposure to the test agents might also have had a differential effect on memory in the APP/PS1 mice. Future studies using naïve APP/PS1 mice would help resolve this issue.

The difference between genotypes for latency to find the platform in the first three phases may be accounted by the tendency of APP/PS1 to display thigmotaxis and excessive floating as a stress response[587]. This behaviour was observed in some of the APP/PS1 mice over the course of the experiment and these mice were removed from analysis if the behaviour persisted across consecutive training days (Table A2). However, these mice were allowed to swim in subsequent training phases and were included in analysis if they did not display excessive stress behaviour. Interestingly, there was no difference in latency to find the platform during training between control mice and APP/PS1 mice for

the final training phase indicating that these mice are capable of spatial learning at 18 months of age given repeated testing. This analysis also showed no overt toxicity from acute injection of Isosafrol or DCA given that all mice were able to recover 2 weeks after chemical administration and perform just as well during the next training phase.

At each individual phase of the experiment, the chemical treatment of vehicle, Isosafrol, DCA, or saline, was given to the mice 30 minutes before entering the probe trial. This time point was chosen due to previous reports showing a physiological effect on the brain at this time for both Isosafrol at 300 mg/kg[491] and DCA at 200 mg/kg[493]. During each probe trial, the percent time spent in the correct quadrant was recorded as a measure of memory and the total distance covered was recorded as a measure of physical ability to swim in the water tank (Figure 26). A two-way ANOVA revealed a significant effect of genotype and treatment, as well as an interaction between genotype and treatment. When compared to the initial injection of the vehicle (1% Carboxymethylcellulose), Isosafrol had no effect on the ability of control mice or APP/PS1 mice to remember the location of the platform. In contrast, DCA administration had a significant effect on control mice, yet had no effect on APP/PS1 mice, when compared to either the first injection with vehicle or the last injection with saline. The same analysis was performed on the total distance travelled during the probe trial and this revealed no significant effect from genotype or treatment, suggesting that all mice were equally capable of physically performing the memory task. These observations suggest that DCA may influence memory for control mice and support the hypothesis that aerobic glycolysis contributes to memory processes. These results also complement the earlier correlation analysis, which demonstrated an inverse relationship between expression of aerobic glycolysis enzymes in the frontal cortex and memory performance in control mice and APP/PS1 mice. There appeared to be no effect from chemical administration in APP/PS1 mice, indicating that aerobic glycolysis may not contribute to memory recall in these mice.

4.2.5   Acute injection of dichloroacetate has a physiological effect on the brain

Considering that chronic exposure through drinking water did not exhibit a physiological response in the brains of affected mice at 12 months of age, it was important to determine

if acute injection of DCA had a measurable effect. Western blot analysis was performed on extracts from the frontal cortex of control mice euthanized after injection of either saline or DCA at 200 mg/kg (Figure 24A). This analysis revealed that mice injected with DCA had a significantly lower ratio of phosphorylated PDH to total PDH. This suggests that acute DCA exposure resulted in a physiological response in the brains of affected animals and is in agreement with other reports showing DCA causes a decline of phosphorylated PDH levels in mouse liver extracts[597], and isolated mitochondria from the mouse brain[598]. Intraperitoneal injection of DCA has also been shown to increase PDH activity in the brain[599,600], yet to the best of my knowledge this is the first report of DCA intraperitoneal injection demonstrating a reduction in phosphorylation levels of PDH in the brain. The relative band density of PDK1 was also measured to determine if there was any difference in the levels of the target of DCA. A significant decrease in PDK1 expression was detected in animals injected with DCA compared to saline. It is unclear if a 30 minute exposure to DCA is long enough to induce changes in transcription and translation, but long-term exposure to DCA has been shown to reduce PDK4 expression through the Forkhead box protein O1 (FOXO1) transcription factor[601]. In addition to the direct chemical inhibition of PDK, DCA exposure may also promote a decline in PDK1 expression further potentiating the decrease in PDH phosphorylation and promoting oxidative phosphorylation. Altogether, these results demonstrate that an acute injection of DCA causes an observable reduction in phosphorylation levels of PDH in the frontal cortex of affected mice.

4.2.6 The inhibition of memory performance from acute injection of dichloroacetate is not reproducible

One of the main goals of scientific experimentation is to ensure that the outcomes are reproducible. In animal behaviour experiments, there may be several confounding variables that influence the outcome of a particular test. One possible confounding factor is repeated testing, in which a previous experience influences the outcome of subsequent tasks. Animals that have been exposed to a behavioural test often perform differently than naïve animals[494], although the relative influence of repeated testing depends on the specific test being administered[602], the strain of the animal[603], and time interval between

behavioural tests[604]. One study using C57BL/6J and 129S2/Sv strains in the MWM reported that mice who had previously experienced the test did not perform any differently than naïve mice during training or during the probe trial[605]. Another study using C57BL/6J and NMRI strains showed that training at 2 months of age did not improve performance in the MWM at 10 months of age compared to naïve mice, and also did not affect from their performance when they were tested again at 18 months of age[606]. A similar study using C57BL/6J and NMRI strains showed that training at 2 months of age improved performance at 6 and 10 months of age in NMRI mice when compared to naïve mice, but this effect was not observed in C57BL/6J mice who showed no difference to naïve mice[603]. However, in the case of this study the time interval between training was approximately 2 weeks, and it is unclear if previous experiences changed the outcome of subsequent trials with a different chemical treatment. Another confounding variable that may have influenced the outcome of these tests is age. Control mice and APP/PS1 mice started the first training phase at approximately 12 months of age and finished the last probe trial at approximately 16 months of age. It is unclear if aging negatively affected mice at later experimental phases. In an attempt to address these confounding variables and determine if repeated trials or age had an influence on subsequent outcomes, a saline injection phase was performed as the final treatment (Figure 26). This analysis revealed no difference between either control mice or APP/PS1 mice injected with saline at the very end of the study or vehicle at the very beginning of the study. Although these results need to be taken with caution, they suggest that these confounding variables did not impair the ability of these mice to perform during the final probe trial.

In order to further test the hypothesis that aerobic glycolysis contributes to memory processes, a new experiment was conducted where each of the previous confounding variables was removed. DCA was selected as the treatment instead of Isosafrol because control mice showed a greater impairment in memory from DCA injection than Isosafrol treatment in the previous study. The latency time required to find the platform was recorded over the course of four training days and a one-way repeated measure ANOVA revealed no difference between mice assigned to saline or DCA treatments (Figure 27). This indicated that there was no inherent difference in the ability of mice from either

treatment group to learn the location of the hidden platform. Several measures of performance were recorded during the probe trial including the total distance traveled, the percent time spent in the correct quadrant, the number of platform entries, the latency to the first platform entry, and the difference in latency to the platform between the probe trial and the average of the final training day (Figure 27). Mice injected with DCA travelled the same total distance as mice injected with saline, suggesting that DCA had no effect on the ability of mice to swim in the tank. Mice injected with DCA spent the same percent of time in the correct quadrant as mice injected with saline, and crossed the boundary of the platform the same number of times. These measures suggest that there was no significant difference in memory performance between saline and DCA-injected mice at 9 months of age. The latency to the first platform entry was also recorded and there was no difference between DCA-injected mice and saline-injected mice. In contrast, the difference between the latency to find the platform boundary during the probe trial and the average latency to find the platform on training day 4 revealed that saline mice found the platform boundary faster than their previous average time (-4.88 ± 1.09 seconds), while the DCA mice did not find the platform any faster than their previous average time (0.16 ± 1.96 seconds). There was a considerable difference between these two groups ($p = 0.042$), yet it did not reach the significance threshold set by the Bonferroni correction for multiple comparisons ($\alpha < 0.01$). This finding should be interpreted with caution, but suggests that DCA may cause a delay in memory recall and could have had an effect on the ability of mice to continue to learn the location of platform. Future experiments should examine the effect of DCA injection before each training day in order to determine if DCA impairs learning ability in these mice. Moreover, the previous study was performed with mice at 12 months of age. The effect of DCA on mice at different ages should also be considered.

Following the probe trial, a flag trial was performed where the platform was placed back into the tank in the opposite quadrant and a red flag was attached as a visual cue. The latency to find the platform during this trial found no difference between DCA-injected mice and saline-injected mice, suggesting that DCA did not interfere with the ability of mice to use visual cues to find the platform. Altogether, these data indicate that acute

exposure to DCA does not impair memory performance in naïve mice, which is counter to the previous study showing a significant decline in memory performance of DCA-injected mice. However, there was indication that learning might be compromised by DCA exposure. Further studies using different ages of mice and repeated injection strategies will be required to formally determine the effect of DCA-mediated inhibition of aerobic glycolysis on learning and memory.

4.2.7   Acute injection of dichloroacetate may reduce conversion of pyruvate to lactate in the brain

Recent advances in MRI technology have enabled the monitoring of brain metabolism non-invasively with the use of hyperpolarized ^{13}C-labelled metabolites coupled with MRS. Injection of hyperpolarized ^{13}C-pyruvate generates pyruvate and lactate peaks that are linearly proportional to their concentration, and thus can be used to quantify the conversion of pyruvate-to-lactate in the brain[607]. Considering that acute exposure to DCA had no effect on memory performance of naïve mice, DCA was tested for a physiological response on the brain using hyperpolarized ^{13}C-pyruvate MRS. The target of DCA is PDK, which phosphorylates and inhibits the PDH complex resulting in higher activity and a drop in brain lactate levels[600]. In order to measure the conversion of pyruvate to lactate in the brain, 9-month-old naïve mice ($n = 5$) were injected via tail vein with ^{13}C-pyruvate and the resulting peaks of pyruvate and lactate were measured 30 minutes before and 30 minutes after tail vein injection of DCA (200 mg/kg). The whole brain was imaged by ^{1}H-MRI and individual ^{13}C-pyruvate spectra were overlaid to a coronal field of view (Figure 28). The average of all spectra for each individual mouse was calculated for both before and after DCA injection and the average of all mice in the experiment was then compiled. This analysis revealed a decline in the ratio of lactate-to-pyruvate from before (0.10 ± 0.01) to after (0.06 ± 0.02) DCA injection (Figure 28). A paired Welch's t-test revealed that this difference was not statistically significant ($p = 0.07$), however, only five mice were analyzed and there was considerable variability in lactate levels detected using this scanning technique. Further ^{13}C-pyruvate MRS experiments should be completed to improve the sample size and increase the power of

the analysis in order to conclusively determine that DCA causes a decline in brain lactate production.

4.2.8   Acute injection of dichloroacetate causes a decline in phosphorylated PDH levels in the brain

To determine if DCA injection in these mice caused a change in phosphorylation levels of PDH, mice were euthanized 30 minutes after intraperitoneal injection with either saline or DCA (200 mg/kg) and brain extracts from the frontal cortex and hippocampus were examined by western blotting (Figure 30 and Figure 32). This analysis revealed that DCA caused a significant reduction in levels of phosphorylated PDH to total PDH in both the frontal cortex and the hippocampus, indicating that DCA caused a physiological response in the affected animals. This analysis also revealed a significant increase in PDK1 expression and a significant decrease in MCT4 expression in the frontal cortex of DCA-injected mice. There was no significant difference between saline- and DCA-injected mice for any of the proteins investigated in the hippocampus. A decrease in expression of LDHA and MCT2 was noted but these differences did not pass the significance threshold as determined by the Bonferroni correction for multiple comparisons. Altogether, these results confirm the previous observations that DCA injection causes a decline in levels of phosphorylated PDH in the frontal cortex and hippocampus of affected mice.

4.2.9   The correlation between the expression of aerobic glycolysis enzymes in the frontal cortex and memory performance is reproducible

In order to further examine the relationship between aerobic glycolysis and memory, the percent time spent in the correct quadrant during the probe trial of the MWM was correlated to the band density from western blots of aerobic glycolysis and lactate transporter proteins in the frontal cortex and hippocampus of saline- and DCA-injected mice (Figure 33 and Figure 34). A multiple linear regression revealed that the ratio of phosphorylated PDH to total PDH in the frontal cortex positively correlated with memory performance for saline-injected mice. This suggests that mice with higher phosphorylation of PDH in the frontal cortex performed better on the memory task than

mice with lower phosphorylation of PDH. It is intriguing that DCA-injected mice had a significant reduction in levels of phosphorylated-PDH and yet this did not confer impairment in memory performance. This suggests that compensatory responses may have been activated to maintain energetic demand during memory testing despite the drop in PDH phosphorylation. A significant positive correlation was also observed between memory performance and the expression of the astrocyte-specific lactate transporter, MCT4, in the frontal cortex of DCA-injected mice. This indicates that mice with higher MCT4 expression performed better on the memory test than mice with lower expression. Previous reports have demonstrated that inhibition of MCT4 leads to amnesia, which can be rescued by lactate but not equicaloric glucose, yet the inhibition of MCT2 leads to amnesia that cannot be rescued by lactate or glucose[462]. Assuming that DCA caused a decline in lactate levels by inhibiting PDK and thus reducing phosphorylation of PDH, an increase in lactate transport may have arisen to maintain neuronal activity. The positive correlation between memory performance and levels of phosphorylated-PDH in the frontal cortex is consistent with previous observations in control mice (Figure 19). However, these mice also displayed a positive correlation for lactate-producing enzymes LDHA and PKM2/PKM1, suggesting a relationship between lactate production and improved memory. This collective trend is absent from saline-injected mice in this analysis, which showed no correlation for LDHA, LDHB, PKM2, or PKM1. In agreement with previous observations, there were no significant correlations between memory and expression of aerobic glycolysis proteins or lactate transporters in the hippocampus. These results indicate that aerobic glycolysis in the frontal cortex may play a more fundamental role than it does in the hippocampus.

It is also possible that aerobic glycolysis does not contribute to memory processes. Mice injected with DCA did not exhibit impaired memory despite a decline in levels of phosphorylated-PDH in both the frontal cortex and hippocampus. In addition, memory performance did not correlate with expression of any marker of aerobic glycolysis other than phosphorylation of PDH. However, earlier results from the correlation analysis of control and APP/PS1 mice demonstrated a clear positive correlation between memory and expression of lactate producing enzymes whereas the opposite effect was observed for the lactate consuming enzyme (Figure 19). Furthermore, a significant decline in

memory performance was measured from DCA-injected control mice when compared to vehicle-injected and saline-injected control mice (Figure 26). These observations highlight the need to reproduce experiments and test the hypothesis under different conditions. In order to further examine the relationship between memory and aerobic glycolysis, each measure of memory performance from the MWM was correlated to levels of phosphorylated PDH in the frontal cortex of saline- and DCA-injected mice (Figure 35). As previously demonstrated, a multiple linear regression revealed a significant correlation between levels of phosphorylated PDH and percent time spent in the correct quadrant.

Chapter 5

5 Conclusions

There are two main conclusions that can be drawn from this work: (1) the deposition of Aβ in the AD brain perturbs lactate metabolism as indicated by the maintained lactate levels with age in the frontal cortex of APP/PS1 mice, which interferes with memory processes normally beneficial to the healthy aging brain, and (2) aerobic glycolysis plays a role in spatial memory as demonstrated by the correlation analysis between protein expression and memory performance, yet is not explicitly required for proper memory function. There are several strengths and limitations to this study that are addressed in this chapter, as well as future directions for further addressing these emergent hypotheses.

5.1 Thesis summary

Alzheimer's disease is a neurodegenerative disorder characterized by the accumulation of intracellular amyloid plaques and extracellular neurofibrillary tangles. The amyloid plaques are comprised of aggregated Aβ peptides that cause mitochondrial dysfunction and neuronal death. Nerve cells can become resistant to Aβ-toxicity by up-regulating aerobic glycolysis, a metabolic phenotype that predominantly uses glycolysis for energy production despite the availability of oxygen. Yet, it is currently unknown if neurons are capable of escaping Aβ-mediated toxicity by up-regulating aerobic glycolysis *in vivo*, and whether aerobic glycolysis contributes to memory. The studies outlined in this dissertation tested the hypotheses that neurons upregulate aerobic glycolysis to promote Aβ resistance, and that aerobic glycolysis contributes to memory processes. *In vivo* ^{1}H-MRS revealed an age-dependent decline in lactate levels within the frontal cortex of control mice, whereas lactate levels remained unaltered in APP/PS1 mice from 3 to 12 months of age. In the hippocampus, lactate levels declined with age for both genotypes, but sampling of ISF found elevated levels of lactate in APP/PS1 mice. An age-dependent decline in levels of aerobic glycolysis enzymes in both control mice and APP/PS1 mice was detected along with a concomitant increase in lactate transporter expression in control mice. Immunofluorescence microscopy revealed the expression of aerobic

glycolysis enzymes PDK1 and LDHA primarily in neurons within the frontal cortex and hippocampus, and also in activated astrocytes in APP/PS1 mice. These findings suggest that aerobic glycolysis plays an important role in memory in control mice but may be detrimental in AD mice.

In order to test the hypothesis that aerobic glycolysis contributes to memory processes, a single cohort of mice were injected with an acute dose of Isosafrol, an inhibitor of LDHA, and also DCA, an inhibitor of PDK, in consecutive independent trials immediately before entering the MWM. Control mice exposed to DCA performed worse in the memory task compared to vehicle or saline injections, while APP/PS1 mice were unaffected. A second experiment was performed to confirm these observations using two independent groups of randomly assigned naïve control mice. In this case, mice injected with DCA were found to have similar memory performance to mice injected with saline. *In vivo* hyperpolarized ^{13}C-pyruvate MRS was used to validate the effectiveness of DCA by demonstrating a reduction in conversion of pyruvate to lactate in the brain. Western blots from extracts of the frontal cortex and hippocampus of DCA-injected mice revealed a significant decline in phosphorylation of PDH. In support of previous findings, phosphorylation of PDH correlated with better memory performance in saline-injected mice. These observations support the hypothesis that aerobic glycolysis contributes to memory, yet is likely not the only contributing factor. Together, this evidence indicates that production of lactate, via aerobic glycolysis, is beneficial for memory function during normal aging. Aβ deposition may perturb lactate processing and contribute to cognitive decline in AD.

5.2 Strengths and limitations of the study

5.2.1 Disparity between human patients and the APP/PS1 mouse model of Alzheimer's disease

Transgenic mouse models of AD offer a unique opportunity to examine pathogenic mechanisms and test novel therapeutics. However, given the high failure rate of clinical trials, several questions have arisen about the validity of using laboratory animals to model a complex age-related neurodegenerative disease in humans[608,609]. All transgenic

mouse models of AD carry autosomal dominant mutations identified from early-onset variants of the disease in humans, yet this accounts for less than 1% of all AD cases, while the vast majority of AD cases are sporadic in nature and arise as a consequence of age and genetic or lifestyle risk factors[610]. This means that these animals are good models of a small subset of AD patients, but do not accurately represent the pathophysiological changes associated with sporadic AD in the general public. In addition, most transgenic mouse models only recapitulate amyloid accumulation, yet fail to develop other pathological hallmarks including neurofibrillary tangles and neuronal loss[611]. Transgenic mice that do carry mutations driving both amyloid plaques and neurofibrillary tangles develop neurodegeneration and early cognitive deficits in a supra-physiological manner[612]. These models are efficient for experimental purposes because of the rapid onset of pathology and early cognitive decline, yet the progression of pathophysiology in humans with sporadic AD occurs over the course of decades and this cannot be accurately recapitulated in experimental models.

All of my experiments were performed using the APP/PS1 mouse model of AD. These mice carry the Swedish mutation (K670N:M671L) in the *APP* gene that results in increased production and secretion of the Aβ peptide[562–566], while expression of PSEN1 lacking exon 9 (ΔE9) shifts the cleavage of APP to favor $A\beta_{(1-42)}$ over $A\beta_{(1-40)}$[96]. I chose this model for several reasons: (1) the resistance mechanism in immortalized nerve cultures was identified in Aβ toxicity independent of tau pathology[260]; (2) these mice develop cognitive impairment between 8 and 14 months of age[481], which is suitable for the purposes of finishing experiments within a doctoral timeline; and (3) these mice do not develop neurodegeneration at the age of cognitive impairment[613], suggesting that a resistance mechanism to Aβ may exist in order to facilitate neuron survival despite the widespread accumulation of plaque at this age. Yet, if these mice do not experience neurodegeneration, then why do they develop cognitive impairment? It was recently discovered that APP/PS1 mice have impaired synaptic rewiring of cholinergic interneurons in the hippocampus that is required for fear-conditioned learning[614]. In addition, hippocampal pyramidal cells of APP/PS1 mice have early deficits in long-term potentiation (LTP) that are independent of altered dendritic spine morphology[615]. These

studies highlight a key disparity between these mice and human AD patients, where cognitive decline is highly correlated with neurofibrillary tangles and neuron loss[616–619]. The results of this dissertation suggest that memory deficit in APP/PS1 mice may also lie in altered lactate metabolism, although further experiments are needed to confirm this hypothesis.

5.2.2   Protein expression may not reflect enzyme activity

Western blot analysis of protein expression levels and phosphorylation of PDH may not accurately reflect enzyme activity or the direction of metabolic pathways. A recent ^{1}H-MRS study demonstrated that brain lactate levels increase with age and this is characterized by a shift in the ratio of LDH isozyme expression of high LDHA and low LDHB[330]. This change in the ratio of LDHA to LDHB has also been described in different tissues of the rat, including brain, in response to hypoxia[620]. However, considering that the equilibrium constant is the same for all isozymes, because it is the same reaction being catalyzed, it can be assumed that the LDH reaction is a near-equilibrium reaction and steady state conditions apply. This means that the isozyme pattern cannot have an influence on the equilibrium lactate concentration[331]. If non-steady state conditions apply, such as a rapid glycolytic flux or lactate export from the cell, then the isozyme pattern may influence lactate concentration. In support of the expression analysis of LDH isozyme pattern, Ross and colleagues also performed LDH activity assays and demonstrated a significant increase in LDH activity in the direction of the reaction from pyruvate to lactate[330]. In this dissertation, the ratio of LDHA to LDHB was measured using western blot analysis from brain extracts, yet the activity of this reaction was not measured and it was assumed that a shift in the ratio of LDHA/LDHB would translate to a change in the direction of the pyruvate to lactate reaction.

By the same measure, it was assumed that a change in the level of PDH phosphorylation was an indication of the activity of the enzyme, yet this is not always the case. Purified PDH from bovine kidney mitochondria could be inactivated in a dose-dependent manner by incubating the reaction mixture in ATP independent of PDH kinases or phosphatases[592]. The regulation of PDH by phosphorylation is also site-specific. In an elegant study by Korotchikina and Patel, the three phosphorylation sites of mammalian

PDH were mutated from Serine to Alanine either individually or in combination. The activity of these PDH mutants demonstrated little decline in activity for mutations in 2 of the 3 phosphorylation sites, yet a 50-70% decline in activity of the mutant at Serine-293[621]. One study using human mitochondria from muscle found that the phosphorylation of PDH at two independent sites, Serine-293 and Serine-300, were negatively correlated with PDH activity using an exponential model (R^2 = 0.43 and 0.46, respectively), yet this accounts for only 43% and 46% of the variation in PDH activity suggesting alternate regulatory mechanisms may be present[622]. Furthermore, elevated phosphorylation of PDH did not compromise the regulation of PDH activity during exercise. Dynamic changes to the concentrations of substrates (pyruvate, NAD^+, CoA) or products (acetyl-CoA, CO_2, NADH) may also influence the activity of PDH independent of the PDH kinases or phosphatates[623]. Considering that the acute exposure to DCA reduced phosphorylation levels of PDH at both sites Serine-232 and Serine-293 in the brains of affected mice (Figure 24), it was assumed that PDH activity was increased. However, this was not measured and it is possible that the change in phosphorylation level was not reflective of activity. If phosphorylation does not accurately reflect PDH activity, it is possible that DCA failed to inhibit memory performance because PDH activity was maintained following DCA exposure. Future experiments should measure activity of PDH from these samples to confirm that DCA exposure affects the activity of the enzyme *in vivo*.

Western blot analysis of protein expression and phosphorylation of PDH were correlated to memory performance in the MWM. Interestingly, the expression of lactate-producing enzymes in the frontal cortex correlated with better memory whereas expression of LDHB correlated with worse memory in control mice. In addition, saline-injected mice showed a positive correlation between phosphorylation of PDH in the frontal cortex and memory. Correlations of gene expression in the brain and behavioural changes have previously been described[624–627], indicating a relevant relationship between expression of certain proteins in the brain and behavioural phenotype. It was assumed that the protein levels from brain extracts of euthanized mice were reflective of actual protein expression during the memory test. However, it is currently unknown how stable these expression patterns are during stressful conditions of memory testing or over the course of time.

Several different factors are known to influence gene expression of glycolytic enzymes, including physical exercise[628], hypoxia[629], glucose availability[630], circadian rhythm[631], and neuronal activation[632]. Protein phosphorylation is an especially labile regulatory mechanism that changes rapidly in response to cellular environment[633]. In terms of metabolic signaling, phosphorylation is especially sensitive to changes in nutrient availability and energetic status of the cell considering that ATP is the donor of phosphate groups[634]. Phosphorylation of PDH can occur as quickly as 2 minutes in response to glucose stimulation in pancreatic β-cells[635]. In response to hypoxia, PDH phosphorylation occurs within 30 minutes, while transcriptional upregulation of HIF-1 target genes occurs after 4-6 hours[636]. Given that protein expression and phosphorylation is constantly changing in response to a dynamic cellular environment, future experiments should aim to euthanize mice immediately following memory testing to ensure accurate correlations are made.

5.2.3   Off-target effects and increased variability with chemical modulation from Isosafrol and dichloroacetate

In order to modulate the activity of key aerobic glycolysis enzymes, the chemicals DCA and Isosafrol were used to inhibit the aerobic glycolysis enzymes PDK and LDHA, respectively. Chemical modulation is a simple, effective, and inexpensive way to test the effect of target molecules on a biological system. Chemical modulation is used extensively *in vitro* in part due to the simplicity of the cell culture system, yet there are certain challenges associated with *in vivo* biological systems. The single largest limitation discovered in this work was the loss of effect in chronic exposure to DCA. Thus the ability to test the hypothesis that aerobic glycolysis is upregulated in neurons to promote Aβ resistance, could not be properly investigated. Other main limitations of chemical modulation in laboratory animals are potential off-target effects and variable bioavailability and clearance of these agents.

Despite several studies demonstrating the high affinity of DCA for PDK[599] and Isosafrol for LDHA[491], these chemicals have several additional off-target effects. DCA is transported across the plasma membrane by the MCT family of transporters that are also responsible for shuttling lactate, pyruvate, and ketone bodies[637]. This means that DCA

could interfere with transport of metabolites within the brain and across the blood-brain barrier by directly competing with these substrates. The primary site of DCA metabolism is the liver, where it is dehalogenated to glyoxylate in a reaction that requires glutathione and eventually converted to glycine, oxalate, and CO_2[637,638]. Yet, a minority of DCA may also undergo reductive dechlorination to monochloracetate, which is highly neurotoxic[596]. Peripheral neuropathy is a common side effect of DCA in humans[595] and laboratory animals[639]. This likely occurs via reduction in expression of myelin-related proteins in Schwann cells[640]. Over the course of this dissertation, several mice had to be euthanized after months of chronic exposure to DCA due to tissue damage to the ends of their tails and hindfeet. While all other mice appeared to tolerate DCA during the course of exposure, and there was no observable effect of DCA on the ability of mice to swim in the MWM, it was assumed that nerve toxicity did not have an effect on cerebral lactate metabolism. Isosafrol has a shorter history than DCA and so less is known about its pharmacology or pharmacotoxicology. Oral administration of isosafrol in rats resulted in 89% of the dose excreted in urine after 72 hours suggesting it has less bioavailability than DCA[641]. Isosafrol is an analog of stiripentol, which indirectly inhibits cytochrome P450 enzymes[642] and may affect detoxification reactions in the liver or synthesis of hormones, cholesterol, or vitamin D[643].

Chemical modulation also introduces a source of individual variability between animals of the same treatment. The mode of delivery of chronic DCA exposure was oral administration in the drinking water. The dosage of DCA was calculated based on an average weight of all animals in the same cage and an assumed daily consumption of 5 mL per animal. Given that animals in the same cage had different weights and likely consumed different amounts of water, the specific dose of each animal would have been slightly different. Precise dosages of DCA and Isosafrol were achieved by intraperitoneal injection. The dose of each injection was calculated by weight of each individual animal, which was more accurate than oral administration, yet there were likely subtle differences in the site of injection of each animal that introduced variability in biological measurements. In addition, mice that were injected with DCA or Isosafrol were memory tested or euthanized 30 minutes after delivery, yet the half-life of the drug is dependent on its detoxification in the liver or clearance in the kidney and would be slightly different

for each animal. For these reasons, the introduction of chemicals to a biological system as a means to study the effect of inhibiting an enzyme introduces addition sources of variability between individuals within a treatment group.

5.3 Future directions

Due to technical limitations of chemical-induced inhibition of enzymes, future work should be aimed at using more reliable and robust methods of modifying the expression or activity of these enzymes in order to reduce off-target effects and limit additional sources of variation. Genetic manipulation allows precise temporal and spatial control over expression of gene targets. This gives researchers the tools for examining the biological consequence of altered expression within a given age of an animal's lifespan and within specific tissues of interest.

Future projects will be aimed at over-expressing or knocking-out LDHA in either neurons or astrocytes and testing the behavioural outcome at an appropriate age. In addition, crossing these mice to a mouse model of AD would greatly help towards identifying the role of LDHA expression, and associated lactate production, on AD progression. Some of this work has already been accomplished. In consultation with Christopher Pin and the London Regional Transgenic and Gene Targeting Facility (LRTGT), I created a new transgenic mouse line over-expressing mouse LDHA with a C-terminal HA tag. Founder mice for this transgenic line are currently in our colony. The *Ldha* gene was cloned into the pTRE-Tight (Clontech) tetracycline-inducible expression vector, which contains a minimal CMV promoter ($P_{minCMV\Delta}$) immediately downstream of a tetracycline response element (TRE_{mod}) consisting of seven direct repeats of a 36 bp sequence containing the 19 bp tetracycline operator sequence (tet-O). In order to test the efficiency of expression in response to tetracycline, the mLDHA-HA-pTight construct was transfected into HeLa cells that stably express the reverse tetracycline transactivator (rtTA). The HeLa-rtTA cells were kindly provided by Dr. Nina Jones of Guelph University. A dose-dependent increase in mLDHA-HA protein level was found with a 24 hour exposure to tetracycline as determined by western blot analysis of cell lysates using anti-HA antibodies (Figure A1B). The mLDHA-HA-pTight construct was then digested with the *Xho1* restriction enzyme to isolate the fragment containing the P_{tight} promoter and the mLDHA-HA gene

with a polyadenylation tail. This fragment was used for pronuclear injection into fertilized embryos for the creation of a novel transgenic mouse at the LRTGT facility. Tail samples from weaned pups were tested for the presence of the mLDHA-HA transgene using primers within the P_{tight} promoter and the first exon of the LDHA gene. This analysis identified two female mice positive for the mLDHA-HA transgene. These founders were bred to male C57BL/6J mice and the litters were tested for the presence of the transgene using ear punch tissue from weaning. One of the founder females produced a single female pup that was positive for mLDHA-HA, indicating that the transgene was within the germline and could be passed through breeding (Figure A1C).

This mLDHA-HA transgenic mouse line will be crossed to mice containing the reverse tetracycline transactivator (rtTA) under control of the neuron-specific *CaMKIIα* promoter in order to drive expression of mLDHA-HA specifically in neurons in response to oral administration of doxycycline[644]. In order to drive expression in astrocytes, tet-O-mLDHA-HA transgenic mice will be crossed to mice containing the rtTA element under control of the astrocyte-specific *Gfap* promoter[645,646]. In a preliminary experiment to confirm the tight inducible expression of the mLDHA-HA construct, 1-month-old mice that express either the mLDHA-HA alone or rtTA alone, or mice expressing both mLDHA-HA and rtTA will be switched to a doxycycline chow for a time course of 2 weeks and then euthanized. Western blot analysis using HA-specific monoclonal antibodies will be used to confirm the expression of the mLDHA-HA construct in double transgenic mice alone. A sub-cohort of double transgenic mice will be treated with doxycycline for 2 weeks and removed from doxycycline for 2 weeks to demonstrate that removal of doxycycline after induction can suppress expression of the transgene. Once the regulation of transgene expression has been confirmed, double-transgenic mice will be allowed to age to 12 months and exposed to doxycycline chow for 2 weeks that will activate mLDHA-HA expression in either neurons or astrocytes.

In order to knock-out LDHA expression in either neurons or astrocytes, an alternate approach will be taken. Transgenic mice containing loxP sites flanking exon 2 in the *Ldha* alleles (LDHA^{fl/fl}) will be crossed to mice containing Cre-recombinase under control of the tet-O promoter (tet-O-Cre)[647]. The LDHA^{fl/fl} mouse line is commercially

available and has successfully been used to conditionally knockout the Ldha gene only in bone marrow stem cells[648]. These double-transgenic mice will be crossed to mice containing the tetracycline-transactivator (tTA) cassette under control of the *CaMKIIα* promoter to drive expression in neurons[649] or the *Gfap* promoter to drive expression in astrocytes[650]. The tTA element will repress expression of Cre in the presence of doxycycline and activate Cre when doxycycline is removed. Considering that complete knockout of LDHA is embryonic lethal[651], pregnant mothers will be put on doxycycline chow to prevent the expression of Cre during gestation and neonatal development in triple-transgenic mice. In a preliminary experiment to confirm the absence of LDHA expression, 1-month-old triple-transgenic mice will be switched from a doxycycline chow to a normal chow for a time course of 2 weeks and then euthanized. Western blot analysis of brain extracts using LDHA-specific antibodies will be used to determine the expression of LDHA protein relative to double-transgenic mice that lack the tet-O-Cre cassette. A sub-cohort of triple transgenic mice will be switched to normal food for 2 weeks and then back to doxycycline for 2 weeks to demonstrate that removal of doxycycline induces a permanent excision of the floxed *Ldha* gene. Once the regulation of the transgenic elements have been established, triple-transgenic mice will be maintained on doxycycline until 12 months of age and switched to normal chow to remove LDHA expression in either neurons or astrocytes.

These genetic mouse lines allow for convenient temporal and spatial control over expression of LDHA response to doxycycline chow. Transgenic mice that are either not exposed to doxycycline chow (for over-expression line) or exposed to doxycycline chow (for knock-out line) can be conveniently used as littermate controls. The behaviour of LDHA over-expression mice or LDHA knock-out mice will be evaluated using several different memory tests, including the MWM, the Barnes maze[652], and the novel object recognition test[653]. In order to assess stress and anxiety of these animals, the open-field test[654], the elevated plus maze[655], and the light-dark exploration test[656] will be used. All of these behavioural tests are available to our laboratory. The amount of lactate will be measured *in vivo* using ^{1}H-MRS examining different brain regions including the frontal cortex, the hippocampus, and the cerebellum. Mice will be euthanized and brain tissue

harvested for western blot analysis of the frontal cortex, the hippocampus, and the cerebellum, in order to confirm the expression of the mLDHA-HA construct using HA-specific antibodies or the deletion of LDHA using LDHA-specific antibodies. The tissue-specific expression or knock-out of LDHA in neurons or astrocytes will be evaluated using cryo-immunofluorescence microscopy with TUJ1 antibodies to target neurons and GFAP antibodies to target astrocytes with co-immunostaining using HA-specific antibodies and LDHA-specific antibodies. It is predicted that mice over-expressing mLDHA-HA in neurons or astrocytes will display higher levels of cerebral lactate and have enhanced memory performance. In contrast, mice that lack LDHA expression will display decreased levels of cerebral lactate and will have memory deficits. These results will offer robust evidence to accept or reject the hypothesis that aerobic glycolysis contributes to memory processes. Any differences between the genetic manipulations of LDHA in neurons or astrocytes will indicate a functionally distinct role of aerobic glycolysis in these two different cell types.

In order to test the hypothesis that aerobic glycolysis promotes $A\beta$ resistance in AD, double-transgenic LDHA over-expression mice and triple-transgenic LDHA knock-out mice will each be crossed to the 5xTg mouse line. These mice contain 5 different mutations targeting the $A\beta$ pathway: $APP_{KM670/671NL}$ (Swedish), APP_{I716V} (Florida), APP_{V7171} (London), $PSEN_{1M146L}$, and $PSEN_{L286V}$. This mouse model of AD has several benefits over the APP/PS1 mouse line; including deficits in spatial learning that occur at 4-5 months of age and apparent neurodegeneration at 9-12 months of age[657]. Considering that these mice exhibit dramatic rises in $A\beta_{(1-42)}$ levels beginning at 1.5 months of age, the induction of LDHA over-expression or knock-out will be initialized immediately after weaning. These mice will be monitored over the course of age and behavioural testing will be administered at 4 months of age. The progression of amyloid pathology will be examined over the course of aging by euthanizing mice at regular intervals of age. Brain cryo-sections will be stained with Thioflavin S to visualize amyloid plaques via immunofluorescence, while cerebral levels of $A\beta_{(1-40)}$ and $A\beta_{(1-42)}$ will be measured using ELISAs. Synaptic dysfunction and neurodegeneration will be evaluated by western blot analysis measuring levels of syntaxin and post-synaptic density protein 95 (PSD-95),

both synaptic markers, and p25 as a marker for the neurodegeneration pathway[657]. It is anticipated that over-expression of LDHA in neurons or astrocytes will maintain neuron survival in 5xTg mice at 9 months of age, while the opposite trend is expected with LDHA knock-out mice. These experiments will provide sufficient evidence to accept or reject the hypothesis that aerobic glycolysis promotes Aβ resistance in AD.

5.4   Concluding remarks

A number of significant and novel findings were realized in this study. First, lactate levels in the frontal cortex decline with age, yet are maintained in APP/SP1 mice. A significant correlation exists between expression of lactate producing enzymes and memory performance in control mice, but not in APP/PS1 mice. These findings suggest that lactate production plays a beneficial role in memory in the healthy aging brain but might contribute to memory decline in the AD brain. Second, expression of PDK1 and LDHA, two central regulators of aerobic glycolysis was found primarily in the soma of neurons, but also in reactive astrocytes surrounding amyloid plaques. These observations indicate that neurons can also generate lactate, and that reactive astrocytes may play a role in the elevated lactate levels detected in the AD brain. Finally, chemical inhibition of aerobic glycolysis appeared to inhibit learning in mice whereas it had little to no effect on spatial memory. Thus, aerobic glycolysis may play a more prominent role in different regions of the brain affecting other cognitive processes and behaviours independent of memory. Each of these observations need to be examined further in order to provide a more complete mechanistic overview of cerebral lactate metabolism in the healthy brain and its role in memory. This work will also lead to a better understanding of how aerobic glycolysis and cerebral Aβ interact in the AD brain and could lead to the development of novel metabolic strategies to treat this devastating disease.

Bibliography

1. Prevalence and Monetary Costs of Dementia in Canada. (2016).

2. Campion, D. *et al.* Early-onset autosomal dominant Alzheimer disease: prevalence, genetic heterogeneity, and mutation spectrum. *Am. J. Hum. Genet.* **65,** 664–670 (1999).

3. Janssen, J. C. *et al.* Early onset familial Alzheimer's disease: Mutation frequency in 31 families. *Neurology* **60,** 235–239 (2003).

4. Imtiaz, B., Tolppanen, A.-M., Kivipelto, M. & Soininen, H. Future directions in Alzheimer's disease from risk factors to prevention. *Biochem. Pharmacol.* **88,** 661–670 (2014).

5. Alzheimer's Association. 2015 Alzheimer's disease facts and figures. *Alzheimers Dement. J. Alzheimers Assoc.* **11,** 332–384 (2015).

6. Brookmeyer, R., Corrada, M. M., Curriero, F. C. & Kawas, C. Survival following a diagnosis of Alzheimer disease. *Arch. Neurol.* **59,** 1764–1767 (2002).

7. Small, D. H. & Cappai, R. Alois Alzheimer and Alzheimer's disease: a centennial perspective. *J. Neurochem.* **99,** 708–710 (2006).

8. Grundke-Iqbal, I. *et al.* Abnormal phosphorylation of the microtubule-associated protein tau (tau) in Alzheimer cytoskeletal pathology. *Proc. Natl. Acad. Sci.* **83,** 4913–4917 (1986).

9. Kosik, K. S., Joachim, C. L. & Selkoe, D. J. Microtubule-associated protein tau (tau) is a major antigenic component of paired helical filaments in Alzheimer disease. *Proc. Natl. Acad. Sci.* **83,** 4044–4048 (1986).

10. Wood, J. G., Mirra, S. S., Pollock, N. J. & Binder, L. I. Neurofibrillary tangles of Alzheimer disease share antigenic determinants with the axonal microtubule-associated protein tau (tau). *Proc. Natl. Acad. Sci.* **83,** 4040–4043 (1986).

11. Glenner, G. G. & Wong, C. W. Alzheimer's disease: initial report of the purification and characterization of a novel cerebrovascular amyloid protein. *Biochem. Biophys. Res. Commun.* **120,** 885–890 (1984).

12. Wong, C. W., Quaranta, V. & Glenner, G. G. Neuritic plaques and cerebrovascular amyloid in Alzheimer disease are antigenically related. *Proc. Natl. Acad. Sci. U. S. A.* **82,** 8729–8732 (1985).

13. Hyman, B. T. & Trojanowski, J. Q. Consensus recommendations for the postmortem diagnosis of Alzheimer disease from the National Institute on Aging and the Reagan Institute Working Group on diagnostic criteria for the

neuropathological assessment of Alzheimer disease. *J. Neuropathol. Exp. Neurol.* **56,** 1095–1097 (1997).

14. Iqbal, K. *et al.* Defective brain microtubule assembly in Alzheimer's disease. *Lancet Lond. Engl.* **2,** 421–426 (1986).

15. Gu, Y., Oyama, F. & Ihara, Y. Tau is widely expressed in rat tissues. *J. Neurochem.* **67,** 1235–1244 (1996).

16. Drechsel, D. N., Hyman, A. A., Cobb, M. H. & Kirschner, M. W. Modulation of the dynamic instability of tubulin assembly by the microtubule-associated protein tau. *Mol. Biol. Cell* **3,** 1141–1154 (1992).

17. Jameson, L., Frey, T., Zeeberg, B., Dalldorf, F. & Caplow, M. Inhibition of microtubule assembly by phosphorylation of microtubule-associated proteins. *Biochemistry (Mosc.)* **19,** 2472–2479 (1980).

18. Lindwall, G. & Cole, R. D. Phosphorylation affects the ability of tau protein to promote microtubule assembly. *J. Biol. Chem.* **259,** 5301–5305 (1984).

19. Hutton, M. *et al.* Association of missense and 5'-splice-site mutations in tau with the inherited dementia FTDP-17. *Nature* **393,** 702–705 (1998).

20. Poorkaj, P. *et al.* Tau is a candidate gene for chromosome 17 frontotemporal dementia. *Ann. Neurol.* **43,** 815–825 (1998).

21. Spillantini, M. G. *et al.* Mutation in the tau gene in familial multiple system tauopathy with presenile dementia. *Proc. Natl. Acad. Sci.* **95,** 7737–7741 (1998).

22. Tanzi, R. E. & Bertram, L. Twenty years of the Alzheimer's disease amyloid hypothesis: a genetic perspective. *Cell* **120,** 545–555 (2005).

23. Lemere, C. A. *et al.* Sequence of Deposition of Heterogeneous Amyloid β-Peptides and APO E in Down Syndrome: Implications for Initial Events in Amyloid Plaque Formation. *Neurobiol. Dis.* **3,** 16–32 (1996).

24. Lemere, C. A. *et al.* The E280A presenilin 1 Alzheimer mutation produces increased Aβ42 deposition and severe cerebellar pathology. *Nat. Med.* **2,** 1146–1150 (1996).

25. Bateman, R. J. *et al.* Clinical and biomarker changes in dominantly inherited Alzheimer's disease. *N. Engl. J. Med.* **367,** 795–804 (2012).

26. Arriagada, P. V., Growdon, J. H., Hedley-Whyte, E. T. & Hyman, B. T. Neurofibrillary tangles but not senile plaques parallel duration and severity of Alzheimer's disease. *Neurology* **42,** 631–639 (1992).

27. Li, T. *et al.* The neuritic plaque facilitates pathological conversion of tau in an Alzheimer/'s disease mouse model. *Nat. Commun.* **7,** 12082 (2016).

28. Hardy, J. A. & Higgins, G. A. Alzheimer's disease: the amyloid cascade hypothesis. *Science* **256,** 184–185 (1992).

29. Bagyinszky, E., Youn, Y. C., An, S. & Kim, S. The genetics of Alzheimer&#39;s disease. *Clin. Interv. Aging* 535 (2014). doi:10.2147/CIA.S51571

30. Jonsson, T. *et al.* A mutation in APP protects against Alzheimer's disease and age-related cognitive decline. *Nature* **488,** 96–99 (2012).

31. Masters, C. L. *et al.* Amyloid plaque core protein in Alzheimer disease and Down syndrome. *Proc. Natl. Acad. Sci. U. S. A.* **82,** 4245–4249 (1985).

32. Kang, J. *et al.* The precursor of Alzheimer's disease amyloid A4 protein resembles a cell-surface receptor. *Nature* **325,** 733–736 (1987).

33. Wisniewski, K. E., Wisniewski, H. M. & Wen, G. Y. Occurrence of neuropathological changes and dementia of Alzheimer's disease in Down's syndrome. *Ann. Neurol.* **17,** 278–282 (1985).

34. Bayer, T. A., Cappai, R., Masters, C. L., Beyreuther, K. & Multhaup, G. It all sticks together--the APP-related family of proteins and Alzheimer's disease. *Mol. Psychiatry* **4,** 524–528 (1999).

35. Lorent, K. *et al.* Expression in mouse embryos and in adult mouse brain of three members of the amyloid precursor protein family, of the alpha-2-macroglobulin receptor/low density lipoprotein receptor-related protein and of its ligands apolipoprotein E, lipoprotein lipase, alpha-2-macroglobulin and the 40,000 molecular weight receptor-associated protein. *Neuroscience* **65,** 1009–1025 (1995).

36. Schubert, D., Jin, L. W., Saitoh, T. & Cole, G. The regulation of amyloid beta protein precursor secretion and its modulatory role in cell adhesion. *Neuron* **3,** 689–694 (1989).

37. Araki, W. *et al.* Trophic effect of beta-amyloid precursor protein on cerebral cortical neurons in culture. *Biochem. Biophys. Res. Commun.* **181,** 265–271 (1991).

38. Roch, J. M. *et al.* Increase of synaptic density and memory retention by a peptide representing the trophic domain of the amyloid beta/A4 protein precursor. *Proc. Natl. Acad. Sci. U. S. A.* **91,** 7450–7454 (1994).

39. Small, D. H. *et al.* A heparin-binding domain in the amyloid protein precursor of Alzheimer's disease is involved in the regulation of neurite outgrowth. *J. Neurosci. Off. J. Soc. Neurosci.* **14,** 2117–2127 (1994).

40. Zheng, H. *et al.* beta-Amyloid precursor protein-deficient mice show reactive gliosis and decreased locomotor activity. *Cell* **81,** 525–531 (1995).

41. Heber, S. *et al.* Mice with combined gene knock-outs reveal essential and partially redundant functions of amyloid precursor protein family members. *J. Neurosci. Off. J. Soc. Neurosci.* **20,** 7951–7963 (2000).

42. Wang, P. *et al.* Defective neuromuscular synapses in mice lacking amyloid precursor protein (APP) and APP-Like protein 2. *J. Neurosci. Off. J. Soc. Neurosci.* **25,** 1219–1225 (2005).

43. Jacobsen, K. T. & Iverfeldt, K. Amyloid precursor protein and its homologues: a family of proteolysis-dependent receptors. *Cell. Mol. Life Sci. CMLS* **66,** 2299–2318 (2009).

44. Koo, E. H. *et al.* Precursor of amyloid protein in Alzheimer disease undergoes fast anterograde axonal transport. *Proc. Natl. Acad. Sci. U. S. A.* **87,** 1561–1565 (1990).

45. Querfurth, H. W. & LaFerla, F. M. Alzheimer's Disease. *N. Engl. J. Med.* **362,** 329–344 (2010).

46. Levy-Lahad, E. *et al.* Candidate gene for the chromosome 1 familial Alzheimer's disease locus. *Science* **269,** 973–977 (1995).

47. Rogaev, E. I. *et al.* Familial Alzheimer's disease in kindreds with missense mutations in a gene on chromosome 1 related to the Alzheimer's disease type 3 gene. *Nature* **376,** 775–778 (1995).

48. Sherrington, R. *et al.* Cloning of a gene bearing missense mutations in early-onset familial Alzheimer's disease. *Nature* **375,** 754–760 (1995).

49. Jarrett, J. T., Berger, E. P. & Lansbury, P. T. The carboxy terminus of the beta amyloid protein is critical for the seeding of amyloid formation: implications for the pathogenesis of Alzheimer's disease. *Biochemistry (Mosc.)* **32,** 4693–4697 (1993).

50. Hardy, J. & Selkoe, D. J. The amyloid hypothesis of Alzheimer's disease: progress and problems on the road to therapeutics. *Science* **297,** 353–356 (2002).

51. Kumar, D. K. V. *et al.* Amyloid-β peptide protects against microbial infection in mouse and worm models of Alzheimer's disease. *Sci. Transl. Med.* **8,** 340ra72 (2016).

52. Mawuenyega, K. G. *et al.* Decreased clearance of CNS beta-amyloid in Alzheimer's disease. *Science* **330,** 1774 (2010).

53. Selkoe, D. J. Preventing Alzheimer's disease. *Science* **337,** 1488–1492 (2012).

54. Strittmatter, W. J. *et al.* Apolipoprotein E: high-avidity binding to beta-amyloid and increased frequency of type 4 allele in late-onset familial Alzheimer disease. *Proc. Natl. Acad. Sci. U. S. A.* **90,** 1977–1981 (1993).

55. Corder, E. H. *et al.* Gene dose of apolipoprotein E type 4 allele and the risk of Alzheimer's disease in late onset families. *Science* **261,** 921–923 (1993).

56. Farrer LA, Cupples L, Haines JL & et al. Effects of age, sex, and ethnicity on the association between apolipoprotein e genotype and alzheimer disease: A meta-analysis. *JAMA* **278,** 1349–1356 (1997).

57. Roses, A. D. Apolipoprotein E Affects the Rate of Alzheimer Disease Expression: β-Amyloid Burden Is a Secondary Consequence Dependent on APOE Genotype and Duration of Disease. *J. Neuropathol. Exp. Neurol.* **53,** 429–437 (1994).

58. Mahley, R. W. Apolipoprotein E: cholesterol transport protein with expanding role in cell biology. *Science* **240,** 622–630 (1988).

59. Weisgraber, K. H., Rall, S. C. & Mahley, R. W. Human E apoprotein heterogeneity. Cysteine-arginine interchanges in the amino acid sequence of the apo-E isoforms. *J. Biol. Chem.* **256,** 9077–9083 (1981).

60. Hatters, D. M., Peters-Libeu, C. A. & Weisgraber, K. H. Apolipoprotein E structure: insights into function. *Trends Biochem. Sci.* **31,** 445–454 (2006).

61. Keeney, J. T.-R., Ibrahimi, S. & Zhao, L. Human ApoE Isoforms Differentially Modulate Glucose and Amyloid Metabolic Pathways in Female Brain: Evidence of the Mechanism of Neuroprotection by ApoE2 and Implications for Alzheimer's Disease Prevention and Early Intervention. *J. Alzheimers Dis. JAD* **48,** 411–424 (2015).

62. LaDu, M. J. *et al.* Isoform-specific binding of apolipoprotein E to beta-amyloid. *J. Biol. Chem.* **269,** 23403–23406 (1994).

63. Holtzman, D. M. *et al.* Expression of human apolipoprotein E reduces amyloid-beta deposition in a mouse model of Alzheimer's disease. *J. Clin. Invest.* **103,** R15–R21 (1999).

64. Holtzman, D. M. *et al.* Apolipoprotein E isoform-dependent amyloid deposition and neuritic degeneration in a mouse model of Alzheimer's disease. *Proc. Natl. Acad. Sci. U. S. A.* **97,** 2892–2897 (2000).

65. Schmechel, D. E. *et al.* Increased amyloid beta-peptide deposition in cerebral cortex as a consequence of apolipoprotein E genotype in late-onset Alzheimer disease. *Proc. Natl. Acad. Sci. U. S. A.* **90,** 9649–9653 (1993).

66. Bogdanovic, N., Corder, E., Lannfelt, L. & Winblad, B. APOE polymorphism and clinical duration determine regional neuropathology in Swedish APP(670, 671)

mutation carriers: implications for late-onset Alzheimer's disease. *J. Cell. Mol. Med.* **6,** 199–214 (2002).

67. Small, G. W. *et al.* Influence of cognitive status, age, and APOE-4 genetic risk on brain FDDNP positron-emission tomography imaging in persons without dementia. *Arch. Gen. Psychiatry* **66,** 81–87 (2009).

68. Theendakara, V. *et al.* Direct Transcriptional Effects of Apolipoprotein E. *J. Neurosci. Off. J. Soc. Neurosci.* **36,** 685–700 (2016).

69. Greenberg, S. M., Rebeck, G. W., Vonsattel, J. P., Gomez-Isla, T. & Hyman, B. T. Apolipoprotein E epsilon 4 and cerebral hemorrhage associated with amyloid angiopathy. *Ann. Neurol.* **38,** 254–259 (1995).

70. Josephs, K. A., Tsuboi, Y., Cookson, N., Watt, H. & Dickson, D. W. Apolipoprotein E epsilon 4 is a determinant for Alzheimer-type pathologic features in tauopathies, synucleinopathies, and frontotemporal degeneration. *Arch. Neurol.* **61,** 1579–1584 (2004).

71. Martinez, M. *et al.* Apolipoprotein E4 is probably responsible for the chromosome 19 linkage peak for Parkinson's disease. *Am. J. Med. Genet. Part B Neuropsychiatr. Genet. Off. Publ. Int. Soc. Psychiatr. Genet.* **136B,** 72–74 (2005).

72. Masterman, T. & Hillert, J. The telltale scan: APOE epsilon4 in multiple sclerosis. *Lancet Neurol.* **3,** 331 (2004).

73. Hendrie, H. C. Epidemiology of dementia and Alzheimer's disease. *Am. J. Geriatr. Psychiatry Off. J. Am. Assoc. Geriatr. Psychiatry* **6,** S3-18 (1998).

74. Fratiglioni, L., De Ronchi, D. & Agüero-Torres, H. Worldwide prevalence and incidence of dementia. *Drugs Aging* **15,** 365–375 (1999).

75. Canadian Study of Health and Aging Working Group. Canadian study of health and aging: study methods and prevalence of dementia. *CMAJ Can. Med. Assoc. J.* **150,** 899–913 (1994).

76. Scahill, R. I. *et al.* A longitudinal study of brain volume changes in normal aging using serial registered magnetic resonance imaging. *Arch. Neurol.* **60,** 989–994 (2003).

77. Enzinger, C. *et al.* Risk factors for progression of brain atrophy in aging: six-year follow-up of normal subjects. *Neurology* **64,** 1704–1711 (2005).

78. Fotenos, A. F., Snyder, A. Z., Girton, L. E., Morris, J. C. & Buckner, R. L. Normative estimates of cross-sectional and longitudinal brain volume decline in aging and AD. *Neurology* **64,** 1032–1039 (2005).

79. Hedman, A. M., van Haren, N. E. M., Schnack, H. G., Kahn, R. S. & Hulshoff Pol, H. E. Human brain changes across the life span: a review of 56 longitudinal magnetic resonance imaging studies. *Hum. Brain Mapp.* **33,** 1987–2002 (2012).

80. Du, A. T. *et al.* Atrophy rates of entorhinal cortex in AD and normal aging. *Neurology* **60,** 481–486 (2003).

81. Du, A.-T. *et al.* Age effects on atrophy rates of entorhinal cortex and hippocampus. *Neurobiol. Aging* **27,** 733–740 (2006).

82. Fjell, A. M. *et al.* One-year brain atrophy evident in healthy aging. *J. Neurosci. Off. J. Soc. Neurosci.* **29,** 15223–15231 (2009).

83. Koivisto, K. *et al.* Prevalence of age-associated memory impairment in a randomly selected population from eastern Finland. *Neurology* **45,** 741–747 (1995).

84. Nyberg, L., Lövdén, M., Riklund, K., Lindenberger, U. & Bäckman, L. Memory aging and brain maintenance. *Trends Cogn. Sci.* **16,** 292–305 (2012).

85. Dickson, D. W. *et al.* Identification of normal and pathological aging in prospectively studied nondemented elderly humans. *Neurobiol. Aging* **13,** 179–189 (1992).

86. Vlassenko, A. G. *et al.* Amyloid-Beta Plaque Growth in Cognitively Normal Adults: Longitudinal PIB Data. *Ann. Neurol.* **70,** 857–861 (2011).

87. Rodrigue, K. M., Kennedy, K. M. & Park, D. C. Beta-Amyloid Deposition and the Aging Brain. *Neuropsychol. Rev.* **19,** 436–450 (2009).

88. Swerdlow, R. H. Is aging part of Alzheimer's disease, or is Alzheimer's disease part of aging? *Neurobiol. Aging* **28,** 1465–1480 (2007).

89. Dubois, B. *et al.* Revising the definition of Alzheimer's disease: a new lexicon. *Lancet Neurol.* **9,** 1118–1127 (2010).

90. Albert, M. S. *et al.* The diagnosis of mild cognitive impairment due to Alzheimer's disease: recommendations from the National Institute on Aging-Alzheimer's Association workgroups on diagnostic guidelines for Alzheimer's disease. *Alzheimers Dement. J. Alzheimers Assoc.* **7,** 270–279 (2011).

91. Jack, C. R. *et al.* Introduction to the recommendations from the National Institute on Aging-Alzheimer's Association workgroups on diagnostic guidelines for Alzheimer's disease. *Alzheimers Dement. J. Alzheimers Assoc.* **7,** 257–262 (2011).

92. Sperling, R. A. *et al.* Toward defining the preclinical stages of Alzheimer's disease: recommendations from the National Institute on Aging-Alzheimer's Association workgroups on diagnostic guidelines for Alzheimer's disease. *Alzheimers Dement. J. Alzheimers Assoc.* **7,** 280–292 (2011).

93. Cirrito, J. R. *et al.* In vivo assessment of brain interstitial fluid with microdialysis reveals plaque-associated changes in amyloid-beta metabolism and half-life. *J. Neurosci. Off. J. Soc. Neurosci.* **23,** 8844–8853 (2003).

94. Kress, B. T. *et al.* Impairment of paravascular clearance pathways in the aging brain. *Ann. Neurol.* **76,** 845–861 (2014).

95. Jack, C. R. *et al.* Amyloid-first and neurodegeneration-first profiles characterize incident amyloid PET positivity. *Neurology* **81,** 1732–1740 (2013).

96. Jankowsky, J. L. *et al.* Mutant presenilins specifically elevate the levels of the 42 residue beta-amyloid peptide in vivo: evidence for augmentation of a 42-specific gamma secretase. *Hum. Mol. Genet.* **13,** 159–170 (2004).

97. Lalonde, R., Kim, H. D., Maxwell, J. A. & Fukuchi, K. Exploratory activity and spatial learning in 12-month-old APP(695)SWE/co+PS1/DeltaE9 mice with amyloid plaques. *Neurosci. Lett.* **390,** 87–92 (2005).

98. Cummings, J. L., Morstorf, T. & Zhong, K. Alzheimer's disease drug-development pipeline: few candidates, frequent failures. *Alzheimers Res. Ther.* **6,** 37 (2014).

99. Reisberg, B. *et al.* Memantine in Moderate-to-Severe Alzheimer's Disease. *N. Engl. J. Med.* **348,** 1333–1341 (2003).

100. Wenk, G. L., Parsons, C. G. & Danysz, W. Potential role of N-methyl-D-aspartate receptors as executors of neurodegeneration resulting from diverse insults: focus on memantine. *Behav. Pharmacol.* **17,** 411–424 (2006).

101. Winblad, B., Jones, R. W., Wirth, Y., Stöffler, A. & Möbius, H. J. Memantine in moderate to severe Alzheimer's disease: a meta-analysis of randomised clinical trials. *Dement. Geriatr. Cogn. Disord.* **24,** 20–27 (2007).

102. Mecocci, P., Bladström, A. & Stender, K. Effects of memantine on cognition in patients with moderate to severe Alzheimer's disease: post-hoc analyses of ADAS-cog and SIB total and single-item scores from six randomized, double-blind, placebo-controlled studies. *Int. J. Geriatr. Psychiatry* **24,** 532–538 (2009).

103. Atri, A. *et al.* Memantine in patients with Alzheimer's disease receiving donepezil: new analyses of efficacy and safety for combination therapy. *Alzheimers Res. Ther.* **5,** 6 (2013).

104. Berk, C. & Sabbagh, M. Successes and Failures for Drugs in Late-Stage Development for Alzheimer's Disease. *Drugs Aging* **30,** 783–792 (2013).

105. Holtzman, D. M., John, C. M. & Goate, A. Alzheimer's Disease: The Challenge of the Second Century. *Sci. Transl. Med.* **3,** 77sr1 (2011).

106. Callaway, E. Alzheimer's drugs take a new tack. *Nature* **489,** 13–4 (2012).

107. Sperling, R. A., Jack, C. R. & Aisen, P. S. Testing the right target and right drug at the right stage. *Sci. Transl. Med.* **3,** 111cm33 (2011).

108. Mueller, S. G. *et al.* The Alzheimer's disease neuroimaging initiative. *Neuroimaging Clin. N. Am.* **15,** 869–877, xi–xii (2005).

109. Mueller, S. G. *et al.* Ways toward an early diagnosis in Alzheimer's disease: the Alzheimer's Disease Neuroimaging Initiative (ADNI). *Alzheimers Dement. J. Alzheimers Assoc.* **1,** 55–66 (2005).

110. Morris, J. C. *et al.* Developing an international network for Alzheimer research: The Dominantly Inherited Alzheimer Network. *Clin. Investig.* **2,** 975–984 (2012).

111. Reiman, E. M., Langbaum, J. B. S. & Tariot, P. N. Alzheimer's prevention initiative: a proposal to evaluate presymptomatic treatments as quickly as possible. *Biomark. Med.* **4,** 3–14 (2010).

112. Reiman, E. M. *et al.* Alzheimer's Prevention Initiative: A Plan to Accelerate the Evaluation of Presymptomatic Treatments. *J. Alzheimers Dis.* **26,** 321–329 (2011).

113. Snider, B. J. *et al.* Novel presenilin 1 mutation (S170F) causing Alzheimer disease with Lewy bodies in the third decade of life. *Arch. Neurol.* **62,** 1821–1830 (2005).

114. Bateman, R. J. *et al.* Autosomal-dominant Alzheimer's disease: a review and proposal for the prevention of Alzheimer's disease. *Alzheimers Res. Ther.* **3,** 1 (2011).

115. Fagan, A. M. *et al.* Cerebrospinal fluid tau/beta-amyloid(42) ratio as a prediction of cognitive decline in nondemented older adults. *Arch. Neurol.* **64,** 343–349 (2007).

116. Morris, J. C. *et al.* Pittsburgh compound B imaging and prediction of progression from cognitive normality to symptomatic Alzheimer disease. *Arch. Neurol.* **66,** 1469–1475 (2009).

117. Villemagne, V. L. *et al.* Longitudinal assessment of Aβ and cognition in aging and Alzheimer disease. *Ann. Neurol.* **69,** 181–192 (2011).

118. Andreasen, N. & Blennow, K. CSF biomarkers for mild cognitive impairment and early Alzheimer's disease. *Clin. Neurol. Neurosurg.* **107,** 165–173 (2005).

119. Mattsson, N. *et al.* CSF biomarkers and incipient Alzheimer disease in patients with mild cognitive impairment. *JAMA* **302,** 385–393 (2009).

120. Shaw, L. M. *et al.* Cerebrospinal fluid biomarker signature in Alzheimer's disease neuroimaging initiative subjects. *Ann. Neurol.* **65,** 403–413 (2009).

121. Snider, B. J. *et al.* Cerebrospinal fluid biomarkers and rate of cognitive decline in very mild dementia of the Alzheimer type. *Arch. Neurol.* **66,** 638–645 (2009).

122. Klunk, W. E. *et al.* Imaging brain amyloid in Alzheimer's disease with Pittsburgh Compound-B. *Ann. Neurol.* **55,** 306–319 (2004).

123. Minoshima, S. *et al.* Metabolic reduction in the posterior cingulate cortex in very early Alzheimer's disease. *Ann. Neurol.* **42,** 85–94 (1997).

124. Kadir, A. *et al.* Dynamic changes in PET amyloid and FDG imaging at different stages of Alzheimer's disease. *Neurobiol. Aging* **33,** 198.e1-14 (2012).

125. Ingelsson, M. *et al.* Early Abeta accumulation and progressive synaptic loss, gliosis, and tangle formation in AD brain. *Neurology* **62,** 925–931 (2004).

126. Jack, C. R. *et al.* 11C PiB and structural MRI provide complementary information in imaging of Alzheimer's disease and amnestic mild cognitive impairment. *Brain J. Neurol.* **131,** 665–680 (2008).

127. Jack, C. R. *et al.* Serial PIB and MRI in normal, mild cognitive impairment and Alzheimer's disease: implications for sequence of pathological events in Alzheimer's disease. *Brain J. Neurol.* **132,** 1355–1365 (2009).

128. Jack, C. R. *et al.* Evidence for ordering of Alzheimer disease biomarkers. *Arch. Neurol.* **68,** 1526–1535 (2011).

129. Walhovd, K. B. *et al.* Multi-modal imaging predicts memory performance in normal aging and cognitive decline. *Neurobiol. Aging* **31,** 1107–1121 (2010).

130. Roe, C. M. *et al.* Amyloid imaging and CSF biomarkers in predicting cognitive impairment up to 7.5 years later. *Neurology* **80,** 1784–1791 (2013).

131. Villemagne, V. L. *et al.* Amyloid β deposition, neurodegeneration, and cognitive decline in sporadic Alzheimer's disease: a prospective cohort study. *Lancet Neurol.* **12,** 357–367 (2013).

132. Vos, S. J. *et al.* Preclinical Alzheimer's disease and its outcome: a longitudinal cohort study. *Lancet Neurol.* **12,** 957–965 (2013).

133. Fagan, A. M. *et al.* Longitudinal change in CSF biomarkers in autosomal-dominant Alzheimer's disease. *Sci. Transl. Med.* **6,** 226ra30 (2014).

134. Jansen, W. J. *et al.* Prevalence of cerebral amyloid pathology in persons without dementia: a meta-analysis. *JAMA* **313,** 1924–1938 (2015).

135. van Rossum, I. A. *et al.* Injury markers but not amyloid markers are associated with rapid progression from mild cognitive impairment to dementia in Alzheimer's disease. *J. Alzheimers Dis. JAD* **29,** 319–327 (2012).

136. van Rossum, I. A. *et al.* Injury markers predict time to dementia in subjects with MCI and amyloid pathology. *Neurology* **79,** 1809–1816 (2012).

137. Roe, C. M., Fagan, A. M., Grant, E. A., Holtzman, D. M. & Morris, J. C. CSF biomarkers of Alzheimer disease: 'noncognitive' outcomes. *Neurology* **81,** 2028–2031 (2013).

138. De Meyer G, Shapiro F, Vanderstichele H & et al. DIagnosis-independent alzheimer disease biomarker signature in cognitively normal elderly people. *Arch. Neurol.* **67,** 949–956 (2010).

139. Tomlinson, B. E., Blessed, G. & Roth, M. Observations on the brains of non-demented old people. *J. Neurol. Sci.* **7,** 331–356 (1968).

140. Burns, A., Tomlinson, B. & Mann, D. m. a. Observations on the brains of demented old people. B.E. Tomlinson, G. Blessed and M. Roth, Journal of the Neurological Sciences (1970) 11, 205–242; (1968) 7, 331–356. *Int. J. Geriatr. Psychiatry* **12,** 785–790 (1997).

141. Price, J. L. & Morris, J. C. Tangles and plaques in nondemented aging and 'preclinical' Alzheimer's disease. *Ann. Neurol.* **45,** 358–368 (1999).

142. Aizenstein, H. J. *et al.* Frequent Amyloid Deposition Without Significant Cognitive Impairment Among the Elderly. *Arch. Neurol.* **65,** 1509–1517 (2008).

143. Crystal, H. *et al.* Clinico-pathologic studies in dementia: nondemented subjects with pathologically confirmed Alzheimer's disease. *Neurology* **38,** 1682–1687 (1988).

144. Hulette, C. M. *et al.* Neuropathological and neuropsychological changes in 'normal' aging: evidence for preclinical Alzheimer disease in cognitively normal individuals. *J. Neuropathol. Exp. Neurol.* **57,** 1168–1174 (1998).

145. Katzman, R. *et al.* Clinical, pathological, and neurochemical changes in dementia: a subgroup with preserved mental status and numerous neocortical plaques. *Ann. Neurol.* **23,** 138–144 (1988).

146. Knopman, D. S. *et al.* Neuropathology of cognitively normal elderly. *J. Neuropathol. Exp. Neurol.* **62,** 1087–1095 (2003).

147. Price, J. L., Davis, P. B., Morris, J. C. & White, D. L. The distribution of tangles, plaques and related immunohistochemical markers in healthy aging and Alzheimer's disease. *Neurobiol. Aging* **12,** 295–312 (1991).

148. Schmitt, F. A. *et al.* 'Preclinical' AD revisited: neuropathology of cognitively normal older adults. *Neurology* **55,** 370–376 (2000).

149. Arriagada, P. V., Marzloff, K. & Hyman, B. T. Distribution of Alzheimer-type pathologic changes in nondemented elderly individuals matches the pattern in Alzheimer's disease. *Neurology* **42,** 1681–1688 (1992).

150. Haroutunian, V. *et al.* Regional distribution of neuritic plaques in the nondemented elderly and subjects with very mild Alzheimer disease. *Arch. Neurol.* **55,** 1185–1191 (1998).

151. Haroutunian, V. *et al.* Neurofibrillary tangles in nondemented elderly subjects and mild Alzheimer disease. *Arch. Neurol.* **56,** 713–718 (1999).

152. Tagliavini, F., Giaccone, G., Frangione, B. & Bugiani, O. Preamyloid deposits in the cerebral cortex of patients with Alzheimer's disease and nondemented individuals. *Neurosci. Lett.* **93,** 191–196 (1988).

153. Reiman, E. M. *et al.* Preclinical evidence of Alzheimer's disease in persons homozygous for the epsilon 4 allele for apolipoprotein E. *N. Engl. J. Med.* **334,** 752–758 (1996).

154. Hyman, B. T. The neuropathological diagnosis of Alzheimer's disease: clinical-pathological studies. *Neurobiol. Aging* **18,** S27-32 (1997).

155. Morris, J. C. Mild cognitive impairment and preclinical Alzheimer's disease. *Geriatrics* **Suppl,** 9–14 (2005).

156. Dubois, B. *et al.* Preclinical Alzheimer's disease: Definition, natural history, and diagnostic criteria. *Alzheimers Dement. J. Alzheimers Assoc.* **12,** 292–323 (2016).

157. Mrak, R. E., Griffin, S. T. & Graham, D. I. Aging-associated changes in human brain. *J. Neuropathol. Exp. Neurol.* **56,** 1269–1275 (1997).

158. Gustafson, D. R., Skoog, I., Rosengren, L., Zetterberg, H. & Blennow, K. Cerebrospinal fluid beta-amyloid 1-42 concentration may predict cognitive decline in older women. *J. Neurol. Neurosurg. Psychiatry* **78,** 461–464 (2007).

159. Stomrud, E., Hansson, O., Blennow, K., Minthon, L. & Londos, E. Cerebrospinal fluid biomarkers predict decline in subjective cognitive function over 3 years in healthy elderly. *Dement. Geriatr. Cogn. Disord.* **24,** 118–124 (2007).

160. Steenland, K., Zhao, L., Goldstein, F., Cellar, J. & Lah, J. Biomarkers for Predicting Cognitive Decline in those with Normal Cognition. *J. Alzheimers Dis. JAD* **40,** 587–594 (2014).

161. Bennett, D. A. *et al.* Neuropathology of older persons without cognitive impairment from two community-based studies. *Neurology* **66,** 1837–1844 (2006).

162. Vemuri, P. *et al.* Cognitive reserve and Alzheimer's disease biomarkers are independent determinants of cognition. *Brain J. Neurol.* **134,** 1479–1492 (2011).

163. Baumgart, M. *et al.* Summary of the evidence on modifiable risk factors for cognitive decline and dementia: A population-based perspective. *Alzheimers Dement. J. Alzheimers Assoc.* **11,** 718–726 (2015).

164. Barnard, N. D. *et al.* Dietary and lifestyle guidelines for the prevention of Alzheimer's disease. *Neurobiol. Aging* **35, Supplement 2,** S74–S78 (2014).

165. Liang, K. Y. *et al.* Exercise and Alzheimer's disease biomarkers in cognitively normal older adults. *Ann. Neurol.* **68,** 311–318 (2010).

166. Landau, S. M. *et al.* Association of lifetime cognitive engagement and low β-amyloid deposition. *Arch. Neurol.* **69,** 623–629 (2012).

167. Okonkwo, O. C. *et al.* Physical activity attenuates age-related biomarker alterations in preclinical AD. *Neurology* **83,** 1753–1760 (2014).

168. Vemuri, P. *et al.* Effect of lifestyle activities on Alzheimer disease biomarkers and cognition. *Ann. Neurol.* **72,** 730–738 (2012).

169. Stern, Y. What is cognitive reserve? Theory and research application of the reserve concept. *J. Int. Neuropsychol. Soc. JINS* **8,** 448–460 (2002).

170. Stern, Y. Cognitive reserve. *Neuropsychologia* **47,** 2015–2028 (2009).

171. Mortimer, J. A., Borenstein, A. R., Gosche, K. M. & Snowdon, D. A. Very early detection of Alzheimer neuropathology and the role of brain reserve in modifying its clinical expression. *J. Geriatr. Psychiatry Neurol.* **18,** 218–223 (2005).

172. Roe CM *et al.* Alzheimer disease and cognitive reserve: Variation of education effect with carbon 11–labeled pittsburgh compound b uptake. *Arch. Neurol.* **65,** 1467–1471 (2008).

173. Hall, C. B. *et al.* Education delays accelerated decline on a memory test in persons who develop dementia. *Neurology* **69,** 1657–1664 (2007).

174. Hall, C. B. *et al.* Cognitive activities delay onset of memory decline in persons who develop dementia. *Neurology* **73,** 356–361 (2009).

175. Craik, F. I. M., Bialystok, E. & Freedman, M. Delaying the onset of Alzheimer disease Bilingualism as a form of cognitive reserve. *Neurology* **75,** 1726–1729 (2010).

176. Stern, Y., Tang, M. X., Denaro, J. & Mayeux, R. Increased risk of mortality in Alzheimer's disease patients with more advanced educational and occupational attainment. *Ann. Neurol.* **37,** 590–595 (1995).

177. Stern, Y., Albert, S., Tang, M. X. & Tsai, W. Y. Rate of memory decline in AD is related to education and occupation: cognitive reserve? *Neurology* **53,** 1942–1947 (1999).

178. Scarmeas, N., Albert, S. M., Manly, J. J. & Stern, Y. Education and rates of cognitive decline in incident Alzheimer's disease. *J. Neurol. Neurosurg. Psychiatry* **77,** 308–316 (2006).

179. Helzner, E. P., Scarmeas, N., Cosentino, S., Portet, F. & Stern, Y. Leisure activity and cognitive decline in incident Alzheimer disease. *Arch. Neurol.* **64,** 1749–1754 (2007).

180. Scheibel, A., Conrad, T., Perdue, S., Tomiyasu, U. & Wechsler, A. A quantitative study of dendrite complexity in selected areas of the human cerebral cortex. *Brain Cogn.* **12,** 85–101 (1990).

181. Jacobs, B., Schall, M. & Scheibel, A. B. A quantitative dendritic analysis of Wernicke's area in humans. II. Gender, hemispheric, and environmental factors. *J. Comp. Neurol.* **327,** 97–111 (1993).

182. Riudavets, M. A. *et al.* Resistance to Alzheimer's pathology is associated with nuclear hypertrophy in neurons. *Neurobiol. Aging* **28,** 1484–1492 (2007).

183. Iacono, D. *et al.* Neuronal hypertrophy in asymptomatic Alzheimer disease. *J. Neuropathol. Exp. Neurol.* **67,** 578–589 (2008).

184. Kempermann, G. The neurogenic reserve hypothesis: what is adult hippocampal neurogenesis good for? *Trends Neurosci.* **31,** 163–169 (2008).

185. Honer, W. G. *et al.* Cognitive reserve, presynaptic proteins and dementia in the elderly. *Transl. Psychiatry* **2,** e114 (2012).

186. Arnold, S. E. *et al.* Cellular, synaptic, and biochemical features of resilient cognition in Alzheimer's disease. *Neurobiol. Aging* **34,** 157–168 (2013).

187. de Leon, M. J. *et al.* Positron emission tomographic studies of aging and Alzheimer disease. *AJNR Am. J. Neuroradiol.* **4,** 568–571 (1983).

188. de Leon, M. J. *et al.* Prediction of cognitive decline in normal elderly subjects with 2-[(18)F]fluoro-2-deoxy-D-glucose/poitron-emission tomography (FDG/PET). *Proc. Natl. Acad. Sci. U. S. A.* **98,** 10966–10971 (2001).

189. Small, G. W. *et al.* Apolipoprotein E type 4 allele and cerebral glucose metabolism in relatives at risk for familial Alzheimer disease. *JAMA* **273,** 942–947 (1995).

190. Mosconi, L. *et al.* Hypometabolism exceeds atrophy in presymptomatic early-onset familial Alzheimer's disease. *J. Nucl. Med. Off. Publ. Soc. Nucl. Med.* **47,** 1778–1786 (2006).

191. Mosconi, L. *et al.* Hippocampal hypometabolism predicts cognitive decline from normal aging. *Neurobiol. Aging* **29,** 676–692 (2008).

192. Cunnane, S. *et al.* Brain fuel metabolism, aging, and Alzheimer's disease. *Nutrition* **27,** 3–20 (2011).

193. Jack, C. R. *et al.* Hypothetical model of dynamic biomarkers of the Alzheimer's pathological cascade. *Lancet Neurol.* **9,** 119–128 (2010).

194. Reiman, E. M. *et al.* Functional brain abnormalities in young adults at genetic risk for late-onset Alzheimer's dementia. *Proc. Natl. Acad. Sci. U. S. A.* **101,** 284–289 (2004).

195. Costantini, L. C., Barr, L. J., Vogel, J. L. & Henderson, S. T. Hypometabolism as a therapeutic target in Alzheimer's disease. *BMC Neurosci.* **9,** S16 (2008).

196. Caldwell, C. C., Yao, J. & Brinton, R. D. Targeting the Prodromal Stage of Alzheimer's Disease: Bioenergetic and Mitochondrial Opportunities. *Neurotherapeutics* **12,** 66–80 (2015).

197. Lustbader, J. W. *et al.* ABAD directly links Abeta to mitochondrial toxicity in Alzheimer's disease. *Science* **304,** 448–452 (2004).

198. Manczak, M. *et al.* Mitochondria are a direct site of A beta accumulation in Alzheimer's disease neurons: implications for free radical generation and oxidative damage in disease progression. *Hum. Mol. Genet.* **15,** 1437–1449 (2006).

199. Yao, J. *et al.* Mitochondrial bioenergetic deficit precedes Alzheimer's pathology in female mouse model of Alzheimer's disease. *Proc. Natl. Acad. Sci. U. S. A.* **106,** 14670–14675 (2009).

200. Hernandez-Zimbron, L. F. *et al.* Amyloid-β peptide binds to cytochrome C oxidase subunit 1. *PloS One* **7,** e42344 (2012).

201. Beal, M. F. Mitochondria take center stage in aging and neurodegeneration. *Ann. Neurol.* **58,** 495–505 (2005).

202. Cardoso, S. M., Santos, S., Swerdlow, R. H. & Oliveira, C. R. Functional mitochondria are required for amyloid beta-mediated neurotoxicity. *FASEB J. Off. Publ. Fed. Am. Soc. Exp. Biol.* **15,** 1439–1441 (2001).

203. Parks, J. K., Smith, T. S., Trimmer, P. A., Bennett, J. P. & Parker, W. D. Neurotoxic Abeta peptides increase oxidative stress in vivo through NMDA-receptor and nitric-oxide-synthase mechanisms, and inhibit complex IV activity and induce a mitochondrial permeability transition in vitro. *J. Neurochem.* **76,** 1050–1056 (2001).

204. Casley, C. S., Canevari, L., Land, J. M., Clark, J. B. & Sharpe, M. A. Beta-amyloid inhibits integrated mitochondrial respiration and key enzyme activities. *J. Neurochem.* **80,** 91–100 (2002).

205. Casley, C. S. *et al.* Beta-amyloid fragment 25-35 causes mitochondrial dysfunction in primary cortical neurons. *Neurobiol. Dis.* **10,** 258–267 (2002).

206. Morais Cardoso, S., Swerdlow, R. H. & Oliveira, C. R. Induction of cytochrome c-mediated apoptosis by amyloid beta 25-35 requires functional mitochondria. *Brain Res.* **931,** 117–125 (2002).

207. Aleardi, A. M. *et al.* Gradual alteration of mitochondrial structure and function by beta-amyloids: importance of membrane viscosity changes, energy deprivation, reactive oxygen species production, and cytochrome c release. *J. Bioenerg. Biomembr.* **37,** 207–225 (2005).

208. Crouch, P. J. *et al.* Copper-dependent inhibition of human cytochrome c oxidase by a dimeric conformer of amyloid-beta1-42. *J. Neurosci. Off. J. Soc. Neurosci.* **25,** 672–679 (2005).

209. Hauptmann, S. *et al.* Mitochondrial dysfunction: an early event in Alzheimer pathology accumulates with age in AD transgenic mice. *Neurobiol. Aging* **30,** 1574–1586 (2009).

210. Dragicevic, N. *et al.* Mitochondrial amyloid-beta levels are associated with the extent of mitochondrial dysfunction in different brain regions and the degree of cognitive impairment in Alzheimer's transgenic mice. *J. Alzheimers Dis. JAD* **20 Suppl 2,** S535-550 (2010).

211. Mao, P. & Reddy, P. H. Aging and amyloid beta-induced oxidative DNA damage and mitochondrial dysfunction in Alzheimer's disease: implications for early intervention and therapeutics. *Biochim. Biophys. Acta* **1812,** 1359–1370 (2011).

212. Du, H. *et al.* Early deficits in synaptic mitochondria in an Alzheimer's disease mouse model. *Proc. Natl. Acad. Sci. U. S. A.* **107,** 18670–18675 (2010).

213. Arispe, N., Rojas, E. & Pollard, H. B. Alzheimer disease amyloid beta protein forms calcium channels in bilayer membranes: blockade by tromethamine and aluminum. *Proc. Natl. Acad. Sci.* **90,** 567–571 (1993).

214. Simmons, M. A. & Schneider, C. R. Amyloid β peptides act directly on single neurons. *Neurosci. Lett.* **150,** 133–136 (1993).

215. Glabe, C. G. & Kayed, R. Common structure and toxic function of amyloid oligomers implies a common mechanism of pathogenesis. *Neurology* **66,** S74–S78 (2006).

216. Reddy, P. H. & Beal, M. F. Amyloid beta, mitochondrial dysfunction and synaptic damage: implications for cognitive decline in aging and Alzheimer's disease. *Trends Mol. Med.* **14,** 45–53 (2008).

217. Devi, L., Prabhu, B. M., Galati, D. F., Avadhani, N. G. & Anandatheerthavarada, H. K. Accumulation of Amyloid Precursor Protein in the Mitochondrial Import Channels of Human Alzheimer's Disease Brain Is Associated with Mitochondrial Dysfunction. *J. Neurosci.* **26,** 9057–9068 (2006).

218. Hansson Petersen, C. A. *et al.* The amyloid beta-peptide is imported into mitochondria via the TOM import machinery and localized to mitochondrial cristae. *Proc. Natl. Acad. Sci. U. S. A.* **105,** 13145–13150 (2008).

219. Caspersen, C. *et al.* Mitochondrial Abeta: a potential focal point for neuronal metabolic dysfunction in Alzheimer's disease. *FASEB J. Off. Publ. Fed. Am. Soc. Exp. Biol.* **19,** 2040–2041 (2005).

220. Manczak, M., Park, B. S., Jung, Y. & Reddy, P. H. Differential expression of oxidative phosphorylation genes in patients with Alzheimer's disease: implications for early mitochondrial dysfunction and oxidative damage. *Neuromolecular Med.* **5,** 147–162 (2004).

221. Brooks, W. M. *et al.* Gene expression profiles of metabolic enzyme transcripts in Alzheimer's disease. *Brain Res.* **1127,** 127–135 (2007).

222. Liang, W. S. *et al.* Alzheimer's disease is associated with reduced expression of energy metabolism genes in posterior cingulate neurons. *Proc. Natl. Acad. Sci. U. S. A.* **105,** 4441–4446 (2008).

223. Covarrubias, L., Hernández-García, D., Schnabel, D., Salas-Vidal, E. & Castro-Obregón, S. Function of reactive oxygen species during animal development: passive or active? *Dev. Biol.* **320,** 1–11 (2008).

224. Marchi, S. *et al.* Mitochondria-Ros Crosstalk in the Control of Cell Death and Aging. *J. Signal Transduct.* **2012,** (2012).

225. Butterfield, D. A. beta-Amyloid-associated free radical oxidative stress and neurotoxicity: implications for Alzheimer's disease. *Chem. Res. Toxicol.* **10,** 495–506 (1997).

226. Smith, M. A., Rottkamp, C. A., Nunomura, A., Raina, A. K. & Perry, G. Oxidative stress in Alzheimer's disease. *Biochim. Biophys. Acta BBA - Mol. Basis Dis.* **1502,** 139–144 (2000).

227. Behl, C., Davis, J. B., Lesley, R. & Schubert, D. Hydrogen peroxide mediates amyloid beta protein toxicity. *Cell* **77,** 817–827 (1994).

228. Harris, M. E., Hensley, K., Butterfield, D. A., Leedle, R. A. & Carney, J. M. Direct evidence of oxidative injury produced by the Alzheimer's beta-amyloid peptide (1-40) in cultured hippocampal neurons. *Exp. Neurol.* **131,** 193–202 (1995).

229. Rhein, V. *et al.* Amyloid-beta and tau synergistically impair the oxidative phosphorylation system in triple transgenic Alzheimer's disease mice. *Proc. Natl. Acad. Sci. U. S. A.* **106,** 20057–20062 (2009).

230. Leuner, K. *et al.* Mitochondrion-derived reactive oxygen species lead to enhanced amyloid beta formation. *Antioxid. Redox Signal.* **16,** 1421–1433 (2012).

231. Markesbery, W. R. Oxidative Stress Hypothesis in Alzheimer's Disease. *Free Radic. Biol. Med.* **23,** 134–147 (1997).

232. Benzinger, T. L. S. *et al.* Regional variability of imaging biomarkers in autosomal dominant Alzheimer's disease. *Proc. Natl. Acad. Sci. U. S. A.* **110,** E4502-4509 (2013).

233. Johnson, S. C. *et al.* Amyloid burden and neural function in people at risk for Alzheimer's Disease. *Neurobiol. Aging* **35,** 576–584 (2014).

234. Poisnel, G. *et al.* Increased regional cerebral glucose uptake in an APP/PS1 model of Alzheimer's disease. *Neurobiol. Aging* **33,** 1995–2005 (2012).

235. Reddy, P. H. *et al.* Gene expression profiles of transcripts in amyloid precursor protein transgenic mice: up-regulation of mitochondrial metabolism and apoptotic genes is an early cellular change in Alzheimer's disease. *Hum. Mol. Genet.* **13,** 1225–1240 (2004).

236. Iwangoff, P., Armbruster, R., Enz, A. & Meier-Ruge, W. Glycolytic enzymes from human autoptic brain cortex: normal aged and demented cases. *Mech. Ageing Dev.* **14,** 203–209 (1980).

237. Bigl, M. *et al.* Changes of activity and isozyme pattern of phosphofructokinase in the brains of patients with Alzheimer's disease. *J. Neurochem.* **67,** 1164–1171 (1996).

238. Bigl, M., Brückner, M. K., Arendt, T., Bigl, V. & Eschrich, K. Activities of key glycolytic enzymes in the brains of patients with Alzheimer's disease. *J. Neural Transm.* **106,** 499–511 (1999).

239. Newington, J. T. *et al.* Amyloid Beta Resistance in Nerve Cell Lines Is Mediated by the Warburg Effect. *PLoS ONE* **6,** e19191 (2011).

240. Newington, J. T. *et al.* Overexpression of pyruvate dehydrogenase kinase 1 and lactate dehydrogenase A in nerve cells confers resistance to amyloid beta and other toxins by decreasing mitochondrial respiration and ROS production. *J. Biol. Chem.* **287,** 37245–58 (2012).

241. Soane, L., Kahraman, S., Kristian, T. & Fiskum, G. Mechanisms of impaired mitochondrial energy metabolism in acute and chronic neurodegenerative disorders. *J. Neurosci. Res.* **85,** 3407–3415 (2007).

242. Nielsen, T. H. *et al.* Cerebral energy metabolism during induced mitochondrial dysfunction. *Acta Anaesthesiol. Scand.* **57,** 229–235 (2013).

243. Warburg, O. On the origin of cancer cells. *Science* **123,** 309–314 (1956).

244. Cairns, R. A., Harris, I. S. & Mak, T. W. Regulation of cancer cell metabolism. *Nat. Rev. Cancer* **11,** 85–95 (2011).

245. Oren, R., Farnham, A. E., Saito, K., Milofsky, E. & Karnovsky, M. L. Metabolic patterns in three types of phagocytizing cells. *J. Cell Biol.* **17,** 487–501 (1963).

246. Campbell, J. D. & Paul, R. J. The nature of fuel provision for the Na+,K(+)-ATPase in porcine vascular smooth muscle. *J. Physiol.* **447,** 67–82 (1992).

247. Pellerin, L. & Magistretti, P. J. Excitatory amino acids stimulate aerobic glycolysis in astrocytes via an activation of the Na+/K+ ATPase. *Dev. Neurosci.* **18,** 336–342 (1996).

248. Wu, K., Aoki, C., Elste, A., Rogalski-Wilk, A. A. & Siekevitz, P. The synthesis of ATP by glycolytic enzymes in the postsynaptic density and the effect of endogenously generated nitric oxide. *Proc. Natl. Acad. Sci. U. S. A.* **94,** 13273–13278 (1997).

249. Okamoto, K., Wang, W., Rounds, J., Chambers, E. A. & Jacobs, D. O. ATP from glycolysis is required for normal sodium homeostasis in resting fast-twitch rodent skeletal muscle. *Am. J. Physiol. Endocrinol. Metab.* **281,** E479-488 (2001).

250. Pellerin, L. *et al.* Activity-dependent regulation of energy metabolism by astrocytes: an update. *Glia* **55,** 1251–1262 (2007).

251. De Bock, K. *et al.* Role of PFKFB3-driven glycolysis in vessel sprouting. *Cell* **154,** 651–663 (2013).

252. Cheng, S.-C. *et al.* mTOR- and HIF-1α-mediated aerobic glycolysis as metabolic basis for trained immunity. *Science* **345,** 1250684 (2014).

253. Zu, X. L. & Guppy, M. Cancer metabolism: facts, fantasy, and fiction. *Biochem. Biophys. Res. Commun.* **313,** 459–465 (2004).

254. Pfeiffer, T., Schuster, S. & Bonhoeffer, S. Cooperation and Competition in the Evolution of ATP-Producing Pathways. *Science* **292,** 504–507 (2001).

255. Howarth, C., Gleeson, P. & Attwell, D. Updated energy budgets for neural computation in the neocortex and cerebellum. *J. Cereb. Blood Flow Metab. Off. J. Int. Soc. Cereb. Blood Flow Metab.* **32,** 1222–1232 (2012).

256. Hume, D. A. & Weidemann, M. J. Role and regulation of glucose metabolism in proliferating cells. *J. Natl. Cancer Inst.* **62,** 3–8 (1979).

257. Lunt, S. Y. & Vander Heiden, M. G. Aerobic Glycolysis: Meeting the Metabolic Requirements of Cell Proliferation. *Annu. Rev. Cell Dev. Biol.* **27,** 441–464 (2011).

258. Lin, S.-J., Defossez, P.-A. & Guarente, L. Requirement of NAD and SIR2 for Life-Span Extension by Calorie Restriction in Saccharomyces cerevisiae. *Science* **289,** 2126–2128 (2000).

259. Ying, W. NAD+/NADH and NADP+/NADPH in cellular functions and cell death: regulation and biological consequences. *Antioxid. Redox Signal.* **10,** 179–206 (2008).

260. Soucek, T., Cumming, R., Dargusch, R., Maher, P. & Schubert, D. The regulation of glucose metabolism by HIF-1 mediates a neuroprotective response to amyloid beta peptide. *Neuron* **39,** 43–56 (2003).

261. Hroudová, J., Singh, N. & Fišar, Z. Mitochondrial dysfunctions in neurodegenerative diseases: relevance to Alzheimer's disease. *BioMed Res. Int.* **2014,** 175062 (2014).

262. Vlassenko, A. G. *et al.* Spatial correlation between brain aerobic glycolysis and amyloid-β (Aβ) deposition. *Proc. Natl. Acad. Sci.* **107,** 17763–17767 (2010).

263. Mergenthaler, P., Lindauer, U., Dienel, G. A. & Meisel, A. Sugar for the brain: the role of glucose in physiological and pathological brain function. *Trends Neurosci.* **36,** 587–597 (2013).

264. Macheda, M. L., Rogers, S. & Best, J. D. Molecular and cellular regulation of glucose transporter (GLUT) proteins in cancer. *J. Cell. Physiol.* **202,** 654–662 (2005).

265. Schubert, D. Glucose metabolism and Alzheimer's disease. *Ageing Res. Rev.* **4,** 240–257 (2005).

266. Simpson, I. A., Carruthers, A. & Vannucci, S. J. Supply and demand in cerebral energy metabolism: the role of nutrient transporters. *J. Cereb. Blood Flow Metab. Off. J. Int. Soc. Cereb. Blood Flow Metab.* **27,** 1766–1791 (2007).

267. Rouach, N., Koulakoff, A., Abudara, V., Willecke, K. & Giaume, C. Astroglial metabolic networks sustain hippocampal synaptic transmission. *Science* **322,** 1551–1555 (2008).

268. Gandhi, G. K., Cruz, N. F., Ball, K. K. & Dienel, G. A. Astrocytes are poised for lactate trafficking and release from activated brain and for supply of glucose to neurons. *J. Neurochem.* **111,** 522–536 (2009).

269. Simpson, I. A., Chundu, K. R., Davies-Hill, T., Honer, W. G. & Davies, P. Decreased concentrations of GLUT1 and GLUT3 glucose transporters in the brains of patients with Alzheimer's disease. *Ann. Neurol.* **35,** 546–551 (1994).

270. Liu, Y., Liu, F., Iqbal, K., Grundke-Iqbal, I. & Gong, C.-X. Decreased glucose transporters correlate to abnormal hyperphosphorylation of tau in Alzheimer disease. *FEBS Lett.* **582,** 359–364 (2008).

271. Mooradian, A. D., Chung, H. C. & Shah, G. N. GLUT-1 expression in the cerebra of patients with Alzheimer's disease. *Neurobiol. Aging* **18,** 469–474 (1997).

272. Harr, S. D., Simonian, N. A. & Hyman, B. T. Functional alterations in Alzheimer's disease: decreased glucose transporter 3 immunoreactivity in the perforant pathway terminal zone. *J. Neuropathol. Exp. Neurol.* **54,** 38–41 (1995).

273. Boado, R. J., Wang, L. & Pardridge, W. M. Enhanced expression of the blood-brain barrier GLUT1 glucose transporter gene by brain-derived factors. *Brain Res. Mol. Brain Res.* **22,** 259–267 (1994).

274. Mani, N., Khaibullina, A., Krum, J. M. & Rosenstein, J. M. Activation of receptor-mediated angiogenesis and signaling pathways after VEGF administration in fetal rat CNS explants. *J. Cereb. Blood Flow Metab. Off. J. Int. Soc. Cereb. Blood Flow Metab.* **23,** 1420–1429 (2003).

275. Okino, S. T., Chichester, C. H. & Whitlock, J. P., Jr. Hypoxia-inducible mammalian gene expression analyzed in vivo at a TATA-driven promoter and at an initiator-driven promoter. *J. Biol. Chem.* **273,** 23837–23843 (1998).

276. Berg, J., Tymoczko, J. & Stryer, L. in *Glycolysis is an energy-conversion pathway in many organisms* Section 16.1 (W H Freeman, 2002).

277. Patra, K. C. & Hay, N. The pentose phosphate pathway and cancer. *Trends Biochem. Sci.* **39,** 347–354 (2014).

278. Ayala, A., Fabregat, I. & Machado, A. The role of NADPH in the regulation of glucose-6-phosphate and 6-phosphogluconate dehydrogenases in rat adipose tissue. *Mol. Cell. Biochem.* **105,** 1–5 (1991).

279. Au, S. W., Gover, S., Lam, V. M. & Adams, M. J. Human glucose-6-phosphate dehydrogenase: the crystal structure reveals a structural NADP(+) molecule and provides insights into enzyme deficiency. *Struct. Lond. Engl. 1993* **8,** 293–303 (2000).

280. Przybytkowski, E. & Averill-Bates, D. A. Correlation between glutathione and stimulation of the pentose phosphate cycle in situ in Chinese hamster ovary cells exposed to hydrogen peroxide. *Arch. Biochem. Biophys.* **325,** 91–98 (1996).

281. Bensaad, K. *et al.* TIGAR, a p53-inducible regulator of glycolysis and apoptosis. *Cell* **126,** 107–120 (2006).

282. Jiang, P. *et al.* p53 regulates biosynthesis through direct inactivation of glucose-6-phosphate dehydrogenase. *Nat. Cell Biol.* **13,** 310–316 (2011).

283. Nelson, T., Kaufman, E. E. & Sokoloff, L. 2-Deoxyglucose incorporation into rat brain glycogen during measurement of local cerebral glucose utilization by the 2-deoxyglucose method. *J. Neurochem.* **43,** 949–956 (1984).

284. Swanson, R. A. & Choi, D. W. Glial glycogen stores affect neuronal survival during glucose deprivation in vitro. *J. Cereb. Blood Flow Metab. Off. J. Int. Soc. Cereb. Blood Flow Metab.* **13,** 162–169 (1993).

285. Wender, R. *et al.* Astrocytic glycogen influences axon function and survival during glucose deprivation in central white matter. *J. Neurosci. Off. J. Soc. Neurosci.* **20,** 6804–6810 (2000).

286. Brown, A. M. *et al.* Astrocyte glycogen metabolism is required for neural activity during aglycemia or intense stimulation in mouse white matter. *J. Neurosci. Res.* **79,** 74–80 (2005).

287. Suh, S. W. *et al.* Astrocyte glycogen sustains neuronal activity during hypoglycemia: studies with the glycogen phosphorylase inhibitor CP-316,819 ([R-R*,S*]-5-chloro-N-[2-hydroxy-3-(methoxymethylamino)-3-oxo-1-(phenylmethyl)propyl]-1H-indole-2-carboxamide). *J. Pharmacol. Exp. Ther.* **321,** 45–50 (2007).

288. Dienel, G. A., Ball, K. K. & Cruz, N. F. A glycogen phosphorylase inhibitor selectively enhances local rates of glucose utilization in brain during sensory stimulation of conscious rats: implications for glycogen turnover. *J. Neurochem.* **102,** 466–478 (2007).

289. Sickmann, H. M., Walls, A. B., Schousboe, A., Bouman, S. D. & Waagepetersen, H. S. Functional significance of brain glycogen in sustaining glutamatergic neurotransmission. *J. Neurochem.* **109 Suppl 1,** 80–86 (2009).

290. Sickmann, H. M., Waagepetersen, H. S., Schousboe, A., Benie, A. J. & Bouman, S. D. Brain glycogen and its role in supporting glutamate and GABA homeostasis in a type 2 diabetes rat model. *Neurochem. Int.* **60,** 267–275 (2012).

291. Walls, A. B., Heimbürger, C. M., Bouman, S. D., Schousboe, A. & Waagepetersen, H. S. Robust glycogen shunt activity in astrocytes: Effects of glutamatergic and adrenergic agents. *Neuroscience* **158,** 284–292 (2009).

292. Swanson, R. A., Morton, M. M., Sagar, S. M. & Sharp, F. R. Sensory stimulation induces local cerebral glycogenolysis: demonstration by autoradiography. *Neuroscience* **51,** 451–461 (1992).

293. Swanson, R. A. Physiologic coupling of glial glycogen metabolism to neuronal activity in brain. *Can. J. Physiol. Pharmacol.* **70 Suppl,** S138-144 (1992).

294. Gibbs, M. E., Hutchinson, D. & Hertz, L. Astrocytic involvement in learning and memory consolidation. *Neurosci. Biobehav. Rev.* **32,** 927–944 (2008).

295. Hertz, L. & Gibbs, M. E. What learning in day-old chickens can teach a neurochemist: focus on astrocyte metabolism. *J. Neurochem.* **109 Suppl 1,** 10–16 (2009).

296. Newman, L. A., Korol, D. L. & Gold, P. E. Lactate Produced by Glycogenolysis in Astrocytes Regulates Memory Processing. *PLoS ONE* **6,** e28427 (2011).

297. DiNuzzo, M., Mangia, S., Maraviglia, B. & Giove, F. Glycogenolysis in astrocytes supports blood-borne glucose channeling not glycogen-derived lactate shuttling to neurons: evidence from mathematical modeling. *J. Cereb. Blood Flow Metab. Off. J. Int. Soc. Cereb. Blood Flow Metab.* **30,** 1895–1904 (2010).

298. Mazurek, S., Boschek, C. B., Hugo, F. & Eigenbrodt, E. Pyruvate kinase type M2 and its role in tumor growth and spreading. *Semin. Cancer Biol.* **15,** 300–308 (2005).

299. David, C. J., Chen, M., Assanah, M., Canoll, P. & Manley, J. L. HnRNP proteins controlled by c-Myc deregulate pyruvate kinase mRNA splicing in cancer. *Nature* **463,** 364–368 (2010).

300. Jurica, M. S. *et al.* The allosteric regulation of pyruvate kinase by fructose-1,6-bisphosphate. *Struct. Lond. Engl. 1993* **6,** 195–210 (1998).

301. Christofk, H. R. *et al.* The M2 splice isoform of pyruvate kinase is important for cancer metabolism and tumour growth. *Nature* **452,** 230–233 (2008).

302. Clower, C. V. *et al.* The alternative splicing repressors hnRNP A1/A2 and PTB influence pyruvate kinase isoform expression and cell metabolism. *Proc. Natl. Acad. Sci.* **107,** 1894–1899 (2010).

303. Anastasiou, D. *et al.* Pyruvate kinase M2 activators promote tetramer formation and suppress tumorigenesis. *Nat. Chem. Biol.* **8,** 839–847 (2012).

304. Lunt, S. Y. *et al.* Pyruvate Kinase Isoform Expression Alters Nucleotide Synthesis to Impact Cell Proliferation. *Mol. Cell* **57,** 95–107 (2015).

305. Anastasiou, D. *et al.* Inhibition of pyruvate kinase M2 by reactive oxygen species contributes to cellular antioxidant responses. *Science* **334,** 1278–1283 (2011).

306. Patel, M. S., Korotchkina, L. G. & Sidhu, S. Interaction of E1 and E3 components with the core proteins of the human pyruvate dehydrogenase complex. *J. Mol. Catal. B Enzym.* **61,** 2–6 (2009).

307. Zhang, F., Xu, X., Zhou, B., He, Z. & Zhai, Q. Gene expression profile change and associated physiological and pathological effects in mouse liver induced by fasting and refeeding. *PloS One* **6,** e27553 (2011).

308. Behal, R. H., Buxton, D. B., Robertson, J. G. & Olson, M. S. Regulation of the pyruvate dehydrogenase multienzyme complex. *Annu. Rev. Nutr.* **13,** 497–520 (1993).

309. Patel, M. S. & Korotchkina, L. G. Regulation of the pyruvate dehydrogenase complex. *Biochem. Soc. Trans.* **34,** 217–222 (2006).

310. Kato, M. *et al.* Structural basis for inactivation of the human pyruvate dehydrogenase complex by phosphorylation: role of disordered phosphorylation loops. *Struct. Lond. Engl. 1993* **16,** 1849–1859 (2008).

311. Yeaman, S. J. *et al.* Sites of phosphorylation on pyruvate dehydrogenase from bovine kidney and heart. *Biochemistry (Mosc.)* **17,** 2364–2370 (1978).

312. Gudi, R., Bowker-Kinley, M. M., Kedishvili, N. Y., Zhao, Y. & Popov, K. M. Diversity of the pyruvate dehydrogenase kinase gene family in humans. *J. Biol. Chem.* **270,** 28989–28994 (1995).

313. Korotchkina, L. G. & Patel, M. S. Site specificity of four pyruvate dehydrogenase kinase isoenzymes toward the three phosphorylation sites of human pyruvate dehydrogenase. *J. Biol. Chem.* **276,** 37223–37229 (2001).

314. Jeong, J. Y., Jeoung, N. H., Park, K.-G. & Lee, I.-K. Transcriptional Regulation of Pyruvate Dehydrogenase Kinase. *Diabetes Metab. J.* **36,** 328–335 (2012).

315. Wu, P. *et al.* Starvation and diabetes increase the amount of pyruvate dehydrogenase kinase isoenzyme 4 in rat heart. *Biochem. J.* **329 (Pt 1),** 197–201 (1998).

316. Wu, P. *et al.* Starvation increases the amount of pyruvate dehydrogenase kinase in several mammalian tissues. *Arch. Biochem. Biophys.* **381,** 1–7 (2000).

317. Kim, J., Tchernyshyov, I., Semenza, G. L. & Dang, C. V. HIF-1-mediated expression of pyruvate dehydrogenase kinase: a metabolic switch required for cellular adaptation to hypoxia. *Cell Metab.* **3,** 177–185 (2006).

318. Papandreou, I., Cairns, R. A., Fontana, L., Lim, A. L. & Denko, N. C. HIF-1 mediates adaptation to hypoxia by actively downregulating mitochondrial oxygen consumption. *Cell Metab.* **3,** 187–197 (2006).

319. McFate, T. *et al.* Pyruvate dehydrogenase complex activity controls metabolic and malignant phenotype in cancer cells. *J. Biol. Chem.* **283,** 22700–22708 (2008).

320. Nakai, N. *et al.* The abundance of mRNAs for pyruvate dehydrogenase kinase isoenzymes in brain regions of young and aged rats. *Life Sci.* **68,** 497–503 (2000).

321. Sheu, K. F., Kim, Y. T., Blass, J. P. & Weksler, M. E. An immunochemical study of the pyruvate dehydrogenase deficit in Alzheimer's disease brain. *Ann. Neurol.* **17,** 444–449 (1985).

322. Parnetti, L. *et al.* Increased cerebrospinal fluid pyruvate levels in Alzheimer's disease. *Neurosci. Lett.* **199,** 231–233 (1995).

323. Krieg, A. F., Rosenblum, L. J. & Henry, J. B. Lactate dehydrogenase isoenzymes a comparison of pyruvate-to-lactate and lactate-to-pyruvate assays. *Clin. Chem.* **13,** 196–203 (1967).

324. Markert, C. L., Shaklee, J. B. & Whitt, G. S. Evolution of a gene. Multiple genes for LDH isozymes provide a model of the evolution of gene structure, function and regulation. *Science* **189,** 102–114 (1975).

325. Semenza, G. L. *et al.* Hypoxia response elements in the aldolase A, enolase 1, and lactate dehydrogenase A gene promoters contain essential binding sites for hypoxia-inducible factor 1. *J. Biol. Chem.* **271,** 32529–32537 (1996).

326. Doherty, J. R. & Cleveland, J. L. Targeting lactate metabolism for cancer therapeutics. *J. Clin. Invest.* **123,** 3685–3692 (2013).

327. Allison, S. J. *et al.* Identification of LDH-A as a therapeutic target for cancer cell killing via (i) p53/NAD(H)-dependent and (ii) p53-independent pathways. *Oncogenesis* **3,** e102 (2014).

328. Bittar, P. G., Charnay, Y., Pellerin, L., Bouras, C. & Magistretti, P. J. Selective distribution of lactate dehydrogenase isoenzymes in neurons and astrocytes of human brain. *J. Cereb. Blood Flow Metab. Off. J. Int. Soc. Cereb. Blood Flow Metab.* **16,** 1079–1089 (1996).

329. O'Brien, J., Kla, K. M., Hopkins, I. B., Malecki, E. A. & McKenna, M. C. Kinetic parameters and lactate dehydrogenase isozyme activities support possible lactate utilization by neurons. *Neurochem. Res.* **32,** 597–607 (2007).

330. Ross, J. M. *et al.* High brain lactate is a hallmark of aging and caused by a shift in the lactate dehydrogenase A/B ratio. *Proc. Natl. Acad. Sci. U. S. A.* **107,** 20087–20092 (2010).

331. Quistorff, B. & Grunnet, N. High brain lactate is not caused by a shift in the lactate dehydrogenase A/B ratio. *Proc. Natl. Acad. Sci.* **108,** E21–E21 (2011).

332. Wang, G. L., Jiang, B. H., Rue, E. A. & Semenza, G. L. Hypoxia-inducible factor 1 is a basic-helix-loop-helix-PAS heterodimer regulated by cellular O2 tension. *Proc. Natl. Acad. Sci.* **92,** 5510–5514 (1995).

333. Salceda, S. & Caro, J. Hypoxia-inducible factor 1alpha (HIF-1alpha) protein is rapidly degraded by the ubiquitin-proteasome system under normoxic conditions. Its

stabilization by hypoxia depends on redox-induced changes. *J. Biol. Chem.* **272,** 22642–22647 (1997).

334. Semenza, G. L., Nejfelt, M. K., Chi, S. M. & Antonarakis, S. E. Hypoxia-inducible nuclear factors bind to an enhancer element located 3' to the human erythropoietin gene. *Proc. Natl. Acad. Sci.* **88,** 5680–5684 (1991).

335. Semenza, G. L. HIF-1: upstream and downstream of cancer metabolism. *Curr. Opin. Genet. Dev.* **20,** 51–56 (2010).

336. Sun, Q. *et al.* Mammalian target of rapamycin up-regulation of pyruvate kinase isoenzyme type M2 is critical for aerobic glycolysis and tumor growth. *Proc. Natl. Acad. Sci. U. S. A.* **108,** 4129–4134 (2011).

337. Zhong, H. *et al.* Overexpression of hypoxia-inducible factor 1alpha in common human cancers and their metastases. *Cancer Res.* **59,** 5830–5835 (1999).

338. Jiang, B. H., Agani, F., Passaniti, A. & Semenza, G. L. V-SRC induces expression of hypoxia-inducible factor 1 (HIF-1) and transcription of genes encoding vascular endothelial growth factor and enolase 1: involvement of HIF-1 in tumor progression. *Cancer Res.* **57,** 5328–5335 (1997).

339. Maxwell, P. H. *et al.* Hypoxia-inducible factor-1 modulates gene expression in solid tumors and influences both angiogenesis and tumor growth. *Proc. Natl. Acad. Sci. U. S. A.* **94,** 8104–8109 (1997).

340. Ryan, H. E., Lo, J. & Johnson, R. S. HIF-1 alpha is required for solid tumor formation and embryonic vascularization. *EMBO J.* **17,** 3005–3015 (1998).

341. Zhang, Z., Yan, J., Chang, Y., ShiDu Yan, S. & Shi, H. Hypoxia inducible factor-1 as a target for neurodegenerative diseases. *Curr. Med. Chem.* **18,** 4335–4343 (2011).

342. Schubert, D., Soucek, T. & Blouw, B. The induction of HIF-1 reduces astrocyte activation by amyloid beta peptide. *Eur. J. Neurosci.* **29,** 1323–1334 (2009).

343. Mink, J. W., Blumenschine, R. J. & Adams, D. B. Ratio of central nervous system to body metabolism in vertebrates: its constancy and functional basis. *Am. J. Physiol.* **241,** R203-212 (1981).

344. Raichle, M. E. & Gusnard, D. A. Appraising the brain's energy budget. *Proc. Natl. Acad. Sci.* **99,** 10237–10239 (2002).

345. Attwell, D. & Laughlin, S. B. An Energy Budget for Signaling in the Grey Matter of the Brain. *J. Cereb. Blood Flow Metab.* **21,** 1133–1145 (2001).

346. Fox, P. T., Raichle, M. E., Mintun, M. A. & Dence, C. Nonoxidative glucose consumption during focal physiologic neural activity. *Science* **241,** 462–464 (1988).

347. Blomqvist, G. *et al.* Regional cerebral oxidative and total glucose consumption during rest and activation studied with positron emission tomography. *Acta Physiol. Scand.* **151,** 29–43 (1994).

348. Boyle, P. J. *et al.* Diminished brain glucose metabolism is a significant determinant for falling rates of systemic glucose utilization during sleep in normal humans. *J. Clin. Invest.* **93,** 529–535 (1994).

349. Madsen, P. L. *et al.* Persistent resetting of the cerebral oxygen/glucose uptake ratio by brain activation: evidence obtained with the Kety-Schmidt technique. *J. Cereb. Blood Flow Metab. Off. J. Int. Soc. Cereb. Blood Flow Metab.* **15,** 485–491 (1995).

350. Powers, W. J. *et al.* Selective defect of in vivo glycolysis in early Huntington's disease striatum. *Proc. Natl. Acad. Sci. U. S. A.* **104,** 2945–2949 (2007).

351. Vaishnavi, S. N. *et al.* Regional aerobic glycolysis in the human brain. *Proc. Natl. Acad. Sci.* 201010459 (2010). doi:10.1073/pnas.1010459107

352. Raichle, M. E. *et al.* A default mode of brain function. *Proc. Natl. Acad. Sci. U. S. A.* **98,** 676–682 (2001).

353. Braver, T. S. & Barch, D. M. Extracting core components of cognitive control. *Trends Cogn. Sci.* **10,** 529–532 (2006).

354. Morcom, A. M. & Fletcher, P. C. Does the brain have a baseline? Why we should be resisting a rest. *NeuroImage* **37,** 1073–1082 (2007).

355. Vincent, J. L., Kahn, I., Snyder, A. Z., Raichle, M. E. & Buckner, R. L. Evidence for a frontoparietal control system revealed by intrinsic functional connectivity. *J. Neurophysiol.* **100,** 3328–3342 (2008).

356. Azevedo, F. A. C. *et al.* Equal numbers of neuronal and nonneuronal cells make the human brain an isometrically scaled-up primate brain. *J. Comp. Neurol.* **513,** 532–541 (2009).

357. Raichle, M. E. Behind the scenes of functional brain imaging: a historical and physiological perspective. *Proc. Natl. Acad. Sci. U. S. A.* **95,** 765–772 (1998).

358. Brain energy metabolism by B. K. Siesjo, John Wiley & Sons, New York, 1978. *Ann. Neurol.* **5,** 308–308 (1979).

359. Plum, F., Posner, J. B. & Troy, B. Cerebral metabolic and circulatory responses to induced convulsions in animals. *Arch. Neurol.* **18,** 1–13 (1968).

360. Howse, D. C., Plum, F., Duffy, T. E. & Salford, L. G. Cerebral energy metabolism and the regulation of cerebral blood flow. *Trans. Am. Neurol. Assoc.* **98,** 153–155 (1973).

361. Madsen, P. L., Linde, R., Hasselbalch, S. G., Paulson, O. B. & Lassen, N. A. Activation-induced resetting of cerebral oxygen and glucose uptake in the rat. *J. Cereb. Blood Flow Metab. Off. J. Int. Soc. Cereb. Blood Flow Metab.* **18,** 742–748 (1998).

362. Newberg, A. B. *et al.* Concurrent CBF and CMRGlc changes during human brain activation by combined fMRI-PET scanning. *NeuroImage* **28,** 500–506 (2005).

363. Madsen, P. L., Cruz, N. F., Sokoloff, L. & Dienel, G. A. Cerebral oxygen/glucose ratio is low during sensory stimulation and rises above normal during recovery: excess glucose consumption during stimulation is not accounted for by lactate efflux from or accumulation in brain tissue. *J. Cereb. Blood Flow Metab. Off. J. Int. Soc. Cereb. Blood Flow Metab.* **19,** 393–400 (1999).

364. Prichard, J. *et al.* Lactate rise detected by 1H NMR in human visual cortex during physiologic stimulation. *Proc. Natl. Acad. Sci. U. S. A.* **88,** 5829–5831 (1991).

365. Sappey-Marinier, D. *et al.* Effect of photic stimulation on human visual cortex lactate and phosphates using 1H and 31P magnetic resonance spectroscopy. *J. Cereb. Blood Flow Metab. Off. J. Int. Soc. Cereb. Blood Flow Metab.* **12,** 584–592 (1992).

366. Hu, Y. & Wilson, G. S. A temporary local energy pool coupled to neuronal activity: fluctuations of extracellular lactate levels in rat brain monitored with rapid-response enzyme-based sensor. *J. Neurochem.* **69,** 1484–1490 (1997).

367. Urrila, A. S. *et al.* Metabolic imaging of human cognition: an fMRI/1H-MRS study of brain lactate response to silent word generation. *J. Cereb. Blood Flow Metab. Off. J. Int. Soc. Cereb. Blood Flow Metab.* **23,** 942–948 (2003).

368. Mangia, S. *et al.* Sustained neuronal activation raises oxidative metabolism to a new steady-state level: evidence from 1H NMR spectroscopy in the human visual cortex. *J. Cereb. Blood Flow Metab. Off. J. Int. Soc. Cereb. Blood Flow Metab.* **27,** 1055–1063 (2007).

369. Ido, Y., Chang, K. & Williamson, J. R. NADH augments blood flow in physiologically activated retina and visual cortex. *Proc. Natl. Acad. Sci. U. S. A.* **101,** 653–658 (2004).

370. Mintun, M. A., Vlassenko, A. G., Rundle, M. M. & Raichle, M. E. Increased lactate/pyruvate ratio augments blood flow in physiologically activated human brain. *Proc. Natl. Acad. Sci. U. S. A.* **101,** 659–664 (2004).

371. Vlassenko, A. G., Rundle, M. M., Raichle, M. E. & Mintun, M. A. Regulation of blood flow in activated human brain by cytosolic NADH/NAD+ ratio. *Proc. Natl. Acad. Sci. U. S. A.* **103,** 1964–1969 (2006).

372. Wolin, M. S. Reactive oxygen species and vascular signal transduction mechanisms. *Microcirc. N. Y. N 1994* **3,** 1–17 (1996).

373. Volk, T., Hensel, M. & Kox, W. J. Transient Ca2+ changes in endothelial cells induced by low doses of reactive oxygen species: role of hydrogen peroxide. *Mol. Cell. Biochem.* **171,** 11–21 (1997).

374. Iadecola, C. Regulation of the cerebral microcirculation during neural activity: is nitric oxide the missing link? *Trends Neurosci.* **16,** 206–214 (1993).

375. Gordon, G. R. J., Choi, H. B., Ellis-Davies, G. C. R. & MacVicar, B. A. Brain metabolic state dictates the polarity of astrocyte control over the cerebrovasculature. *Nature* **456,** 745–749 (2008).

376. Volterra, A. & Meldolesi, J. Astrocytes, from brain glue to communication elements: the revolution continues. *Nat. Rev. Neurosci.* **6,** 626–640 (2005).

377. Pellerin, L. & Magistretti, P. J. Glutamate uptake into astrocytes stimulates aerobic glycolysis: a mechanism coupling neuronal activity to glucose utilization. *Proc. Natl. Acad. Sci. U. S. A.* **91,** 10625–10629 (1994).

378. Pellerin, L. & Magistretti, P. J. Sweet sixteen for ANLS. *J. Cereb. Blood Flow Metab.* **32,** 1152–1166 (2012).

379. Gasic, G. P. & Hollmann, M. Molecular neurobiology of glutamate receptors. *Annu. Rev. Physiol.* **54,** 507–536 (1992).

380. Magistretti, P. J. & Chatton, J.-Y. Relationship between L-glutamate-regulated intracellular Na+ dynamics and ATP hydrolysis in astrocytes. *J. Neural Transm. Vienna Austria 1996* **112,** 77–85 (2005).

381. Magistretti, P. J. Neuron-glia metabolic coupling and plasticity. *J. Exp. Biol.* **209,** 2304–2311 (2006).

382. Magistretti, P. J., Morrison, J. H., Shoemaker, W. J., Sapin, V. & Bloom, F. E. Vasoactive intestinal polypeptide induces glycogenolysis in mouse cortical slices: a possible regulatory mechanism for the local control of energy metabolism. *Proc. Natl. Acad. Sci. U. S. A.* **78,** 6535–6539 (1981).

383. Suzuki, A. *et al.* Astrocyte-neuron lactate transport is required for long-term memory formation. *Cell* **144,** 810–823 (2011).

384. Poole, R. C. & Halestrap, A. P. Transport of lactate and other monocarboxylates across mammalian plasma membranes. *Am. J. Physiol.* **264,** C761-782 (1993).

385. Gerhart, D. Z., Enerson, B. E., Zhdankina, O. Y., Leino, R. L. & Drewes, L. R. Expression of monocarboxylate transporter MCT1 by brain endothelium and glia in adult and suckling rats. *Am. J. Physiol.* **273,** E207-213 (1997).

386. Debernardi, R., Pierre, K., Lengacher, S., Magistretti, P. J. & Pellerin, L. Cell-specific expression pattern of monocarboxylate transporters in astrocytes and neurons observed in different mouse brain cortical cell cultures. *J. Neurosci. Res.* **73,** 141–155 (2003).

387. Rafiki, A., Boulland, J. L., Halestrap, A. P., Ottersen, O. P. & Bergersen, L. Highly differential expression of the monocarboxylate transporters MCT2 and MCT4 in the developing rat brain. *Neuroscience* **122,** 677–688 (2003).

388. Pellerin, L., Halestrap, A. P. & Pierre, K. Cellular and subcellular distribution of monocarboxylate transporters in cultured brain cells and in the adult brain. *J. Neurosci. Res.* **79,** 55–64 (2005).

389. Pierre, K. & Pellerin, L. Monocarboxylate transporters in the central nervous system: distribution, regulation and function. *J. Neurochem.* **94,** 1–14 (2005).

390. Rinholm, J. E. *et al.* Regulation of oligodendrocyte development and myelination by glucose and lactate. *J. Neurosci. Off. J. Soc. Neurosci.* **31,** 538–548 (2011).

391. Gerhart, D. Z., Enerson, B. E., Zhdankina, O. Y., Leino, R. L. & Drewes, L. R. Expression of the monocarboxylate transporter MCT2 by rat brain glia. *Glia* **22,** 272–281 (1998).

392. Halestrap, A. P. & Price, N. T. The proton-linked monocarboxylate transporter (MCT) family: structure, function and regulation. *Biochem. J.* **343,** 281–299 (1999).

393. Juel, C. Symmetry and pH dependency of the lactate/proton carrier in skeletal muscle studied with rat sarcolemmal giant vesicles. *Biochim. Biophys. Acta* **1283,** 106–110 (1996).

394. Dimmer, K. S., Friedrich, B., Lang, F., Deitmer, J. W. & Bröer, S. The low-affinity monocarboxylate transporter MCT4 is adapted to the export of lactate in highly glycolytic cells. *Biochem. J.* **350 Pt 1,** 219–227 (2000).

395. Vinnakota, K. C. & Beard, D. A. Kinetic Analysis and Design of Experiments to Identify the Catalytic Mechanism of the Monocarboxylate Transporter Isoforms 4 and 1. *Biophys. J.* **100,** 369–380 (2011).

396. Pellerin, L. *et al.* Evidence supporting the existence of an activity-dependent astrocyte-neuron lactate shuttle. *Dev. Neurosci.* **20,** 291–299 (1998).

397. Bouzier-Sore, A.-K., Merle, M., Magistretti, P. J. & Pellerin, L. Feeding active neurons: (re)emergence of a nursing role for astrocytes. *J. Physiol. Paris* **96,** 273–282 (2002).

398. Morgello, S., Uson, R. R., Schwartz, E. J. & Haber, R. S. The human blood-brain barrier glucose transporter (GLUT1) is a glucose transporter of gray matter astrocytes. *Glia* **14,** 43–54 (1995).

399. Yu, S. & Ding, W. G. The 45 kDa form of glucose transporter 1 (GLUT1) is localized in oligodendrocyte and astrocyte but not in microglia in the rat brain. *Brain Res.* **797,** 65–72 (1998).

400. Derouiche, A. & Frotscher, M. Astroglial processes around identified glutamatergic synapses contain glutamine synthetase: evidence for transmitter degradation. *Brain Res.* **552,** 346–350 (1991).

401. Bak, L. K., Schousboe, A. & Waagepetersen, H. S. The glutamate/GABA-glutamine cycle: aspects of transport, neurotransmitter homeostasis and ammonia transfer. *J. Neurochem.* **98,** 641–653 (2006).

402. McKenna, M. C. The glutamate-glutamine cycle is not stoichiometric: fates of glutamate in brain. *J. Neurosci. Res.* **85,** 3347–3358 (2007).

403. Itoh, Y. *et al.* Dichloroacetate effects on glucose and lactate oxidation by neurons and astroglia in vitro and on glucose utilization by brain in vivo. *Proc. Natl. Acad. Sci. U. S. A.* **100,** 4879–4884 (2003).

404. Serres, S., Bezancon, E., Franconi, J.-M. & Merle, M. Ex vivo NMR study of lactate metabolism in rat brain under various depressed states. *J. Neurosci. Res.* **79,** 19–25 (2005).

405. Bouzier-Sore, A.-K. *et al.* Competition between glucose and lactate as oxidative energy substrates in both neurons and astrocytes: a comparative NMR study. *Eur. J. Neurosci.* **24,** 1687–1694 (2006).

406. Lovatt, D. *et al.* The transcriptome and metabolic gene signature of protoplasmic astrocytes in the adult murine cortex. *J. Neurosci. Off. J. Soc. Neurosci.* **27,** 12255–12266 (2007).

407. Herrero-Mendez, A. *et al.* The bioenergetic and antioxidant status of neurons is controlled by continuous degradation of a key glycolytic enzyme by APC/C-Cdh1. *Nat. Cell Biol.* **11,** 747–752 (2009).

408. Bittner, C. X. *et al.* High resolution measurement of the glycolytic rate. *Front. Neuroenergetics* **2,** (2010).

409. Laughton, J. D. *et al.* Metabolic compartmentalization in the human cortex and hippocampus: evidence for a cell- and region-specific localization of lactate dehydrogenase 5 and pyruvate dehydrogenase. *BMC Neurosci.* **8,** 35 (2007).

410. Halim, N. D. *et al.* Phosphorylation status of pyruvate dehydrogenase distinguishes metabolic phenotypes of cultured rat brain astrocytes and neurons. *Glia* **58,** 1168–1176 (2010).

411. Schurr, A., Payne, R. S., Miller, J. J. & Rigor, B. M. Brain lactate is an obligatory aerobic energy substrate for functional recovery after hypoxia: further in vitro validation. *J. Neurochem.* **69,** 423–426 (1997).

412. Bouzier, A. K. *et al.* The metabolism of [3-(13)C]lactate in the rat brain is specific of a pyruvate carboxylase-deprived compartment. *J. Neurochem.* **75,** 480–486 (2000).

413. Qu, H., Håberg, A., Haraldseth, O., Unsgård, G. & Sonnewald, U. (13)C MR spectroscopy study of lactate as substrate for rat brain. *Dev. Neurosci.* **22,** 429–436 (2000).

414. Lebon, V. *et al.* Astroglial contribution to brain energy metabolism in humans revealed by 13C nuclear magnetic resonance spectroscopy: elucidation of the dominant pathway for neurotransmitter glutamate repletion and measurement of astrocytic oxidative metabolism. *J. Neurosci. Off. J. Soc. Neurosci.* **22,** 1523–1531 (2002).

415. Boumezbeur, F. *et al.* Altered brain mitochondrial metabolism in healthy aging as assessed by in vivo magnetic resonance spectroscopy. *J. Cereb. Blood Flow Metab. Off. J. Int. Soc. Cereb. Blood Flow Metab.* **30,** 211–221 (2010).

416. Boumezbeur, F. *et al.* The contribution of blood lactate to brain energy metabolism in humans measured by dynamic 13C nuclear magnetic resonance spectroscopy. *J. Neurosci. Off. J. Soc. Neurosci.* **30,** 13983–13991 (2010).

417. Schousboe, A. *et al.* Trafficking between glia and neurons of TCA cycle intermediates and related metabolites. *Glia* **21,** 99–105 (1997).

418. Hassel, B. & Bråthe, A. Cerebral metabolism of lactate in vivo: evidence for neuronal pyruvate carboxylation. *J. Cereb. Blood Flow Metab. Off. J. Int. Soc. Cereb. Blood Flow Metab.* **20,** 327–336 (2000).

419. Waagepetersen, H. S., Sonnewald, U., Larsson, O. M. & Schousboe, A. A Possible Role of Alanine for Ammonia Transfer Between Astrocytes and Glutamatergic Neurons. *J. Neurochem.* **75,** 471–479 (2000).

420. Chih, C. P., Lipton, P. & Roberts, E. L. Do active cerebral neurons really use lactate rather than glucose? *Trends Neurosci.* **24,** 573–578 (2001).

421. Chih, C.-P. & Roberts Jr, E. L. Energy substrates for neurons during neural activity: a critical review of the astrocyte-neuron lactate shuttle hypothesis. *J. Cereb. Blood Flow Metab. Off. J. Int. Soc. Cereb. Blood Flow Metab.* **23,** 1263–1281 (2003).

422. Korf, J. Is brain lactate metabolized immediately after neuronal activity through the oxidative pathway? *J. Cereb. Blood Flow Metab. Off. J. Int. Soc. Cereb. Blood Flow Metab.* **26,** 1584–1586 (2006).

423. Schurr, A. Lactate: the ultimate cerebral oxidative energy substrate? *J. Cereb. Blood Flow Metab. Off. J. Int. Soc. Cereb. Blood Flow Metab.* **26,** 142–152 (2006).

424. Mangia, S., Simpson, I. A., Vannucci, S. J. & Carruthers, A. The in vivo neuron-to-astrocyte lactate shuttle in human brain: evidence from modeling of measured lactate levels during visual stimulation. *J. Neurochem.* **109 Suppl 1,** 55–62 (2009).

425. Dienel, G. A. Brain lactate metabolism: the discoveries and the controversies. *J. Cereb. Blood Flow Metab.* **32,** 1107–1138 (2012).

426. Walz, W. & Mukerji, S. Lactate release from cultured astrocytes and neurons: a comparison. *Glia* **1,** 366–370 (1988).

427. Lundgaard, I. *et al.* Direct neuronal glucose uptake heralds activity-dependent increases in cerebral metabolism. *Nat. Commun.* **6,** 6807 (2015).

428. Silver, I. A. & Erecińska, M. Energetic demands of the Na+/K+ ATPase in mammalian astrocytes. *Glia* **21,** 35–45 (1997).

429. Eriksson, G., Peterson, A., Iverfeldt, K. & Walum, E. Sodium-dependent glutamate uptake as an activator of oxidative metabolism in primary astrocyte cultures from newborn rat. *Glia* **15,** 152–156 (1995).

430. Kauppinen, R. A. & Nicholls, D. G. Synaptosomal bioenergetics. The role of glycolysis, pyruvate oxidation and responses to hypoglycaemia. *Eur. J. Biochem. FEBS* **158,** 159–165 (1986).

431. Kauppinen, R. A., Taipale, H. T. & Komulainen, H. Interrelationships between glucose metabolism, energy state, and the cytosolic free calcium concentration in cortical synaptosomes from the guinea pig. *J. Neurochem.* **53,** 766–771 (1989).

432. Erecińska, M., Nelson, D. & Chance, B. Depolarization-induced changes in cellular energy production. *Proc. Natl. Acad. Sci. U. S. A.* **88,** 7600–7604 (1991).

433. Gjedde, A. & Marrett, S. Glycolysis in neurons, not astrocytes, delays oxidative metabolism of human visual cortex during sustained checkerboard stimulation in vivo. *J. Cereb. Blood Flow Metab. Off. J. Int. Soc. Cereb. Blood Flow Metab.* **21,** 1384–1392 (2001).

434. Ide, K., Horn, A. & Secher, N. H. Cerebral metabolic response to submaximal exercise. *J. Appl. Physiol. Bethesda Md 1985* **87,** 1604–1608 (1999).

435. Ide, K., Schmalbruch, I. K., Quistorff, B., Horn, A. & Secher, N. H. Lactate, glucose and O2 uptake in human brain during recovery from maximal exercise. *J. Physiol.* **522 Pt 1,** 159–164 (2000).

436. Quistorff, B., Secher, N. H. & Van Lieshout, J. J. Lactate fuels the human brain during exercise. *FASEB J. Off. Publ. Fed. Am. Soc. Exp. Biol.* **22,** 3443–3449 (2008).

437. van Hall, G. *et al.* Blood lactate is an important energy source for the human brain. *J. Cereb. Blood Flow Metab. Off. J. Int. Soc. Cereb. Blood Flow Metab.* **29,** 1121–1129 (2009).

438. Rasmussen, P., Wyss, M. T. & Lundby, C. Cerebral glucose and lactate consumption during cerebral activation by physical activity in humans. *FASEB J.* **25,** 2865–2873 (2011).

439. Dienel, G. A. Astrocytes are 'good scouts': being prepared also helps neighboring neurons. *J. Cereb. Blood Flow Metab. Off. J. Int. Soc. Cereb. Blood Flow Metab.* **30,** 1893–1894 (2010).

440. DiNuzzo, M., Mangia, S., Maraviglia, B. & Giove, F. Changes in glucose uptake rather than lactate shuttle take center stage in subserving neuroenergetics: evidence from mathematical modeling. *J. Cereb. Blood Flow Metab. Off. J. Int. Soc. Cereb. Blood Flow Metab.* **30,** 586–602 (2010).

441. Mangia, S. *et al.* Response to 'comment on recent modeling studies of astrocyte-neuron metabolic interactions': much ado about nothing. *J. Cereb. Blood Flow Metab. Off. J. Int. Soc. Cereb. Blood Flow Metab.* **31,** 1346–1353 (2011).

442. Abel, T. & Lattal, K. M. Molecular mechanisms of memory acquisition, consolidation and retrieval. *Curr. Opin. Neurobiol.* **11,** 180–187 (2001).

443. Anagnostaras, S. G., Maren, S. & Fanselow, M. S. Temporally graded retrograde amnesia of contextual fear after hippocampal damage in rats: within-subjects examination. *J. Neurosci. Off. J. Soc. Neurosci.* **19,** 1106–1114 (1999).

444. Bontempi, B., Laurent-Demir, C., Destrade, C. & Jaffard, R. Time-dependent reorganization of brain circuitry underlying long-term memory storage. *Nature* **400,** 671–675 (1999).

445. Holt, W. & Maren, S. Muscimol inactivation of the dorsal hippocampus impairs contextual retrieval of fear memory. *J. Neurosci. Off. J. Soc. Neurosci.* **19,** 9054–9062 (1999).

446. Lisman, J. E. Relating hippocampal circuitry to function: recall of memory sequences by reciprocal dentate-CA3 interactions. *Neuron* **22,** 233–242 (1999).

447. Riedel, G. *et al.* Reversible neural inactivation reveals hippocampal participation in several memory processes. *Nat. Neurosci.* **2,** 898–905 (1999).

448. Hebb, D. O. *The Organization of Behaviour*. (Wiley & Sons, 1949).

449. Hughes, J. R. Post-tetanic potentiation. *Physiol. Rev.* **38,** 91–113 (1958).

450. Klann, E. & Sweatt, J. D. Altered protein synthesis is a trigger for long-term memory formation. *Neurobiol. Learn. Mem.* **89,** 247–259 (2008).

451. Bliss, T. V. & Collingridge, G. L. A synaptic model of memory: long-term potentiation in the hippocampus. *Nature* **361,** 31–39 (1993).

452. Malenka, R. C. & Nicoll, R. A. Long-term potentiation--a decade of progress? *Science* **285,** 1870–1874 (1999).

453. Martin, S. J., Grimwood, P. D. & Morris, R. G. Synaptic plasticity and memory: an evaluation of the hypothesis. *Annu. Rev. Neurosci.* **23,** 649–711 (2000).

454. Malenka, R. C. The long-term potential of LTP. *Nat. Rev. Neurosci.* **4,** 923–926 (2003).

455. Riedel, G., Platt, B. & Micheau, J. Glutamate receptor function in learning and memory. *Behav. Brain Res.* **140,** 1–47 (2003).

456. Fischer, A., Sananbenesi, F., Schrick, C., Spiess, J. & Radulovic, J. Distinct roles of hippocampal de novo protein synthesis and actin rearrangement in extinction of contextual fear. *J. Neurosci. Off. J. Soc. Neurosci.* **24,** 1962–1966 (2004).

457. Chen, L. Y., Rex, C. S., Casale, M. S., Gall, C. M. & Lynch, G. Changes in synaptic morphology accompany actin signaling during LTP. *J. Neurosci. Off. J. Soc. Neurosci.* **27,** 5363–5372 (2007).

458. Mantzur, L., Joels, G. & Lamprecht, R. Actin polymerization in lateral amygdala is essential for fear memory formation. *Neurobiol. Learn. Mem.* **91,** 85–88 (2009).

459. Bourtchuladze, R. *et al.* Deficient long-term memory in mice with a targeted mutation of the cAMP-responsive element-binding protein. *Cell* **79,** 59–68 (1994).

460. Kida, S. *et al.* CREB required for the stability of new and reactivated fear memories. *Nat. Neurosci.* **5,** 348–355 (2002).

461. Pittenger, C. *et al.* Reversible inhibition of CREB/ATF transcription factors in region CA1 of the dorsal hippocampus disrupts hippocampus-dependent spatial memory. *Neuron* **34,** 447–462 (2002).

462. Suzuki, A. *et al.* Astrocyte-neuron lactate transport is required for long-term memory formation. *Cell* **144,** 810–823 (2011).

463. Goyal, M. S., Hawrylycz, M., Miller, J. A., Snyder, A. Z. & Raichle, M. E. Aerobic glycolysis in the human brain is associated with development and neotenous gene expression. *Cell Metab.* **19,** 49–57 (2014).

464. Yang, J. *et al.* Lactate promotes plasticity gene expression by potentiating NMDA signaling in neurons. *Proc. Natl. Acad. Sci.* **111,** 12228–12233 (2014).

465. Giffard, R. G., Monyer, H., Christine, C. W. & Choi, D. W. Acidosis reduces NMDA receptor activation, glutamate neurotoxicity, and oxygen-glucose deprivation neuronal injury in cortical cultures. *Brain Res.* **506,** 339–342 (1990).

466. Tang, C. M., Dichter, M. & Morad, M. Modulation of the N-methyl-D-aspartate channel by extracellular H+. *Proc. Natl. Acad. Sci. U. S. A.* **87,** 6445–6449 (1990).

467. Mosienko, V., Teschemacher, A. G. & Kasparov, S. Is L-lactate a novel signaling molecule in the brain? *J. Cereb. Blood Flow Metab. Off. J. Int. Soc. Cereb. Blood Flow Metab.* (2015). doi:10.1038/jcbfm.2015.77

468. Cai, T.-Q. *et al.* Role of GPR81 in lactate-mediated reduction of adipose lipolysis. *Biochem. Biophys. Res. Commun.* **377,** 987–991 (2008).

469. Liu, C. *et al.* Lactate inhibits lipolysis in fat cells through activation of an orphan G-protein-coupled receptor, GPR81. *J. Biol. Chem.* **284,** 2811–2822 (2009).

470. Liu, C. *et al.* 3,5-Dihydroxybenzoic acid, a specific agonist for hydroxycarboxylic acid 1, inhibits lipolysis in adipocytes. *J. Pharmacol. Exp. Ther.* **341,** 794–801 (2012).

471. Lauritzen, K. H. *et al.* Lactate receptor sites link neurotransmission, neurovascular coupling, and brain energy metabolism. *Cereb. Cortex N. Y. N 1991* **24,** 2784–2795 (2014).

472. Bozzo, L., Puyal, J. & Chatton, J.-Y. Lactate modulates the activity of primary cortical neurons through a receptor-mediated pathway. *PloS One* **8,** e71721 (2013).

473. Gilbert, E., Tang, J. M., Ludvig, N. & Bergold, P. J. Elevated lactate suppresses neuronal firing in vivo and inhibits glucose metabolism in hippocampal slice cultures. *Brain Res.* **1117,** 213–223 (2006).

474. O'Dowd, B. S., Gibbs, M. E., Ng, K. T., Hertz, E. & Hertz, L. Astrocytic glycogenolysis energizes memory processes in neonate chicks. *Brain Res. Dev. Brain Res.* **78,** 137–141 (1994).

475. Hertz, L., O'Dowd, B. S., Ng, K. T. & Gibbs, M. E. Reciprocal changes in forebrain contents of glycogen and of glutamate/glutamine during early memory consolidation in the day-old chick. *Brain Res.* **994,** 226–233 (2003).

476. Gibbs, M. E., Anderson, D. G. & Hertz, L. Inhibition of glycogenolysis in astrocytes interrupts memory consolidation in young chickens. *Glia* **54,** 214–222 (2006).

477. Gibbs, M. E., Lloyd, H. G. E., Santa, T. & Hertz, L. Glycogen is a preferred glutamate precursor during learning in 1-day-old chick: biochemical and behavioral evidence. *J. Neurosci. Res.* **85,** 3326–3333 (2007).

478. Boury-Jamot, B. *et al.* Disrupting astrocyte-neuron lactate transfer persistently reduces conditioned responses to cocaine. *Mol. Psychiatry* (2015). doi:10.1038/mp.2015.157

479. Zhang, Y. *et al.* Inhibition of Lactate Transport Erases Drug Memory and Prevents Drug Relapse. *Biol. Psychiatry* **79,** 928–939 (2016).

480. Rupp, N. J., Wegenast-Braun, B. M., Radde, R., Calhoun, M. E. & Jucker, M. Early onset amyloid lesions lead to severe neuritic abnormalities and local, but not global neuron loss in APPPS1 transgenic mice. *Neurobiol. Aging* **32,** 2324.e1-6 (2011).

481. Jankowsky, J. L. *et al.* Co-expression of multiple transgenes in mouse CNS: a comparison of strategies. *Biomol. Eng.* **17,** 157–165 (2001).

482. Kassem, M. N. E. & Bartha, R. Quantitative proton short-echo-time LASER spectroscopy of normal human white matter and hippocampus at 4 Tesla incorporating macromolecule subtraction. *Magn. Reson. Med.* **49,** 918–927 (2003).

483. Macauley, S. L. *et al.* Hyperglycemia modulates extracellular amyloid-β concentrations and neuronal activity in vivo. *J. Clin. Invest.* **125,** 2463–2467 (2015).

484. Morris, R. Developments of a water-maze procedure for studying spatial learning in the rat. *J. Neurosci. Methods* **11,** 47–60 (1984).

485. Vorhees, C. V. & Williams, M. T. Morris water maze: procedures for assessing spatial and related forms of learning and memory. *Nat. Protoc.* **1,** 848–858 (2006).

486. Uden, P. C. & Miller, J. W. Chlorinated acids and chloral in drinking water. *J. Am. Water Works Assoc.* **75,** 524–527 (1983).

487. McAllister, A., Allison, S. P. & Randle, P. J. Effects of dichloroacetate on the metabolism of glucose, pyruvate, acetate, 3-hydroxybutyrate and palmitate in rat diaphragm and heart muscle in vitro and on extraction of glucose, lactate, pyruvate and free fatty acids by dog heart in vivo. *Biochem. J.* **134,** 1067–1081 (1973).

488. Lukas, G., Vyas, K. H., Brindle, S. D., Le Sher, A. R. & Wagner, W. E. Biological disposition of sodium dichloroacetate in animals and humans after intravenous administration. *J. Pharm. Sci.* **69,** 419–421 (1980).

489. Whitehouse, S., Cooper, R. H. & Randle, P. J. Mechanism of activation of pyruvate dehydrogenase by dichloroacetate and other halogenated carboxylic acids. *Biochem. J.* **141,** 761–774 (1974).

490. Chiron, C. *et al.* Stiripentol in severe myoclonic epilepsy in infancy: a randomised placebo-controlled syndrome-dedicated trial. STICLO study group. *Lancet Lond. Engl.* **356,** 1638–1642 (2000).

491. Sada, N., Lee, S., Katsu, T., Otsuki, T. & Inoue, T. Epilepsy treatment. Targeting LDH enzymes with a stiripentol analog to treat epilepsy. *Science* **347,** 1362–1367 (2015).

492. Stacpoole, P. W. The pharmacology of dichloroacetate. *Metabolism.* **38,** 1124–1144 (1989).

493. Stacpoole, P. W., Nagaraja, N. V. & Hutson, A. D. Efficacy of dichloroacetate as a lactate-lowering drug. *J. Clin. Pharmacol.* **43,** 683–691 (2003).

494. van der Staay, F. J. Animal models of behavioral dysfunctions: basic concepts and classifications, and an evaluation strategy. *Brain Res. Rev.* **52,** 131–159 (2006).

495. Ardenkjaer-Larsen, J. H. *et al.* Increase in signal-to-noise ratio of > 10,000 times in liquid-state NMR. *Proc. Natl. Acad. Sci. U. S. A.* **100,** 10158–10163 (2003).

496. Duarte, J. M. N., Do, K. Q. & Gruetter, R. Longitudinal neurochemical modifications in the aging mouse brain measured in vivo by 1H magnetic resonance spectroscopy. *Neurobiol. Aging* **35,** 1660–1668 (2014).

497. Li, X.-Y. *et al.* Age- and Brain Region-Specific Changes of Glucose Metabolic Disorder, Learning, and Memory Dysfunction in Early Alzheimer's Disease Assessed in APP/PS1 Transgenic Mice Using 18F-FDG-PET. *Int. J. Mol. Sci.* **17,** (2016).

498. Luo, F. *et al.* Characterization of 7- and 19-month-old Tg2576 mice using multimodal in vivo imaging: limitations as a translatable model of Alzheimer's disease. *Neurobiol. Aging* **33,** 933–944 (2012).

499. Reiman, E. M. *et al.* Tracking Alzheimer's disease in transgenic mice using fluorodeoxyglucose autoradiography. *Neuroreport* **11,** 987–991 (2000).

500. Valla, J., Gonzalez-Lima, F. & Reiman, E. M. FDG autoradiography reveals developmental and pathological effects of mutant amyloid in PDAPP transgenic mice. *Int. J. Dev. Neurosci. Off. J. Int. Soc. Dev. Neurosci.* **26,** 253–258 (2008).

501. Valla, J., Schneider, L. & Reiman, E. M. Age- and transgene-related changes in regional cerebral metabolism in PSAPP mice. *Brain Res.* **1116,** 194–200 (2006).

502. Rojas, S. *et al.* In vivo evaluation of amyloid deposition and brain glucose metabolism of 5XFAD mice using positron emission tomography. *Neurobiol. Aging* **34,** 1790–1798 (2013).

503. Nicholson, R. M. *et al.* Regional cerebral glucose uptake in the 3xTG model of Alzheimer's disease highlights common regional vulnerability across AD mouse models. *Brain Res.* **1347,** 179–185 (2010).

504. Deleye, S. *et al.* The Effects of Physiological and Methodological Determinants on 18F-FDG Mouse Brain Imaging Exemplified in a Double Transgenic Alzheimer Model. *Mol. Imaging* **15,** (2016).

505. Kuntner, C. *et al.* Limitations of small animal PET imaging with [18F]FDDNP and FDG for quantitative studies in a transgenic mouse model of Alzheimer's disease. *Mol. Imaging Biol. MIB Off. Publ. Acad. Mol. Imaging* **11,** 236–240 (2009).

506. I.R, M. *et al.* Early Detection of Cerebral Glucose Uptake Changes in the 5XFAD Mouse. *Curr. Alzheimer Res.* **11,** 450–460 (2014).

507. Chen, S.-Q. *et al.* Role of myo-inositol by magnetic resonance spectroscopy in early diagnosis of Alzheimer's disease in APP/PS1 transgenic mice. *Dement. Geriatr. Cogn. Disord.* **28,** 558–566 (2009).

508. Chen, S. *et al.* Age-related changes in brain metabolites and cognitive function in APP/PS1 transgenic mice. *Behav. Brain Res.* **235,** 1–6 (2012).

509. Woo, D.-C. *et al.* Regional metabolic alteration of Alzheimer's disease in mouse brain expressing mutant human APP-PS1 by 1H HR-MAS. *Behav. Brain Res.* **211,** 125–131 (2010).

510. Li, X. *et al.* Relationship of MR-derived lactate, mobile lipids, and relative blood volume for gliomas in vivo. *AJNR Am. J. Neuroradiol.* **26,** 760–769 (2005).

511. Harris, L. M. *et al.* Evaluation of lactate detection using selective multiple quantum coherence in phantoms and brain tumours. *Nmr Biomed.* **28,** 338–343 (2015).

512. Salek, R. M. *et al.* A metabolomic study of the CRND8 transgenic mouse model of Alzheimer's disease. *Neurochem. Int.* **56,** 937–947 (2010).

513. González-Domínguez, R., García-Barrera, T., Vitorica, J. & Gómez-Ariza, J. L. Region-specific metabolic alterations in the brain of the APP/PS1 transgenic mice of Alzheimer's disease. *Biochim. Biophys. Acta* **1842,** 2395–2402 (2014).

514. von Kienlin, M. *et al.* Altered metabolic profile in the frontal cortex of PS2APP transgenic mice, monitored throughout their life span. *Neurobiol. Dis.* **18,** 32–39 (2005).

515. Nordengen, K., Heuser, C., Rinholm, J. E., Matalon, R. & Gundersen, V. Localisation of N-acetylaspartate in oligodendrocytes/myelin. *Brain Struct. Funct.* **220,** 899–917 (2015).

516. Makaryus, R. *et al.* The metabolomic profile during isoflurane anesthesia differs from propofol anesthesia in the live rodent brain. *J. Cereb. Blood Flow Metab. Off. J. Int. Soc. Cereb. Blood Flow Metab.* **31,** 1432–1442 (2011).

517. De Santi, S. *et al.* Age-related changes in brain: II. Positron emission tomography of frontal and temporal lobe glucose metabolism in normal subjects. *Psychiatr. Q.* **66,** 357–370 (1995).

518. Willis, M. W. *et al.* Age, sex and laterality effects on cerebral glucose metabolism in healthy adults. *Psychiatry Res.* **114,** 23–37 (2002).

519. Fujimoto, T. *et al.* Changes in glucose metabolism due to aging and gender-related differences in the healthy human brain. *Psychiatry Res.* **164,** 58–72 (2008).

520. Marano, C. M. *et al.* Longitudinal studies of cerebral glucose metabolism in late-life depression and normal aging. *Int. J. Geriatr. Psychiatry* **28,** 417–423 (2013).

521. Nugent, S. *et al.* Brain glucose and acetoacetate metabolism: a comparison of young and older adults. *Neurobiol. Aging* **35,** 1386–1395 (2014).

522. Yanase, D. *et al.* Brain FDG PET study of normal aging in Japanese: effect of atrophy correction. *Eur. J. Nucl. Med. Mol. Imaging* **32,** 794–805 (2005).

523. Nugent, S. *et al.* Glucose hypometabolism is highly localized, but lower cortical thickness and brain atrophy are widespread in cognitively normal older adults. *Am. J. Physiol. Endocrinol. Metab.* **306,** E1315-1321 (2014).

524. Shulman, R. G., Hyder, F. & Rothman, D. L. Lactate efflux and the neuroenergetic basis of brain function. *NMR Biomed.* **14,** 389–396 (2001).

525. Giulian, D., Woodward, J., Young, D. G., Krebs, J. F. & Lachman, L. B. Interleukin-1 injected into mammalian brain stimulates astrogliosis and neovascularization. *J. Neurosci. Off. J. Soc. Neurosci.* **8,** 2485–2490 (1988).

526. Van Wagoner, N. J., Oh, J. W., Repovic, P. & Benveniste, E. N. Interleukin-6 (IL-6) production by astrocytes: autocrine regulation by IL-6 and the soluble IL-6 receptor. *J. Neurosci. Off. J. Soc. Neurosci.* **19,** 5236–5244 (1999).

527. Ridet, J. L., Malhotra, S. K., Privat, A. & Gage, F. H. Reactive astrocytes: cellular and molecular cues to biological function. *Trends Neurosci.* **20,** 570–577 (1997).

528. Akiyama, H. *et al.* Inflammation and Alzheimer's disease. *Neurobiol. Aging* **21,** 383–421 (2000).

529. Galea, E. *et al.* Topological analyses in APP/PS1 mice reveal that astrocytes do not migrate to amyloid-β plaques. *Proc. Natl. Acad. Sci. U. S. A.* **112,** 15556–15561 (2015).

530. Fuller, S., Steele, M. & Münch, G. Activated astroglia during chronic inflammation in Alzheimer's disease--do they neglect their neurosupportive roles? *Mutat. Res.* **690,** 40–49 (2010).

531. Steele, M. L. & Robinson, S. R. Reactive astrocytes give neurons less support: implications for Alzheimer's disease. *Neurobiol. Aging* **33,** 423.e1-13 (2012).

532. Scoville, W. B. & Milner, B. Loss of recent memory after bilateral hippocampal lesions. *J. Neurol. Neurosurg. Psychiatry* **20,** 11–21 (1957).

533. Eichenbaum, H. What H.M. taught us. *J. Cogn. Neurosci.* **25,** 14–21 (2013).

534. Shimamura, A. P., Jurica, P. J., Mangels, J. A., Gershberg, F. B. & Knight, R. T. Susceptibility to Memory Interference Effects following Frontal Lobe Damage: Findings from Tests of Paired-Associate Learning. *J. Cogn. Neurosci.* **7,** 144–152 (1995).

535. Dias, R., Robbins, T. W. & Roberts, A. C. Dissociation in prefrontal cortex of affective and attentional shifts. *Nature* **380,** 69–72 (1996).

536. Birrell, J. M. & Brown, V. J. Medial frontal cortex mediates perceptual attentional set shifting in the rat. *J. Neurosci. Off. J. Soc. Neurosci.* **20,** 4320–4324 (2000).

537. Ragozzino, M. E., Kim, J., Hassert, D., Minniti, N. & Kiang, C. The contribution of the rat prelimbic-infralimbic areas to different forms of task switching. *Behav. Neurosci.* **117,** 1054–1065 (2003).

538. Miller, E. K. & Cohen, J. D. An integrative theory of prefrontal cortex function. *Annu. Rev. Neurosci.* **24,** 167–202 (2001).

539. Preston, A. R. & Eichenbaum, H. Interplay of hippocampus and prefrontal cortex in memory. *Curr. Biol. CB* **23,** R764-773 (2013).

540. Vlassenko, A. G. *et al.* Spatial correlation between brain aerobic glycolysis and amyloid-β (Aβ) deposition. *Proc. Natl. Acad. Sci. U. S. A.* **107,** 17763–17767 (2010).

541. Yang, W. *et al.* ERK1/2-dependent phosphorylation and nuclear translocation of PKM2 promotes the Warburg effect. *Nat. Cell Biol.* **14,** 1295–1304 (2012).

542. Yang, W. & Lu, Z. Nuclear PKM2 regulates the Warburg effect. *Cell Cycle Georget. Tex* **12,** 3154–3158 (2013).

543. Yang, W. *et al.* EGFR-induced and PKCε monoubiquitylation-dependent NF-κB activation upregulates PKM2 expression and promotes tumorigenesis. *Mol. Cell* **48,** 771–784 (2012).

544. Lee, J., Kim, H. K., Han, Y.-M. & Kim, J. Pyruvate kinase isozyme type M2 (PKM2) interacts and cooperates with Oct-4 in regulating transcription. *Int. J. Biochem. Cell Biol.* **40,** 1043–1054 (2008).

545. Tamada, M., Suematsu, M. & Saya, H. Pyruvate kinase M2: multiple faces for conferring benefits on cancer cells. *Clin. Cancer Res. Off. J. Am. Assoc. Cancer Res.* **18,** 5554–5561 (2012).

546. Fox, P. T. & Raichle, M. E. Focal physiological uncoupling of cerebral blood flow and oxidative metabolism during somatosensory stimulation in human subjects. *Proc. Natl. Acad. Sci. U. S. A.* **83,** 1140–1144 (1986).

547. Bero, A. W. *et al.* Neuronal activity regulates the regional vulnerability to amyloid-β deposition. *Nat. Neurosci.* **14,** 750–756 (2011).

548. Cirrito, J. R. *et al.* Endocytosis is required for synaptic activity-dependent release of amyloid-beta in vivo. *Neuron* **58,** 42–51 (2008).

549. Li, X. *et al.* Neuronal Activity and Secreted Amyloid β Lead to Altered Amyloid β Precursor Protein and Presenilin 1 Interactions. *Neurobiol. Dis.* **50,** 127–134 (2013).

550. Lesné, S. *et al.* NMDA receptor activation inhibits alpha-secretase and promotes neuronal amyloid-beta production. *J. Neurosci. Off. J. Soc. Neurosci.* **25,** 9367–9377 (2005).

551. Buckner, R. L. *et al.* Molecular, structural, and functional characterization of Alzheimer's disease: evidence for a relationship between default activity, amyloid, and memory. *J. Neurosci. Off. J. Soc. Neurosci.* **25,** 7709–7717 (2005).

552. Raichle, M. E. & Snyder, A. Z. A default mode of brain function: a brief history of an evolving idea. *NeuroImage* **37,** 1083-1090; discussion 1097-1099 (2007).

553. Horovitz, S. G. *et al.* Low frequency BOLD fluctuations during resting wakefulness and light sleep: a simultaneous EEG-fMRI study. *Hum. Brain Mapp.* **29,** 671–682 (2008).

554. Larson-Prior, L. J. *et al.* Cortical network functional connectivity in the descent to sleep. *Proc. Natl. Acad. Sci. U. S. A.* **106,** 4489–4494 (2009).

555. Horovitz, S. G. *et al.* Decoupling of the brain's default mode network during deep sleep. *Proc. Natl. Acad. Sci. U. S. A.* **106,** 11376–11381 (2009).

556. Kang, J.-E. *et al.* Amyloid-beta dynamics are regulated by orexin and the sleep-wake cycle. *Science* **326,** 1005–1007 (2009).

557. Roh, J. H. *et al.* Sleep-wake cycle and diurnal fluctuation of amyloid-β as biomarkers of brain amyloid pathology. *Sci. Transl. Med.* **4,** 150ra122 (2012).

558. Liao, F., Zhang, T. J., Mahan, T. E., Jiang, H. & Holtzman, D. M. Effects of growth hormone-releasing hormone on sleep and brain interstitial fluid amyloid-β in an APP transgenic mouse model. *Brain. Behav. Immun.* **47,** 163–171 (2015).

559. Vitiello, M. V. & Prinz, P. N. Alzheimer's disease. Sleep and sleep/wake patterns. *Clin. Geriatr. Med.* **5,** 289–299 (1989).

560. Bateman, R. J., Wen, G., Morris, J. C. & Holtzman, D. M. Fluctuations of CSF amyloid-beta levels: implications for a diagnostic and therapeutic biomarker. *Neurology* **68,** 666–669 (2007).

561. Huang, Y. *et al.* Effects of age and amyloid deposition on Aβ dynamics in the human central nervous system. *Arch. Neurol.* **69,** 51–58 (2012).

562. Citron, M. *et al.* Mutation of the beta-amyloid precursor protein in familial Alzheimer's disease increases beta-protein production. *Nature* **360,** 672–674 (1992).

563. Citron, M. *et al.* Excessive production of amyloid beta-protein by peripheral cells of symptomatic and presymptomatic patients carrying the Swedish familial Alzheimer disease mutation. *Proc. Natl. Acad. Sci. U. S. A.* **91,** 11993–11997 (1994).

564. Johnston, J. A. *et al.* Increased beta-amyloid release and levels of amyloid precursor protein (APP) in fibroblast cell lines from family members with the Swedish Alzheimer's disease APP670/671 mutation. *FEBS Lett.* **354,** 274–278 (1994).

565. Scheuner, D. *et al.* Secreted amyloid beta-protein similar to that in the senile plaques of Alzheimer's disease is increased in vivo by the presenilin 1 and 2 and APP mutations linked to familial Alzheimer's disease. *Nat. Med.* **2,** 864–870 (1996).

566. Nilsberth, C. *et al.* The 'Arctic' APP mutation (E693G) causes Alzheimer's disease by enhanced Abeta protofibril formation. *Nat. Neurosci.* **4,** 887–893 (2001).

567. Jankowsky, J. L., Xu, G., Fromholt, D., Gonzales, V. & Borchelt, D. R. Environmental enrichment exacerbates amyloid plaque formation in a transgenic mouse model of Alzheimer disease. *J. Neuropathol. Exp. Neurol.* **62,** 1220–1227 (2003).

568. Trinchese, F. *et al.* Progressive age-related development of Alzheimer-like pathology in APP/PS1 mice. *Ann. Neurol.* **55,** 801–814 (2004).

569. Savonenko, A. *et al.* Episodic-like memory deficits in the APPswe/PS1dE9 mouse model of Alzheimer's disease: relationships to beta-amyloid deposition and neurotransmitter abnormalities. *Neurobiol. Dis.* **18,** 602–617 (2005).

570. Zhang, W. *et al.* Soluble Aβ levels correlate with cognitive deficits in the 12-month-old APPswe/PS1dE9 mouse model of Alzheimer's disease. *Behav. Brain Res.* **222,** 342–350 (2011).

571. Tholey, G., Roth-Schechter, B. F. & Mandel, P. Activity and isoenzyme pattern of lactate dehydrogenase in neurons and astroblasts cultured from brains of chick embryos. *J. Neurochem.* **36,** 77–81 (1981).

572. Fu, W., Shi, D., Westaway, D. & Jhamandas, J. H. Bioenergetic Mechanisms in Astrocytes May Contribute to Amyloid Plaque Deposition and Toxicity. *J. Biol. Chem.* **290,** 12504–12513 (2015).

573. Delatour, B. & Gisquet-Verrier, P. Prelimbic cortex specific lesions disrupt delayed-variable response tasks in the rat. *Behav. Neurosci.* **110,** 1282–1298 (1996).

574. Ragozzino, M. E., Adams, S. & Kesner, R. P. Differential involvement of the dorsal anterior cingulate and prelimbic-infralimbic areas of the rodent prefrontal cortex in spatial working memory. *Behav. Neurosci.* **112,** 293–303 (1998).

575. Porter, M. C., Burk, J. A. & Mair, R. G. A comparison of the effects of hippocampal or prefrontal cortical lesions on three versions of delayed non-matching-to-sample based on positional or spatial cues. *Behav. Brain Res.* **109,** 69–81 (2000).

576. Lee, I. & Kesner, R. P. Time-Dependent Relationship between the Dorsal Hippocampus and the Prefrontal Cortex in Spatial Memory. *J. Neurosci.* **23,** 1517–1523 (2003).

577. Jo, Y. S. *et al.* The medial prefrontal cortex is involved in spatial memory retrieval under partial-cue conditions. *J. Neurosci. Off. J. Soc. Neurosci.* **27,** 13567–13578 (2007).

578. Dienel, G. A. & Hertz, L. Glucose and lactate metabolism during brain activation. *J. Neurosci. Res.* **66,** 824–838 (2001).

579. Weaver, K. E. *et al.* Posterior Cingulate Lactate as a Metabolic Biomarker in Amnestic Mild Cognitive Impairment. *BioMed Res. Int.* **2015,** 610605 (2015).

580. Liguori, C. *et al.* Cerebrospinal fluid lactate levels and brain [18F]FDG PET hypometabolism within the default mode network in Alzheimer's disease. *Eur. J. Nucl. Med. Mol. Imaging* **43,** 2040–2049 (2016).

581. Liguori, C. *et al.* CSF lactate levels, τ proteins, cognitive decline: a dynamic relationship in Alzheimer's disease. *J. Neurol. Neurosurg. Psychiatry* **86,** 655–659 (2015).

582. Kálmán, J. *et al.* Lactate infusion fails to improve semantic categorization in Alzheimer's disease. *Brain Res. Bull.* **65,** 533–539 (2005).

583. Zhang, W. *et al.* Early memory deficits precede plaque deposition in APPswe/PS1dE9 mice: involvement of oxidative stress and cholinergic dysfunction. *Free Radic. Biol. Med.* **52,** 1443–1452 (2012).

584. Izco, M. *et al.* Changes in the brain and plasma Aβ peptide levels with age and its relationship with cognitive impairment in the APPswe/PS1dE9 mouse model of Alzheimer's disease. *Neuroscience* **263,** 269–279 (2014).

585. Edwards, S. R., Hamlin, A. S., Marks, N., Coulson, E. J. & Smith, M. T. Comparative studies using the Morris water maze to assess spatial memory deficits in two transgenic mouse models of Alzheimer's disease. *Clin. Exp. Pharmacol. Physiol.* **41,** 798–806 (2014).

586. Taniuchi, N., Niidome, T. & Sugimoto, H. [Fundamental study of memory impairment and non-cognitive behavioral alterations in APPswe/PS1dE9 mice]. *Yakugaku Zasshi* **135,** 323–329 (2015).

587. Janus, C., Flores, A. Y., Xu, G. & Borchelt, D. R. Behavioral abnormalities in APPSwe/PS1dE9 mouse model of AD-like pathology: comparative analysis across multiple behavioral domains. *Neurobiol. Aging* **36,** 2519–2532 (2015).

588. Kerr, D. S. Treatment of mitochondrial electron transport chain disorders: a review of clinical trials over the past decade. *Mol. Genet. Metab.* **99,** 246–255 (2010).

589. Kankotia, S. & Stacpoole, P. W. Dichloroacetate and cancer: new home for an orphan drug? *Biochim. Biophys. Acta* **1846,** 617–629 (2014).

590. Howlett, R. A., Heigenhauser, G. J., Hultman, E., Hollidge-Horvat, M. G. & Spriet, L. L. Effects of dichloroacetate infusion on human skeletal muscle metabolism at the onset of exercise. *Am. J. Physiol.* **277,** E18-25 (1999).

591. Parolin, M. L. *et al.* Effects of PDH activation by dichloroacetate in human skeletal muscle during exercise in hypoxia. *Am. J. Physiol. Endocrinol. Metab.* **279,** E752-761 (2000).

592. Linn, T. C., Pettit, F. H. & Reed, L. J. Alpha-keto acid dehydrogenase complexes. X. Regulation of the activity of the pyruvate dehydrogenase complex from beef kidney mitochondria by phosphorylation and dephosphorylation. *Proc. Natl. Acad. Sci. U. S. A.* **62,** 234–241 (1969).

593. Mori, M., Yamagata, T., Goto, T., Saito, S. & Momoi, M. Y. Dichloroacetate treatment for mitochondrial cytopathy: long-term effects in MELAS. *Brain Dev.* **26,** 453–458 (2004).

594. Kaufmann, P. *et al.* Dichloroacetate causes toxic neuropathy in MELAS A randomized, controlled clinical trial. *Neurology* **66,** 324–330 (2006).

595. Stacpoole, P. W., Kurtz, T. L., Han, Z. & Langaee, T. Role of Dichloroacetate in the Treatment of Genetic Mitochondrial Diseases. *Adv. Drug Deliv. Rev.* **60,** 1478–1487 (2008).

596. Shroads, A. L. *et al.* Age-dependent kinetics and metabolism of dichloroacetate: possible relevance to toxicity. *J. Pharmacol. Exp. Ther.* **324,** 1163–1171 (2008).

597. Rardin, M. J., Wiley, S. E., Naviaux, R. K., Murphy, A. N. & Dixon, J. E. Monitoring phosphorylation of the pyruvate dehydrogenase complex. *Anal. Biochem.* **389,** 157–164 (2009).

598. Browning, M., Baudry, M., Bennett, W. F. & Lynch, G. Phosphorylation-mediated changes in pyruvate dehydrogenase activity influence pyruvate-supported calcium accumulation by brain mitochondria. *J. Neurochem.* **36,** 1932–1940 (1981).

599. Abemayor, E., Kovachich, G. B. & Haugaard, N. Effects of dichloroacetate on brain pyruvate dehydrogenase. *J. Neurochem.* **42,** 38–42 (1984).

600. Kuroda, Y. *et al.* Effects of dichloroacetate on pyruvate metabolism in rat brain in vivo. *Pediatr. Res.* **18,** 936–938 (1984).

601. Piao, L. *et al.* FOXO1-mediated Upregulation of Pyruvate Dehydrogenase Kinase-4 (PDK4) Decreases Glucose Oxidation and Impairs Right Ventricular Function in Pulmonary Hypertension: Therapeutic Benefits of Dichloroacetate. *J. Mol. Med. Berl. Ger.* **91,** 333–346 (2013).

602. McIlwain, K. L., Merriweather, M. Y., Yuva-Paylor, L. A. & Paylor, R. The use of behavioral test batteries: effects of training history. *Physiol. Behav.* **73,** 705–717 (2001).

603. Vicens, P., Bernal, M. C., Carrasco, M. C. & Redolat, R. Previous training in the water maze: differential effects in NMRI and C57BL mice. *Physiol. Behav.* **67,** 197–203 (1999).

604. Paylor, R., Spencer, C. M., Yuva-Paylor, L. A. & Pieke-Dahl, S. The use of behavioral test batteries, II: effect of test interval. *Physiol. Behav.* **87,** 95–102 (2006).

605. Võikar, V., Vasar, E. & Rauvala, H. Behavioral alterations induced by repeated testing in C57BL/6J and 129S2/Sv mice: implications for phenotyping screens. *Genes Brain Behav.* **3,** 27–38 (2004).

606. Vicens, P., Redolat, R. & Carrasco, M. C. Effects of early spatial training on water maze performance: a longitudinal study in mice. *Exp. Gerontol.* **37,** 575–581 (2002).

607. Daniels, C. J. *et al.* A comparison of quantitative methods for clinical imaging with hyperpolarized (13)C-pyruvate. *NMR Biomed.* **29,** 387–399 (2016).

608. Cummings, J. L., Morstorf, T. & Zhong, K. Alzheimer's disease drug-development pipeline: few candidates, frequent failures. *Alzheimers Res. Ther.* **6,** 37 (2014).

609. Schneider, L. S. *et al.* Clinical trials and late-stage drug development for Alzheimer's disease: an appraisal from 1984 to 2014. *J. Intern. Med.* **275,** 251–283 (2014).

610. Drummond, E. & Wisniewski, T. Alzheimer's disease: experimental models and reality. *Acta Neuropathol. (Berl.)* **133,** 155–175 (2017).

611. Banik, A. *et al.* Translation of Pre-Clinical Studies into Successful Clinical Trials for Alzheimer's Disease: What are the Roadblocks and How Can They Be Overcome? *J. Alzheimers Dis. JAD* **47,** 815–843 (2015).

612. Oddo, S., Caccamo, A., Kitazawa, M., Tseng, B. P. & LaFerla, F. M. Amyloid deposition precedes tangle formation in a triple transgenic model of Alzheimer's disease. *Neurobiol. Aging* **24,** 1063–1070 (2003).

613. Wirths, O. & Bayer, T. A. Neuron Loss in Transgenic Mouse Models of Alzheimer's Disease. *Int. J. Alzheimers Dis.* **2010,** (2010).

614. Schmid, L. C. *et al.* Dysfunction of Somatostatin-Positive Interneurons Associated with Memory Deficits in an Alzheimer's Disease Model. *Neuron* **92,** 114–125 (2016).

615. Silva, S. V. da *et al.* Early synaptic deficits in the APP/PS1 mouse model of Alzheimer's disease involve neuronal adenosine A2A receptors. *Nat. Commun.* **7,** 11915 (2016).

616. West, M. J., Coleman, P. D., Flood, D. G. & Troncoso, J. C. Differences in the pattern of hippocampal neuronal loss in normal ageing and Alzheimer's disease. *Lancet Lond. Engl.* **344,** 769–772 (1994).

617. Gómez-Isla, T. *et al.* Profound loss of layer II entorhinal cortex neurons occurs in very mild Alzheimer's disease. *J. Neurosci. Off. J. Soc. Neurosci.* **16,** 4491–4500 (1996).

618. Price, J. L. *et al.* Neuron number in the entorhinal cortex and CA1 in preclinical Alzheimer disease. *Arch. Neurol.* **58,** 1395–1402 (2001).

619. Rodrigue, K. M. & Raz, N. Shrinkage of the entorhinal cortex over five years predicts memory performance in healthy adults. *J. Neurosci. Off. J. Soc. Neurosci.* **24,** 956–963 (2004).

620. Rossignol, F., Solares, M., Balanza, E., Coudert, J. & Clottes, E. Expression of lactate dehydrogenase A and B genes in different tissues of rats adapted to chronic hypobaric hypoxia. *J. Cell. Biochem.* **89,** 67–79 (2003).

621. Korotchkina, L. G. & Patel, M. S. Mutagenesis studies of the phosphorylation sites of recombinant human pyruvate dehydrogenase. Site-specific regulation. *J. Biol. Chem.* **270,** 14297–14304 (1995).

622. Pilegaard, H. *et al.* PDH-E1α Dephosphorylation and Activation in Human Skeletal Muscle During Exercise. *Diabetes* **55,** 3020–3027 (2006).

623. Spriet, L. L. & Heigenhauser, G. J. F. Regulation of pyruvate dehydrogenase (PDH) activity in human skeletal muscle during exercise. *Exerc. Sport Sci. Rev.* **30,** 91–95 (2002).

624. Sabatini, M. J. *et al.* Amygdala gene expression correlates of social behavior in monkeys experiencing maternal separation. *J. Neurosci. Off. J. Soc. Neurosci.* **27,** 3295–3304 (2007).

625. Hodges, A. *et al.* Brain gene expression correlates with changes in behavior in the R6/1 mouse model of Huntington's disease. *Genes Brain Behav.* **7,** 288–299 (2008).

626. Sharma, H. R. & Thakur, M. K. Correlation of ERα/ERβ expression with dendritic and behavioural changes in CUMS mice. *Physiol. Behav.* **145,** 71–83 (2015).

627. De Ron, P. *et al.* Correlating behaviour and gene expression endpoints in the dopaminergic system after modafinil administration in mouse. *Eur. Neuropsychopharmacol. J. Eur. Coll. Neuropsychopharmacol.* **26,** 729–740 (2016).

628. Barberio, M. D. *et al.* Pyruvate Dehydrogenase Phosphatase Regulatory Gene Expression Correlates with Exercise Training Insulin Sensitivity Changes. *Med. Sci. Sports Exerc.* **48,** 2387–2397 (2016).

629. Kumar, G. K. & Klein, J. B. Analysis of expression and posttranslational modification of proteins during hypoxia. *J. Appl. Physiol.* **96,** 1178–1186 (2004).

630. Spriet, L. L. *et al.* Pyruvate dehydrogenase activation and kinase expression in human skeletal muscle during fasting. *J. Appl. Physiol. Bethesda Md 1985* **96,** 2082–2087 (2004).

631. Peek, C. B. *et al.* Circadian clock NAD+ cycle drives mitochondrial oxidative metabolism in mice. *Science* **342,** 1243417 (2013).

632. Tadi, M., Allaman, I., Lengacher, S., Grenningloh, G. & Magistretti, P. J. Learning-Induced Gene Expression in the Hippocampus Reveals a Role of Neuron -Astrocyte Metabolic Coupling in Long Term Memory. *PLOS ONE* **10,** e0141568 (2015).

633. Humphrey, S. J., James, D. E. & Mann, M. Protein Phosphorylation: A Major Switch Mechanism for Metabolic Regulation. *Trends Endocrinol. Metab. TEM* **26,** 676–687 (2015).

634. Hunter, T. Why nature chose phosphate to modify proteins. *Philos. Trans. R. Soc. B Biol. Sci.* **367,** 2513–2516 (2012).

635. Akhmedov, D., De Marchi, U., Wollheim, C. B. & Wiederkehr, A. Pyruvate dehydrogenase E1α phosphorylation is induced by glucose but does not control

metabolism-secretion coupling in INS-1E clonal β-cells. *Biochim. Biophys. Acta* **1823,** 1815–1824 (2012).

636. Zimmer, A. D., Walbrecq, G., Kozar, I., Behrmann, I. & Haan, C. Phosphorylation of the pyruvate dehydrogenase complex precedes HIF-1-mediated effects and pyruvate dehydrogenase kinase 1 upregulation during the first hours of hypoxic treatment in hepatocellular carcinoma cells. *Hypoxia* **4,** 135–145 (2016).

637. Ammini, C. V. & Stacpoole, P. W. in *Natural Production of Organohalogen Compounds* (ed. Gribble, G.) 215–234 (Springer Berlin Heidelberg, 2003). doi:10.1007/b10453

638. Stacpoole, P. W., Henderson, G. N., Yan, Z., Cornett, R. & James, M. O. Pharmacokinetics, metabolism and toxicology of dichloroacetate. *Drug Metab. Rev.* **30,** 499–539 (1998).

639. Calcutt, N. A. *et al.* Peripheral neuropathy in rats exposed to dichloroacetate. *J. Neuropathol. Exp. Neurol.* **68,** 985–993 (2009).

640. Felitsyn, N., Stacpoole, P. W. & Notterpek, L. Dichloroacetate causes reversible demyelination in vitro: potential mechanism for its neuropathic effect. *J. Neurochem.* **100,** 429–436 (2007).

641. Klungsøyr, J. & Scheline, R. R. Metabolism of isosafrole and dihydrosafrole in the rat. *Biomed. Mass Spectrom.* **9,** 323–329 (1982).

642. Tran, A. *et al.* Influence of stiripentol on cytochrome P450-mediated metabolic pathways in humans: in vitro and in vivo comparison and calculation of in vivo inhibition constants. *Clin. Pharmacol. Ther.* **62,** 490–504 (1997).

643. Dhers, L., Ducassou, L., Boucher, J.-L. & Mansuy, D. Cytochrome P450 2U1, a very peculiar member of the human P450s family. *Cell. Mol. Life Sci. CMLS* (2017). doi:10.1007/s00018-016-2443-3

644. Mansuy, I. M. *et al.* Inducible and Reversible Gene Expression with the rtTA System for the Study of Memory. *Neuron* **21,** 257–265 (1998).

645. Johnson, W. B. *et al.* Indicator expression directed by regulatory sequences of the glial fibrillary acidic protein (GFAP) gene: in vivo comparison of distinct GFAP-lacZ transgenes. *Glia* **13,** 174–184 (1995).

646. Kim, B. O. *et al.* Neuropathologies in Transgenic Mice Expressing Human Immunodeficiency Virus Type 1 Tat Protein under the Regulation of the Astrocyte-Specific Glial Fibrillary Acidic Protein Promoter and Doxycycline. *Am. J. Pathol.* **162,** 1693–1707 (2003).

647. Perl, A.-K. T., Wert, S. E., Nagy, A., Lobe, C. G. & Whitsett, J. A. Early restriction of peripheral and proximal cell lineages during formation of the lung. *Proc. Natl. Acad. Sci. U. S. A.* **99,** 10482–10487 (2002).

648. Wang, Y.-H. *et al.* Cell state-specific metabolic dependency in hematopoiesis and leukemogenesis. *Cell* **158,** 1309–1323 (2014).

649. Mayford, M. *et al.* Control of memory formation through regulated expression of a CaMKII transgene. *Science* **274,** 1678–1683 (1996).

650. Wang, J., Lin, W., Popko, B. & Campbell, I. L. Inducible production of interferon-gamma in the developing brain causes cerebellar dysplasia with activation of the Sonic hedgehog pathway. *Mol. Cell. Neurosci.* **27,** 489–496 (2004).

651. Xie, H. *et al.* Targeting Lactate Dehydrogenase-A Inhibits Tumorigenesis and Tumor Progression in Mouse Models of Lung Cancer and Impacts Tumor-Initiating Cells. *Cell Metab.* **19,** 795–809 (2014).

652. Sunyer, B., Patil, S., Höger, H. & Luber, G. Barnes maze, a useful task to assess spatial reference memory in the mice. *Protoc. Exch.* (2007). doi:10.1038/nprot.2007.390

653. Antunes, M. & Biala, G. The novel object recognition memory: neurobiology, test procedure, and its modifications. *Cogn. Process.* **13,** 93–110 (2012).

654. Prut, L. & Belzung, C. The open field as a paradigm to measure the effects of drugs on anxiety-like behaviors: a review. *Eur. J. Pharmacol.* **463,** 3–33 (2003).

655. Rodgers, R. J. & Dalvi, A. Anxiety, defence and the elevated plus-maze. *Neurosci. Biobehav. Rev.* **21,** 801–810 (1997).

656. Crawley, J. & Goodwin, F. K. Preliminary report of a simple animal behavior model for the anxiolytic effects of benzodiazepines. *Pharmacol. Biochem. Behav.* **13,** 167–170 (1980).

657. Oakley, H. *et al.* Intraneuronal beta-amyloid aggregates, neurodegeneration, and neuron loss in transgenic mice with five familial Alzheimer's disease mutations: potential factors in amyloid plaque formation. *J. Neurosci. Off. J. Soc. Neurosci.* **26,** 10129–10140 (2006).

Appendix A: Supplementary Figures and Tables

A

B

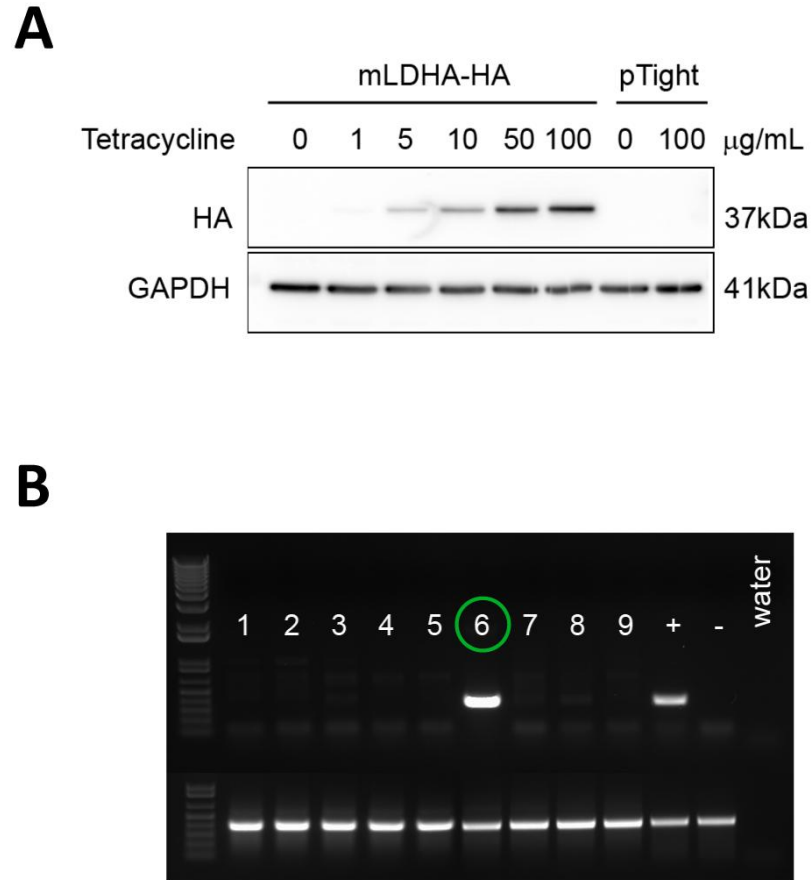**Figure A1. Creation of novel transgenic mouse line containing mLDHA-HA-pTight expression cassette.**

(A) Western blot analysis of cell lysates probed using HA- and GAPDH-antibodies showing tetracycline-inducible expression of mLDHA-HA in HeLa-rtTA cells. (B) PCR-based genotyping of ear punch from litter of female founder mouse #849 with positive pup #6 demonstrating germline transmission of the mLDHA-HA-pTight transgene.

Table A2. List of mice removed from analysis due to stress effects in a particular training phase.

Mice could be removed from analysis if they display behaviour that clearly demonstrates no attempt to actively search for the platform during the training phase. The number of control mice and APP/PS1 mice out of the total for each training phase is displayed.

	Number of mice removed from analysis due to stress	
Training Phase	**Control**	**APP/PS1**
Vehicle	0 / 17	3 / 11
Isosafrol	0 / 16	1 / 9
DCA	0 / 15	1 / 9
Saline	0 / 13	1 / 7

Appendix B: Reprint Permissions

RightsLink Printable License

**SPRINGER LICENSE
TERMS AND CONDITIONS**

Feb 17, 2017

This Agreement between Richard Harris ("You") and Springer ("Springer") consists of your license details and the terms and conditions provided by Springer and Copyright Clearance Center.

License Number	4051380502203
License date	Feb 17, 2017
Licensed Content Publisher	Springer
Licensed Content Publication	Biogerontology
Licensed Content Title	Age-dependent metabolic dysregulation in cancer and Alzheimer's disease
Licensed Content Author	Richard A. Harris
Licensed Content Date	Jan 1, 2014
Licensed Content Volume	15
Licensed Content Issue	6
Type of Use	Thesis/Dissertation
Portion	Full text
Number of copies	1
Author of this Springer article	Yes and you are the sole author of the new work
Order reference number	
Title of your thesis / dissertation	Cerebral lactate metabolism and memory: Implications in Alzheimer's disease
Expected completion date	Apr 2017
Estimated size(pages)	200
Requestor Location	███████████
Billing Type	Invoice
Billing Address	███████████
Total	0.00 CAD

Terms and Conditions

Introduction
The publisher for this copyrighted material is Springer. By clicking "accept" in connection

with completing this licensing transaction, you agree that the following terms and conditions apply to this transaction (along with the Billing and Payment terms and conditions established by Copyright Clearance Center, Inc. ("CCC"), at the time that you opened your Rightslink account and that are available at any time at http://myaccount.copyright.com).

Limited License

With reference to your request to reuse material on which Springer controls the copyright, permission is granted for the use indicated in your enquiry under the following conditions:

- Licenses are for one-time use only with a maximum distribution equal to the number stated in your request.

- Springer material represents original material which does not carry references to other sources. If the material in question appears with a credit to another source, this permission is not valid and authorization has to be obtained from the original copyright holder.

- This permission

• is non-exclusive

• is only valid if no personal rights, trademarks, or competitive products are infringed.

• explicitly excludes the right for derivatives.

- Springer does not supply original artwork or content.

- According to the format which you have selected, the following conditions apply accordingly:

• **Print and Electronic:** This License include use in electronic form provided it is password protected, on intranet, or CD-Rom/DVD or E-book/E-journal. It may not be republished in electronic open access.

• **Print:** This License excludes use in electronic form.

• **Electronic:** This License only pertains to use in electronic form provided it is password protected, on intranet, or CD-Rom/DVD or E-book/E-journal. It may not be republished in electronic open access.

For any electronic use not mentioned, please contact Springer at permissions.springer@spi-global.com.

- Although Springer controls the copyright to the material and is entitled to negotiate on rights, this license is only valid subject to courtesy information to the author (address is given in the article/chapter).

- If you are an STM Signatory or your work will be published by an STM Signatory and you are requesting to reuse figures/tables/illustrations or single text extracts, permission is granted according to STM Permissions Guidelines: http://www.stm-assoc.org/permissions-guidelines/

For any electronic use not mentioned in the Guidelines, please contact Springer at ▮▮▮▮▮▮▮▮▮▮▮▮▮▮. If you request to reuse more content than stipulated in the STM Permissions Guidelines, you will be charged a permission fee for the excess content.

Permission is valid upon payment of the fee as indicated in the licensing process. If permission is granted free of charge on this occasion, that does not prejudice any rights we might have to charge for reproduction of our copyrighted material in the future.

-If your request is for reuse in a Thesis, permission is granted free of charge under the following conditions:

This license is valid for one-time use only for the purpose of defending your thesis and with a maximum of 100 extra copies in paper. If the thesis is going to be published, permission needs to be reobtained.

- includes use in an electronic form, provided it is an author-created version of the thesis on his/her own website and his/her university's repository, including UMI (according to the definition on the Sherpa website: http://www.sherpa.ac.uk/romeo/);

- is subject to courtesy information to the co-author or corresponding author.

Geographic Rights: Scope

Licenses may be exercised anywhere in the world.

Altering/Modifying Material: Not Permitted

Figures, tables, and illustrations may be altered minimally to serve your work. You may not alter or modify text in any manner. Abbreviations, additions, deletions and/or any other alterations shall be made only with prior written authorization of the author(s).

Reservation of Rights

Springer reserves all rights not specifically granted in the combination of (i) the license details provided by you and accepted in the course of this licensing transaction and (ii) these terms and conditions and (iii) CCC's Billing and Payment terms and conditions.

License Contingent on Payment

While you may exercise the rights licensed immediately upon issuance of the license at the end of the licensing process for the transaction, provided that you have disclosed complete and accurate details of your proposed use, no license is finally effective unless and until full payment is received from you (either by Springer or by CCC) as provided in CCC's Billing and Payment terms and conditions. If full payment is not received by the date due, then any license preliminarily granted shall be deemed automatically revoked and shall be void as if never granted. Further, in the event that you breach any of these terms and conditions or any of CCC's Billing and Payment terms and conditions, the license is automatically revoked and shall be void as if never granted. Use of materials as described in a revoked license, as well as any use of the materials beyond the scope of an unrevoked license, may constitute copyright infringement and Springer reserves the right to take any and all action to protect its copyright in the materials.

Copyright Notice: Disclaimer

You must include the following copyright and permission notice in connection with any reproduction of the licensed material:

"Springer book/journal title, chapter/article title, volume, year of publication, page, name(s) of author(s), (original copyright notice as given in the publication in which the material was originally published) "With permission of Springer"

In case of use of a graph or illustration, the caption of the graph or illustration must be included, as it is indicated in the original publication.

Warranties: None

Springer makes no representations or warranties with respect to the licensed material and adopts on its own behalf the limitations and disclaimers established by CCC on its behalf in its Billing and Payment terms and conditions for this licensing transaction.

Indemnity

You hereby indemnify and agree to hold harmless Springer and CCC, and their respective officers, directors, employees and agents, from and against any and all claims arising out of your use of the licensed material other than as specifically authorized pursuant to this license.

No Transfer of License

This license is personal to you and may not be sublicensed, assigned, or transferred by you without Springer's written permission.

No Amendment Except in Writing

This license may not be amended except in a writing signed by both parties (or, in the case of Springer, by CCC on Springer's behalf).

Objection to Contrary Terms

Springer hereby objects to any terms contained in any purchase order, acknowledgment, check endorsement or other writing prepared by you, which terms are inconsistent with these terms and conditions or CCC's Billing and Payment terms and conditions. These terms and conditions, together with CCC's Billing and Payment terms and conditions (which are incorporated herein), comprise the entire agreement between you and Springer (and CCC) concerning this licensing transaction. In the event of any conflict between your obligations established by these terms and conditions and those established by CCC's Billing and Payment terms and conditions, these terms and conditions shall control.

Jurisdiction
All disputes that may arise in connection with this present License, or the breach thereof, shall be settled exclusively by arbitration, to be held in the Federal Republic of Germany, in accordance with German law.
Other conditions:
V 12AUG2015

Questions? ███████████████████████
████████████

SOCIETY FOR NEUROSCIENCE ORDER DETAILS

Feb 23, 2017

Order Number	501236809
Order date	Feb 17, 2017
Licensed content publisher	Society for Neuroscience
Licensed content title	The journal of neuroscience : the official journal of the Society for Neuroscience
Licensed content date	Jan 1, 1981
Type of Use	Thesis/Dissertation
Requestor type	Author of requested content
Format	Print, Electronic
Portion	chapter/article
Title or numeric reference of the portion(s)	Aerobic Glycolysis in the Frontal Cortex Correlates with Memory Performance in Wild-Type Mice But Not the APP/PS1 Mouse Model of Cerebral Amyloidosis, Figures 1-4
Title of the article or chapter the portion is from	Aerobic Glycolysis in the Frontal Cortex Correlates with Memory Performance in Wild-Type Mice But Not the APP/PS1 Mouse Model of Cerebral Amyloidosis
Editor of portion(s)	N/A
Author of portion(s)	Richard Harris
Volume of serial or monograph.	N/A
Page range of the portion	
Publication date of portion	February 10, 2016
Rights for	Main product
Duration of use	Life of current edition
Creation of copies for the disabled	no
With minor editing privileges	yes
For distribution to	Canada
In the following language(s)	Original language of publication
With incidental promotional use	no
The lifetime unit quantity of new product	Up to 499
Made available in the following markets	Education
Specified additional information	Minor editing privileges
The requesting person/organization is:	Richard Harris
Order reference number	
Author/Editor	Richard Harris
The standard identifier of New Work	Thesis/Dissertation

RightsLink Printable Job Ticket

Title of New Work	Cerebral lactate metabolism and memory: Implications in Alzheimer's disease
Publisher of New Work	The University of Western Ontario
Expected publication date	Apr 2017
Estimated size (pages)	200
Total (may include CCC user fee)	0.00 USD

Curriculum Vitae

Name: Richard Harris

Post-secondary   Carleton University
Education and   Ottawa, Ontario, Canada
Degrees: 2003-2007 B.Sc.

                     The University of Guelph
                     Guelph, Ontario, Canada
                     2007-2009 M.Sc.

                     The University of Western Ontario
                     London, Ontario, Canada
                     2012-2017 Ph.D.

Honours and   Province of Ontario Graduate Scholarship
Awards: 2014, 2015
                     Western Science Dean's Doctoral Scholarship
                     2012

Related Work   Teaching Assistant
Experience   The University of Western Ontario
                     2012-2017

Publications:

Harris RA, Scholl T, Cumming RC (2017). Chemical inhibition of aerobic glycolysis does not impair memory performance. Manuscript in preparation

Harris RA, Tindale L, Lone A, Singh O, Macauley SL, Stanley M, Holtzman DM, Bartha R, Cumming RC (2016) Aerobic glycolysis in the frontal cortex correlates with memory performance in wild-type mice but not in the APP/PS1 mouse model of cerebral amyloidosis. *J. Neurosci.* 36(6):1871-8

Harris RA*, Clouthier DL*, Harris CN*, Martin CE, Puri MC, Jones N. (2015) Requisite role for Nck adaptors in cardiovascular development, endothelial-to-mesenchymal transition and directed migration. *Mol. Cell Biol.* 35(9):1573-87.*Denotes equal author contributions.

Harris RA, Tindale L, Cumming RC (2014) Age-dependent dysregulation in cancer and Alzheimer's disease. *Biogerontology.* 15(6):559-77

Newington JT, Harris R, Cumming RC (2013) Re-evaluating metabolism in Alzheimer's disease from the perspective of the astrocyte-neuron lactate shuttle model. *J. of Neurodegen. Dis.*